TECHNICAL REPORT NO. 5

EFFECT OF JOINTS ON THE STRENGTH OF TUNNELS

RESEARCH ON ROCK BOLT REINFORCEMENT

by

RICHARD E. GOODMAN

SEPTEMBER 1968

OMAHA DISTRICT, CORPS OF ENGINEERS
OMAHA, NEBRASKA 68102

THIS RESEARCH WAS FUNDED BY OFFICE,
CHIEF OF ENGINEERS, DEPARTMENT OF THE ARMY

PREPARED UNDER CONTRACT DACA45-67-C-0015 MOD. P001
BY THE UNIVERSITY OF CALIFORNIA, BERKELEY, CALIFORNIA

ABSTRACT

Rock and joint properties were reviewed as a basis for developing the analyses. The review discussed: failure criteria for the rock; and joint properties. Improved methods of sampling and testing joints were explored in detail. Pile Driver test sections were used as a basis for analysis.

Two approaches of analysis of the rock to predict performance of rock bolted and unlined test sections were used. The first method called finite element was used on one section only. This method's complexity prevented its application to other sections. Discontinuities, heterogeneities, and local failures can be taken into account by finite elements, but the representation is only two dimensional. Joint influence analysis, the second method, was applied to many sections. In comparison to the finite element method, joint influence analysis is relatively simple to use. Joints and rock bolts are assumed not to modify the stress distribution in the joint influence analysis; however, the method represents a three dimensional approach.

Comparisons were made to post-shot cross sections of the Pile Driver openings to evaluate the methods of analysis. The finite element method is more powerful; the joint influence analysis is easier to use. ( )

PREFACE

This investigation was authorized by the Chief of Engineers (ENGMC-EM) and was performed in FY 1968 under Contract No. DACA45-67-C-0015, Mod. P001, between the Omaha District, Corps of Engineers and Dr. Richard E. Goodman, Berkeley, California.

This report was prepared under the supervision of Dr. R. E. Goodman, Principal Investigator. Personnel contributing to the report were Michael Cleary, Ashraf Mahtab, and Fred Sage.

During the work period covered by this report, Colonel William H. McKenzie III was District Engineer; Charles L. Hipp was Chief, Engineering Division; C. J. Distefano was technical monitor for the Omaha District under the general supervision of D. C. Aardappel, Acting Chief, Protective Structures Branch. D. G. Heitmann participated in the monitoring work.

TABLE OF CONTENTS

TABLES

FIGURES

FIGURES - continued

FIGURES - continued

FIGURES - continued

FIGURES - continued

EFFECT OF JOINTS ON THE STRENGTH OF TUNNELS

1. INTRODUCTION

This is a report of an investigation performed under Contract Number DACA45-67-C-0015 Mod. P001, between the Corps of Engineers, Omaha District, and Dr. Richard E. Goodman, as contractor. It describes results of research on an application of analysis techniques to the Piledriver Drift. The work was performed during the period, July 1, 1967 to June 30, 1968. This work was specifically tied to the Piledriver Project. An effort was made to apply previously developed analytical techniques to evaluate the influence of jointing and faulting in the bedrock on the performance of Piledriver test drifts. Frequent reference is made to the final reports of two previous contracts[1,2].

In the first contract, the principal investigators studied the effect of geological factors on the behavior of several experimental lined and unlined sections of the Piledriver test. Particular attention was paid to the effect of joint planes on the strength of a tunnel under static load. Consideration was also given to the strengthening effect of rock bolts and of composite steel-concrete linings. The first contract was a specifically directed investigation of short duration. In the second contract, several ideas for analysis of geological factors which had been considered in the first contract were given further attention and the importance of weakness surfaces on the mechanics of tunnels was underscored. It was stated that the technology of description and prediction of joints and fractures was sufficiently far advanced to permit analysis but that the mechanics of the

---

[1]Goodman, R. E., Geological Factors in Design of Blast Resistant Tunnels, U.S. Army, Corps of Engineers, Omaha District, Tech. Report No. 2, September 1966.

[2]Goodman, R. E., Analysis of Structures in Jointed Rock, U. S. Army, Corps of Engineers, Omaha District, Tech. Report No. 3, September 1967.

interaction of joint blocks around an opening had not been considered in any depth.

Two methods of analysis were proposed and developed to some extent in the second report. The first was a three-dimensional ubiquitous joint analysis, referred to also by the more simple title of joint influence analysis. It involves the calculation of the area around the tunnel within which the traction across a joint of fixed orientation and given cohesion and friction is sufficient to induce sliding along or opening of the joint.

The second method of analysis discussed in the second contract report was a joint stiffness analysis using the method of finite element analysis. In this method, an attempt is made to compile a mathematical model of a particular cross section of a tunnel, and to introduce into the model, representations for the deformability and strength of both the solid rock blocks and the joints and fractures between them.

In this report, the two above methods have been applied to analysis of selected portions of the Piledriver experiment. The Piledriver experiment includes test galleries of various distances from a blast as depicted in Fig. 1.1. In this study, the CR and DL Drifts shown in Fig. 1.1 were considered. These drifts include unlined sections, rock-bolted sections, and lined sections with various combinations of concrete, steel and compressible back-packing. Detailed descriptions of the test openings are given in a number of other reports and are summarized in Technical Report Number 2[3].

The principal investigator studied general descriptive information about the Piledriver test, including geological maps and logs compiled before the experiment. He made two trips -- one with Dr. Robert Taylor and one alone -- to examine the failure pattern and damage patterns of drifts after the blast. He also studied post-blast cross sections and profiles, portions of the Corps of Engineers Report describing damage in the drifts[4], and post-shock geological notes made by the geologist on the pre-construction logs. Work was performed at 131 Montrose Road, Berkeley, California, and at the University of California Computer Center. One progress report was

---

[3]op. cit., p. 1.

[4]Chapter 4, Piledriver Report POR 4015.

sent on January 12, describing joint influence analysis in DL drift. This document includes all the information contained in that progress report.

This report is organized as follows. Section 2 describes the method of mathematical modeling for tunnels in jointed rock including modifications made to finite element analysis methods used herein. Methods of developing geologic cross sections from construction logs are described and there is a discussion of the properties to be assigned to the rock blocks, including deformability and strength. A new criterion of failure for Piledriver rock was incorporated in the study and is described in this section. The properties of joint surfaces are discussed and the methods of sampling and testing joints to determine their deformability and strength properties are reviewed. Typical shear-displacement curves are presented for the various kinds of joint surfaces that are known to occur. Extensive data on joint strength and deformability properties are presented in a series of tables compiled from many sources around the world. Finally, at the end of this section, the application of the modeling technique to the DL drift is discussed.

Section 3 describes the use of the joint influence diagram method to DL and CR drifts. The method of constructing and using joint influence diagrams is reviewed, and the state of stress around each of the tunnels adopted for the analysis is presented. Analyses were made every 10 feet throughout CR lateral and CR north drift and throughout DL 1 and DL 2. At every cross section considered, the results of analysis are presented in a series of figures and compared with the actual damage patterns revealed after the blast. Computer programs used in this work are presented in the Appendix.

PILE DRIVER

PERSPECTIVE OF DRIFT COMPLEX

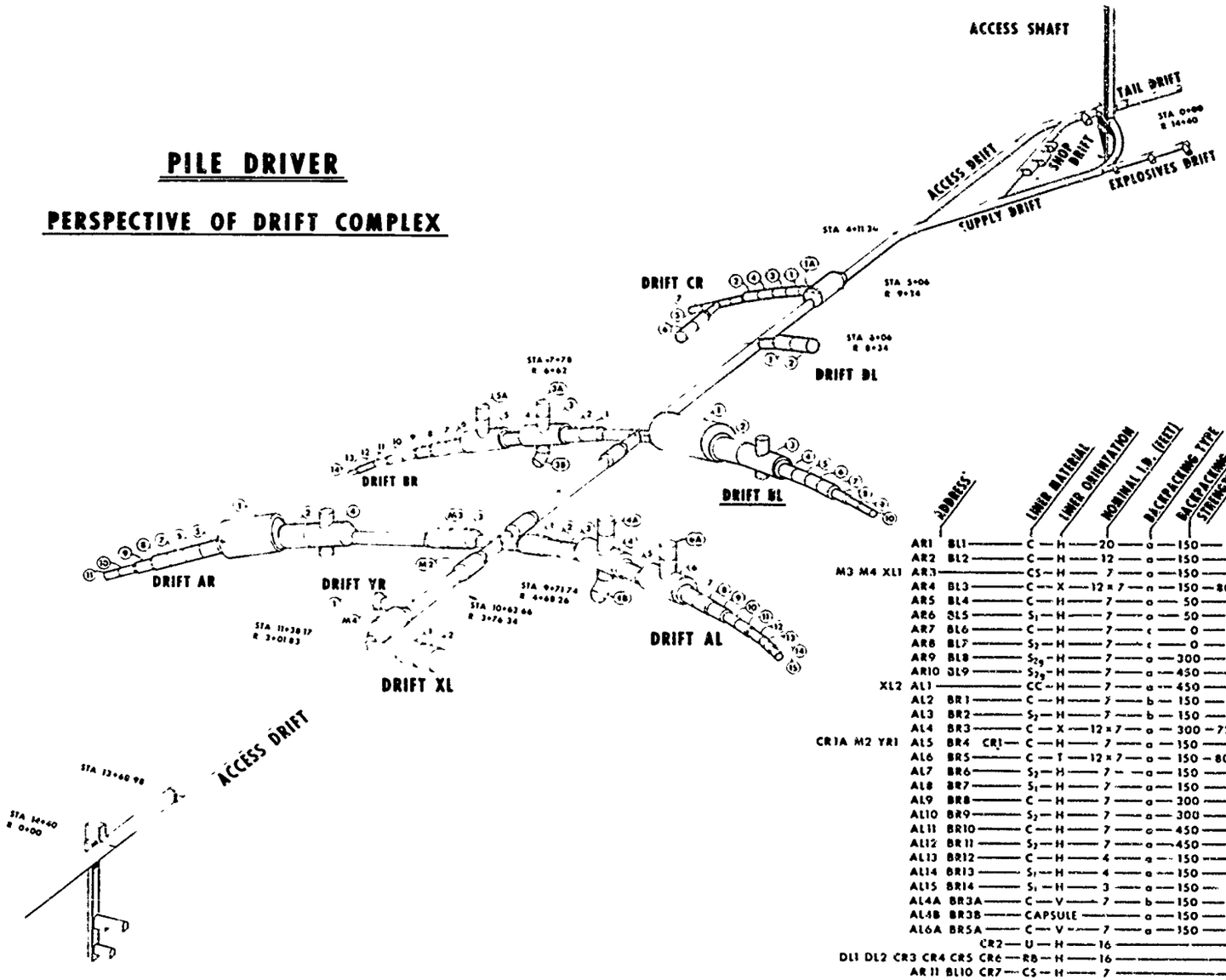

	ADDRESS	LINER MATERIAL	LINER ORIENTATION	NOMINAL I.D. (FEET)	BACKPACKING TYPE	BACKPACKING COMPRESSIVE STRENGTH (P.S.I.)	BACKPACKING THICKNESS (IN.)	LINER THICKNESS	ROCK DIAMETER
	AR1 BL1	C — H	20	a	150	132	12"		44'-0"
	AR2 BL2	C — H	12	a	150	80	8"		26'-8"
M3 M4 XL1	AR3	CS — H	7	a	150	57	15" → 1 GA		21'-6"
	AR4 BL3	C — X	12 x 7	a	150	80 x 48	8" x 6"		26'-8" x 16'-0"
	AR5 BL4	C — H	7	a	50	48	6"		16'-0"
	AR6 BL5	S_1 — H	7	a	50	49	7 G.A.		16'-0"
	AR7 BL6	C — H	7	c	0	48	6"		16'-0"
	AR8 BL7	S_2 — H	7	c	0	49	DBL 1 GA		16'-0"
	AR9 BL8	S_{29} — H	7	a	300	26	DBL 7 GA		11'-6"
	AR10 BL9	S_{29} — H	7	a	450	9	DBL. 1 GA		9'-3"
XL2	AL1	CC — H	7	a	450	57	15"		21'-6"
	AL2 BR1	C — H	7	b	150	48	6"		16'-0'
	AL3 BR2	S_2 — H	7	b	150	48	DBL. 1 GA		16'-0"
	AL4 BR3	C — X	12 x 7	a	300	72 x 44	16" x 10"		26'-8" x 16'-0"
CR1A M2 YR1	AL5 BR4 CR1	C — H	7	a	150	48	6"		16'-0"
	AL6 BR5	C — T	12 x 7	a	150	80 x 48	8" x 6"		26'-8" x 16'-0"
	AL7 BR6	S_2 — H	7	a	150	49	DBL. 1 GA		16'-0"
	AL8 BR7	S_1 — H	7	a	150	49	7 G.A.		16'-0"
	AL9 BR8	C — H	7	a	300	26	10"		13'-0"
	AL10 BR9	S_2 — H	7	a	300	26	DBL. 3/8"		11'-6"
	AL11 BR10	C — H	7	a	450	12	15"		11'-6"
	AL12 BR11	S_2 — H	7	a	450	9	HONEYCOMB		9'-3"
	AL13 BR12	C — H	4	a	150	28	3-1/2"		9'-3"
	AL14 BR13	S_1 — H	4	a	150	29	3 G.A.		9'-3"
	AL15 BR14	S_1 — H	3	a	150	21	8 G A		7'-3"
	AL4A BR3A	C — V	7	b	150	48	6"		16'-0"
	AL4B BR3B	CAPSULE		a	150	48	6"		16'-0"
	AL6A BR5A	C — V	7	a	150	48	6"		16'-0"
	CR2	U — H	16						16'-0"
DL1 DL2 CR3 CR4 CR5 CR6		RB — H	16						16'-0"
	AR11 BL10 CR7	CS — H	7					12"C 1"S/RB	9'-3"

Fig. 1.1

2. MATHEMATICAL MODELING OF TUNNELS IN JOINTED ROCK

2.1 GENERAL - FINITE ELEMENT METHOD

The finite element method was used to construct mathematical models of selected cross sections in C and D drifts. The methods used were described in the two previous reports[5]. Several modifications and additions were introduced in the course of this investigation, to allow for incremental loading of large systems of rock blocks and joints under plane strain conditions with large displacements. The computer program used in the analyses is included in Appendix 1 together with explanatory notes on its operation.

The results of computations can be no better than the quality of the input data: These are: the structural geology of the cross sections; the properties of the rocks; and the properties of the joints.

2.2 GEOLOGICAL DATA

The general geology of the Piledriver drifts is well known from geological logs of the walls and roof of the drifts prepared by Corps of Engineers geologists, J. Zeltinger and Harold Jack. Fig. 2.1 presents, for example, the logs for DL 1 and 2. These logs provide the information for preparation of detailed cross sections showing the outlines of joint bounded blocks around the tunnel. Fig. 2.2 shows how these detailed sections are prepared by projection and extrapolation. Thus, cross sections of the drifts can be constructed as in Fig. 2.3.

The detailed geologic sections present data on the distribution of joints and defects and the shape of rock blocks behind the tunnel walls. From these data, a finite element computing mesh can be compiled. In the subsequent analysis, obviously the shapes of the blocks delimited by the network of discontinuities is very important. The confidence with which this is known is greatest closest to the wall of the tunnel where the extrapolation of geological data required is minimum, fortunately, this is the most important

---

[5] op. cit., p. 1

region for the analysis. Unfortunately, joints which parallel the tunnel axis behind the wall may not be seen in the tunnel and the only way they can be placed on the cross sections is by regularly repeating joints of the same orientation that do intersect the tunnel. However, a slight inaccuracy in the placement of a single joint will lead to fictitious slivers and wedges of rock which may tend to fail by bending and crushing as the joint blocks move; thus, it is important to define the correct cross section as accurately as possible. Use of a bore hole stratascope, camera, or television device would add a new dimension of precision to the development of geologic cross sections and, therefore, is very strongly recommended for studies of this type.

The accuracy of the geologic projections can be checked in transition sections where tunnels go from one size to another, in end sections where a drift terminates and in sharp bends where drifts are passing through joints previously seen around the bend. The quality of projection in the example given for DL 1 and 2 is presented in Fig. 2.4, where the projected end section can be compared with the actually logged section. The general trends are correct but there is much inaccuracy in the configurations of individual blocks. The primary difference is the offsetting of the D joints by the A shears, a factor not considered in making these projections. Greater precision is achieved close to the walls than in the center of the end plate or far behind the walls.

2.3 ROCK PROPERTIES

The properties of the Piledriver rock, previously described[6], were determined by the Missouri River Division Laboratory by direct pull tension, and unconfined and triaxial compression tests. The intact rock specimens acted as brittle, linear elastic solids at confining pressures as high as 3000 psi. The tensile strength was 1450 psi and the average unconfined compressive strength was 30,500 psi. The modulus of elasticity was 11.0 to 12.0 $\times 10^6$ psi in compression and 8.0 $\times 10^6$ psi in tension.

---

[6]Technical Report Number 2 (op. cit., p. 1)

The criterion of failure adopted for previous work based on the test data was adapted from the Griffith and Modified Griffith theories of failure. This is a two dimensional approach in which the intermediate principal stress is ignored. A new approach is introduced herein where the three principal stresses are all considered by using a power law in terms of octahedral stresses.

(1) Power Law Failure Criterion

The criterion of failure of rocks may be expressed in terms of three principal stresses, or invariants formed from them. In a three axis principal stress space, the criterion of failure would delimit a closed solid surface within which the coordinates of any point define a stable combination of principal stresses. In detail, it is not known what the shape of the failure surface is for the various classes of rocks. However, all rocks have a relatively small tensile strength and show an increase in compressive strength with confining pressure at a rate which decreases with higher confinements. Jaeger[7] has suggested that the failure surface for rocks may be a solid of revolution about the line making equal angles with the stress axes (the hydrostatic axis). He suggested a paraboloid of revolution obtained by rotating the Griffith Parabola about the hydrostatic axis. Any solid of revolution about the hydrostatic axis can be expressed as a curve in a plane defined by octahedral shearing stress (τ_{oct}) as ordinate and octahedral normal stress (σ_{oct}) as abscissa; these quantities are expressible in terms of principal stresses as follows:

$$\tau_{oct} = \frac{1}{3}\sqrt{(\sigma_1 - \sigma_2)^2 + (\sigma_2 - \sigma_3)^2 + (\sigma_3 - \sigma_1)^2} \qquad (2\text{-}1)$$

and

$$\sigma_{oct} = \frac{1}{3}(\sigma_1 + \sigma_2 + \sigma_3) \qquad (2\text{-}2)$$

Rather than constraining the failure law to conform to a specific curve, e.g. parabaloid or cone, a more general power law relation between τ_{oct} and σ_{oct} has been adopted, i.e.

---

[7]Proceedings 8th Symposium on Rock Mechanics, AIME, 1966, p. 3-57.

$$\tau_{oct} = N + D\,\sigma_{oct}^{B} \qquad (2\text{-}3)$$

This is simply an empirical criterion of failure conforming to the constraint that it represent a solid of revolution about the hydrostatic axis in principal stress space. To apply this criterion, Eq. 2-3 shall also be written in logarithmic form, as follows:

$$\log_{10}(\tau_{oct} - N) = A + B \log_{10} \sigma_{oct} \qquad (2\text{-}4)$$

$$(\sigma_{oct} > 0)$$

where A has been written in place of $\log_{10} D$. D, B, and N are strength constants of the material. The dimensionless constant B describes the curvature of the failure surface. D and N, whose values depend on the system of units employed, describe something like the friction and cohesion. N is the value of the octahedral shear stress when the octahedral normal stress is 0. It could be determined directly from a pure shear test on a plate of rock ($\sigma_1 = -\sigma_3$; $\sigma_2 = 0$), or from a torsion test of a solid cylinder of rock. N can be estimated as the intercept on the τ_{oct} axis of the failure curve, plotted from test data in the $\sigma_{oct} - \tau_{oct}$ plane. Another method of estimating N would be to calculate N from a formula derived for the special case of Mohr-Coulomb theory.

A three-dimensional generalization of the Mohr-Coulomb theory is represented by Eq. 2-3 if B is equal to 1. From triaxial test data, one may calculate a Mohr-envelope and determine the constants ϕ (the angle of internal friction), and c (the shear strength intercept or cohesion). τ_{oct} and σ_{oct} may also be calculated from triaxial compression test results, as follows (compare with Eqs. 2-1, 2-2)

$$\tau_{oct} = \frac{\sqrt{2}}{3}(\sigma_{1_f} - p) \qquad (2\text{-}5)$$

$$\sigma_{oct} = \frac{\sigma_{1_f} + 2p}{3} \qquad (2\text{-}6)$$

where p equals the confining pressure and σ_{1_f} = the axial pressure at the time of failure. Substituting these expressions in Eq. 2-3 yields the expression

$$\frac{\sqrt{2}}{3}(\sigma_{1_f} - p) = N + D\left[\frac{\sigma_{1_f} + 2p}{3}\right]^B \tag{2-7}$$

For the case where B = 1, Eq. 2-7 simplifies to

$$\sigma_{1_f} = \frac{3N}{\sqrt{2} - D} + \frac{2D + \sqrt{2}}{\sqrt{2} - D} p \tag{2-8}$$

The analogous formula for the Mohr-Coulomb theory is:

$$\sigma_{1_f} = 2\,c\,\tan\alpha + \tan^2\alpha\, p \tag{2-9}$$

where $\alpha = (45 + \phi/2)$.

By comparing Eqs. 2-8 and 2-9, one may write the two identities:

$$\frac{3N}{\sqrt{2} - D} = 2\,c\,\tan\alpha \tag{2-10}$$

$$\frac{2D + \sqrt{2}}{\sqrt{2} - D} = \tan^2\alpha \tag{2-11}$$

which may be solved for N to yield

$$N = 2\sqrt{2}\;c\;\frac{\tan(45 + \phi/2)}{2 + \tan^2(45 + \phi/2)} \tag{2-12}$$

Eq. 2-12 may be used to gain an estimate of N in order to determine the constants A and B from actual failure data. One may also solve Eqs. 2-10 and 2-11 for D to yield:

$$D = \frac{\sqrt{2}\,[\tan^2(45 + \phi/2) - 1]}{2 + \tan^2(45 + \phi/2)} \tag{2-13}$$

Eq. 2-13, together with Eq. 2-12, provides values for the strength constants D and N, with B = 1, representing an extension of the Mohr-Coulomb theory to three dimensions by rotation about the hydrostatic axis to form a cone.

However, it would be more sensible to determine the best values of the strength constants by empirical means.

The procedures for determining the values of D, B, and N to fit actual test data are as follows:

1. Convert the breaking stresses, in laboratory or field strength tests, to octahedral normal and shear stresses using Eqs. 2-1 and 2-2. In the triaxial compression test, for example, with confining pressure p and axial stress at failure σ_{1_f}, ($\sigma_1 = \sigma_{1_f}$ and $\sigma_2 = \sigma_3 = p$)

$$\sigma_{oct} = \frac{(\sigma_{1_f} - p)}{3} + p \qquad (2\text{-}14)$$

and

$$\tau_{oct} = \frac{\sqrt{2}}{3}(\sigma_{1_f} - p) \qquad (2\text{-}15)$$

while in the uniaxial tension test, with tensile strength = $-\sigma_t$,

$$\sigma_{oct} = -\frac{\sigma_t}{3} \qquad (2\text{-}16)$$

and

$$\tau_{oct} = \frac{\sqrt{2}}{3}\sigma_t \qquad (2\text{-}17)$$

2. Determine N. It may be computed from Eq. 2-12 (ϕ and c must be determined first), or, if data exist in the region of low octahedral normal stresses, e.g. tension or torsion or simple shear test, it may be determined graphically by plotting the values of σ_{oct} and τ_{oct} at failure on arithmetic graph paper and sketching a smooth curve to find the value of τ_{oct} when $\sigma_{oct} = 0$. If data are available only from confined and unconfined compression tests, the latter method will not be sufficiently accurate.

3. Determine D and B by plotting the data to log-log scale. The ordinate is $\log_{10}(\tau_{oct} - N)$ and the abscissa is $\log_{10}(\sigma_{oct})$. The best fit straight line yields the constants A and B (Eq. 2-4); then, $D = \log^{-1}A$.

In employing the graphical procedure above, one must be careful to avoid prejudicing the data because of scatter in repeated unconfined compression or tension tests. The octahedral stresses calculated from any set of unconfined compression tests must lie along the straight line $\tau_{oct} = \sqrt{2}\,\sigma_{oct}$. Similarly, scattered data from repeated uniaxial tension tests be along the line $\tau_{oct} = -\sqrt{2}\,\sigma_{oct}$. To avoid prejudicing the data, for results of unconfined compression or tension tests, only one point, the one corresponding to the average strength, should be converted to octahedral stresses and graphed.

Figs. 2.5 and 2.6 show strength data plotted in this way for Piledriver rock. In Fig. 2.5, the arithmetic plot of τ_{oct} versus σ_{oct} based on compression tests is curved slightly downward. The uniaxial tension strength of -1450 psi yields the point τ_{oct} = +685 psi, σ_{oct} = -484 psi. The interpolated value of N is 1300 psi. Eq. 2-12, with $\phi = 56°$ and c = 3600 psi, gives N = 2,540 psi. In Fig. 2-6, $\log_{10}(\tau_{oct} - N)$ is plotted against $\log_{10}(\sigma_{oct})$ for both values of N and for N = 0. The set of points corresponding to N = 1300 psi provide the least scatter about a straight line fit. The rock strength constants for the three cases are as follows:

(1)	(2)	(3)
N = 0	N = 1300 psi	N = 2450 psi
D = 6.60	D = 2.95	D = 1.14
B = 0.88	B = 0.91	B = 1.00

The second case was adopted as the failure law for the Piledriver rock, i.e.

$$\tau_{oct} = 1300 + 2.95\,\sigma_{oct}^{0.91} \qquad (2\text{-}18)$$

For a parabaloid (Griffith theory in three dimensions), B = 0.5, while B = 1.0 for a cone (a generalization of Modified Griffith and Mohr-Coulomb theories). Franklin[8] reviewed data from many triaxial tests and found that most data fall between the modified Griffith and Griffith theories, meaning that the failure surface curves downward slightly as confining pressure is increased, but in general, not so much as predicted by the Griffith

---

[8]Franklin, J. A., A Strength Criterion for Rock, Imperial College Rock Mechanics Research Project Number 6, 1968.

theory. The Piledriver quartz monzonite strength data fall within the observed range.

(2) Failure Law When σ_{oct} Is Negative

When the octahedral normal stress becomes tensile, mathematical difficulty is experienced in working with Eq. 2-3. Hoek[9] suggested that the controlling strength parameter is simply the uniaxial tension test in this region, i.e. the rock breaks when the minor principal stress is less than the uniaxial tensile strength. This criterion has been adopted herein. Another possibility would be to adopt the maximum extension strain criterion advanced by Trollope[10] in which the greatest extension strain, in any combined stress state, is unsafe if it exceeds the strain at failure in a uniaxial tension test. It would be a simple matter to introduce this criterion in the computations.

The properties adopted for the rock are summarized in Table 2.1.

2.4 JOINT PROPERTIES

(1) Importance of Joints

Much has been written in recent years about the significance of planes of weakness on the stability of structures and excavations in hard rock. It is quite possible that a person reviewing the recent publications and reports in the field of rock mechanics might become wearied by all of these references to fractures, discontinuities, faults and their impact, he might feel that the problem has been overstated. Nothing could be farther from the truth. In an excavation in hard rock, such as the granitic rock of the Piledriver Drift, if joints and defects of the rock mass are not considered, it is very hard to demonstrate why a drift should fail, even if it is unlined. Post-shock evaluation of the test sections at intermediate range

---

[9]Hoek, E., Rock Fracture Under Static Stress Conditions, CSIR Report MEG 383, October 1965.

[10]Duncan, J. M. and Goodman, R. E., Methods of Analysis for Rock Slopes, U. S. Army Engineers, Waterways Experiment Station, 1968, p. 45.

reveals conclusively that the relative movement of joint-bounded blocks was the most important single criterion in causing damage to lined and unlined sections.

To demonstrate the importance of joints in a tunnel in hard rock, the computer methods used herein were applied to the study of a circular tunnel section in homogeneous hard rock with the properties of the Piledriver quartz monzonite. (These properties are listed in Table 2.1.) Fig. 2.7 shows the finite element mesh (PD-5) used for this analysis. A static pressure was applied horizontally in increments of 4000 psi, reaching a peak pressure of 32,000 psi. Simultaneously, vertical compression of 0.43 × the blast pressure was applied to represent the confinement in the wave front. With these boundary conditions, there is no tension developed, theoretically, at any point around the opening, but very significant compressive stresses developed in the tangential direction at the roof and floor. No element in the finite element mesh experienced failure at any stage in the incremental loading process, even when 32,000 psi had been reached. Unquestionably, the wall rock at the top and bottom of the opening would have broken. However, the surface layer of finite elements cannot represent the stresses on the surface but rather at the element centers, which for this mesh were approximately 1/32 of a radius behind the wall. Even though this is a short distance behind the wall, the stress gradient is so steep that the stresses had already reached tolerable values and no failure was predicted by the failure criterion adopted.

In order to examine a situation with more severe loading conditions a second case was investigated where the ratio of free field pressures was 0.25, i.e. the vertical pressure was 25% of the blast pressure. This would correspond to a value of Poisson's ratio of 0.2 and is more drastic than the actual wave motion believed to have been experienced in the Piledriver Drifts. At this confining ratio, some tension develops in the 0° and 180° walls. The progress of failure with increasing increments of applied pressure is plotted in Fig. 2.8. With the first increment, 4,000 psi blast pressure, no elements had failed; at 8,000 psi, two elements had failed in the tensile region (Fig. 2.8a). The volume of rock which was actually disturbed by this very significant stress is not great and it is quite possible that had there been a rock bolt reinforcement or steel lining, nothing very

severe in the way of change would have occurred in the tunnel. By the time pressure of 32,000 psi had been reached, damage had extended to only five elements, encompassing only those elements near the horizontal diameter adjacent to or just behind the wall (Fig. 2.8c). No elements are shown as failed at 90° (roof) as the stresses at element centers were tolerable, even at p_1 = 32,000 psi.

While the type of failure pattern described above may be relevant to the case of an unreinforced hole of small diameter for the installation of telephone conduit, it has very little to do with the case of lined or bolted 16 foot diameter opening in rock. The localized crushing and slabbing of rock which was observed underground in some of the drifts must represent the stress concentration effect of geological weakness planes on the intervening blocks. In order to make an analysis of this factor, it is necessary to gain samples of the weakness planes, to test them, to determine their strength and stiffness, and to construct a finite element mesh. The subject of sampling and testing natural joint surfaces is not well known in the United States but has been advanced in the last two years to a significant level of achievement in Western Europe. The following discussion relates to some of the findings of these investigations.

(2) Methods of Sampling Joints

In order to determine the mechanical properties of natural joint surfaces, it is necessary to produce samples of significant size in the laboratory for shear testing. In some cases, the natural joint surfaces are so regular, smooth and planar, that the creation of artificial joints by sawing of otherwise intact cores provides realistic specimens for analysis. Another method is by breaking beams in the field or in the laboratory and testing the artificial shear or extension features as developed. One may also sample joints by selecting blocks in an outcrop which are mated, carefully sculpting and removing them and fitting them into a laboratory shear machine. It is also possible to drill across joints in the field, either normal to the joints, parallel to the joints, or at a pre-set angle to the joints. Finally, it is possible to remove blocks containing joints by drilling, trepanning or even wire sawing in the field. All of these methods will be discussed.

Artificial Joints. A large number of friction tests have been conducted in laboratories by sawing intact cores of rock. The two pieces may then be mounted in a direct shear box by setting in Portland cement or epoxy resin, or fitted inside a triaxial device. In the latter case, the diamond saw cut must be at about 45-60° to the ends of the core. Tests of this type were conducted by the Corps of Engineers in the Missouri River Div. Laboratory. They will be discussed in the next section. It is doubtful that an unmodified diamond saw cut is a very good model of a natural joint surface. Joints owe their origin to breakage of rock under extension or shear. Extensional joints are characteristically rough. While shear features are smooth, they invariably contain a filling of gouge, clay, or crushed rock. A diamond saw specimen can model a natural joint if a gouge-like layer is developed on the diamond cut surface. Research in this area is being pursued at the University of Illinois by Mr. J. Coulson under the direction of Professor Donald Deere. Diamond saw specimens are polished to specified smoothness and then sheared at high normal pressure. This produces slickensides and crushed material on the joint surface which resembles slickensided surfaces sometimes seen on naturally occurring shear joints. The repeated cycles of loading of such specimens are then reasonable models of the actual in situ mechanical characteristics of the joint surface. Fig. 2.9 shows a typical specimen of an artificial joint in the University of Illinois test series.

Dr. M. DeFreitas and Dr. John Knill in the Department of Geology at Imperial College, London, have been studying the shear behavior of artificially induced extension joints in granite. Rock blocks containing joints are brought to the laboratory from the quarry where they have been produced in hard rock by impact of simple beams. The matching rock pieces are laid on the laboratory table and a mold for the shear box is accurately positioned (Fig. 2.10a). The joint specimen is cemented into the mold with epoxy cement and then the mold is removed and the specimen is placed in the direct shear machine for testing. The joints produced and tested in this manner are typically rough extension joints, with a waviness of several centimeters (Fig. 2.10b). Dr. DeFreitas has been studying the effect of joint roughness on the shear characteristics and in fact has been measuring the shape of the

surface with a wheel and stylus. Joints produced in this way may be very realistic models of actually occurring joints of extension origin.

Artificial joints may also be produced in the testing machine by incipient shear failure of intact specimens. Both triaxial and direct shear specimens can be used. Dr. Jaeger, at Australian National University, has experimented along these lines.

Field Sampling of Open Joints. Very often, joint surfaces of interest in the field are loose or open so that one block rests on another with perfect fit but without any cohesion. In this case, it is possible, with a geology pick or crowbar, to remove blocks containing joints. It may not be necessary to hold the upper and lower blocks together for shipment, but only to mark their relative positions so that they may be replaced in proper orientation in the laboratory. Professor Krsmanovich in Sarajevo, Yugoslavia, has sampled a large number of joints in limestone by this method. The samples are, of course, disturbed in the sense that any original closing of aperture tangentially or normally which may occur during the actual loading in the field cannot be reproduced in the laboratory specimen.

Drilling Joint Samples. It is possible to obtain a relatively undisturbed sample of a joint by drilling through it with a core barrel. There are three methods of doing this -- normal drilling, parallel drilling, and inclined drilling. The firm Coyne and Bellier, in Paris, France, has obtained samples at several dam sites by drilling perpendicular to joint planes, so that the joint occupies a position parallel to the ends of the core; after trimming in the laboratory and plotting in Portland cement, the circular cross-sectioned joint surface is tested in a direct shear machine. Samples from two inches diameter to as much as nine inches in diameter have been obtained in this manner by Coyne and Bellier (Fig. 2.11). It is possible that drilling across the joint by a rotary drill will seriously disturb the joint surface as one block turns on the other. In fact, it might be impossible to sample very weak joints or open joints by this technique.

A modification of the perpendicular drilling technique is being investigated by Goodman and Mahtab at present in a project at the University of California, Berkeley. In this method, a small hole is first drilled across the joint and a rock anchor is installed and tightened; then the small hole

is over-cored so that the sample is obtained without relative movement between the two blocks. This has worked satisfactorily in the laboratory on cores of sandstone but has not yet been tried in the field.

Coyne and Bellier, the Portugese National Civil Engineering Laboratory and the mining group at Imperial College have drilled samples parallel to the plane of joint features so that the joint specimen occupies a diametral plane of a core sample. Fig. 2.12 shows such specimens after a test; these NX size (2-1/8") specimens were encased in Portland cement. Coyne and Bellier have also drilled larger specimens (Fig. 2.13a). Dr. David Pentz, at Imperial College, England, has also obtained samples by this technique. In this work, he used a nine horsepower diamond drill to obtain cores nine inches in diameter. The cores were drilled without a core spring; when the full depth of drilling had been reached, the diamond bit was removed and a core spring and dummy bit were installed. Then the sample was pulled by the core spring, jacking the drill against the collar, to produce a tension break at the end. The core containing the joint specimen could then be removed from the hole.

After removal, the joint is bound so that it will not be disturbed in transit and paraffined (Fig. 2.13b) or otherwise protected so that the natural moisture content will be preserved. On return to the laboratory, the core is fitted in the shear box by imbedment in either concrete, as Coyne and Bellier have done, or in epoxy resin, as Imperial College has done. Samples obtained this way can be very large, up to 1600 square centimeters. A surprisingly large number of samples have been obtained by Coyne and Bellier and Imperial College (Fig. 2.14).

It is also possible to drill specimens for triaxial joint tests by orienting the drill at 45-60° to a naturally occurring joint. A triaxial test with a naturally occurring joint at this controlled orientation is called a multi-stage triaxial. Tests of this type were performed by the Missouri River Division of the Corps of Engineers on Piledriver rock. Such tests were also performed on limestone by Heuze and Goodman[11]. Professor Jaeger in Australia has conducted many tests of this type.

---

[11]Heuze, F. and Goodman, R. E., Mechanical Properties and In Situ Behavior of the Chino Limestone, Crestmore Mine, Proceedings 9th Symposium on Rock Mechanics, AIME, 1968.

Removal of Blocks Containing Joints. It is possible to remove large chunk samples of rock relatively undisturbed and thus obtain large numbers of samples in the laboratory. One method of obtaining such samples is by drilling overlapping holes with a drilling template to create a series of slots. The U. S. Bureau of Reclamation took several large chunk samples from the Grand Coulee Third Power House by this technique. The firm Coyne and Bellier has introduced a wire sawing technique to speed up and reduce the cost of sampling large blocks. Their technique consists of drilling the corners of the eventual block by conventional drill holes; the wire sawing apparatus consists of two rods with pulleys on the end which are fitted into the drill holes (Fig. 2.15). The wire runs between the pulleys which are fixed into two corner holes of the eventual block and fed out of the drill holes to the continuation of the wire loop. In principle, four slots could be cut in this fashion to outline the four walls of the block; but, in practice, several of the sides were trepanned. Then the bottom of the block is freed by sawing with an ingeniously contrived loop in the wire. Eurenius and Fagerström, of the Swedish firm Vattenbyggnadsbyrån, have taken a large number of block samples at a Syrian dam site in a soft rock by cutting with a power saw. Direct shear specimens were performed in the laboratory by normal drilling of the seams contained within the block samples. Other methods of cutting blocks which may prove eventually to have application for taking block samples are electron beam cutting, laser cutting, and possibly hydrogen arc cutting.

(3) Methods of Testing Joints

Triaxial Test with Oriented Joint -- Multi-stage Triaxial. As stated above, it is possible to conduct a triaxial test with an oriented joint so that the eventual failure is by the mode of slipping along the pre-selected surface. The specimen is first failed under some initial confining pressure, followed by step-wise increase of confinement and sliding by increasing axial pressure. This yields a value for the joint angle of friction. This test may be reasonable in stiff joints where there is no filling or compressible rock zone between the walls of the joint. A finite element analysis of triaxial specimens containing inclined joints more compressible than the surrounding rock was performed as a collateral experiment in the course of the

previous contracts. The results indicated very uneven stress distributions along the joint and totally different concentrations of stress in the upper and lower walls of the joint. Thus, the multi-stage triaxial is probably not a good test for seams or joints of shear origin.

Laboratory Direct Shear Tests. The direct shear test is a pertinent method of test for evaluating the relative sliding tendency of joint blocks in an excavation or foundation. However, it is not a simple matter to produce a reasonably uniform stress distribution inside a direct shear box. If joints were perfectly smooth, it would be possible to align the joint inside a direct shear chamber and displace the top half relative to the bottom with forces almost colinear. Ideally, these forces would be shears along the top and bottom blocks and the blocks would be very thin. However, since the top and bottom blocks must have some thickness in order for the specimen of rock to be sufficiently stiff, it is not practical to force the top over the bottom by shears along the top and bottom surfaces. Therefore, it is customary to push or pull the top relative to the bottom by applied forces and reactions transmitted from the sides of the block. These forces introduce overturning moments into the shear box which must produce contrary moments in reaction from the top and bottom of the shear box, causing non-uniform distribution of normal pressure along the sliding surface. One possible result is indicated in Fig. 2.17. If the joint surface is rough, furthermore, it is necessary to provide a sufficient gap between the top and bottom supporting blocks to allow for the full amplitude of the irregularity of the joint surface. This introduces a further overturning moment and a tendency for non-uniform stress distribution in the shear box. There are further moments in the vertical plane, introduced by hinging around high points of rock along the sliding surfaces.

Another problem of direct shear tests concerns the lateral boundary conditions. In evaluating the strength of rock joints for purposes of slope stability analysis, it is reasonable to conclude that the prototype blocks will be in a condition of plane strain, i.e. that no side displacements will be permitted. In order to achieve this boundary condition in a direct shear machine, only one direction of displacement is permitted. This is the Casagrande boundary condition designed into the Casagrande direct shear machines, distributed in soil mechanics laboratories around the world. With irregular

joint surfaces there is the possibility of rotational tendencies in a horizontal plane because of rotary moments on high points along the joint surface. Thus, the upper or lower block tends to swing into the sides. In the plane strain type of shear box, this is impossible because of the lateral confinement offered by the sides. However, the resulting distribution of side pressures is very irregular and is not known; therefore, the test results may be quite unreal. Another approach to this problem is to omit the sides of the shear box altogether. The problem of achieving a uniform stress distribution in a direct shear box is difficult. A through study by modern analytical methods is needed. Shear strength characteristics determined in direct shear tests depend on the boundary conditions achieved. Unfortunately, there is no uniformity in the construction of machines in use around the world and it is possible that the results of one worker will not agree with the results of another even though identical specimens are tested.

The most impressive and elaborate direct shear machine in the world was developed by Dr. David Pentz and colleagues at the Royal School of Mines at Imperial College, London, England (Fig. 2.16). In this machine, the horizontal force required to maintain the displacement in a single direction is controllable and can be measured. The shear box takes samples up to nine inches in width. Elaborate controls of pressure and rate of displacement have been incorporated in its design. Unfortunately, it is so recent a development that relatively few samples have been tested as of this date.

Casagrande type shear boxes, designed for soil mechanics use, have been adapted for joint samples in many laboratories around the world. In addition, plane strain shear boxes of much larger size and load capacity have been constructed for work on rock specimens. The most important of these machines is the one used by Coyne and Bellier in Paris and developed by the S.E.I.L.* (Fig. 2.18). It takes samples of dimensions 0.3 meters by 0.5 meters or less. It is desirable, in a direct shear machine, that the normal load follow the position of the center of the test surface which is in contact at any time. In the Coyne and Bellier machine, this is achieved by providing hinges that allow the normal pressure ram to displace with the relative displacement across

---

*S.E.I.L. = Société d'Equipment Industriel et de Laboratoir

the joint. Movement of the axis of normal load with the moving block can be allowed by employing dead weights or hangars. The large direct shear machine employed at Imperial College by DeFreitas and Knill (Fig. 2.19), and the fine direct shear machine employed at the University of Illinois by Deere and Coulson (Fig. 2.20), are of the plane strain type and use dead weight loading.

Professor Krsmanovic in Yugoslavia constructed a large machine without sides (Fig. 2.21a). Specimens for this machine have the dimensions 40 × 40 × 20 centimeters, giving a shear surface of about 1600 square centimeters; the maximum normal stress is about 40 kilograms per square centimeter and the maximum shear stress is 80 kilograms per square centimeter on these large areas. The Krsmanovic device is designed in such a way that the applied shear force is inclined about 4° relative to the surface of shearing. Inclination of the applied force is one way of overcoming some of the difficulties with rotary moments described above. However, a large inclination of the applied force causes normal stresses to vary appreciably with the shear stress applied. This makes it very difficult to test specimens under low normal stress. The Krsmanovic device uses jacks on both sides and ball bearings both above and below the shear blocks so that the center of the surface which is in contact at any time does not move during the test (Fig. 2.21b). Therefore, it is possible to use a fixed loading frame to apply the normal pressures.

In Situ Direct Shear Tests. It is possible to perform direct shear tests in the field. These tests are accomplished by selective excavation to form a block on a natural surface of weakness. The surface does not need to be horizontal.

There is no standard method of performing this test*. The block is invariably confined in a reinforced concrete or a composite steel concrete frame. The shear load is usually slightly inclined. The normal load is sometimes provided only by the block's own weight.

Blocks on inclined surfaces are under shear stress before the test begins. To extend the elastic information of the test, the block may be pushed up the hill, through zero.

---

*Standards for in situ shear tests are being considered at present by ASTM.

Few tests of this type have been performed, in hard rocks, in the United States, owing to the expense in labor required. Many such block shear tests have been conducted by European organizations, but relatively few on natural joint surfaces. Several examples are shown in Figs. 2.22, 2.23 and 2.24.

(4) Results of Shear Tests

Results of a large number of laboratory direct shear tests and several in situ block shear tests have been summarized in Tables 2.2 and 2.3. These data were gathered mostly from unpublished reports generously made available by the organizations concerned.

The load-deformation curves for these tests have been represented by values for shear stress and displacement at the peak and residual points. In some cases, a yield point was reported as well in the early part of the curves. Though the possible combinations of values for these quantities are numerous, several generalizations can be made about the characteristics of the results for different types of weakness surfaces. The load deformation curves were classified into four types as drawn in Fig. 2.25 and summarized in Table 2 4.

Type 1 stress deformation curves rise very steeply to peak stress at very low deformations and then quickly fall to a residual value which may be one third or less of the peak. Healed joints, and incipient fractures belong to this class.

Type 2 curves also develop the peak stress at very low deformations but do not fall so sharply to the residual, further, the peak strength is only slightly above the residual. Artificial joints formed by diamond saw cutting rock specimens belong to this class. Polished surfaces, type 2a, show less rate of decay of strength after the peak than do unpolished saw cuts (2b). The shear stiffness is higher than natural joints, but is still low enough in number (ca. 10^4 kg/cm^3) to contribute significant deformation beyond that of the intact rock if the joints are repeated at intervals of several feet in a hard rock such as quartz monzonite.

Type 3 curves show lower stiffness and numerous secondary peaks. Second peaks may be as large as the primary. These curves result when testing clean,

rough joints, such as extension joints in granite. The irregularities in the load-deformation curve result from overriding of successive asperities. Undisturbed samples of such joints may show an initial concavity as tangential aperture is closed (type 3b).

In classes 1-3, it mattered little whether the surfaces were dry or soaked with water. In type 4 curves, on the other hand, the behavior is modified grossly by change in the water content. These curves are typical of sheared zones, clay filled joints, and shale partings. At low moisture contents (4a), the curves show high stiffness and great differences between peak and residual displacements, although generally not as severe as with the healed joints (type 1). When wet, the stiffness is greatly reduced. Thin zones (4b), when wet, show "strain hardening" behavior with ultimate strength considerably greater than the point of maximum curvature (denoted "peak"). Thick seams have elastic-plastic stress deformation curves when wet (4c). All of the in situ tests (Table 2.3) yielded type 4 curves, probably because these expensive tests are reserved for the worst discontinuities.

It is difficult to increase the water content of sheared zones and clay seams to desired values. The field moisture content can be retained by careful sealing in the field. To increase the moisture content beyond this value, soaking is necessary. Soaking the specimens without surcharge may lead to excessive moisture contents -- well beyond those expectable in the field. Since the permeability becomes low under normal pressure, soaking under surcharge tends to wet the edges more than the center. Coyne and Bellier have tried introducing water into drill holes parallel and also perpendicular to the seam, with moderate success.

Typical values for the peak displacements, tangential stiffness, and ratio of peak to residual stresses are given for all types of surfaces in Table 2.4. It is emphasized that these are only typical values; considerable deviation exists in all these quantities. Both the peak displacement and shear stiffness tend to increase with increasing normal stress. When variation in normal pressure is ignored, the deviation of peak displacements is, however, far less than the deviation of stiffness. In fact, if no test were possible, as a rough estimate of initial shear stiffness, one could calculate the strength from the friction angle (which is usually between 30° and 40°) and divide it by the peak displacement value selected from Table 2.3.

One of the most interesting conclusions from the test results reported in Table 2.2 is the large displacement required to reach residual strength values -- frequently several centimeters.

Data on displacements normal to the shear plane were not presented in Tables 2.2 and 2.3. In all laboratory tests where normal displacements were given, shearing displacement was accompanied by dilations (thickening of the joint zone). The peak dilation occurs well after the peak stress at low normal pressures, but occurs right at the peak shear stress in tests run under high normal pressure. Several of the in situ block shear tests showed slight closing of the joint in the early part of the shear-displacement curve; however, dilation always occurred eventually.

2.5 APPLICATION TO PILEDRIVER - DL DRIFT

The methods described in this section were used to model the cross section of DL Drift at station 0 + 70. This section is at the intersection of DL 1 and DL 2. The drift was 16 feet in diameter, containing pre-tensioned rock bolts on a regular pattern, with one bolt per 3.25 square feet of the wall. There are two layers of chain link fabric held by the bolts.

Originally, it was planned to make a number of models at many different cross sections. However, the model became so complex that it demanded a great deal of time. An effort was made to reduce the complexity of each geologic cross section; however, results of study with the DL drift section showed that more, rather than less, complexity would be required to achieve meaningful results. Further refinement would, unfortunately, call for knowledge of the detailed geologic and material properties exceeding that which was known before the test. The purpose of the analysis presented here is to judge our capacity to perform a meaningful quantitative analysis of an actual geological cross section.

The finite element mesh prepared for DL drift is presented, without nodal point and element numbers, in Fig. 2.26a. This is the most complex finite element mesh known to the author. Its 900 nodal points, 667 total elements, and 398 joint elements completely filled the core storage on the IBM 7094 computer available at the time it was prepared. However, the new CDC 6400 computer with extended core storage recently installed at the University of California allows a five-fold increase in the problem size

and a significant enlargement of the allowable bandwidth. Debugging the mesh was made possible by using a plotter to draw the element boundaries as punched on the input cards. (Fig. 2.26 is, in fact, the machine plotted mesh.)

Results of two cases, the parameters of which are summarized in Table 2.5, will be described. In case 1, the joints were assigned very stiff, strong properties, as if they are only incipiently developed, or are healed. In case 2, the joint strength was reduced and the deformability assigned to joint and rock elements after failure was very great. In a third case, the different sets of weakness surfaces were treated differentially; the shears (A joints) were assigned the weakest and most deformable properties and the mineralized B joints were assigned the stiff, strong properties of incipient joints. The results from study of case 3 did not contrast strongly with case 2, and therefore are not presented here.

The failure criterion adopted for the rock in case 2 was more severe than for prototype Piledriver rock as N was taken equal to zero. The actual rock being slightly stronger than this, the extent of rock breakage indicated from computations is somewhat too great.

The results for cases 1 and 2 are presented in Figs. 2.27 and 2.28. The displacements are plotted, to scale, around the walls of the tunnel and at selected points behind the wall. The blast side is to the left in these figures. Elements that have failed are indicated by "R" if they are rock elements and by "J" if they are solid elements. Double lines indicate opening of joints.

(1) Case 1 -- Results

In Fig. 2.27a, displacements are plotted to the scale of the drawing after the second 5000 psi load increment and the failed elements are shown after the total pressure reached 5000 and 10,000 psi. In Fig. 2.27b, displacements and failed rock elements are shown after 15,000 psi (third increment), the failed joints were not shown owing to a mistake which disturbed the printing of joint stresses after the third increment.

The results plotted in Fig. 2.27 show that the elements tended to fail along the steep A joints above and below the tunnel. This joint system is roughly perpendicular to the blast front. A large failed zone

was localized in the tunnel roof above the lee side. Rock blocks in this zone were in tension resulting from eccentric loading as the blocks shifted along joints. Little additional damage was done after the first increment of the blast (9 additional failed elements in the second increment as compared to 32 in the first). The opening of joints and the relative displacement of adjacent nodal points is shown after 15,000 psi on Fig. 2.27b. The whole blast side moved into the opening almost uniformly.

(2) Case 2 -- Results

In Fig. 2.28, a much more drastic but generally similar behavior pattern is shown for case 2. Here the properties of the rock and joints were weaker both before and after failure. The displacements after 10,000 psi were so large that the mesh could not be used for additional increments. Failures were plotted after the first increment of pressure (2500 psi) and the displacements were plotted after the second increment with cumulative pressure equal to 5000 psi. On the blast side of the tunnel, the wall moved in 1.5 feet, while on the lee wall, the movements were negligible. Very small displacements resulted from the first 2500 psi increment but there were numerous failed elements, the great deformability assigned to failed elements for the second increment led to the very large displacements plotted. Joint openings occurred in the lower part of the blast side while blocks slid along flat joints in the roof.

(3) Comparison with Actual Damage

The deformed shape of the tunnel and location of broken rock zones indicated by these analyses can be compared with the actually observed failure pattern shown in Fig. 2.29. The analysis predicts large inward movements of the whole wall, with little rock breakage, on the blast side. The analysis also indicates extensive localized crushing of rock above the roof on the lee side. This, in general, is what occurred.

(4) Conclusion

The computing mesh was far too small, and the geological information was far too imprecise to allow more refined studies of these sections. The indication from the study is, however, that given sufficiently accurate

geological and materials property data, analysis can now predict behavior of tunnels in jointed rock. Further comments are made on the ramifications of this conclusion in Section 4 of the report.

Table 2.1

SUMMARY OF ROCK PROPERTIES

(Compression Positive)

DEFORMABILITY

Modulus of elasticity in compression	11.0×10^6 psi
Modulus of elasticity in compression	8.0×10^6 psi
Poisson's ratio	0.3

STRENGTH

Triaxial Data

$\phi = 56°$

$c = 3600$ psi

Tensile Strength

$-\sigma_t = -1450$ psi

Adopted Equation of Failure Surface (psi units*)

1. $\sigma_{oct} > 0$

   fails when $\tau_{oct} = 1300 + 2.95(\sigma_{oct})^{0.91}$

   $N = 1300$ psi
   $D = 2.95$
   $B = 0.91$

2. $\sigma_{oct} < 0$

   fails when $\sigma_{min} < -1450$ psi

---

*To convert to psf units, multiply N by 144 and solve:

$$D_{psf} = \log^{-1} [\log D_{psi} + (1 - B) \log 144]$$

In psf units:

$N = 1.87 \times 10^5$
$D = 5.04$
$B = 0.91$

TABLE 2.2 RESULTS OF LABORATORY DIRECT SHEAR TESTS ON ROCK SPECIMENS WITH JOINTS

Test Designation	Laboratory and Person in Charge	Description of Specimens	Thickness of Seam (cm)	Cross-section Area (cm^2)	Normal Stress at Start of Test (kg/cm^2)	Tangential Stress (kg/cm^2)			Tangential Displacement (cm)			Shear Stiffness (hundreds of kg/cm^3)		Peak Stress / Residual Stress	Curve Type
						Yield	Peak	Residual	Yield	Peak	Residual	Yield	Peak		
10-14.6 Run 3	U. of Illinois - Coulson and Deere	Dry Berea sandstone-sawed joint, lapped #80		82.0	2.63		1.21			0.0004			30.4		2a
6-14.7 Run 7	" "	Dry limestone-sawed joint, lapped #80		82.0	106.0	48.0	89.0		a	0.10	0.5	a	8.90		2a
Q72	U.C., Berkeley - Mahtab and Goodman	Dry Boise sandstone-rough saw cut		5.0	24.8		19.8	19.8		0.015	>0.5		13.2	1 00	2b
Blockingstone #6	Imperial College - DeFreitas	Dry granite-rough joint from breaking beam		200.0	12.0	23.0	26.9	12.6	0.151	0.265	1.53	1.51	1.01	2.13	3a
7	"	"		172.0	14.5	22.8	22.8		0.178	0.178		1.28	1.28		3a
2	"	"		205.0	14.5	42.5	42.5		0.307	0.307		1.38	1.38		3a
8	"	"		192.0	14.5	48.8	48.8		0 330	0.330		1.48	1 48		3a
4	"	"		144.0	14.5	29.6	29.6		0.186	0.186		1.60	1 60		3a
Dolgado #2	Imperial College - Peats	Dry slate-natural cleavage surface		ca. 300	44.6	28.0	35.0	16.8	0.31*	0.43*	3.2	0.90	0.81	2.07	3b
1	"	Dry porphyry-natural joint surface		" "	51.4	45.5	45.5	37.5	0 46*	0.46*	2.0	0.98	0.98	1.22	3a
3	"	"		" "	81.6	62.0*	67.0	50.0	0.37*	0.49*	3.2	1.67	1.36	1.34	3b
4	"	"		" "	63.0		62.0	56 0		0.63*	4.0		0.99	1.11	3b
5	"	"		" "	103.0		134.5	72.0		0.70*	3.0		1.98	1.86	3b
6	"	"		" "	33.0		34.5	22.0		1.27*	4.4		0.27	1.64	3b
7	"	"		" "	53.0		106.0	36.0		1.33*	5.9		0 78	2.95	3b
8	"	"		" "	67.0		70.3	52.0		0.59*	4.0		1.18	1.35	3b
9	"	"		" "	86.0		77.5	55.0		0.84*	3.9		0.94	1.41	3b
10	"	"		" "	102.0		59.2			0.72*			0.85		
B-1 3	Sarajevo - Kremanovic	Limestone - thin shale seams along bedding		ca. 1500	12.5	7.2	10.2+	15.8	0.095	0.12+	1.8	14.2	8.5	0.66+	4b
5	"	"		" "	28.5	9.5	18.8+	>25.0	0.06	0.56+	2.0	1.58	0 33	0.75+	4b
15	"	"		" "	24.8	7.4	12.8+	16.3	0.03	0.24+	1.5	2.45	0.53	0.78+	4b
12	"	Limestone - mylonite along bedding		" "	21 5	8.2	18.3	12.8	0.01	0.15	>2.0	8.2	1.2	1.43	4a
16	"	"		" "	18.3	16.2	21.0	19 5	0.055	0 38	1.5	2.95	0.55	1.08	4a
21	"	"		" "	24.2	13.6	19.05	16.0	0.02	0.60	1 7	6.8	0 32	1.19	4a
23	"	"		" "	13.3	14.2	14.23	11.0	0.025	0.025	>2.0	5.69	5.7	1.29	4a
26	"	"		" "	8.0	3.2	12.0	9.0	0.03	0.42	1.8	1.06	0.29	1.33	4a
28	"	"		" "	11.8	11.8	15.2	11.6	0.06	0.27	1.8	1.97	0.56	1 31	4a
35	"	"		" "	2.14	1.2	4.44	3.6	0.01	0.15	1.9	1.2	0.29	1.23	4a
B-2 6	Sarajevo - Kremanovic	Limestone - slightly rough bedding		ca. 1500	6.0	14.4	16.8	9.6	0.06	0.12	>2.4	2.4	1.4	1.75	3a
10	"	"		" "	30.5	14.8	37.5	18.0	0.04	0.73	>2.5	4.2	0.51	2.08	3a
13	"	"		" "	11.4	21.5	24.4	14.0	0.10	0.22	>2.4	2.15	1.10	1.74	3a
14	"	"		" "	19.5	27.6	29.6	17.4	0.11	0.22	>2.4	2.50	1 36	1.69	3a
19	"	"		" "	25.75	25.0	32.0	22.2	0.12	0.40	2.4	2.08	0.80	1.44	3a
20	"	"		" "	37.0	32.0	34.5	23.8	0.15	0.47	>2.4	2.14	0.73	1.45	3a
27	"	"		" "	13.4	22.0	23.1	16.6	0.14	0 21	>2.4	1.60	1.10	1.39	3a
32	"	"		" "	1.57	2.0	6.8	4.3	0.01	0 12	2.5	2.0	0 55	1.58	3a
34	"	"		" "	2.09	3.4	6.55	5.2	0.04	0 32	2.3	0.85	0.20	1.26	3a
B-3 1	Sarajevo - Kremanovic	Limestone - rough bedding surfaces		1600	16.6	33.4	36.5	27.5	0.14	0.17	1.8	2.38	2.14	1.33	3a
2	"	"		"	31.5	38.0	42.5	34.0	0.025	0.12	1.8	15.2	3.50	1.23	3a
4	"	"		"	20.0	35.0	38.4	29.0	0.05	0 17	1.8	7.0	2.26	1.32	3a
7	"	"		"	32.7	39.0	41.2	31.4	0.16	0.22	1.5	3.9	1.86	1.31	3a
8	"	"		"	6.8	14.2	20.7	9.1	0.02	0.07	1.8	7.1	2.97	2.28	3a
17	"	"		"	28.0	43.9	43.9	29.8	0.10	0.10	1.8	4.39	4.39	1.47	3a
25	"	"		"	34.3	28.8	41.1	33.2	0.04	0.42	1.8	7.2	0.98	1.34	3a
29	"	"		"	12.65	27.2	27.2	14.3	0.05	0.05	1.8	5.44	5.4	1.90	3a
31	"	"		"	12.25	29.9	29.9	13.8	0.04	0.04	1.8	7.5	7.5	2.17	3a
35	"	"		"	3.05	6.2	6.8	2.7	0.18	0.26	1.7	0.34	0.25	2.52	3a
D-1 14	Sarajevo - Kremanovic	Limestone - smooth unfilled fractures		1600	9.0	6.25	6.6	6.0	0.25	0.23	2.0	0.42	0.28	1.10	4c
16	"	"		"	12.8	6.25	6.5	11.7	0.026	0.051	>2.5	2.4	1.3	0.56	4b
15	"	"		"	15.4	11.5	11.5	11.0	0.26	0.20	2.0	0.44	0.44	1.04	4c
17	"	"		"	24.5	12.5	15.8	14.2	0.10	0.83	>2.5	1.25	0.29	1.18	4c
13	"	"		"	23.9	17.9	23.0	23.0	0.19	0.64	>2.5	0.94	0.36	1.00	4c
D-2 2	Sarajevo - Kremanovic	Limestone - rough unfilled fractures		1600	15.5	30 0	32.0	17.8	0.125	0.230	>2.7	2.4	1.28	1.80	3a
1	"	"		"	24.9	33.0	36.6	24.9	0.025	0.14	>2.7	13.2	2.61	1.53	3a
5	"	"		"	37.3	30.0	38 8	30.3	0.062	0.25	2.7	4.84	1.55	1.28	3a
12	"	"		"	40.8	33.8	42.6	36.5	0.025	0.16	>2.5	14.1	2.66	1.17	3a

[a] Insufficient detail

*Initial displacement occurred as indicated. Peak and yield displacements given are referred to zero after initial displacement had occurred.

+In curves of type 4b top of first segment of stress-deformation curve is listed as "peak", even though later stresses are higher.

TABLE 2.2 RESULTS OF LABORATORY DIRECT SHEAR TESTS ON ROCK SPECIMENS WITH JOINTS

Test Designation	Laboratory and Person in Charge	Description of Specimens	Thickness of Seams (cm)	Cross-section Area (cm^2)	Normal Stress at Start of Test (kg/cm^2)	Tangential Stress (kg/cm^2)			Tangential Displacement (cm)			Shear Stiffness (hundreds of kg/cm^3)		Peak Stress / Residual Stress	Curve Type
						Yield	Peak	Residual	Yield	Peak	Residual	Yield	Peak		
La Rouviere 1965 1	Coyne et Bellier	Marl layers in limestone; saturated	0.1-0.3	680	5.0		6.3	3.2[b]		0.02	5.6		3.1	1.97	1
2	"	"	"	706	4.8		6 5	4.0		0.02	5.2		3.2	1.62	1
3	"	"	"	730	5.0		6.1	3.4		0.03	5.4		2.0	1.79	1
4	"	"	"	605	5.6		8.4	3 6		0.04	5.0		2.1	2.33	1
5	"	"c	"	720	5 0		5.5	3.2		0.03	5.0		1.8	1.72	4a
6	"	"	"	715	5.05	2.7	9.1	3.5	0.01	0.06	>5.4	2.7	1.5	2.60	1
7	"	"	"	730	5.0	3.8	5.2	4.6	0.01	0.10	5.2	3.8	0.52	1.13	4c
8	"	"	"	730	5.55		6.1	3.9		0.02	>5.1		3.0	1.56	1
9	"	"c	"	650	5 7	4.4	4.5	3.9	0.02	0 06	5.1	2.2	0.75	1.15	4a
10	"	"c	"	730	4.95		4.25	3.2		0.02	5.2		2.1	1.33	4c
13	"	"	"	715	5.0		7.7	3.7		0.02	>5.1		3.8	2.08	1
La Rouviere 1964 3	Coyne et Bellier (older d.s. machine)	Marly partings in limestone, saturated	1.5-2.0	62	6.1		13.0	4.35		0.025	0.73		5.2	2.99	1
5	"	" "	1.0	57	7.85		19.7	6.2		0.09	0.82		2.2	3.18	1
6	"	" "	0.3-0.4	62	4.45		4.8	3.2		0.05	0 82		0.96	1.50	1
13	"	dry	5.0	59	3.2		19.8	3.6		0.075	0.83		2.64	5.50	1
15	"	saturated	0.2	51	5.55	6.9	8.3	4.7	0.02	0.04	0.72	3.4	2.08	1 77	1
18	"	"	5.0	63	2.4		2.6	1.6		0.03	0.86		0.87	1.62	1
19	"	"	0.2	58	3.1	14.6	16.5	2.6	0.065	0.115	0.85		1.43	6.35	1
21	"	"	0.1	56	6.75		12.5	4.0		0.03	0.63		4.17	3.13	1
24	"	"	0.1	60	6.35		13.5	5.1		0.025	0.73		5.4	2.65	1
26	"	"	0.1	55	6.85		6.6	3.6		0.06	0.79		1.1	1.83	1
27	"	"	0.3	51	5.85		13.6	3.9		0.03	0.75		4.5	3.49	1
28	"	"	1.0		3.6	8.9	10.0	2.35	0.04	0.06	0.63	2.2	1.7	4 25	1
28b	"	"	0.2	58	6.6	8.0	18.3	5.0		0.055	0.83		3.3	3.66	1
29	"	"	0.2		3.2		8.5	2.6		0.015	0.82		5.7	3.27	1
Malpasset MIII6 A1	Coyne et Bellier (older d.s. machine)	Foliated gneiss and mylonite sample taken in field from sliding plane on left abutment - sheets taken	4.0-5.0	19..	5.0	15.2	23.2	6.9	0.10	0.22	0.99	1.52	1.06	3.37	3a
C2	"	"	"	24.5	4.0		15.2	2.9		0.10	0.83		1.52	5.28	3a
D1	"	"	"	23.0	10.0		12.2	5.75		0.095	0.83		1.29	2.12	3a
D2	"	"	"	18.1	20.0		37.0	17.9		0.17	0.93		2.17	2.07	3a
E1	"	"	"	14.0	30.0		45.5	36.4		0.16	>0.38		2.84	1.25	3a
F1	"	"	"	13.7	20.0		34.4	23.7		0.10	>0.90		3.44	1.45	3a
F2	"	"	"	10.6	10.0		28.7	21.0		0.11	0.79		2.7	1.37	3a
G1	"	"	"	17.2	25.0		36.6	36.6		0.135	0.65		2.71	1.00	3a
H1	"	"	"	22.0	5.0	8.95	13.7	8.8	0.06	0.195	0.99	1.49	0.70	1.55	3a
I1	"	"	"	15.8	15.0		57.5	13.1		0.165	0.74		3.48	4.39	3a
I2	"	"	"	15.3	7.0		25.0	18.5		0.14	0.30		1.8	1.35	3a
I3	"	"	"	14.5	10.0		35.5	13.3		0.125	>0.70		2.84	2.66	3a
I4	"	"	"	14.0	5.0		17.3	5.6		0.09	0.31		1.93	3.11	3a
I5	"	"	"	14.4	30.0		56.5	26.9		0.15	>0.95		3.76	2.10	3a
I6	"	"	"	15.0	30.0	52.0	64.0	32.0	0.11	0.245	>0.79	4.8	2.61	2.00	3a
J1	"	"	"	16.2	15.0		31.8	11.5		0.13	>0.84		2.44	2.76	3a
K1	"	"	"	14.8	10.0		24.0	8.05		0.07	0.92		3.42	2.98	3a
Vouglans Dam 1	Coyne et Bellier	Limestone with marly joints; dry	0.1	35.0	5.0		11.4	4.5		0.02	0.82		5.7	2.54	1
2	"	"	0.05	47.0	5.0		14.0	5.1		0.01	0.83		14.0	2.70	1
3	"	"	0.05	41.5	5.0		17.0	4.55		0.05	0.80		3.4	3.72	1
4	"	"	0.025	37.5	5.0		11.4	7.0		0.05	0.83		2.3	1.6	1
5	"	"	0.2	39.0	9.0		15.8	8.4		0.02	0.82		7.9	1.88	1
6	"	"	0.2	35.0	10.0		29.8	8.3		0.04	0.80		4.9	2.0	1
7	"	"	0.05-2.0	40.0	10.0		24.0	10.1		0.01	0.9		24.0	2.4	1
8	"	"	0.05	36.4	10.0		34.0	12.8		0.03	0.9		11.3	2.65	1
9	"	"	0.025	33.5	15.0		18.4	15.4		0.03	0.9		6.1	1 2	
10	"	"	0.15	28.0	15.0		31.0	12.7		0.06	0.9		5.2	2.4	1
11	"	"	0.05	31.8	15.0		21.0	11.3		0.02	0.9		10.5	1.88	
12	"	"	0.1	34.3	15.0		24.0	10.0		0.01	0.55		24.0	2.4	1
Vouglans Dam 13	Coyne et Bellier	Limestone with marly joints; saturated	0.1	35.2	5.0		5.6	4.15		0.05	0.8		1.1	1.35	4c
14	"	"	0.1	36.4	5.0		9.2	3.7		0.01	0.86		9.2	2.4	4a
15	"	"	0.2	40.0	5.0		5.95	4.0		0.02	0.84		3.0	1.5	4a
16	"	"	0.2	35.7	5.0	3.0	5.0	3.6	0.02	0.35	0.83	1.5	0.14	1.35	4b
17	"	"	0.1	31.7	9.65		7.5	5.9		0.05	0.84		1.5	1.3	4c
18	"	"	0.025	31.8	10.0		37.2	11.5		0.01	0.73		32.2	2.8	1
19	"	"	0.05	28.6	10.0		17.6	13.4		0.05	0.80		3.5	1.35	4a
20	"	"	0.1	38.5	10.0		9.15	7.6		0.05	0.83		1.8	1.22	4c
21	"	"	0.025	32.4	15.0		34.4	12.5		0.05	0.9		6.9	2.76	4a
22	"	"	0.1	30.2	15.0		24.2	15.3		0.05	0.83		4.9	1.6	4a
23	"	"	0.05	26.0	15.0		17.7	9.5		0.03	0.73		5.9	1.8	3a
24	"	"	0.05	24.0	15.0		20.6	13.0		0.01	0.73		20.6	1.6	4a

[b] Residual stress measured in bars instead of kg/cm^2 for La Rouviere test series.

[c] Joint opened in transport

TABLE 2.2 RESULTS OF LABORATORY DIRECT SHEAR TESTS ON ROCK SPECIMENS WITH JOINTS

Test Designation	Laboratory and Person in Charge	Description of Specimens	Thickness of Seam (cm)	Cross-section Area (cm^2)	Normal Stress at Start of Test (kg/cm^2)	Tangential Stress (kg/cm^2)			Tangential Displacement (cm)			Shear Stiffness (hundreds of kg/cm^3)		Peak Stress / Residual Stress	Curve Type
						Yield	Peak	Residual	Yield	Peak	Residual	Yield	Peak		
Vouglans Dam 1	Coyne et Bellier	Limestone, compact (oolitic)		575	5.0	12.5	27.4	5.4	0.02	0.16	3.0	6.2	1.71	5.08	4a
2	"	Limestone, stylolite (oolitic)		575	5.0		27.4	5.3		0.13	>3.0		2.1	5.17	4a
3	"	" " "		575	5.0		28.4	4.9		0.06	>3.0		4.7	5.8	4a
Vouglans Dam 314-3	Coyne et Bellier	Moist marly joint in limestone	2	1090	5.4	4.7	6.3	3.4	0.04	0.15	>6.0	1.2	0.42	1.85	4a
311-3	"	"	2.3	1000	5.45		4.9	3.6		0.02	>6.0		2.4	1.36	4a
305-2	"	"	2.3	1180	8.8	6.8	9.6	5.2	0.02	0.10	>6.0	3.4	0.96	1.84	4a
306-2	"	"	2.0	1235	9.7	6.6	8.0	5.5	0.02	0.04	>5.0	3.3	2.0	1.45	4a
308-2	"	"	2.7	1050	9.9	6.5	8.8	5.9	0.02	0.06	>3.0	3.2	1.5	1.49	4a
308-1	"	"	2.5	1225	10.3	7.0	10.0	5.7	0.03	0.10	>6.0	2.3	1.0	1.75	4a
306-1	"	"	3.0	1175	19.0		9.7	9.7		0.02	>4.8		4.8	1.36	4a
309-1	"	"	1.5	1200	20.0		13.2	10.3		0.08	>6.0		1.6	1.27	4a
310-0	"	"	2.0	1065	20.4		15.3	11.1		0.06	>6.0		2.5	1.38	4a
310-1	"	"	2.2	1200	29.3		19.7	16.5		0.12	>5.0		1.9	1.20	4a
310-5	"	"	2.7	1225	30.0		18.6	15.2		0.12	>2.5		1.5	1.22	4a
312-1	"	"	2.5	1243	30.5		17.7	12.8		0.14	>6.0		1.26	1.38	4a
305-1	"	"	2.3	980	30.5		20.4	14.5		0.34	>6.0		0.6	1.40	4a
Vouglans Dam 308-4	Coyne et Bellier	Marly joint[d]	2.7	1032	20.0		5.0	8.7		0.14	>5.8		0.35	0.58	4b
310-3	"	"	1.3	1240	20.0		4.0	7.7		0.04	>6.0		1.0	0.52	4b
310-4	"	"			20.0		4.0	8.3		0.04	>6.0		1.0	0.49	4b
310-6	"	"	2.2	1126	30.0	5.5	6.9	13.45	0.02	0.3	5	2.8		0.71	4b
312-3	"	Marly joint[e]	2.0	1080	5.0		1.0	2.65		0.02	>5.9		0.5	0.38	4b
311-4	"	Marly joint[f]	1.9	1210			8.45	7.25		0.05	>6.0		1.9	1.17	4a
311-1		Marly joint[g]	3.2	1030	5.0	1.0	1.40	2.25	0.11	0.55	>5.8	0.09	0.023	0.62	4b

[d]Saturated by immersion

[e]Saturated by three holes perpendicular to joint without load

[f]Saturated by three holes perpendicular to joint under normal load

[g]Saturated by a hole parallel to joint

TABLE 2.3 SUMMARY OF RESULTS FROM IN SITU BLOCK SHEAR TESTS ON WEAKNESS PLANES

Test Designation	Location and Organization Performing Test	Description of Rock Conditions	Thickness of Seam	Cross-Section Area	Normal Stress at Start	Normal Stiffness (hundreds of kg/cm³)	Tangential Stress (kg/cm²)		Tangential Displacement (cm)		Shear Stiffness at Peak (hundreds of kg/cm³)	Peak Stress / Residual Stress	Curve Type
							Peak	Residual	Peak	Residual			
C - 2	Dalesice Dam, Czechoslovakia, I.C.M.P. - Brozd	Schistocity plane in amphibolite		5,000	1.25		9.0		0.15		0.60		
1 P	Krivoklat, I.C.M.P. - Brozd	Bedding plane in greywacke	0.5-0.8	2,265	12.6		2.5	7.6	0.11	1.26	0.23	0.33	4b
2 P	"	"	>0.1	3,510	10.3		7.4	12.8	0.06	1.00	1.23	0.58	4b
3 P	"	"	closed, clean	3,460	4.4		23.0	>28.0	0.10	>0.2	2.3		*
K 1	Kurobe IV Dam; Müller and John	Vertical fault	thick, uneven		3.8		4.0		0.23		0.17		4c
K 1	"	"	"		10.9		10.5		0.45		0.23		4c
	Vouglans Dam (E.D.F.), Coyne et Bellier	Marly sand filled joint	0.1-0.2	44,000	10.0	2.9	3.0	> 4.2	0.03	>0.3	2.38		4b
	Jupia Dam, Brazil, I.P.T. - Ruiz and Camargo	Unbonded contact between basalt and sandstone		107,900	1.28		1.0		0.09		0.11		*
SLL 1	Khajuri Kach, Pakistan, Jaroslav Cerni Institute, Yugoslavia - Kujundzic	Closely jointed shale zone in limestone, 47° dip	0.2-0.5	50,000	0.21	Initial Stress 0.25	0.60	0.27	0.30	3.0	0.02	2.20	4a-4c
SLL 2	"	"	"	50,000	0.21	0.20	0.57	0.32	0.25	4.2	0.02	1.78	4c
SLL 3	"	"	"	50 000	0.20	0.28	0.36	0.28	0.3	0.24	0.01	1.28	4c
SLS 2	Khajuri Kach, Pakistan, Jaroslav Cerni Institite, Yugoslavia - Kijundsic	Shale interbed, wet, 44° dip	0.2-0.5	50,000	0.27	>0.20[a]	0.40		0.35		0.01		4c
SLS 3	"	"	"	50,000	0.30	0.32	0.52	< 0.36	0.50	>4.2	0.02	>1.44	4a-4c

[a]Pushed block uphill - thus initial stress is negative relative to direction of test loads.

Table 2.4

TYPICAL LOAD DEFORMATION RELATIONS
FOR DIFFERENT TYPES OF SEAMS AND FRACTURES

Class	Type of Surfaces Typically Exhibiting Behavior in This Class	Peak Displacement (cm)	Tangential Stiffness [10^2(kg/cm^3)]	Peak Strength ÷ Residual Strength
1	Healed joints and incipient joints	0.03	6.0	3.0
2	Clean, smooth fractures			
	2a polished	< 0.01	6.0	1.1
	2b unpolished, e.g. rough saw cut	0.02	1.3	1.2
3	Clean, rough fractures			
	3a artificial extension fractures and disturbed samples	0.20	1.3	1.75
	3b undisturbed samples	0.80	1.0	1.75
4	Filled joints, sheared zones, shale partings, and smooth bedding			
	4a dry or slightly moist	0.12	2.2	1.5
	4b wet; thin seam	0.26	1.5	0.6
	4c wet; thick seam	0.30	0.8	1.0

Table 2.5

ROCK AND JOINT PROPERTIES USED
IN STUDY OF SECTION AT 0 + 70 IN DL DRIFT

	Case 1		Case 2	
	Before Failure	After Failure	Before Failure	After Failure
Rock Deformability				
E in compression (psi)	11.0×10^6	11.0×10^5	11.0×10^6	0.01
E in tension (psi)	8.0×10^6	8.0×10^3	8.0×10^6	0.01
ν (Poisson's ratio)	0.3	0.4	0.3	0.4
Rock Strength Parameters*				
N psi	1300		0	
D (corresponding to psi)	2.95		6.60	
B	0.91		0.88	
Tensile Strength (psi)	1450			
Joint Deformability		**		**
Normal stiffness psi/in	2.9×10^4	2.9×10^4	2.9×10^4	2.9×10^4
Shear stiffness psi/in	2.9×10^5	2.9×10^4	2.9×10^4	0.6×10^{-3}
Maximum closure (inches)	0.12		0.12	
Joint Strength				
Cohesion psi	2,780		100	
Friction	56°		31°	

*See Section 2.4

**Stiffnesses both set to zero if fails in tension (opens)

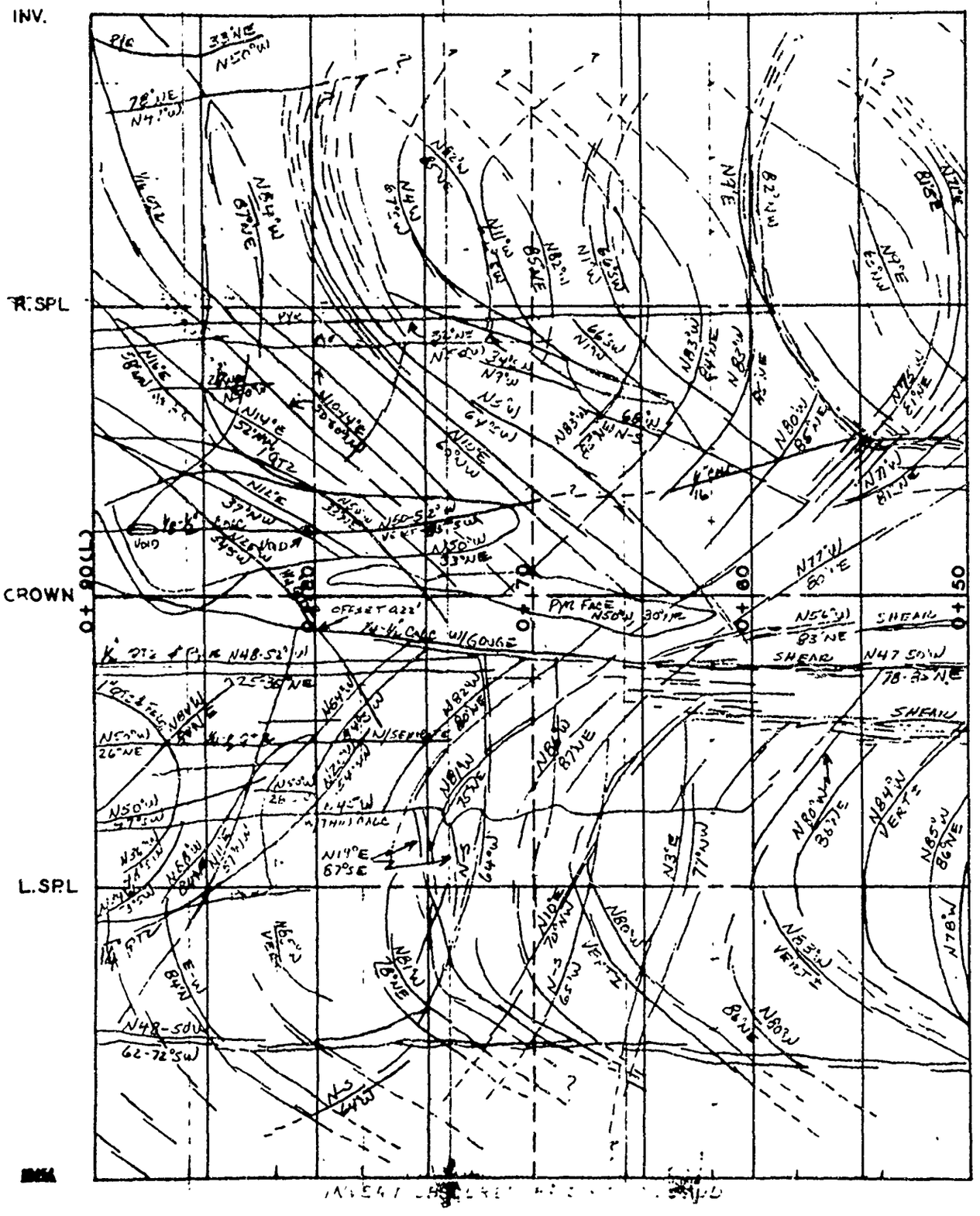

FIGURE 2.1

PRE-SHOT GEOLOGIC LOG

EXPLANATION OF FIGURE 2.2

Method of Projecting Geological Data from Geological Log of Tunnel to Draw Cross Sections

---

1. The strike in relation to the tunnel can be found by three different methods:
   a. Revolve spring line in geological log to tunnel diameter and measure strike a'b';
   b. Measure tangent to curve at the crown;
   c. Use measured strike in the field.

2. Project the intersection of the strike at the crown(s) to sections desired. For example, joint is at crown level at t and r respectively in sections A and B.

3. Project the strike of the joint at spring line level to the sections desired; in the example, joint is at spring line elevation at points n and ℓ respectively in sections A and B.

4. Line $\overset{\frown}{tn}$ is the trace of the plane on section A. Line $\overset{\frown}{rl}$ is the trace of the plane on section B.
   Note: Points x and y show where the joint plane intersects the tunnel boundary in section B. It does not intersect the boundary in section A.

5. Find dip (δ) from distance $\overset{\frown}{sm}$. $\delta = \tan^{-1} \frac{\text{tunnel radius}}{\overset{\frown}{sm}}$, or use dip measured in the field.

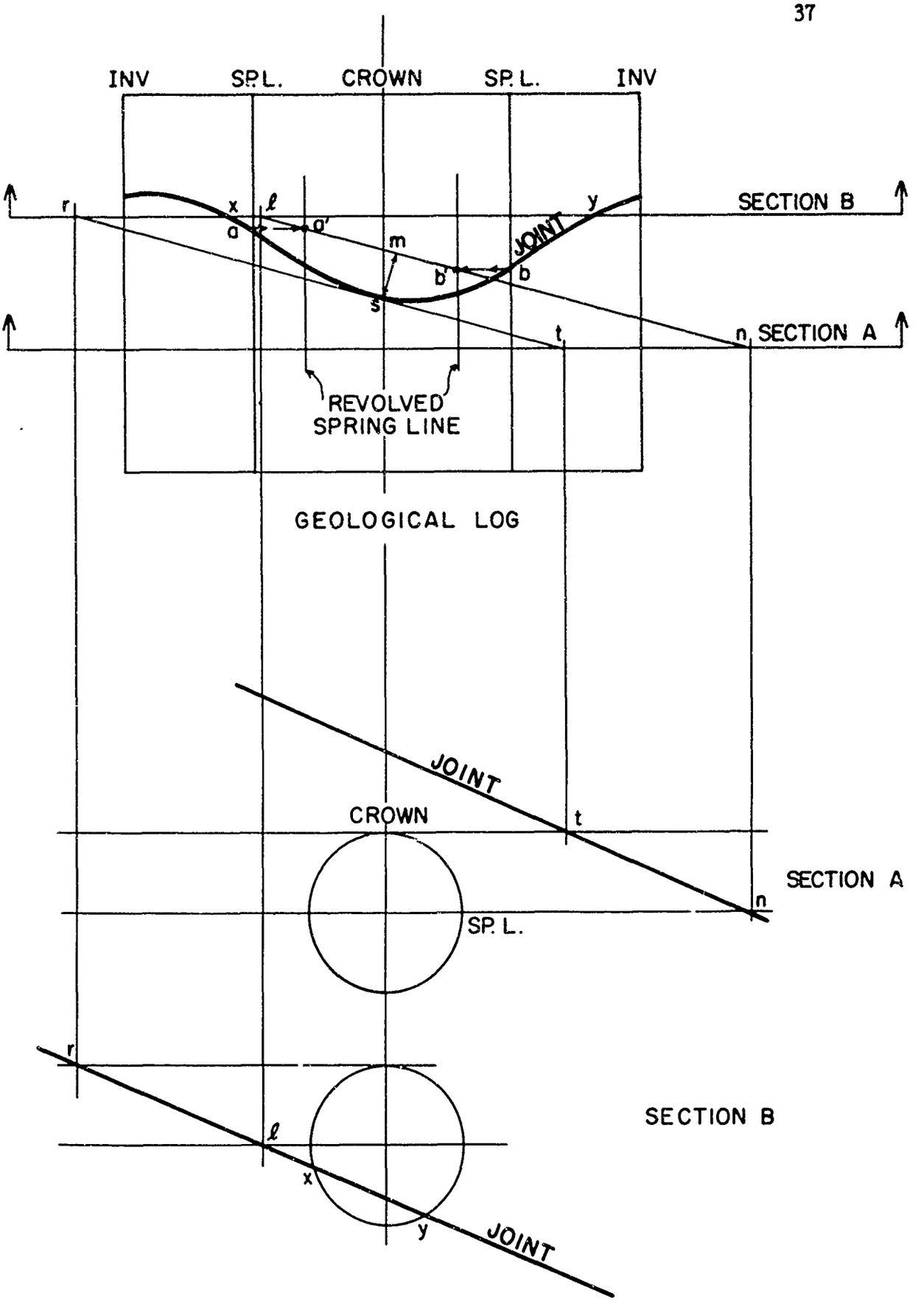

FIGURE 2.2 METHOD OF PROJECTING GEOLOGICAL DATA

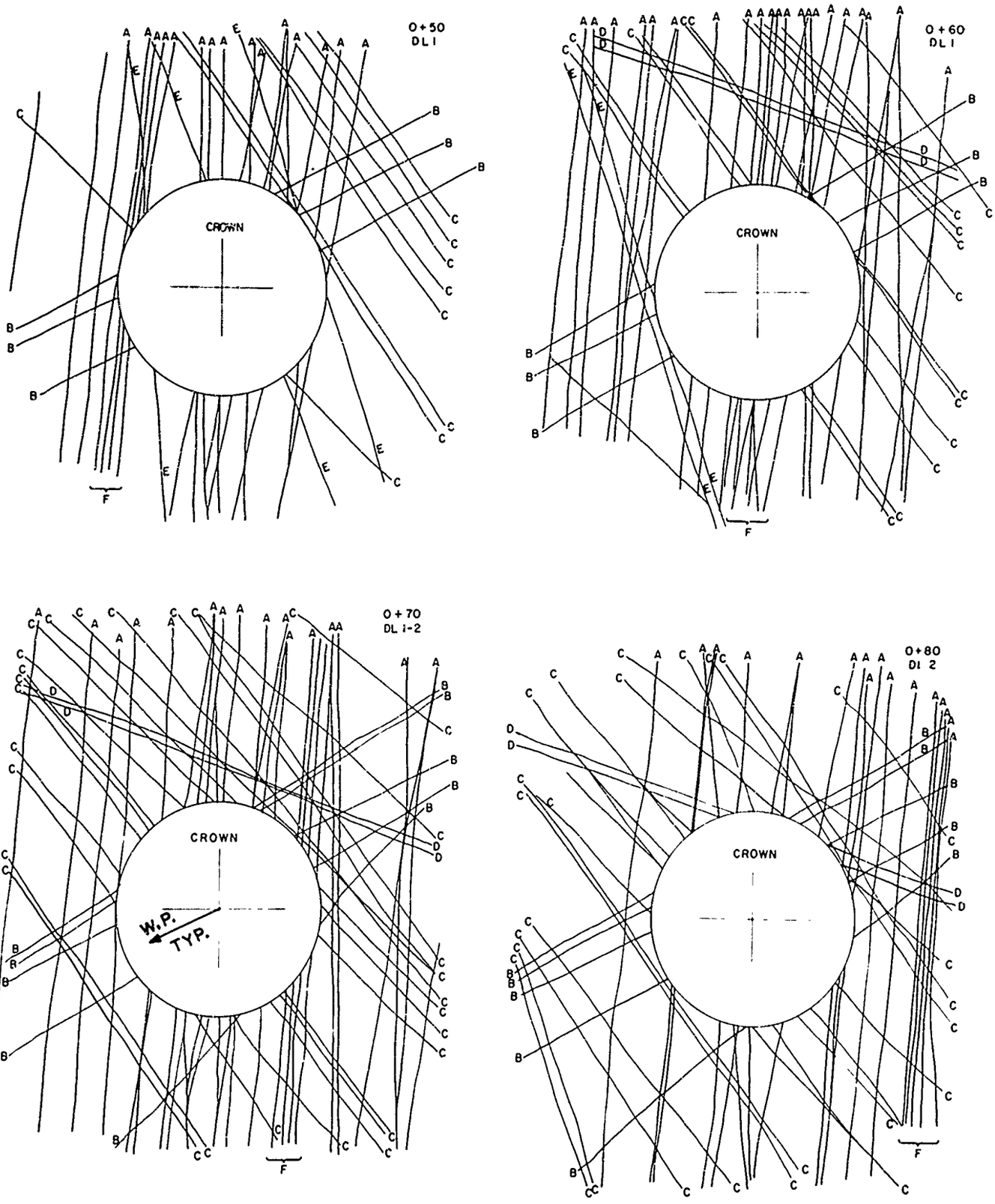

FIGURE 2.3 GEOLOGIC CROSS SECTIONS
DRIFT DL 1-2

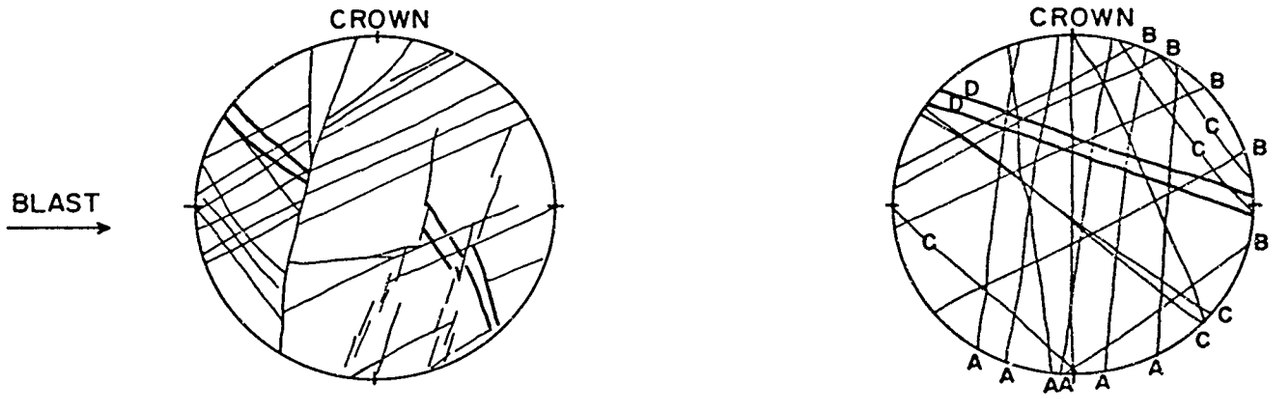

END SECTION OF DL 2
(0+90)
AS LOGGED BY GEOLOGIST.

END SECTION OF DL 2
(0+90)
AS PREDICTED BY PROJECTION
FROM TUNNEL WALLS.

FIGURE 2.4 COMPARISON OF PROJECTED AND ACTUAL END WALL AS A TEST OF THE METHOD OF PROJECTION.

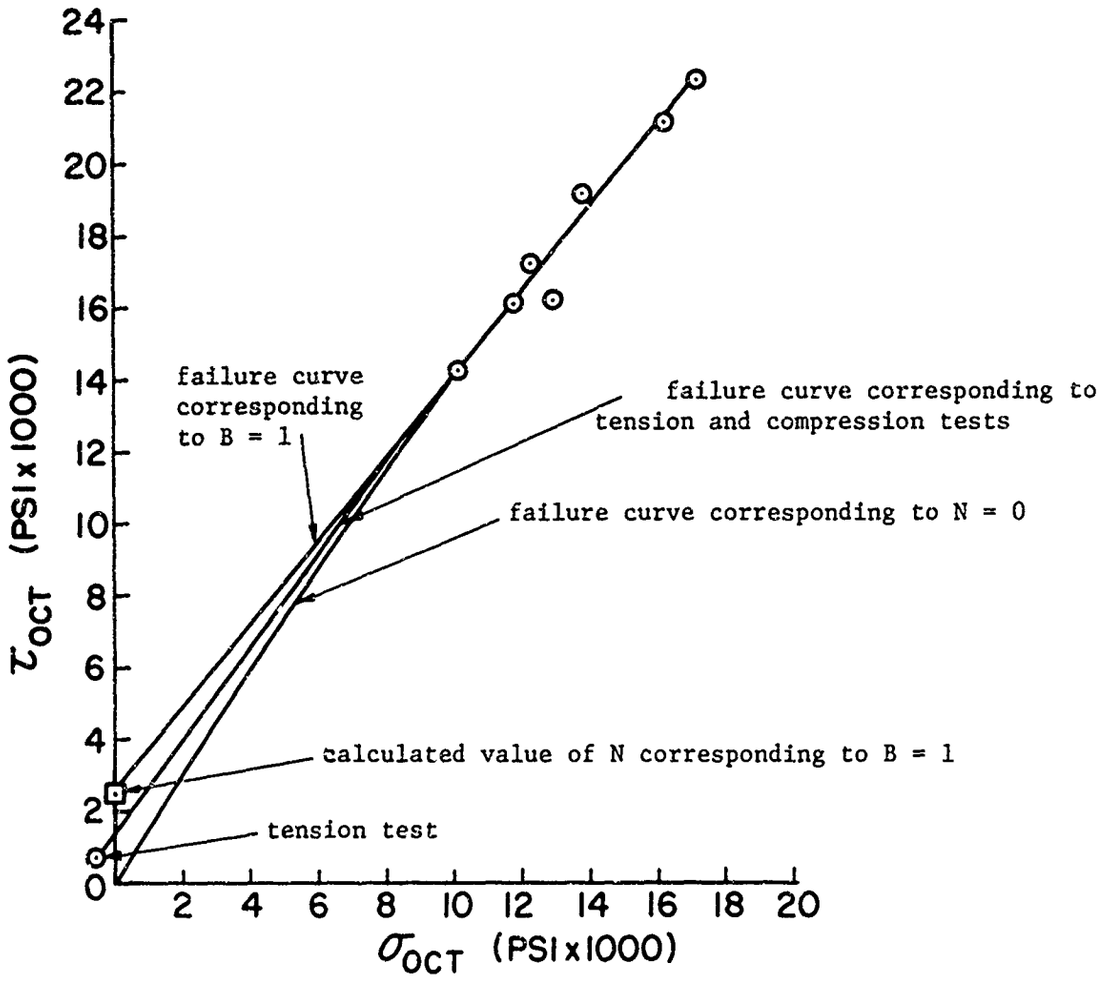

FIGURE 2.5 OCTAHEDRAL STRESSES AT FAILURE FOR PILEDRIVER ROCK

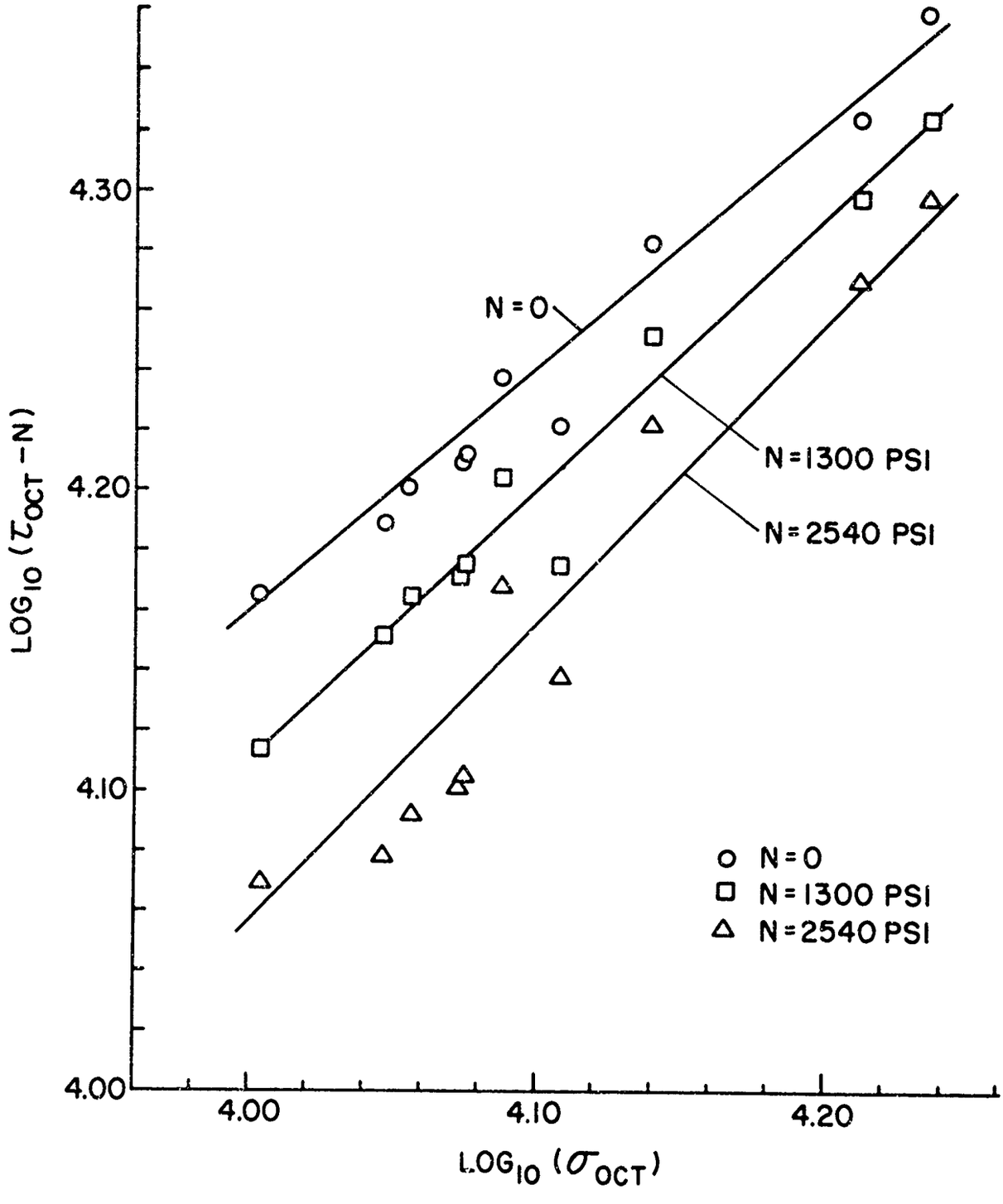

FIGURE 2.6 LOG-LOG PLOT OF OCTAHEDRAL STRESSES AT FAILURE

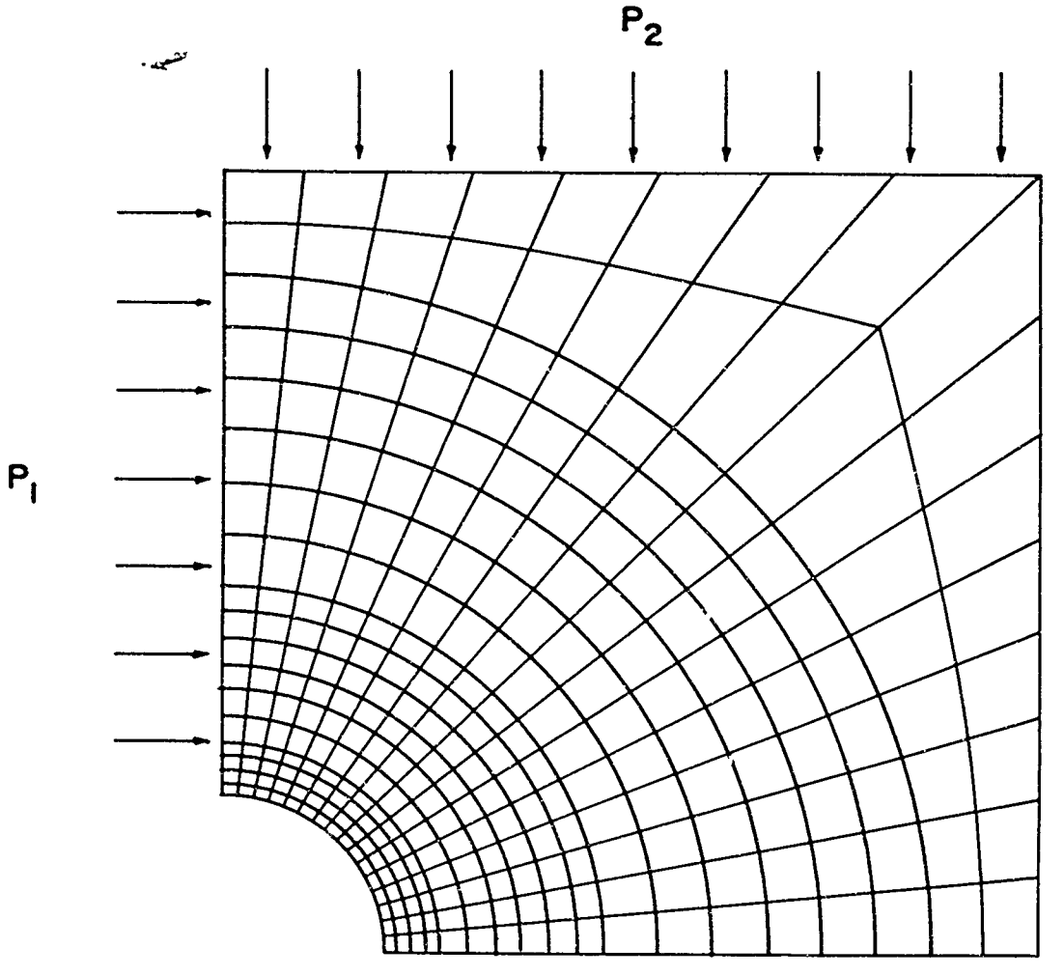

FIG 2.7 FINITE ELEMENT MESH PD5 USED IN EXAMPLE BELOW

FIG 2.8 PROGRESSIVE FAILURE OF ELEMENTS AS P_1 INCREASES FROM 0-32000 PSI IN 8 INCREMENTS ; $P_2/P_1 = 0.25$

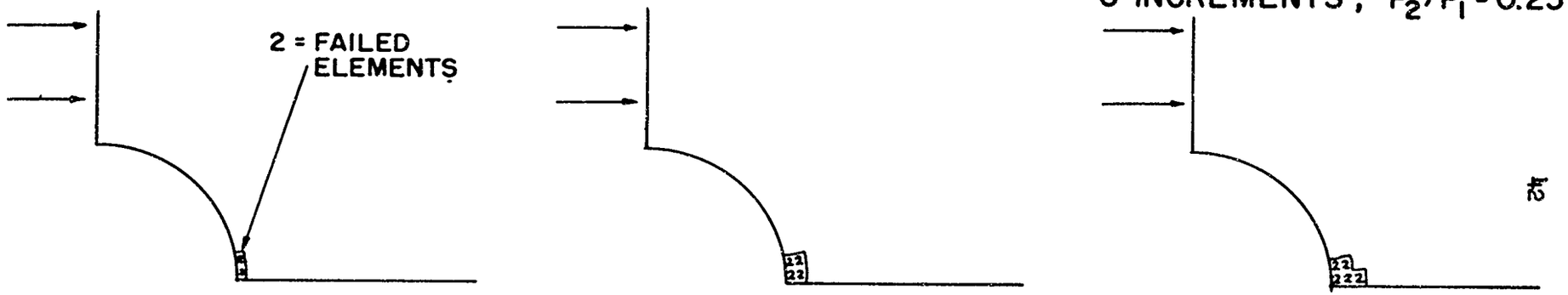

a. P_1 = 8000; 12,000

b. P_1 = 16,000; 20,000; 24, ; 28,

c. P_1 = 32,000

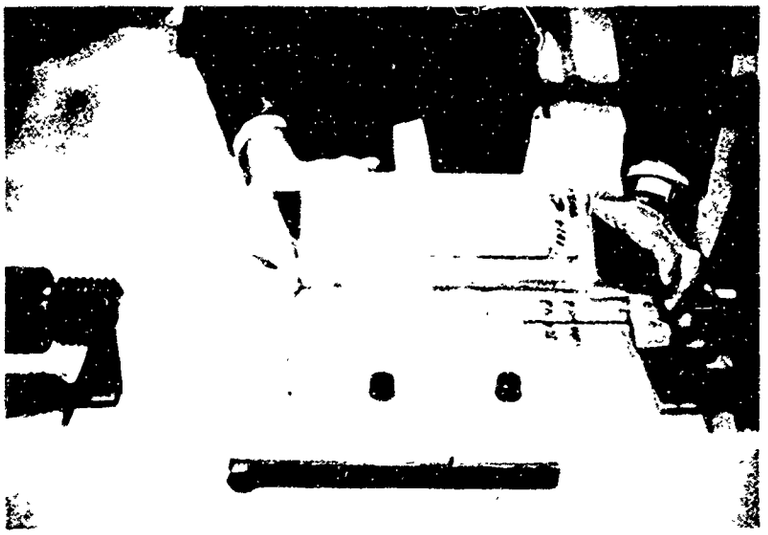

Figure 2.9 Artificial joint specimen produced by longitudinally diamond saw cutting an NX core sample. (Courtesy Univ. Illinois, Dept. C.E.)

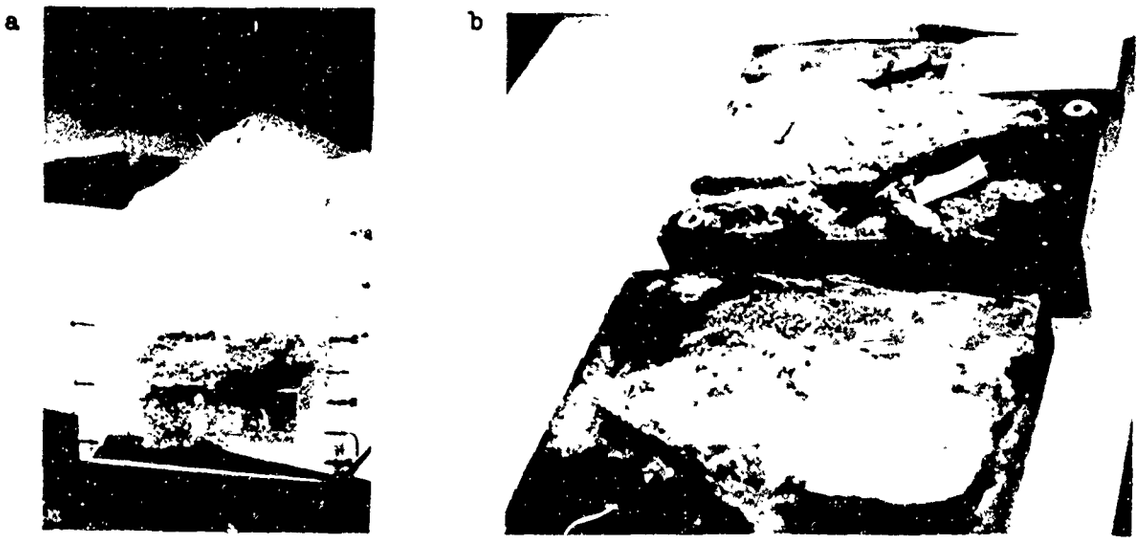

Figure 2.10 Preparation of direct shear specimen containing an artificial extension joint. a) Mold placed around fitted blocks. Plane of joint will be protected with putty while mold is filled with epoxy. b) Direct shear specimens after test. (Courtesy of Imperial College of Science and Technology, Dept. of Geology)

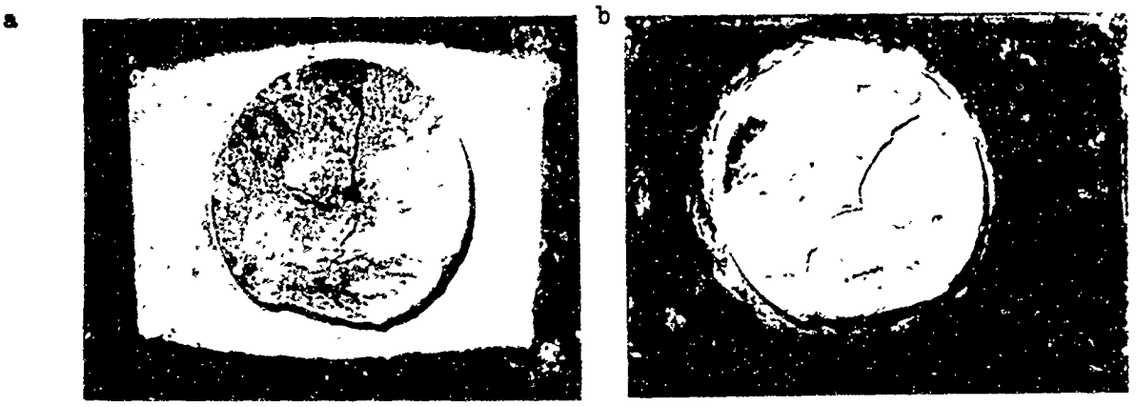

Figure 2.11 Large direct shear specimens of a natural joint obtained by drilling $7\frac{1}{2}$" cores (300 mm) across the joint. Photos a) and b) are of the bottom and top surfaces, respectively, after the test. (Courtesy of Coyne and Bellier)

Figure 2.12 Joint specimens obtained by drilling NX cores parallel to the joint plane. Photos taken after testing of lower (a) and upper (b) halves. Notice clayey filling material. (Courtesy of Coyne and Bellier)

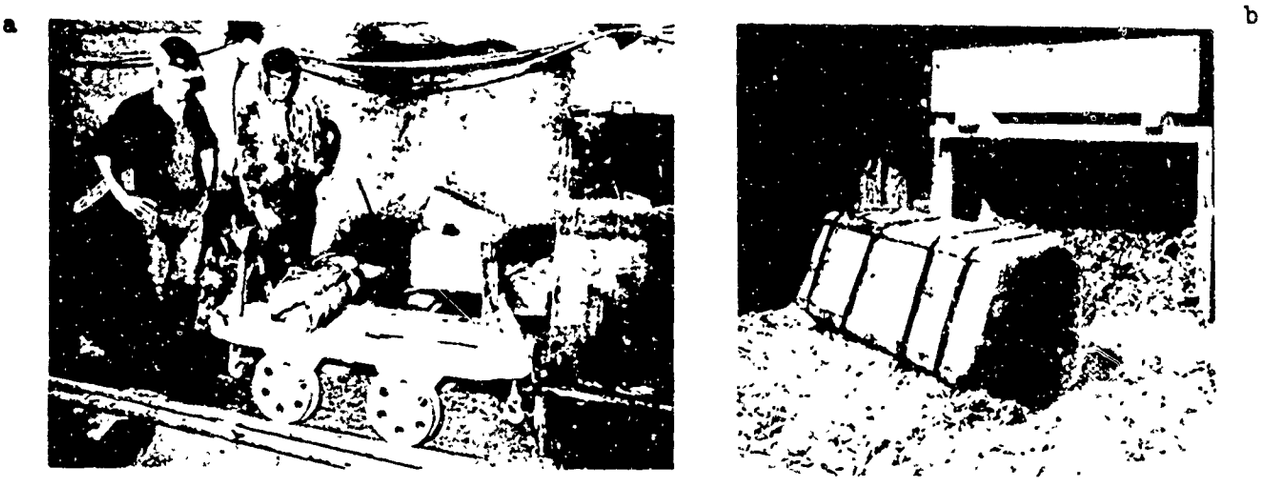

Figure 2.13 Large (8" diameter) core specimens containing joints in the diametral plane. a) After removal from the hole; b) packed in paraffin to preserve natural moisture content. (Courtesy of Coyne and Bellier)

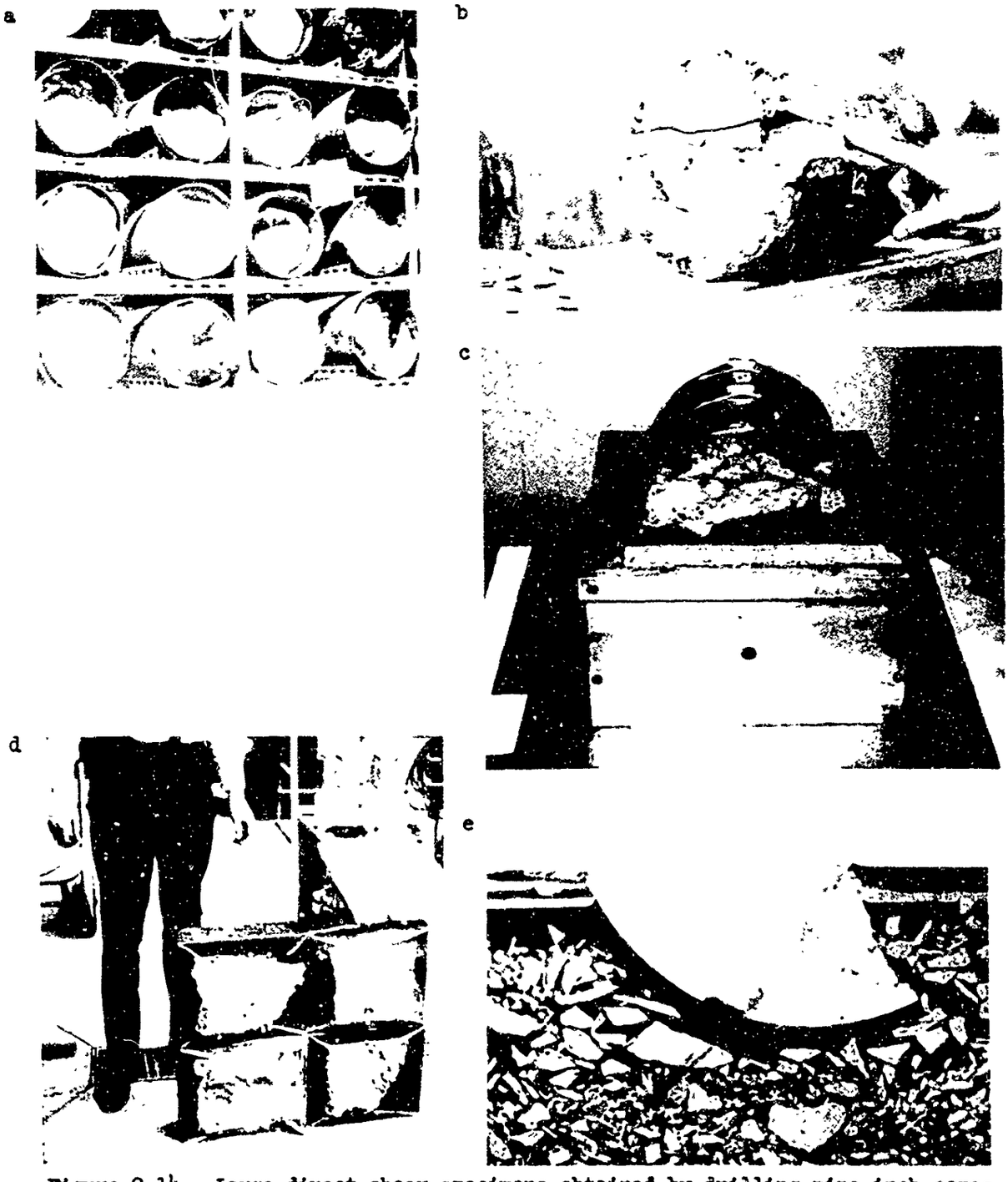

Figure 2.14 Large direct shear specimens obtained by drilling nine inch cores parallel to selected joint surfaces. (Courtesy Imperial College, Royal School of Mines)

a) specimens as received from field
b) after removing protective jacket
c) mounted in shear box, ready for testing (confining bands w be cut before test
d) specimens after test
e) cross section through a specimen showing rock filler in epoxy

Figure 2.15 Wire sawing technique used by Coyne and Bellier to extract block samples containing joints. The wires run around pulleys (not visible) at the ends of the rods. (Courtesy of Coyne and Bellier)

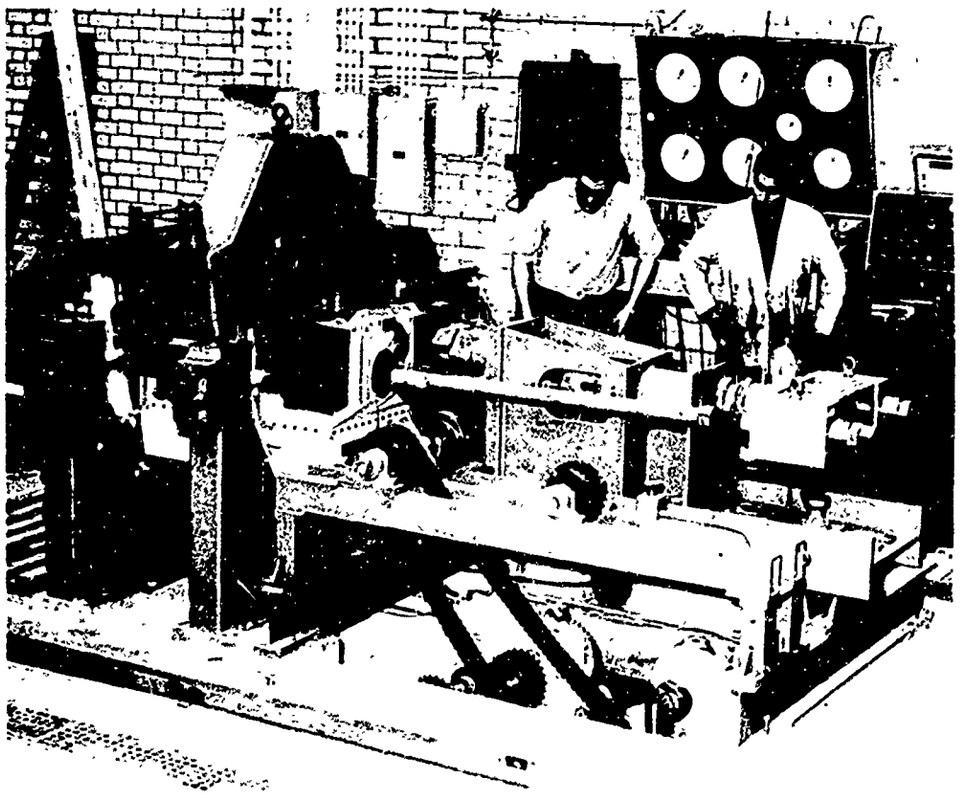

Figure 2.16 Large direct shear machine at Imperial College, Royal School of Mines. (Dr. Pentz to left.) (Courtesy Imperial College)

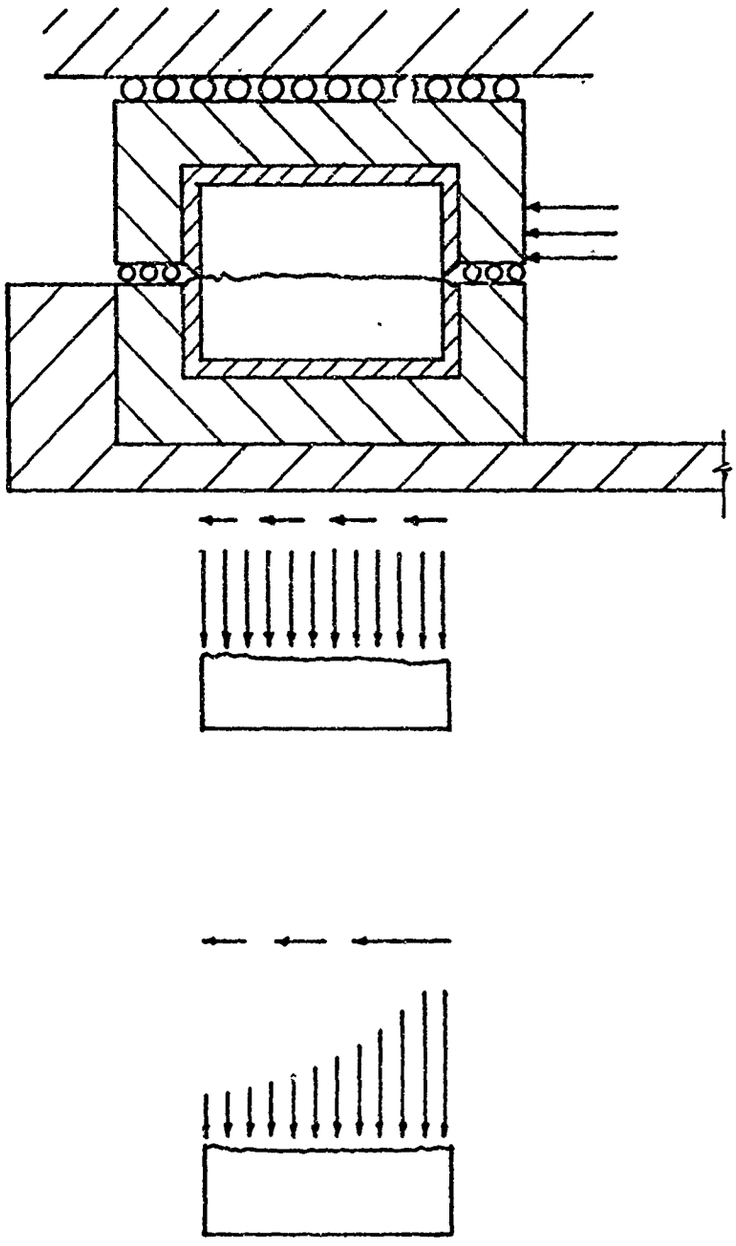

FIGURE 2.17 STRESS DISTRIBUTION IN A DIRECT SHEAR BOX

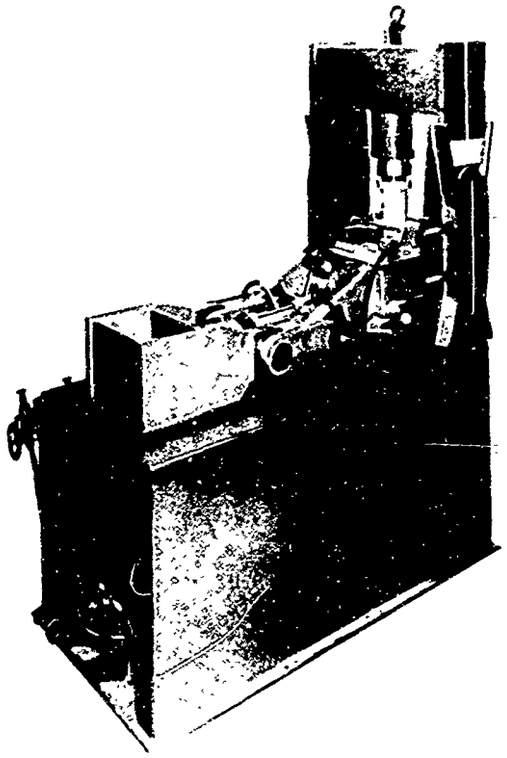

Figure 2.18 Casagrande type (plane strain) direct shear machine used by Coyne and Bellier. Takes samples up to 30 by 50 centimeters. (Courtesy of Coyne and Bellier)

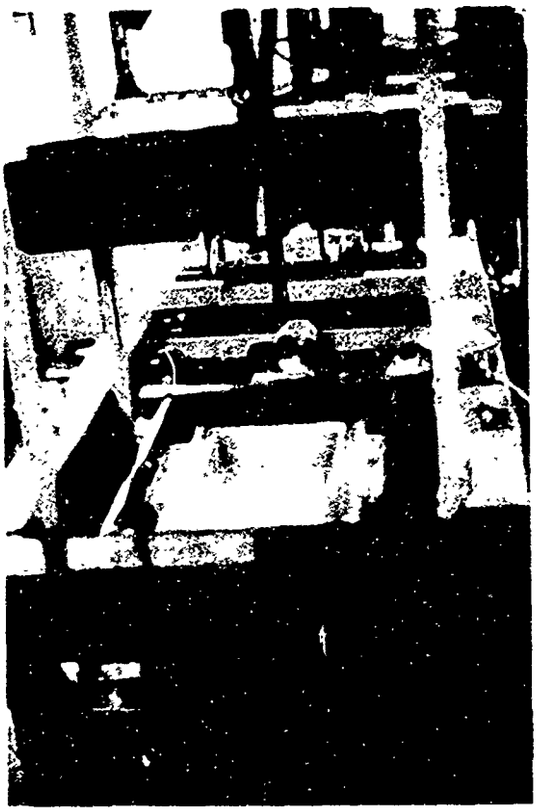

Figure 2.19 Plane strain direct shear machine employed at Dept. of Geology, Imperial College. Uses dead weight loading on hangers. (Courtesy of Dr. DeFreitas)

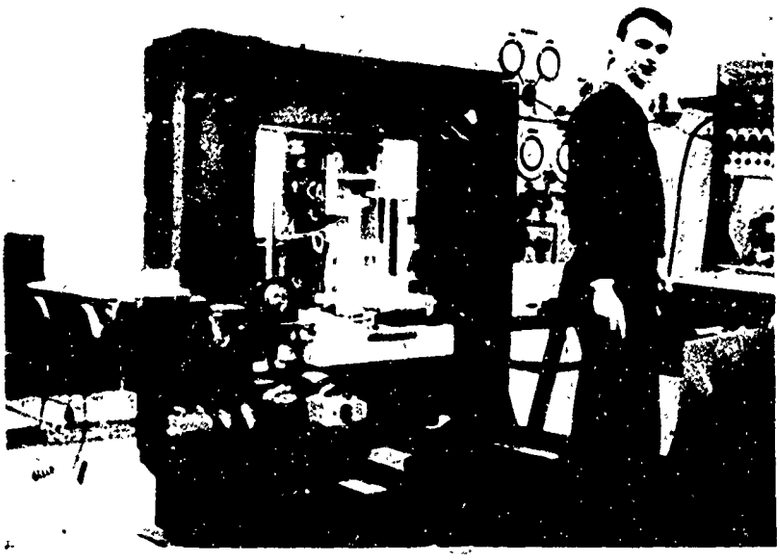

Figure 2.20 Plane strain direct shear machine at University of Illinois, Dept. of Civil Engineering. (Courtesy of Prof. Deere)

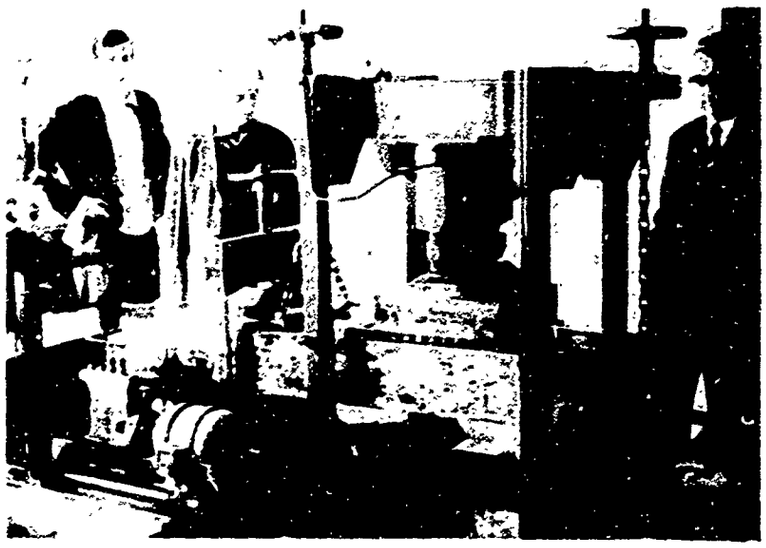

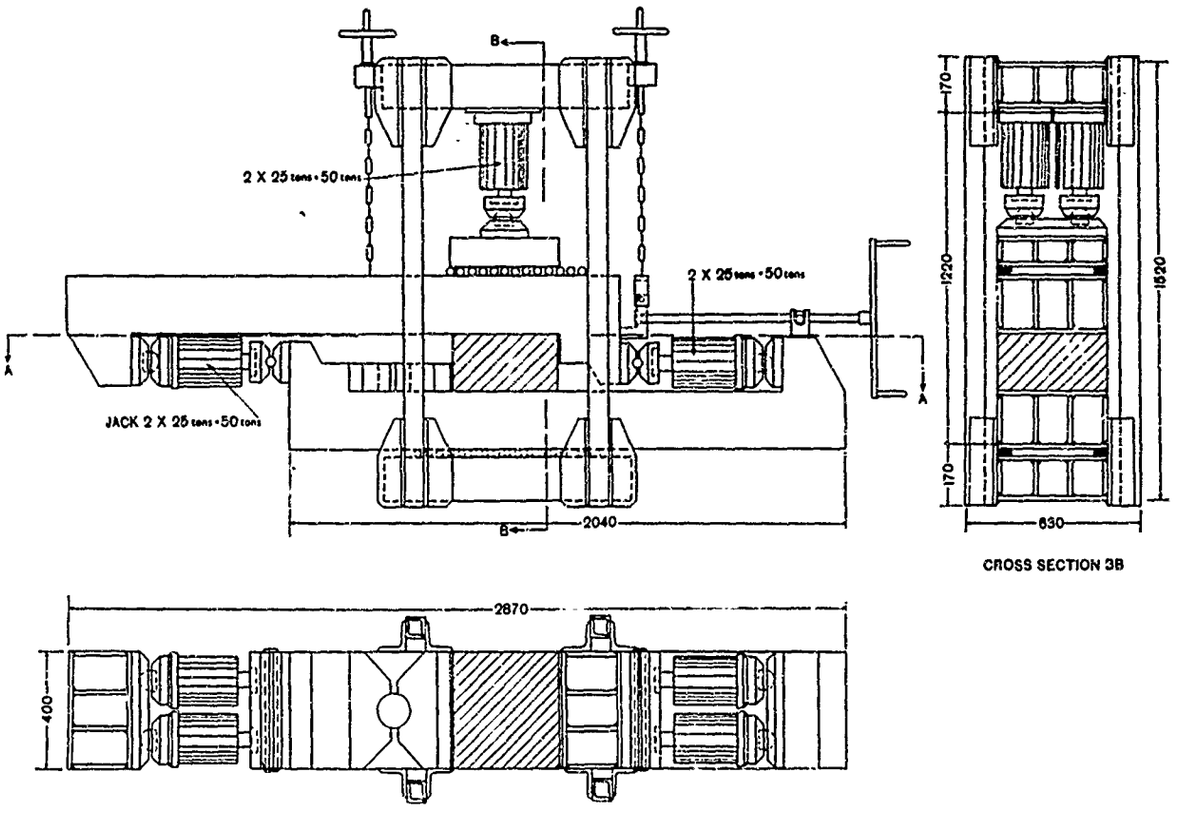

Figure 2.21 Krsmanovic shear machine, Sarajevo, Yugoslavia. a) Prof. Krsmanovic (right) and colleagues at shear machine; b) schematic diagram (from Geotechnique, June 1967, p. 146)

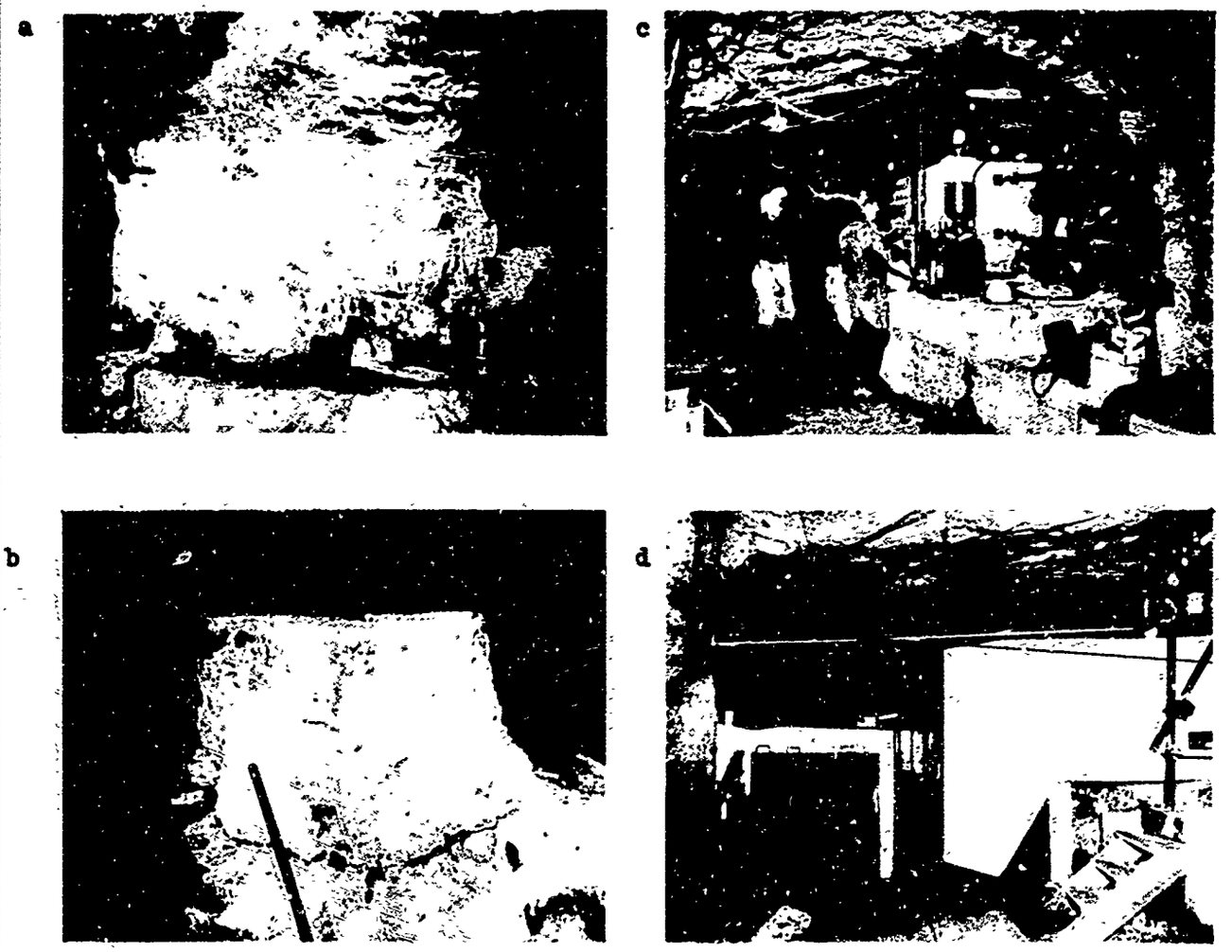

Figure 2.22 In situ shear test conducted at Vouglans dam. (Courtesy of Coyne and Bellier)
a) excavation of a pillar containing the joint to be tested
b) test block before encasing in concrete frame
c) the whole test apparatus
d) jacks used to apply tangential force. Vibration wire gauges used to measure displacements

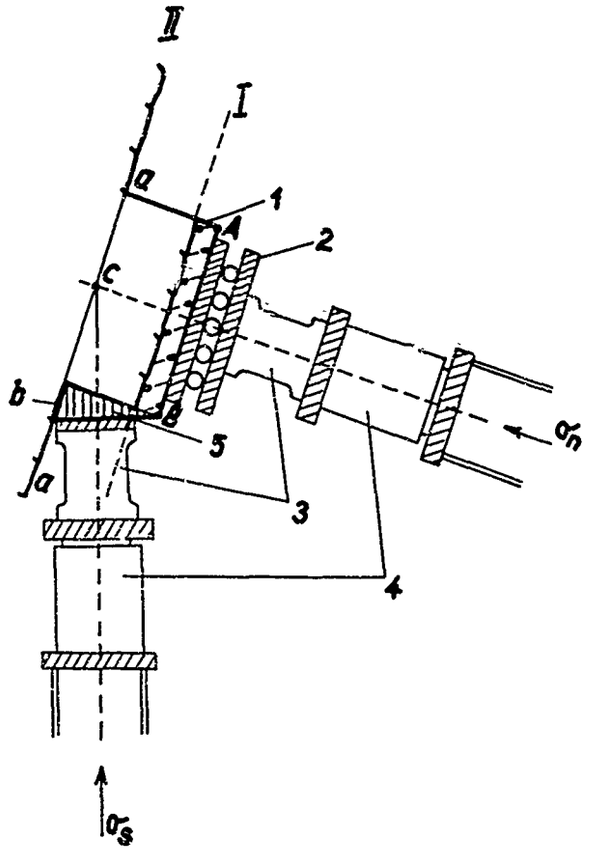

Shear test on a plane of mechanical discontinuity with shear movement within the rock mass.
1) Concrete block with measured points A and B;
2) Roller bearing;
3) Strain gauge dynamometers;
4) Hydraulic presses for pressures of 50 or 100 Mp;
5) Plaster levelling wedge: a) Broken-off rock round the block; b) Cardboard lubricated with vaseline; c) points at which the movement on a plane of mechanical discontinuity is measured; I and II) planes of mechanical discontinuity.

Figure 2.23 In situ shear tests conducted in Czechoslovakia. a) Conventional test, on a horizontal plane; b) test on a steeply inclined plane. (Courtesy Dr. Karel Drozd. Reprinted from Proc. of Geotechnical Conf., Oslo 1967, p. 266.)

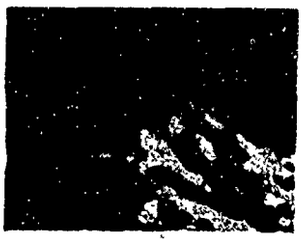

Figure 2.24 In situ shear tests on a clay parting along bedding in shale on a natural slope at Khajuri Kach dam, Pakistan. (Courtesy Dr. Kujundzic, Jaroslav Cerni Institute, Belgrade, Yugoslavia)

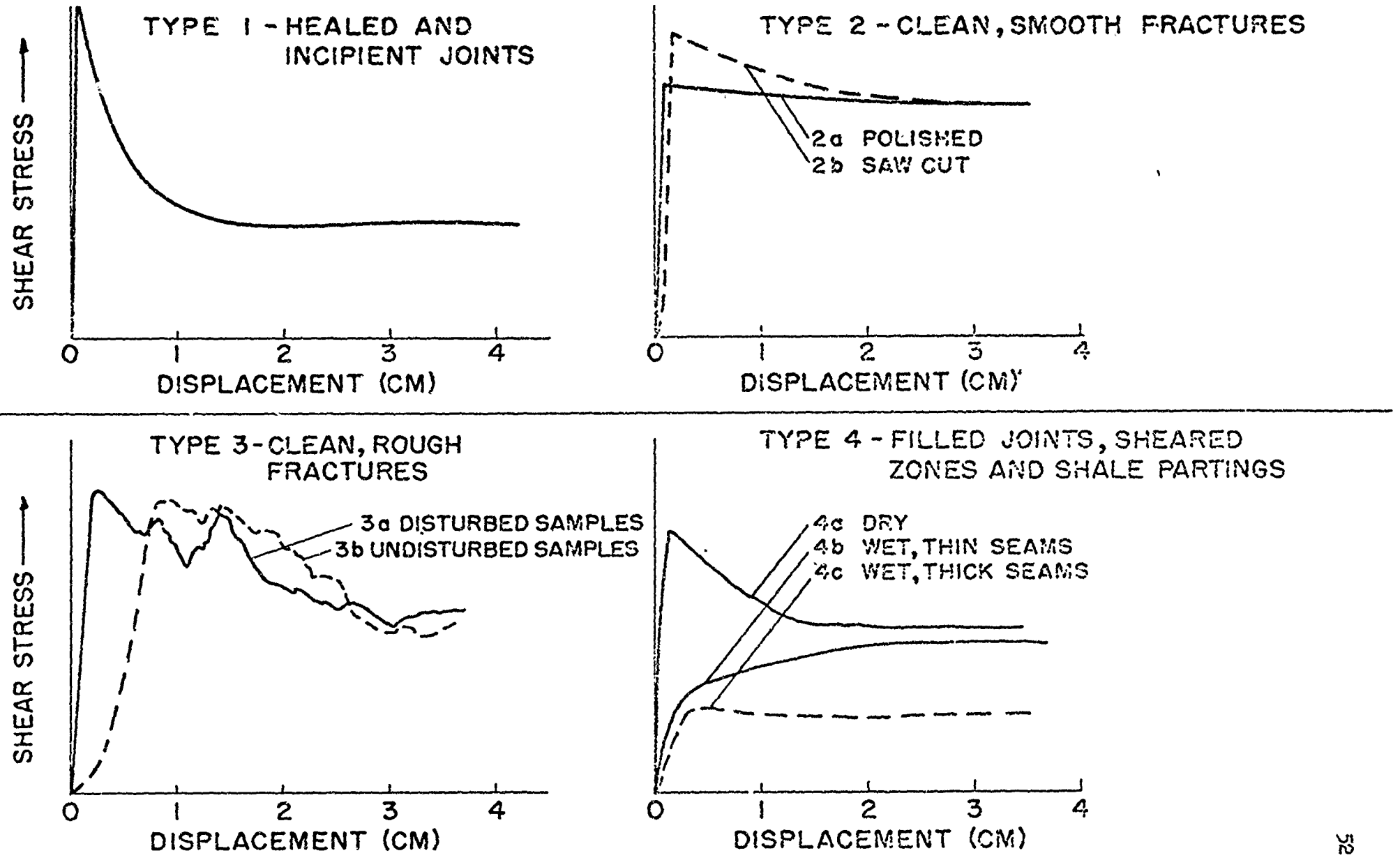

FIGURE 2.25 TYPICAL SHEAR STRESS - DEFORMATION RELATIONSHIPS FOR VARIOUS WEAKNESS SURFACES (STRENGTH DEPENDS ON NORMAL PRESSURE: SHEAR STRESS SCALE IS RELATIVE ONLY)

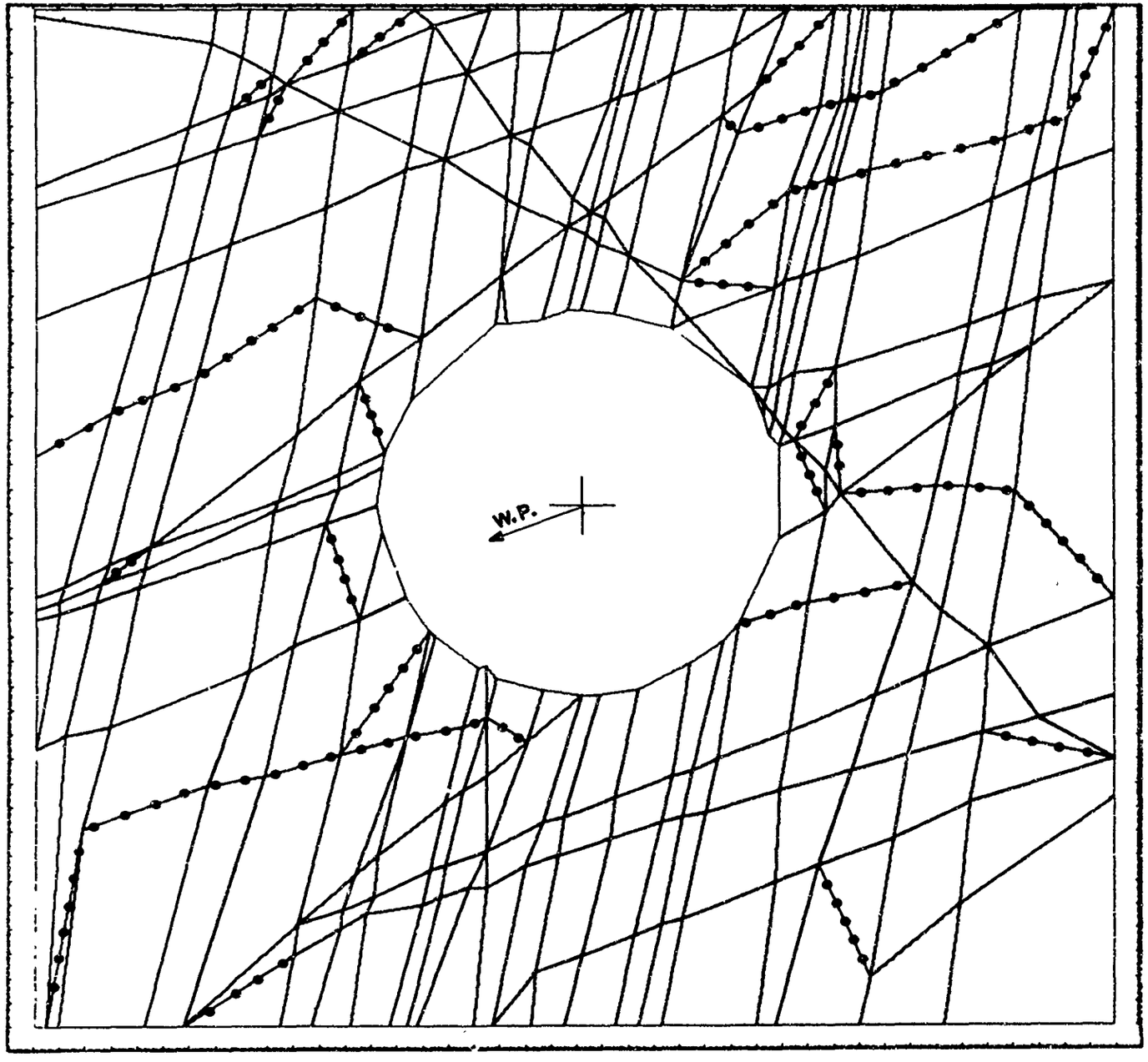

FIGURE 2.26
FINITE ELEMENT MESH
FOR DL DRIFT 0 + 70
667 ELEMENTS
900 NODAL POINTS
398 JOINT ELEMENTS

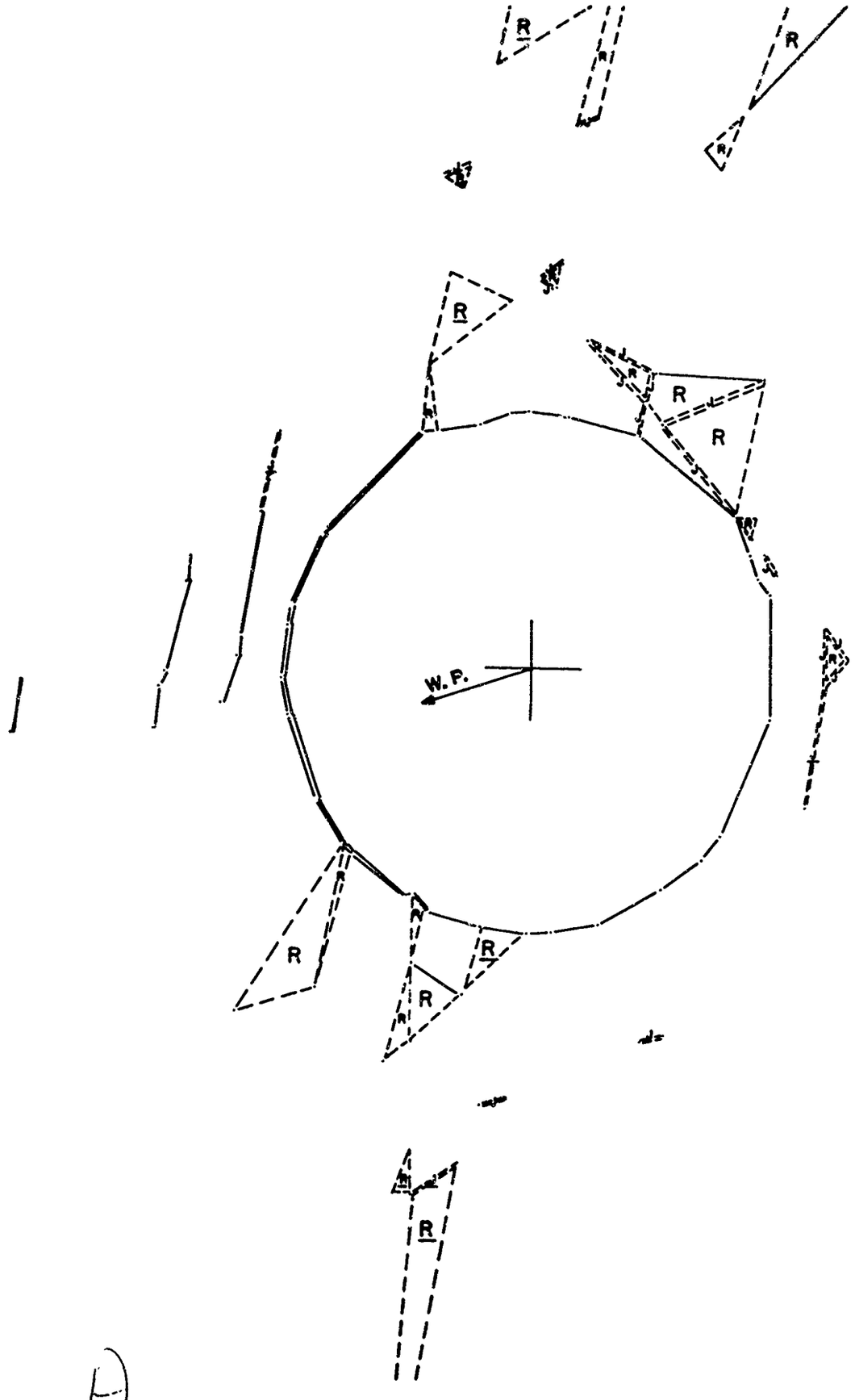
R
R
R
R
R
W.P.
R
R
R
R

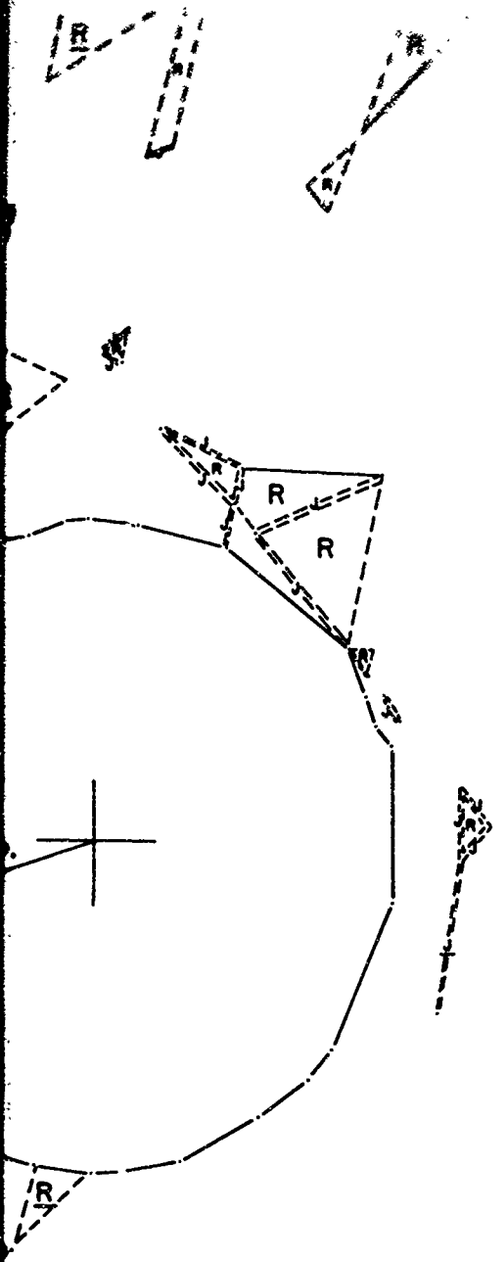

DISPLACEMENTS AFTER 10,000 PSI.
FAILED ELEMENTS AFTER
5000 AND 10,000 PSI.

R = ROCK FAILURE
J = JOINT FAILURE
R AND J SIGNIFY FAILURE
ONLY AFTER 10,000 PSI

0 2 4 FEET

SCALE (OF
DRAWING AND DISPLACEMENT)

------ ORIGINAL POSITION

——— DEFORMED POSITION

—·——·— TUNNEL WALL

FIGURE 2.27 a DL DRIFT 0+70
DISPLACEMENTS AND FAILED
ELEMENTS FOR CASE I

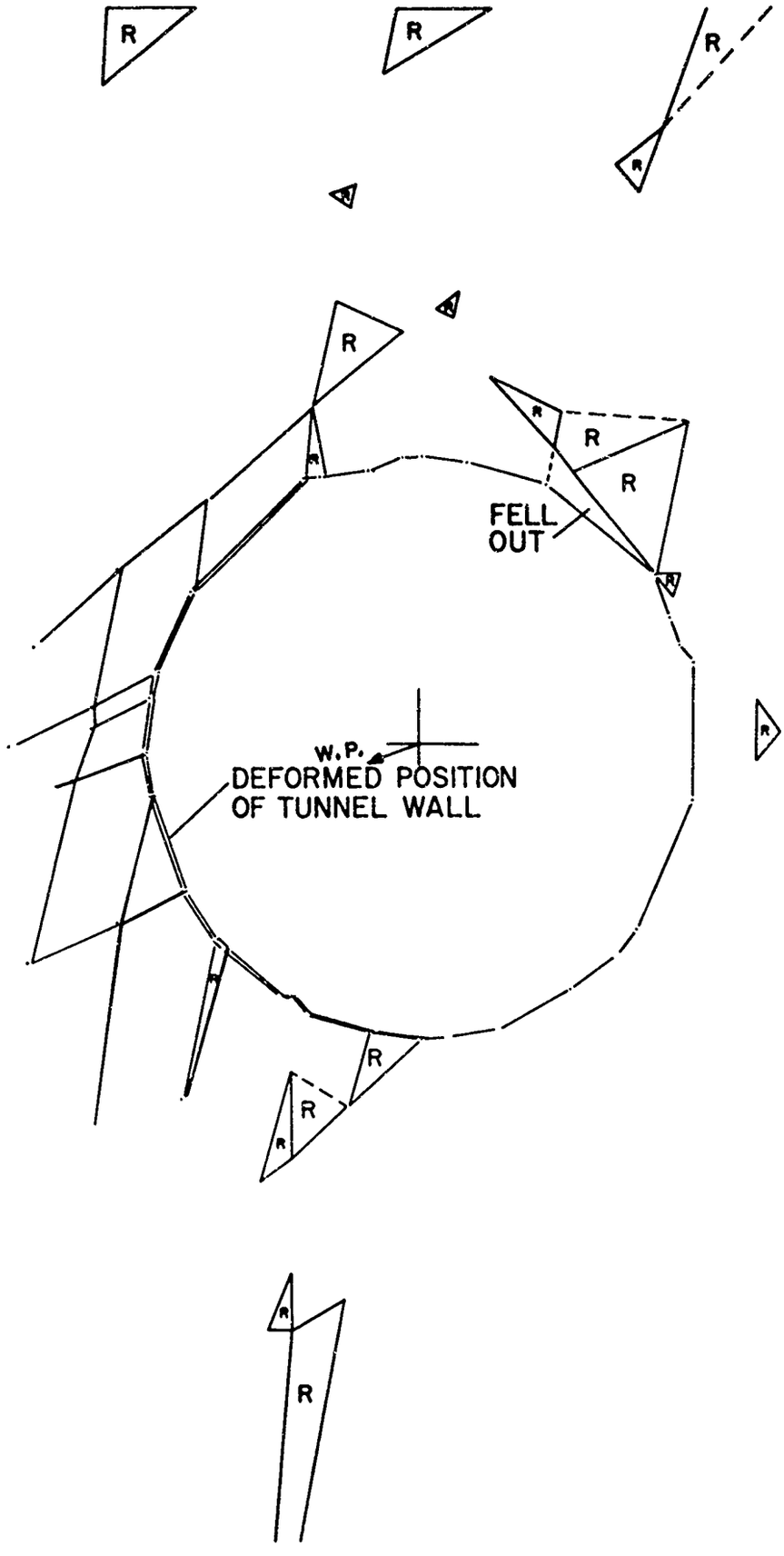
R
R
R
R
R
R
R
R
R
R
R
R
R
R
R
R
FELL
OUT
W.P.
DEFORMED POSITION
OF TUNNEL WALL

41

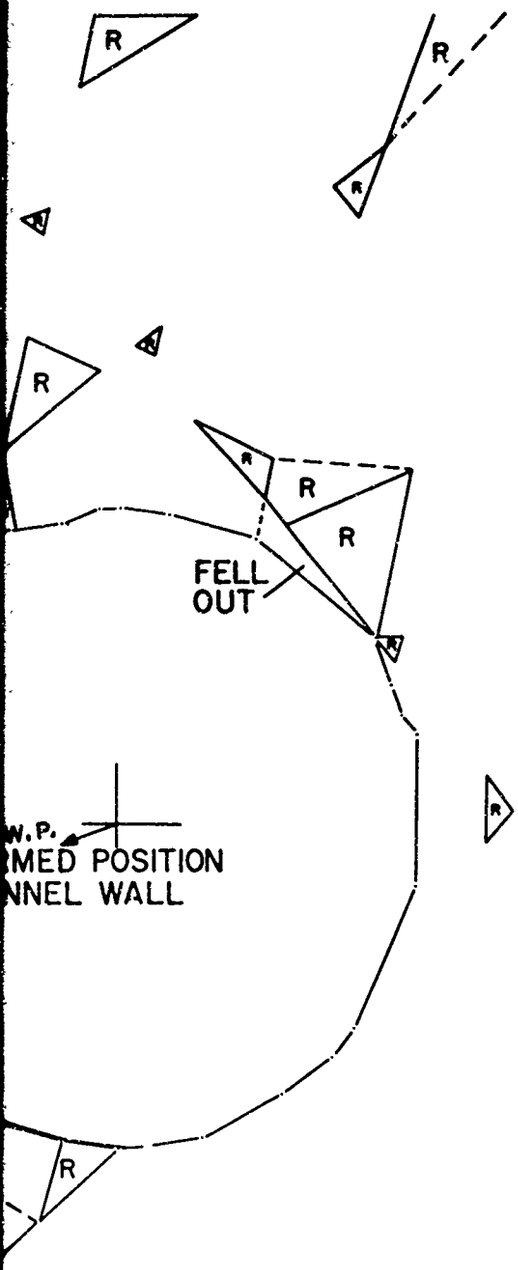

DISPLACEMENTS AND
FAILED SOLID ELEMENTS (R)
AFTER 15,000 PSI.
FAILED JOINTS NOT SHOWN
DOUBLE LINE = OPEN JOINT

0 2 4 FEET

SCALE (OF DRAWING AND
DISPLACEMENT)

----- ORIGINAL POSITION
——— DEFORMED POSITION
—·—·— TUNNEL WALL

FIGURE 2.27b DL DRIFT 0+70
DISPLACEMENTS AND FAILED
ELEMENTS FOR CASE I

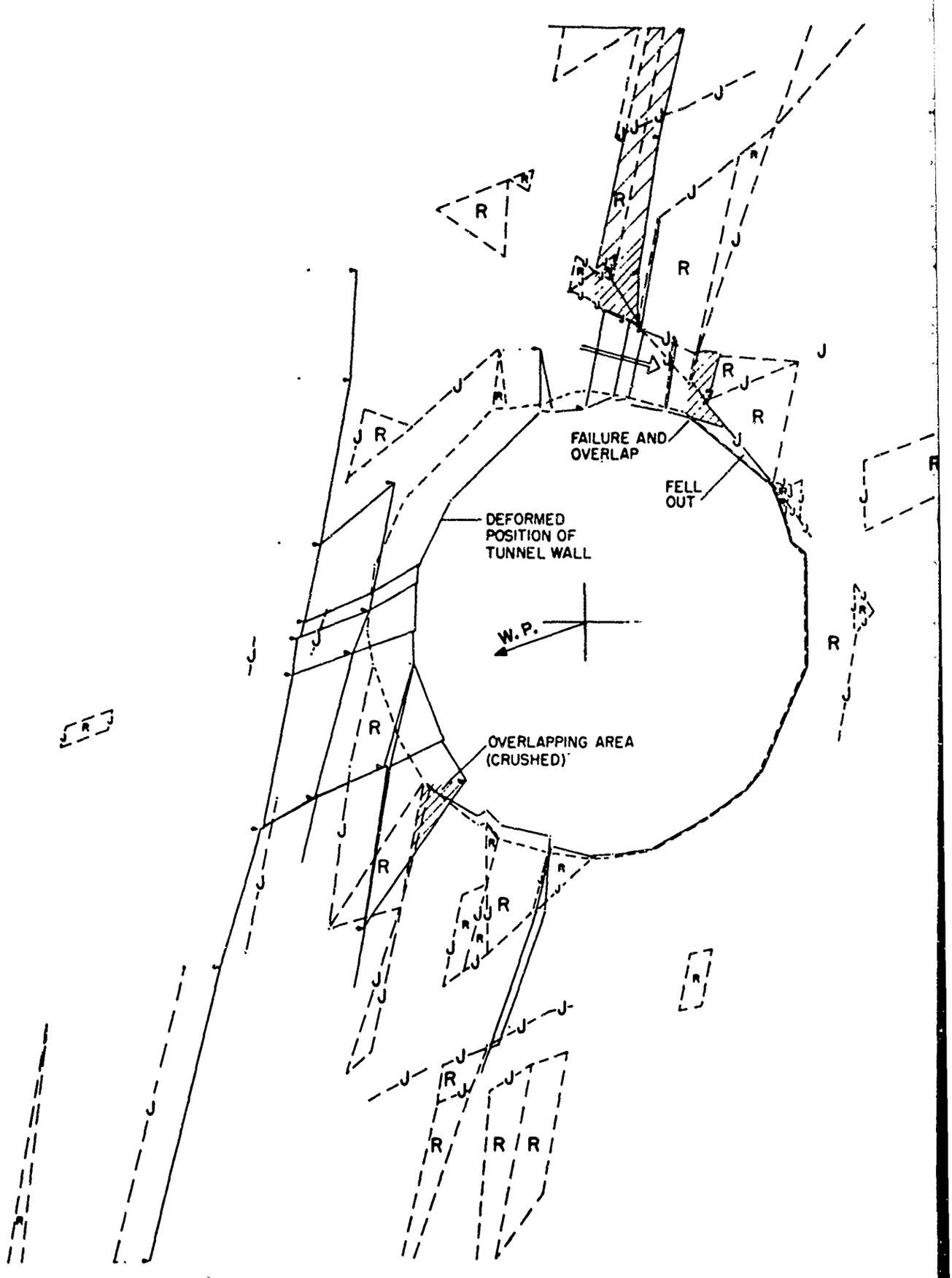
FAILURE AND
OVERLAP
FELL
OUT
DEFORMED
POSITION OF
TUNNEL WALL
W.P.
OVERLAPPING AREA
(CRUSHED)

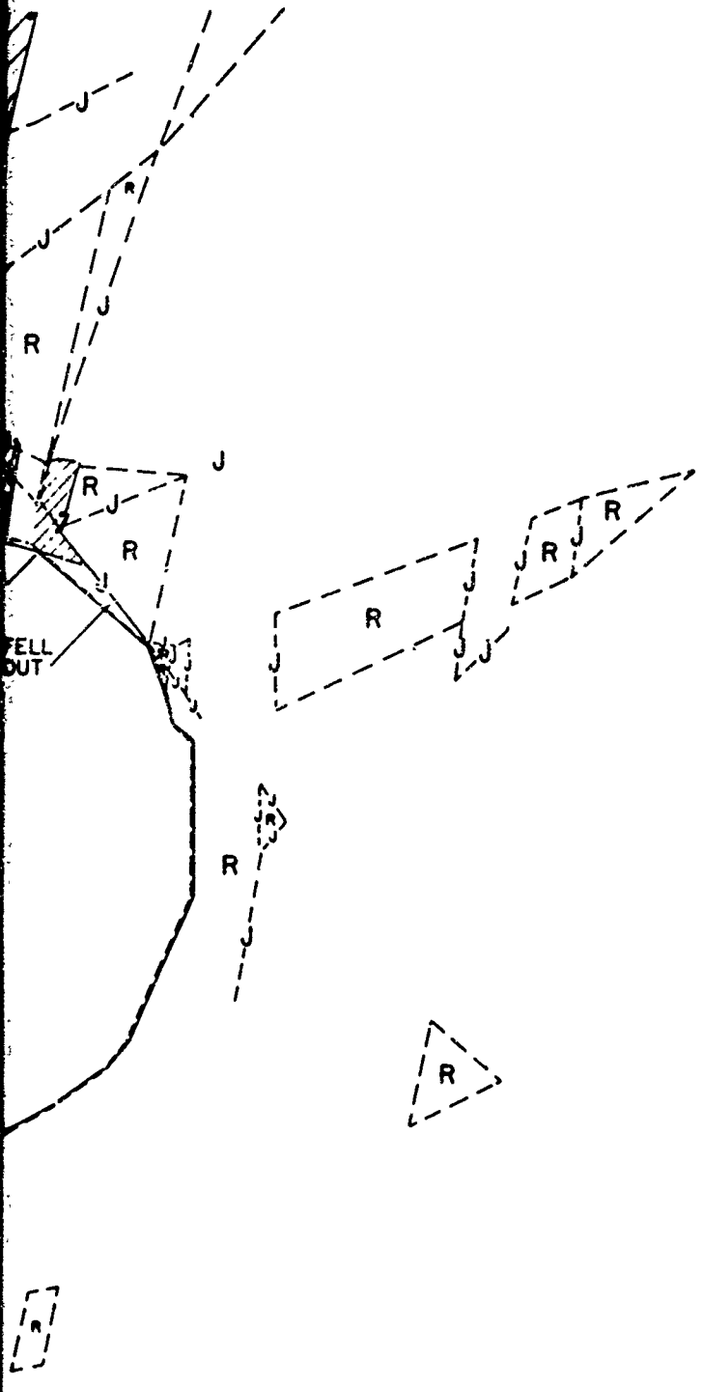

DISPLACEMENTS AFTER 5000 PSI.
FAILED ELEMENTS AFTER 2500 PSI

0 2 4 FEET

SCALE (OF DRAWING AND DISPLACEMENT)

R ROCK FAILURE

J JOINT FAILURE (BY OPENING OR SHEARING)

---- ORIGINAL POSITIONS

——— DEFORMED POSITION

FIGURE 2.28 DL DRIFT 0+70 DISPLACEMENTS AND FAILED ELEMENTS FOR CASE 2

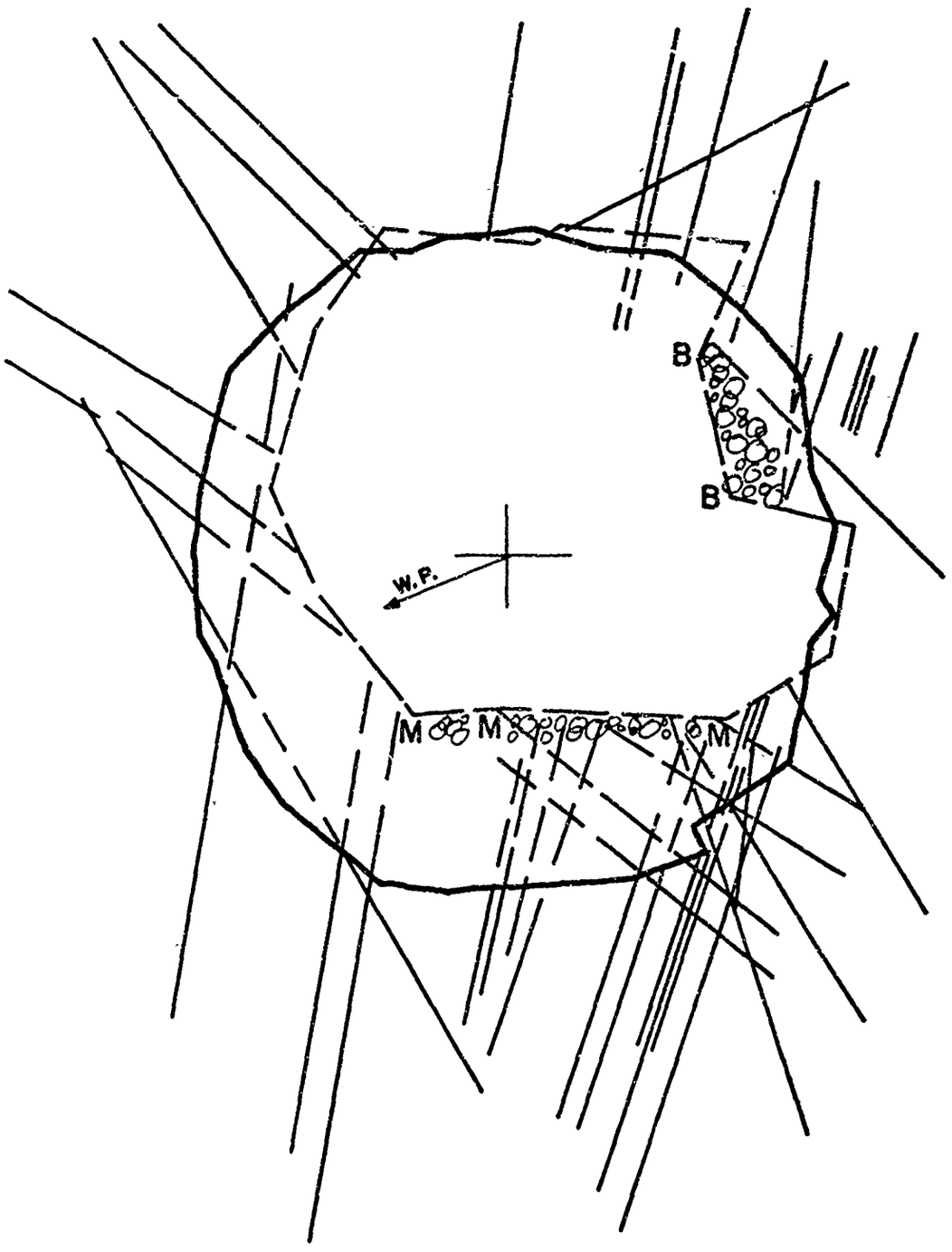

BLAST SIDE TO LEFT
B = BROKEN ROCK IN MESH
M = BROKEN ROCK COVERING INVERT
——ORIGINAL POSITION
– –DEFORMED POSITION

FIGURE 2.29 POST SHOCK CROSS SECTION
STATION 0 + 70 - DL DRIFT

3. ANALYSIS OF CR AND DL DRIFTS BY JOINT INFLUENCE DIAGRAM METHOD

3.1 DESCRIPTION OF PROCEDURES

The inclusion of joint elements with prescribed stiffness and strength values in the powerful finite element method allows testing of sophisticated mathematical models. The stress distributions employed in evaluating the strength of a tunnel section by this method take into account the effect of discontinuities, of heterogeneities, and of local failures. Tunnel liners and rock bolts can be incorporated. However, the discontinuities are entirely two-dimensional in their representation. Further, the method is relatively tedious if large numbers of joints are involved.

Another approach, termed the ubiquitous joint method in previous reports, permits an examination of the influence of varying distributions of joints at a large number of sites with relatively little effort. The method consists of computing regions of influence for prescribed joint orientations in a given stress field and comparing the influence diagrams with site geology. The steps in the analysis are as follows:

1. Construct cross sections of the drifts showing the location and orientation of joints and faults. Divide the joints into sets on the basis of preferred orientation.
2. Calculate the region of influence of each joint set assuming some state of stress acting as a result of the blast. A simple Kirsch solution[12] stress state was assumed, with the blast replaced by a) a static load equal to P and b) confinement in the perpendicular directions equal to $(\nu/1-\nu)(P)$, where P is the peak pressure of the blast and ν is Poisson's ratio.
3. Overlay the geologic sections on the influence diagrams and note the locations where joints of each set can slip.
4. Using the results of (3), and considering the whole network of joints at each section, sketch the probable zones of rock fall-

---

[12]Obert, L. and DuVall, W., Rock Mechanics and the Design of Structures in Rock, Wiley, 1967, p. 101.

out and failure. In rock bolted sections, the capacity of the rock bolts to prevent rock movement is considered at this stage[13].

Fig. 3.1a* shows the sequence of test sections and stationing referred to in this text. Fig. 3.1b* shows the main joints and faults, and labels those sections where major failures occurred. All joints and sheared zones occurring in D drift, CR East West, and CR North were listed and assigned to one of nine joint sets (A-I) on the basis of orientation. Geologic cross sections were constructed, as described in Section 2.1, every 10 feet in CR drift and in DL 1 and 2. At each section, the mean orientations of each of the joint sets were calculated and joint influence areas were determined, assuming ϕ equals 31°, and c equals either 100 or 1000 psi. The stress field used to calculate the joint influence zones correspond to the Kirsch solution[14] for stresses around a circular tunnel, in a biaxial stress field, superimposed on the component of the blast pressure that is longitudinal to the tunnel, as listed in Table 3.1.

The computer programs used in this study are presented in Appendix 2. The computer was used to generate the stress fields around the openings, by the Kirsch solution, and to calculate and plot the joint influence regions for given joint parameters.

In this analysis, it has been assumed that the joints do not modify the stress distribution, i.e. that they are stiff. Further, it is assumed that rock bolted sections and lined sections can be studied without taking into account their strengthening effect until the last step; in other words, that they similarly do not modify the stress distribution. Both of these assumptions are indefensible on detailed examination but they simplify the problem to such a degree that it becomes practical to apply this procedure. The question to be explored here is to what extent this simplified, step by step joint influence analysis yields reasonable tunnel behavior estimates. This will be discussed section by section.

---

*Reproduced from POR 4015, Chapter 4.

[13] U. S. Army Engineer District Omaha, Technical Reports 2 and 3

[14] op. cit., p. 58.

3.2 CR EAST-WEST DRIFT -- RESULTS OF ANALYSIS

Analyses were made every 10 feet in CR drift beginning at station 0 + 20 (CR 1A). The excavated diameters and lining types of the sections in this drift are listed in Table 3.2.

Results of analyses are reported for the rock bolted or unlined section from 0 + 60 to 1 + 70. The strike and dip of joints and sheared zones determined from Figs. 3-1c,d, pre-construction logs, are listed in Table 3.3. In Table 3.4, the strike relative to the tunnel axis (σ), the dip of the joint down from horizontal (D), and the dip (θ) relative to 0° along the radius from the weapon point are listed for each joint set at each station. From these data, the angle (β) between the normal to the joint plane and the axis of the tunnel has been determined as described in Technical Report No. 3[15]. Joint influence diagrams have been constructed for all the sets of joints for the stress state corresponding to a blast pressure of 10,000 psi. Joint sets C and G were found to have no influence region around the tunnel at a number of stations, as described by the note "no joint failure" in Table 3.4. Two cases were analyzed, corresponding to assumptions of joint cohesion of 100 and 1000 psi. Influence diagrams for these cases are shown in Figs. 3.2a,b and 3.3a,b respectively.

Four types of figures (a, b, c, d) have been prepared for the step by step analysis. At each station considered, first a geological cross section is shown (a). (These are to a standard size but varying scale). The second figure in each set (b) shows only the joints and shears which occur within their zone of influence. It is derived by superposition of the influence diagrams, for each joint set in turn, on the geologic cross section (a). The third and fourth figures in each set (c and d) show the expectable post-shock profile for the tunnel; these figures are obtained by superimposing figure b on the geologic cross section to determine which blocks have kinematic freedom to move into the opening. Figures c and d correspond to cohesion of 100 and 1000 psi respectively. No expectable post-shock profiles were prepared for concrete or composite lined tunnels. For rock bolted sections, it was assumed that the bolts and wire mesh could restrain only up to several feet of broken rock from being accelerated into

---

[15] op. cit., p.1

the tunnel. Figs. 3.4 through 3.14 present the results of the analysis for the CR (EW) drift.

(1) Station 0 + 60 CR3 - Fig. 3.4(a-d)

The analysis weights the A joints heavily in the roof and on the blast side just below spring line. D and E joints at 240° and 270° are also significant. The closely fractured zone in the roof is formed of uninfluential C joints but their intersections with the A joints define blocks which would tend to fall into the tunnel. Thus, the analysis predicts rock movement inward at 90-100°, 240-270° and 340-350°.

Actual damage can be seen on the post-shock cross section at 0 + 59 (Fig. 3.16). The closely spaced fractures in the roof did not, in fact, cause roof falls in this section except where they intersected the north 42 west shear and this led to a major rock movement at about 110°. Also, towards the invert at the base of the lee wall, there was a minor rock movement inward. There was very substantial inward movement on the blast wall from slightly above 0° down into the invert. In total, the damage to the section is not substantial. The comparison of the actual damage pattern and its relationship to the geology with the damage pattern predicted by the joint influence diagram analysis shows conformable areas of agreement. It is interesting that rock bolt deformeter data at station 0 + 59 were lost at 100° due to the extensive rock movement in this region. These deformeter data also documented large rock movement on the blast wall side -- 4.7 inches increase in length over the 16 foot long deformeter length.

(2) Station 0 + 70 CR3 - Fig. 3.5(a-d)

The geologic section at 0 + 70 shows flat lying joints closely spaced above the roof, a shear zone, called I-2, in the blast wall with apparent dip towards the opening, and a series of steep B joints behind the lee wall. The cross-section is very complicated. The joint influence analysis predicts very strong influence of 2 A joints which intersect the roof and are inclined with apparent dip towards the weapon point. The results of the analysis are shown in Fig. 3.5 c and d. A major rock fall from the roof was predicted

together with a rock fall from the lee wall down to about spring line delimited by the steeply dipping B joints. Inward movement is also predicted from the blast wall due to the interaction of D and F joints and the I-2 shear zone. The actual damage pattern at this location can be seen on Fig. 3.16 for station 0 + 71. Major rock falls occurred from the roof. Some rock was broken but was restrained by the mesh at about 80°. From 90-120°, major rock movement occurred and this movement continued with decreasing thickness down into the lee wall to about spring line, apparently along the steeply inclined joints. Also there was inward movement on the blast wall. The rock bolt deformeter data at 0 + 71 were lost in the roof because of the rock falls. Also, very large inward movements were observed on the blast wall side. The agreement with the joint influence analysis appears to be good.

(3) Station 0 + 80 CR4 - Fig. 3.6(a-d)

The geological features of the cross section at 0 + 80 are a series of steeply inclined B joints far into the lee wall, a closely fractured zone of G joints below the invert, and a series of shears and joints of the A orientation traversing the tunnel and inclining toward the weapon point. There is also a regular spacing of C joints traversing the tunnel and inclined away from the weapon point. Absent from the section are B joints traversing the tunnel and A joints above the roof of the tunnel. As will be seen in the discussion of CR2 and the unlined unsupported drill slot, the intersection of A and B joints in the roof provides the situation for large rock movements into the tunnel. The joint influence analysis predicts rock movement at 100-120°, mainly on A joints. The actual damage to be seen in Fig. 3.16 and the cross section for station 0 + 79 shows large rock falls restrained by the wire mesh from about 20-90°. These falls were defined by the intersection of vertical B joints and flat lying A joints in the roof. The analysis predicted fall-in of rock from the roof at 100° but totally failed in predicting the major rock breakage between the blast wall and the roof at 20-90°. This is because of the failure of the geological mapping to define the intersecting features in this region of the roof. It again calls need for the use of a stratascope or bore hole camera in a mapping program.

(4) Station 0 + 90 to 1 + 20 CR2 and Drill Slot

Fig. 3.15 is a longitudinal profile along the center line of CF drift from CR3 to the end of the CR Tee intersection. It is clear from examination of this figure that a major rock fall occurred above CR2 and above the drill slot. The drill slot was totally unsupported and it is probable that this area progressed towards CR2 and into the end of CR4. Post shot examination revealed flat-lying joints in the roof above the drill slot and above CR2 which had gone undetected in the mapping program because they do not intesect the walls. Geologic cross sections at station 0 + 90, 1 + 00, 1 + 10 and 1 + 20 are presented in Figs. 3.7, 3.8, 3.9 and 3.10, together with the joint influence analysis for these stations. At 0 + 90, the weakening effect of an intersection of A joints and B joints in the roof is clearly demonstrated. Large fall-out of rock forming a cathedral overbreak from 90-130° is shown in the predicted post shot appearance. At station 1 + 00, A joints in the roof similarly are predicted to cause fall-out from the roof between 90-110°. The predicted fall-out was, in fact, much smaller than that actually occurring, as evidenced by the post shot cross sections in Fig. 3.16. The analysis at station 1 + 10 does not at all correlate with the observed damage. In this station, as can be seen in the cross section in Fig. 3.16, very major roof falls occurred. The geologic cross section at station 1 + 20 shows a profusion of B joints traversing the tunnel and a series of C joints intersecting the B joints in the roof. The jointing is closely spaced above the roof. The joint orientations are favorable to progressive stoping upwards. Thus, the predicted cross section for 1 + 20 shows a very large roof failure between 60-120° in the roof as well as rock movements inward from the walls above the invert. This pattern of fall-out agrees very closely with that actually observed at station 1 + 20, Fig. 3.16.

(5) Station 1 + 30 and Station 1 + 40 CR Tee - Figs. 3.11 and 3.12

The geology in section 1 + 30 is characterized by a series of I shears on the blast wall and a series of A joints inclined towards the blast and traversing the tunnel. This pattern of joints leads to a predicted rock breakage diagram which is not very consequential, consisting principally of a rock fall cathedralling upward between two shears at 100-120°. However, at station 1 + 40, a series of B joints occurred inside the blast wall. Existance of the joints is very well-known because of the log of the perpendicular leg of the Tee in CR north drift. These B joints can be projected from the north leg of the Tee into the wall to their precise positions. They do not continue to 1 + 30 because they are offset by another shear. The effect of the B joints in the wall is to create a large mass of rock bounded by sheared joint planes which could be accelerated into the opening. An inspection of the actual damage at station 1 + 40 in the cross sections of Fig. 3.16 reveals that a large kidney of broken rock supported only by the wire mesh occurred between 0° and 45°. The cross section also showed extensive falls from the lee roof. These are also inferred from the predicted blast damage of the joint analysis. In summary, it appears that the rock damage at 1 + 40 is very well predicted by the joint influence analysis.

(6) Station 1 + 50 CR Tee Intersection

The stress distribution in the Tee intersection is unknown and the joint influence diagram method cannot be applied to this station.

(7) Station 1 + 60 - Fig. 3.13

The geology of this section shows a series of A shears on the lee wall, a series of closely spaced H shears above the region of the lee wall at about 120-140°, and a series of B joints inside the blast wall. The B joints behind the blast wall are a major weakening factor and cause inward movement of rock material above and below 0°. In addition, rock blocks are expected to drop out of the roof at about 140° because of the effect of the H joints. The actual damage at this station can be seen in Fig. 3.16. There was extensive inward movement of rock and failure of rock bolts on the blast wall. In actual fact, the damage was much more extensive than that predicted by the

joint influence analysis. The effect of the Tee intersection on the stress distribution is not known; the use of the Kirsch solution for the stresses around the walls at this station is certainly not correct.

(8) Station 1 + 70 - Fig. 3-14

A, B, and G joints compose the geological section at 1 + 70. A joints are inclined toward the weapon point and primarily intersect only the lee wall. There are only two A joints intersecting the blast wall. Vertically inclined B joints occur at the crown and invert. These joints intersect A and G joints. The G joints traverse the tunnel and are inclined away from the weapon point. Joint influence analysis of 1 + 70 weighs heavily the intersection of A and B joints above the spring line on the lee wall (120°). Intersection A and G joints on the lee wall below the spring line (210°) also produce a weakened area. There are two other minor failure areas. These areas occur at the intersection of A and G joints on the blast wall near spring line (350°) and B and G joints above the spring line (20°). Rock falls are predicted in the roof at 120° and near the invert at 210°. Two minor fallout areas are also predicted in the blast wall at 20° and 350° near the spring line. Fig. 3.16a has no section at 1 + 70 since the last surveyed cross section is at 1 + 67. Section 1 + 67 shows rock falls in the roof. These falls begin just before the crown and extend to the lee wall near the spring line. Rubble so filled the rest of the tunnel that no further comparisons could be made. The visible portion of the tunnel generally conforms with what was predicted.

3.3 CR NORTH DRIFT - RESULTS OF ANALYSIS

CR North drift begins at the CR Tee intersection (station 1 + 52 of CR Drift) and heads towards the weapon point. Analyses were made every 10 feet beginning at station 1 + 60 in the north leg of CR Tee. The excavated diameters and lining types are shown in Table 3.5.

The absolute and relative orientations of joint sets were determined from Fig. 3.17, the pre-construction logs, as previously described for CR lateral drift. Table 3.6 presents the strike and dip data for the different stations. Table 3.7 lists the joint orientation parameters for construction of joint influence diagrams. Joint set H did not occur.

In this drift, the loading is considerably different than in CR lateral, as the applied pressures are less than half of the blast pressure and are hydrostatic (see Table 3.1).

Since this drift is oriented at right angles to CR laterial, the damaging B joints of CR lateral were of no significance in CR north. The I joints were also found to have no influence in the north drift. However, other joint sets were found to have even larger influence regions than in CR lateral. The joint influence diagrams for c = 100 psi and c = 1000 psi are plotted in Fig. 3.18a and b respectively.

(1) Station 1 + 60 North Leg of CR Tee - Fig. 3.19

The geology of this section shows a series of B joints on the right wall and several joints of sets C and G orientations traversing the tunnel. This section was supported by rock bolts. The joint influence analysis predicted breakage of the rock and falls from the right wall. The actual damage can be seen in Fig. 3.28, a long profile along the north drift, and Fig. 3.29, the set of post shock cross sections at varying stations. The cross section at station 1 + 61 shows very extensive damage in the right wall exactly where predicted by the joint influence analysis. (The right wall, looking towards the weapon point, is 0° by convention in CR north drift). The actual extent

of fall-in of rock at this station is much more extensive than predicted by the analysis. However, the agreement on location of damage is excellent.

(2) Station 1 + 70 Transition to Drill Slot - Fig. 3.20

This section is unlined. A series of E joints occur on the right wall at about 0°, inclined steeply from right to left. Another set of E joints cross the tunnel at the invert. It is possible that these are the same joints but have been offset along the shears of set I that occur above the roof. There are also a series of A joints crossing the tunnel at wide spacing. The joint influence analysis shows that the intersection of the A and E joints above the right wall defines an unstable block, and as this section is unlined, it was predicted that a major rock fall would occur from this position. There were no post shot cross section at exactly 1 + 70; however, in Fig. 3.29 there are cross sections at 1 + 67 and 1 + 66, both of which show extensive movement of rock from the roof, more towards the right than towards the left side.

(3) Station 1 + 80 CR North Drill Slot - Fig. 3.21

In this large diameter unlined section, a series of G joints cross the tunnel in vertical diameter and a series of A joints cross roughly horizontally. There are probably more A joints above the roof, but these were not seen. There is also an F joint and an E joint in the right wall. The analysis delimited an unstable block below the right spring line, along the intersection of the two latter joints. The actual damage pattern in the tunnel was very much like that at the previous station, 1 + 70, namely, extensive rock falls from the roof. It is not possible to determine if heave below the right spring line actually occurred as predicted by the analysis as this was covered with rubble.

(4) Station 1 + 90 CR North Drill Slot - Fig. 3.22

This cross section shows extensive jointing with G joints along the left wall, a series of A joints traversing the tunnel, and a shear zone of orientation I above the roof. The intersection of these features leads to an extreme rock breakage prediction, with very extensive rock movement from

the roof above the left wall and a high vault above the right wall. If the joints are considered to possess great cohesion, then the major rock movements remain only in the left wall. The actual damage at this location can be studied on the post shock cross section at station 1 + 92, Fig. 3.29. There is remarkable agreement between the prediction from the joint analysis and the actually observed post shock cross section. It is quite probable that this section would have survived, had it been rock bolted.

(5) Station 2 + 00 to 2 + 38 CR5 and CR6 Drift

The joint influence analysis for station 2 + 00, 2 + 10, 2 + 20, 2 + 30 and 2 + 38 are presented in Figs. 3.23 to 3.27. No extensive damage is predicted at any one of these locations. Though small blocks were delimited by the intersections of unstable joints, it is considered that the direction of the blast would not be such as to cause a small volume of rock to penetrate the wire mesh or pull out the rock bolts. No very large volumes of rock slipping on joints were delimited in the roof or walls and it was believed, in making the analysis, that the wire mesh and rock bolts would be sufficient to handle them. The post shock cross sections for these stations can be seen in Fig. 3.29. There was virtually no distortion or rock falling in these drifts, but the entire drifts were displaced upwards. There is no way that the joint influence analysis can foresee absolute movement of an entire drift.

3.4 DL 1 AND 2 - RESULTS OF ANALYSIS

DL drift is a lateral drift at closer range than CR. Analyses were made every 10 feet in DL 1 and 2, 16 foot diameter rock bolted sections, from station 0 + 50 to 0 + 80.

Fig. 3.30 is a geological log of the walls of DL 1 and DL 2 made before the blast by Corps of Engineers geologists. The data shown on the log were extrapolated beyond the walls, allowing geologic cross sections to be drawn at stations 0 + 50, 0 + 60, 0 + 70 and 0 + 80 (Figs. 3.32 to 3.35). The joints were divided into five sets, A, B, C, D, E, on the basis of orientation as summarized in Table 3.8. Zone F is a group of closely spaced A joints; it probably represents a fault. (The nomenclature of joints is entirely different from that adopted in the previous discussion of CR drift.)

Unfortunately, B joints parallel the tunnel axis and cannot be seen in the roof. Post shock study of DL revealed the occurrence and significant role played by B joints in the roof, particularly above the unreinforced drill slot (not analyzed here).

Joint influence regions for this drift are plotted in Fig. 3.31. Application of this figure to the geologic sections in the manner previously described resulted in the post shock predictions of Figs. 3.32 to 3.35. Major roof falls are predicted at stations 0 + 60 and 0 + 70, and a major rock bolt failure is predicted on the lee side from 0 + 70 to 0 + 80.

The actual damage can be studied in Fig. 3.36, the post shot longitudinal profile, and Fig. 3.37, the post shot cross sections in DL 1 and 2. In these sections, the weapon point is to the right; the post shot predictions, unfortunately, were prepared with the weapon point to the left. So, an inversion of either figure set will be needed to make a comparison.

Rock movement in the rock bolted sections was manifested by: 1) wholesale inward displacement of seemingly intact walls; 2) rock breakage and fall-out at the surface, but sustained by the chain link fabric; 3) rock breakage and fall-out not sustained by the chain link fabric; and 4) rock bolt failure with inward bulging of the wall and pull-away of the rock bolt washer plates from the fabric.

Failure type (3) occurred extensively in the crown from the drill slot to station 0 + 66, the vaulted roof reaching an estimated maximum of 15 feet above the pre-shot crown in the drill slot. This may have been a progressive failure propagating into DL 1 from the less reinforced and larger drill slot opening. A and B joints controlled the rock breakage.

Failure type (4) occurred on the lee wall mainly between 0 + 70 and 0 + 85 in DL 2. Floor heave occurred extensively throughout the drifts.

The multiple depth rock deformeters at station 0 + 70 were destroyed on the lee wall (180°) and in the invert (270°). The response of the blast wall (0°) and the crown (90°) indicates that most of the permanent rock movement at these points occurred within the first 3 feet of depth.

The predicted post shock cross sections have several points of agreement with the observed deformations. Crown failure in DL 1 was much more extensive than the predicted fall-out. This is particularly true at station 0 + 50, where the crown should have held except for pyramiding upward along

the A and C joints above the lee shoulder. The roof failure may have been a progression from the drill slot or may reflect occurrence of several B joints in the roof; as previously noted, these joints parallel the tunnel, therefore cannot be predicted above the tunnel by observations on the walls. In cross sections at 0 + 70 and 0 + 80, the observed movement of the lee wall and bolt failures therein is grossly matched by the predicted cross sections based on joint influence analysis.

3.5 SUMMARY OF RESULTS

The predicted and actual damage patterns in CR East West drift, CR North drift and DL drift are compared in Tables 3.9, 3.10, and 3.11. The joint influence analysis predictions of tunnel damage will not stand up under very detailed comparisons with the actual damage. But in gross features, the comparison is good. It must be noted that the analysis is very sensitive to the quality of geological information. The geological data presented are very complete in comparison with usual geological studies performed for other types of works. However, considerably more detail about the locations and continuity of individual joints and shears is required to refine the quality of the results.

Table 3.1

APPLIED PRESSURES TO DEVELOP

STRESS DISTRIBUTIONS USED IN JOINT ANALYSIS

Sections	Applied Pressures		
	Radial - 0°	Radial - 90°	Longitudinal
DL and CR (EW)	P	$(\nu/1-\nu)P$	$(\nu/1-\nu)P$
CR (North)	$(\nu/1-\nu)P$	$(\nu/1-\nu)P$	P

P = peak pressure of blast

ν = Poisson's ratio

Table 3.2

CR (EW) DRIFT - LINING TYPE AND TUNNEL DIMENSIONS

Section	Station	Excavated Diameter	Lining
CR 1, 1a	0 + 20 - 0 + 54	16'	Reinforced concrete lining with cellular concrete backpacking
CR 3, 4	0 _ 54 - 0 + 94	16'	16' rock bolts at 2.0'
CR 2	0 + 94 - 1 + 12	16'	Unlined
Drill Slot	1 + 12 - 1 + 27	18'	Unlined
CR "T"	1 + 27 - 1 + 67	13'	12' rock bolts at 2.0' (1 + 27 - 1 + 52)
Transition	1 + 67 - 1 + 77	9'3"	Unlined
CR 7	1 + 77 - 1 + 94	9'3"	Composite liner (7' I.D.)
LPI	1 + 94 - 2 + 19	9'3"	Alcove - unlined

Table 3.3

Drift CR - Lateral Joint Set Strikes and Dips at Each Station

Strike

	"A"	"B"	"C"	"D"	"E"	"F"	"G"	"H"	"I"
0+20	N53W(12)	N62W(13)	N32E(4)	N72E(2)	-	-	-	-	N40W(1)
0+30	N50W(5)	N68W(7)	N31E(3)	N72E(3)	N 5E(1)	-	-	-	N41W(4)
0+40	N50W(5)	N67W(5)	N19E(4)	N82E(1)	N 0E(6)	-	-	-	N41W(3)
0+50	N44W(3)	N75W(3)	N19E(1)	-	N46E(6)	N38W(1)	-	-	N29W(1)
0+60	N 0W(8)	N78W(4)	N21E(3)	N85E(3)	N46E(6)	N38W(1)	-	-	N8W (1)
0+70	N 7W(7)	N79W( )	N13E(5)	N80E(1)	N49E(9)	N38W(1)	-	-	-
0+80	N48W( )	N73W(7)	N13E(3)	-	N45E(5)	-	N35E(14)	-	-
0+90	N50W(5)	N73W(10)	-	-	N44E(8)	-	-	-	-
1+00	N 3W(7)	N74W(2)	N 0E(5)	-	N45E(2)	-	N 1E(2)	-	-
1+10	N 9W(8)	N80W(2)	N12E(12)	-	-	-	-	-	-
1+20	N61W(10)	N81W(16)	N10E(9)	-	-	-	N 1E(2)	-	N 2W(2)
1+30	N49W(4)	N83W(1)	-	-	-	-	-	-	N27W(3)
1+40	N 9W(7)	N79W(3)	N13E(1)	-	-	-	N33E(1)	-	-
1+50	N 9W( )	N72W(1)	-	-	-	-	-	-	-
1+60	N 1W(7)	N76W(7)	-	N 4E(1)	-	-	N26E(1)	N53W(1)	N23W(2)
1+70	N 2W(6)	N70W(10)	-	-	-	-	N 2E(9)	-	-
1+80	N 1W(3)	N65W(9)	-	-	N 5E(2)	-	N48W(5)	-	-
1+90	N 9W( )	N64W(8)	N 2E(3)	-	-	-	N46E( )	-	-
2+00	N 2W(1)	N61W( )	N9E( )	-	-	-	N42E(3)	N7 W(1)	-
2+10	N48W( )	N71W(6)	N 0E(1)	-	N60E(1)	N43W(4)	-	N87W(1)	-
2+19	N47W(4)	N73W(4)	-	-	N30E(1)	-	N42E(1)	N87W(1)	N47E(1)

Dip

	"A"	"B"	"C"	"D"	"E"	"F"	"G"	"H"	"I"
0+20	27NE(12)	88SW(3)	77NW( )	62SE(2)	-	-	-	-	Vert(1)
0+30	28NE( )	83SW(7)	62NW( )	64SE(3)	46NW(1)	-	-	-	89NE(1)
0+40	29NE(5)	Vert( )	66NW(4)	69SE(4)	67NW(6)	-	-	-	89NE(3)
0+50	32NE(3)	85NE(3)	66NW(1)	-	67NW(2)	-	-	-	80SW(1)
0+60	26NE(3)	79SW( )	76NW(3)	74SE(3)	61NW(6)	48NE(1)	-	-	77SW(1)
0+70	29NE(7)	78SW(4)	68NW( )	71SE(1)	56NW(9)	49NE(1)	69SE(8)	-	-
0+80	29NE( )	84SW(7)	66NW(3)	-	55NW( )	-	67SE(14)	-	-
0+90	30NE( )	88SW(10)	-	-	56NW(3)	-	-	-	-
0+00	29NE(7)	Vert(2)	74NW(5)	-	55NW(2)	-	84SE(2)	-	-
0+10	31NE(8)	Vert( )	70NW(14)	-	-	-	-	-	-
1+20	26NE(10)	89SW(16)	67NW(9)	-	-	-	78SE( )	-	74SW(2)
1+30	30NE(4)	Vert(1)	-	-	-	-	-	-	79SW(3)
1+40	30NE(7)	Vert(3)	59NW(1)	-	-	-	69SE(1)	-	-
1+50	30NE( )	88NE(1)	-	-	-	-	-	-	-
1+60	31NE(7)	87NE(7)	-	73SE(1)	-	-	69SE(1)	69SE(1)	87SW(2)
1+70	31NE(6)	84NE(10)	-	-	-	-	68SE(9)	-	-
1+80	27NE(3)	Vert(9)	-	-	54NW(2)	-	55SE(5)	-	-
1+90	28NE(4)	83NE(8)	48NW( )	-	-	-	61SE(4)	-	-
2+00	21NE(1)	Vert(3)	70NW( )	-	-	-	60SE(3)	6 NE(1)	-
2+10	30NE( )	79SW(6)	66NW(1)	-	3 NW(1)	9NE	-	89NE(1)	-
2+19	30NE(4)	98SW( )	-	-	46NW(1)	-	79SE(1)	9NE(1)	89SW(1)

( ) total joints considered

Table 3.4

Drift CR - Lateral - Joint Orientation Parameters

STA	Joint Set	σ°	D°	θ°	β°
(12) 0+20	A	6	27	26.8	87
(5) 0+30		9	28	27 6	86
(5) 0+40		14	29	28.3	83.3
(3) 0+50		20	32	30.4	79.6
(8) 0+60		14	26	25.3	83.9
(7) 0+70		16	29	28.0	82 3
(5) 0+80		16	29	28.0	82.3
(5) 0+90		14	30	29.2	83.1
(7) 1+00		11	29	28.5	84.7
(8) 1+10		15	31	30.0	82.5
(10) 1+20		7	25	24.7	86.0
(4) 1+30		19	30	28.6	81.2
(7) 1+40		19	30	28.6	81.2
(5) 1+50		19	30	28.6	81.2
(7) 1+60		17	31	29.8	81.4
(6) 1+70		16	31	30.0	81.8
(3) 1+80		17	27	26.0	82.3
(4) 1+90		19	28	26.7	81.2
(1) 2+00		16	24	23.4	83.6
(5) 2+10		11	30	29.9	84.5
(4) 2+19		12	30	28.5	84.0
121 Mean or range;				27.9	83.0

Joint Set	σ°	D°	θ°	β°
(13) B	-3	88	88.0	-87
(7)	-9	83	82.8	-81.1
(5)	-3	90	90.0	-87.0
(3)	-11	-85	-84.8	79.0
(4)	-14	79	78.7	-76.3
(4)	-15	78	77.6	-75.4
(7)	-9	84	83.8	-81.1
(10)	-9	88	88.0	-81.5
(2)	-10	90	90.0	-80.0
(2)	-16	90	90.0	-74.0
(16)	-13	89	89.0	-77.0
(1)	-15	90	90.0	-75.1
	-11	90	90.0	-79.0
(1)	-4	-88	-39.0	86.0
(7)	-8	-87	-87.0	82.0
(10)	-2	-84	-84.0	88.1
(9)	+3	90	90.0	87.0
(8)	+4	+88	84.0	86.0
(3)	+7	90	90.0	83.0
(6)	-3	79	79.0	-87.0
(4)	-5	88	88.0	-85.0
(125)			+86.4	81.3
			-55.2	83.7

Joint Set	σ°	D°	θ°	β°
(4) C	-89	-77	-4.2	13
(3)	90	-62	0	-28
(4)	83	-66	-15.2	-25
(1)	83	-66	-15.2	-25
(3)	85	-76	-19.3	-15
(5)	77	-68	-29.0	-25.5
(3)	77	-66	-26.7	-27.3
-	-	-	-	-
(5)	74	-74	-41.8	-22.5
(12)	76	-75	-41.9	-20.5
(9)	78	-67	-25.9	-25.7
-	-	-	-	-
(1)	81	-59	-14.4	-32.2
	-	-	-	-
	-	-	-	-
	-	-	-	-
	-	-	-	-
(3)	80	-48	-10.8	-43.0
(2)	77	-50	-14.9	-41.7
(11)	89	-46	-1.0	-44.0
	-	-	-	-
(56)			-10.2	-40.2
				(4)

STA	Joint Set	σ°	D°	θ°	β°
(2) 0+20	D	-49	62	51.0	-48.4
(3) 0+30		-49	68	53.4	-47.4
(6) 0+40		-34	69	65.1	-53.6
0+50		-	-	-	-
(3) 0+60		-31	71	71.5	-60.4
(1) 0+70		-36	71	66.8	-56.4
0+80		-	-	-	-
0+90		-	-	-	-
1+00		-	-	-	-
1+10		-	-	-	-
1+20		-	-	-	-
1+30		-	-	-	-
1+40		-	-	-	-
1+50		-	-	-	-
(1) 1+60		-58	73	60.0	- 6.0
1+70		-	-	-	-
1+80		-	-	-	-
1+90		-	-	-	-
2+00		-	-	-	-
2+10		-	-	-	-
2+19		-	-	-	-
(16) Mean or Range:				62.0	75.0
				67.0	60.0

Joint Set	σ°	D°	θ°	β°
E	-	-	-	-
(1)	-66	-46	-22.7	59.1
(6)	-66	-57	-31.9	40.3
(2)	-66	-57	-31.9	40.3
(6)	-70	-61	-31.6	35.0
(9)	-67	-56	-30.0	0.5
(5)	-71	-55	-24.8	39.4
(8)	-72	-55	-23.8	39.0
(2)	-71	-55	-24.8	39.4
	-	-	-	-
	-	-	-	-
	-	-	-	-
	-	-	-	-
	-	-	-	-
	-	-	-	-
	-	-	-	-
(5)	-47	-54	-36.8	47.5
	-	-	-	-
	-	-	-	-
(1)	-61	-35	-18.8	60.0
	-	-	-	-
(42) Mean			-31.0	40.0
			-23.0	40.0

Joint Set	σ°	D°	θ°	β°
- F	-	-	-	-
	-	-	-	-
	-	-	-	-
	-	-	-	-
(1)	26	48	55.0	71 0
(1)	26	48	55.0	71.0
	-	-	-	-
	-	-	-	-
-	-	-	-	-
-	-	-	-	-
-	-	-	-	-
-	-	-	-	-
-	-	-	-	-
-	-	-	-	-
-	-	-	-	-
-	-	-	-	-
-	16	59	58.0	76.4
(4)	-	-	-	-
(6)			50	72

Table 3.4 Continued

Drift CR-Lateral

STA	Joint Set	σ°	D°	θ°	β°	Joint Set	σ°	D°	θ°	β°	Joint Set	σ°	D°	θ°	β°
0+20	G	-	-	-	-	H	-	-	-	-	(1) I	19	90	90	71.0
0+30		-	-	-	-		-	-	-	-	(4)	18	89	89.0	72.0
0+40		-	-	-	-		-	-	-	-	(3)	23	89	88.9	67.0
0+50		-	-	-	-		-	-	-	-	(1)	35	-80	-77.9	-55.7
0+60		-	-	-	-		-	-	-	-	(1)	56	-77	-67.6	-36.4
(8) 0+70		-84	65	+12.6	-25.9		-	-	-	-		-	-	-	-
(14) 0+80		-81	67	+20.3	-24.6		-	-	-	-		-	-	-	-
0+90		-	-	-	-		-	-	-	-		-	-	-	-
(2) 1+00		-75	84	68.1	-16.4		-	-	-	-		-	-	-	-
1+10		-	-				-	-	-	-		-	-	-	-
(2) 1+20		-71	75	50.5	-24.1		-	-	-	-	(2)	46	-74	-67.6	-46.4
1+30		-	-	-	-		-	-	-	-	(3)	41	-79	-75.6	-50.0
(1) 1+40		-79	65	22.2	-27.5		-	-	-	-		-	-	-	-
1+50		-	-	-	-		-	-	-	-		-	-	-	-
(1) 1+60		-90	64	0	-25.0	(1)	15	-65	-64.2	-76.5	(2)	45	-85	-82.8	-45.
(2) 1+70		-60	68	51.2	-36.7		-	-	-	-		-	-	-	-
(1) 1+80		-64	55	32.0	-42.8		-	-	-	-		-	-	-	-
(1) 1+90		-66	51	26.5	-45.0		-	-	-	-		-	-	-	-
(1) 2+00		-70	60	30.6	-35.7	(1)	-7	-65	-64.8	83.7		-	-	-	-
2+10		-	-	-	-	(1)	-28	-59	-55.8	23.0		-	-	-	-
(1) 2+19 (50)		-79	59	17.6	-33.1	(1) (4)	-28	-59	-55.8	23.0	(1) (18)	12	-89	-89.0	-78.0
Mean or Range:				30.0	-40.0				-65	80				-76.7	51.9
				51	-37									89.0	70.0
				18	-33										

Note: Joints cease to have any weakening effect if their angle with the tunnel axis (β) is less than 30°.[16]

[16] op. cit., p.1

Table 3.5

CR NORTH DRIFT - LINING TYPES AND TUNNEL DIMENSIONS

Section	Station	Excavated Diameter	Lining
CR "T"	1 + 52 - 1 + 67	13'	12' rock bolts at 2' 12' rock anchor at 2'
Transition	1 + 67 - 1 + 75	13'	Unlined
Drill Slot	1 + 75 - 1 + 93	18'	Unlined
Transition	1 + 93 - 1 + 98	16'	Unlined
CR 5, 6	1 + 98 - 2 + 38	16'	16' rock bolts at 2'

Table 3.6

Drift CR-North Joint Set Strikes and Dips at Each Station

Strike

Sta	A	B	C	D	E	F	G	H	I
1+60	N[illegible]W(4)	N62W( )	N32E(3)	-	N3[illegible]E(3)	-	N35E(3)	-	-
1+70	N[illegible]W(4)	N70W( )	-	-	N41E(5)	-	N39E(3)	-	N15W(2)
1+80	N[illegible]W(7)	N[illegible]W(1)		-	N57E(1)	-	N36E(3)	-	-
1+90	N[illegible]W(7)	N6[illegible]W( )		-	-	-	N40E(16)	-	N[illegible]W(2)
2+00	N[illegible]OW(7)	-	-	-	N50E(1)	-	N3 E(2)	-	N[illegible]9W(1)
2+10	N53W( )	-	N30E(1)	-	N[illegible]8E( )	-	N[illegible]2E(3)	-	N16W(3)
2+20	N[illegible]W(6)	-	-	N84E(5)	N50E(3)	-	N[illegible]4E(1)	-	N10W(1)
2+30	N[illegible]W(10)	-	-	N88E(4)	N50E(4)	N21W(1)	N30E(1)	-	N7W(10)
2+38	N[illegible]W(6)	-	-	-	-		-	-	N9W(15)
Mean:	N[illegible].3W	N6[illegible].7W	N[illegible]E	N86E	N[illegible]5.6E		N36.1E		N9.4W N[illegible]3.6

Dip

	A	B	C	D	E	F	G	H	I
[illegible]	[illegible]NE( )	86NE( )	89SE( )	-	62NW(3)	-	63SE(3)	-	-
1+70	[illegible]NE( )	86NE( )	-	-	[illegible]8NW( )	-	86SE(3)	-	8[illegible]SW(2)
1+80	[illegible]2NE(7)	Vert(1)	-	-	80NW(1)	-	Vert(3)	-	-
1+90	[illegible]2NE(7)	8[illegible]NE( )	-	-	-	-	88SE(10)	-	83SW( )
2+00	[illegible]2NE(7)	-	-	-	[illegible]1NW(1)	-	79SE(2)	-	8[illegible]SW(1)
2+10	[illegible]NE( )	-	ONW(1)	-	[illegible]4NW(4)	-	7[illegible]SE(3)	-	78NE(3)
2+20	[illegible]NE(6)	-	-	8[illegible]SE( )	8NW( )	-	87SE(1)	-	87NW(1)
2+30	80NE(10)	-	-	86SE( )	[illegible]8NW( )	52NE(1)	85NE(1)	-	8[illegible]SW(10)
2+38	[illegible]NE(6)	-	-	-	-	-	-	-	87SW(15)
Mean:	[illegible]. NE	87.1NE	89SE	8[illegible]SE	[illegible]9.1W		8[illegible].5NE		87.6SW 8[illegible]SW

( ) total joints considered

Table 3.7

Drift CR-North — Joint Orientation Parameters

	STA	Joint Set	σ°	D°	θ°	β°	Joint Set	σ°	D°	θ°	β°	Joint Set	σ°	D°	θ°	β°
(3)	1+60	A	-63	34	17.0	-60.2	(4) B	90	86	0	4.0	(1) C	0	89	89	90
(4)	1+70		-63	34	17 0	-60.2	(1)	88	86	25.8	5.0	(1)	-	-		
(7)	1+80		-76	31	8.3	-60.1	(3)	-77	90	90	13.0		-	-		
(7)	1+90		-75	31	8.8	-60.2	(5)	-84	88	71.4	7.0		-	-		
(7)	2+00		-72	31	10.5	-60.7		-	-							
(8)	2+10		-75	31	8.8	-60.2		-	-			(1)	8	90	89.8	83.9
(6)	2+20		-73	35	11.5	-56.8		-	-				-	-		
(10)	2+30		-76	30	8.0	-61.1		-	-				-	-		
(6)	2+38		-76	31	8.3	-60.1		-	-				-	-		
	Mean				10 0	-60.1									89.8	83.9

	STA	Joint Set	σ°	D°	θ°	β°	Joint Set	σ°	D°	θ°	β°	Joint Set	σ°	D°	θ°	β°
	1+60	D	-	-			(3) E	13	62	61.4	78.7	F	-	-		
	1+70		-	-			(5)	19	58	56.6	74.0		-	-		
	1+80		-	-			(1)	35	80	77.9	57.4		-	-		
	1+90		-	-				-	-	-	-		-	-		
	2+00		-	-			(1)	28	51	47.6	68.6		-	-		
	2+10		-	-			(4)	26	54	51.0	69.3		-	-		
(5)	2+20		62	-85	-79.9	-28.8	(3)	28	58	54.7	66.6		-	-		
(4)	2+30		66	-86	-80.1	-25.0	(4)	28	58	54.7	66.6	(1)	-43	52	43.1	-57.6
	2+38		-	-				-	-	-	-		-	-		
	Mean									56.2	70.3				43.1	-57.6

	STA	Joint Set	σ°	D°	θ°	β°	Joint Set	σ°	D°	θ°	β°
(3)	1+60	G	13	-63	-62.6	-78.5	I	-	-	-	-
(3)	1+70		17	-86	-54.0	-73.1	(2)	-37	-85	-83.7	53.3
(8)	1+80		14	90	90	-76.0		-	-	-	-
(16)	1+90		18	-78	-69.8	-72.0	(2)	-63	-83	-74.9	28.0
(2)	2+00		13	-79	-78.7	-77.3	(1)	-71	-84	-55.8	20.0
(3)	2+10		20	-74	-73.0	-70.8	(3)	-38	78	-74.9	53.1
(1)	2+20		22	-87	-86 7	-68.0	(1)	-32	-87	-86.5	58.1
(1)	2+30		8	-85	-85.0	-82.1	(10)	-29	-85	-84.3	61.3
	2+38		-	-		-	(15)	-31	-87	-86.5	59.1
	Mean				-74.2	-74 2				-84.1	59.1

No jt failure

( ) total joints considered

Note: Joints cease to have any weakening effect if their angle with the tunnel axis (β) is less than 30°.[17]

[17] op.cit. p. 1

Table 3.8

DL1 and DL2 Joint Set Orientation

Joint Set	θ*	β**	Total Joints Averaged (θ)
"A"	85.0°	60°	23
"B"	29.5°	90°	4
"C"	-50.0°	45°	13
"D"	-21.0°	68°	2
"E"	-70.0°	34°	2

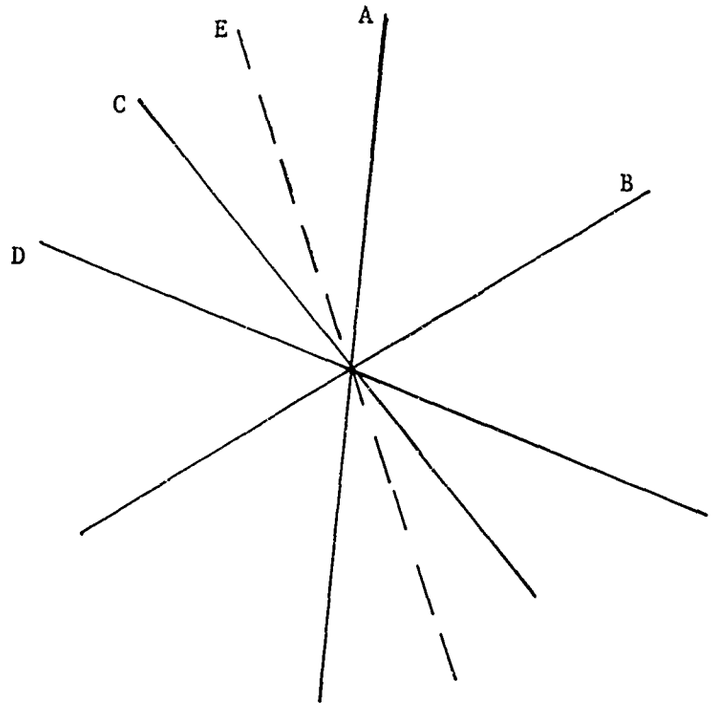

*Trace of joint in plane normal to tunnel axis -- positive counter-clockwise from horizontal

**Angle of joint normal with tunnel axis

Table 3.9

PREDICTED AND ACTUAL TUNNEL DAMAGE -- CR (E-W)

Section	Support	Predicted Damage (Ubiquitous Joint Method - c = 100 psi)	Actual Damage	Agreement
0 + 60	Rock bolts	Local bulging of chain link fabric	Similar to predicted except for 3' heaving of invert	Good
0 + 70	Rock bolts	Crown failure, local bulging of chain link fabric along blast side of tunnel	Slight crown failure; 2' inward bulging along blast side of tunnel, 2' heaving of invert	Good
0 + 80	Rock bolts	Local bulging of chain link fabric at crown	3' inward bulging along blast wall; 1' heaving of invert	Fair
0 + 90	Rock bolts	Crown failure with cathedral overbreak	Major crown failure and breakage from lee wall	Fair
1 + 00	Unlined	Limited crown failure extending maximum of 4' beyond tunnel; local failures near invert	Crown failure extending 7' into rock	Fair
1 + 10	Unlined	Local side failure on side opposite blast (pyramiding)	Major crown failure extending 8' into rock	Poor
1 + 20	Unlined	Major crown failure extending 7' above tunnel	Major crown failure extending 5' into rock	Good
1 + 30	Rock bolts	Local bulging of chain link fabric at crown	Minor crown failure exten- 2'; heaving of invert	Good
1 + 40	Rock bolts	Local bulging of chain link fabric at crown and bulging along blast wall	3' inward bulging along blast wall; 4' heaving of invert	Good
1 + 60	Rock bolts	Local bulging of wall opposite blast and blast wall	Inward movement of wall on blast side; tunnel filled with rubble; wall opposite blast remained intact and stable	Poor

Table 3.9 (cont.)

Section	Support	Predicted Damage (Ubiquitous Joint Method - c = 100 psi)	Actual Damage	Agreement
1 + 70	Unlined	Local wedge-shaped crown failure 4' into rock, minor failure on both walls 2' or less into rock	Inward movement of wall on blast side; 3' of crown failure; tunnel filled with rubble	Poor

Table 3.10

PREDICTED AND ACTUAL TUNNEL DAMAGE -- CR (NORTH)

Section	Support	Predicted Damage (Ubiquitous Joint Method - c = 100 psi)	Actual Damage	Agreement
1 + 60	Rock bolts	7' neck shaped failure at spring line along east wall of tunnel	Similar to predicted damage, heaving of invert	Good
1 + 70	Unlined	5' wedge slip-out at spring line along east wall of tunnel	Major rock fall above right wall	Good
1 + 80	Unlined	East wall: minor failure of 3' wedge at spring line and major failure of 10' wedge near invert	Extensive rock falls from the roof	Fair
1 + 90	Unlined	West wall: major failure of 8' wedge at spring line extending to invert elevation; 8' block failure at crown	Extensive rock fall from the roof	Good
2 + 00	Rock bolts	Bulging of chain link fabric extending from crown and 2/3 around west wall	Heaving of invert with equal displacement of crown	Fair
2 + 10	Rock bolts	Bulging of chain link fabric along west wall spring line	Heaving of invert with equal displacement of crown	Good
2 + 20	Rock bolts	Bulging of chain link fabric along west wall spring line and near invert of east wall	Heaving of invert with equal displacement of crown	Good
2 + 30	Rock bolts	Bulging of chain link fabric at crown and along east wall from tunnel spring line to invert	Heaving of invert with equal displacement of crown	Good
2 + 38	Rock bolts	Same as previous	Same as previous	Good

Table 3.11

PREDICTED AND ACTUAL TUNNEL DAMAGE -- DL 1 AND 2

Section	Support	Predicted Damage (Ubiquitous Joint Method - c = 100 psi)	Actual Damage	Agreement
0 + 50	Rock bolts	Bulge from above lee wall	Major roof cave-in	Poor
0 + 60	Rock bolts	Major roof fall	Major roof cave-in	Fair - Good
0 + 70	Rock bolts	Major roof fall; inward bulge of rock from lee wall	Minor roof fall and rock bolt failure high in lee wall	Good
0 + 80	Rock bolts	Inward bulge of rock from lee wall	Minor roof falls and inward bulge of rock from lee wall	Good

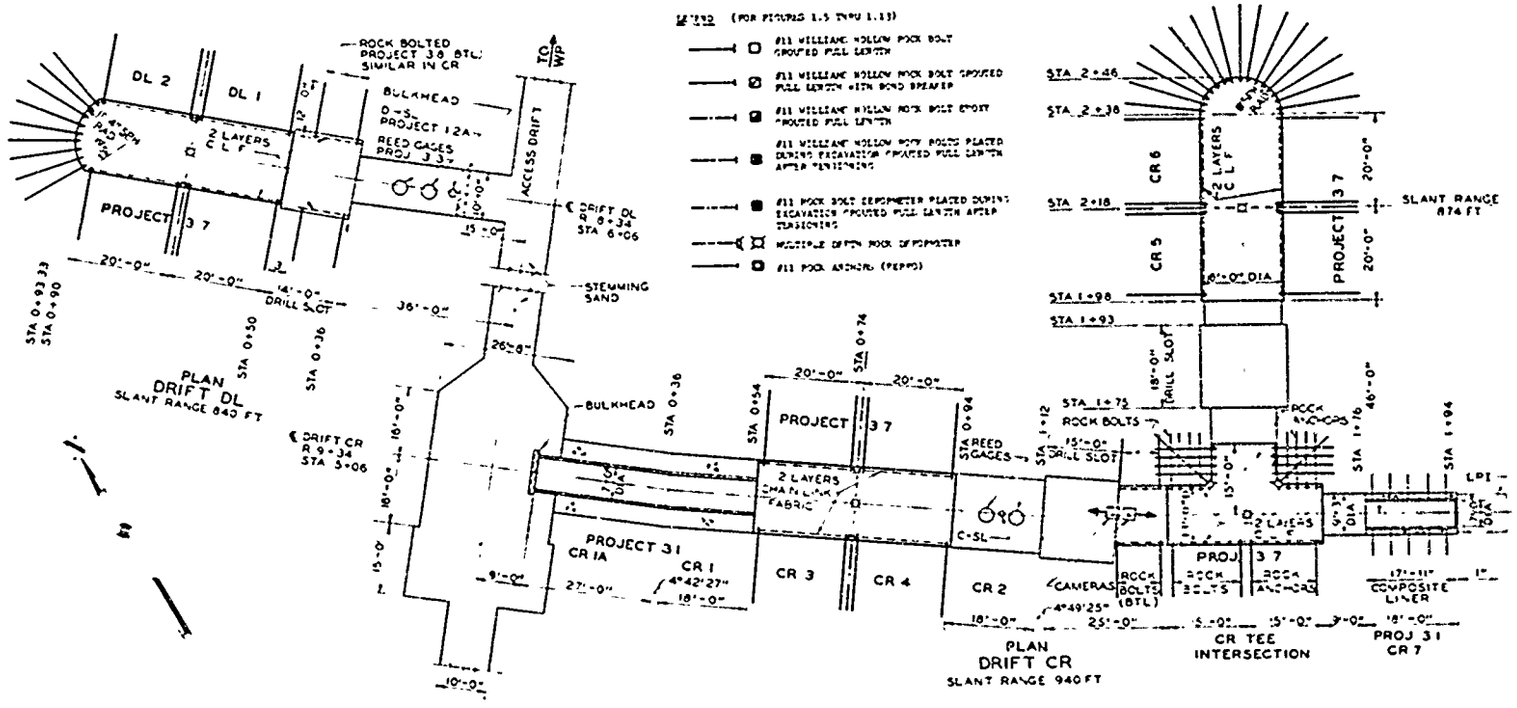

Fig. 3.1a General Plan

(Fig. 1.5 of POR 4015, Chapter 4)

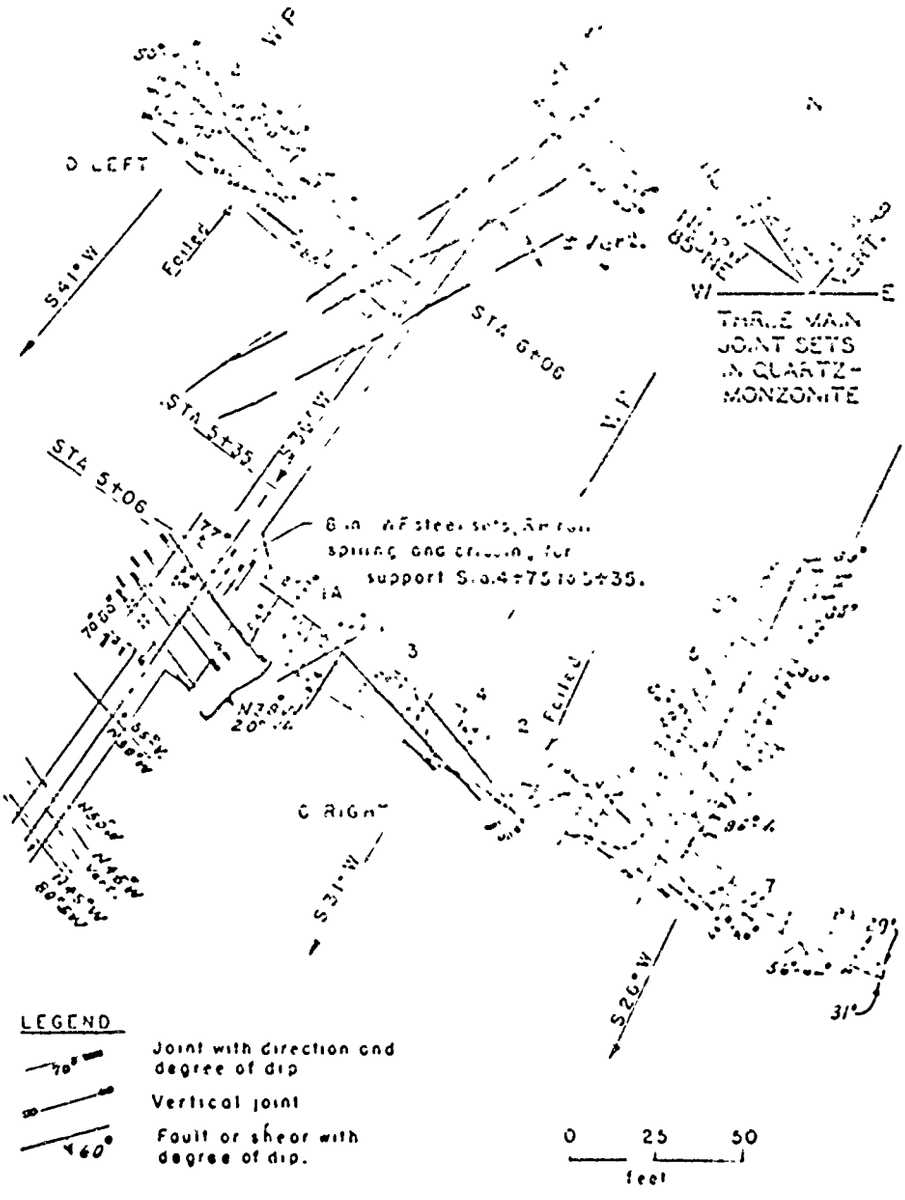

Figure 3.1b Plan of structural geology in vicinity of CR and DL Drifts

(Fig. 2,3 of POR 4015, Chapter 4)

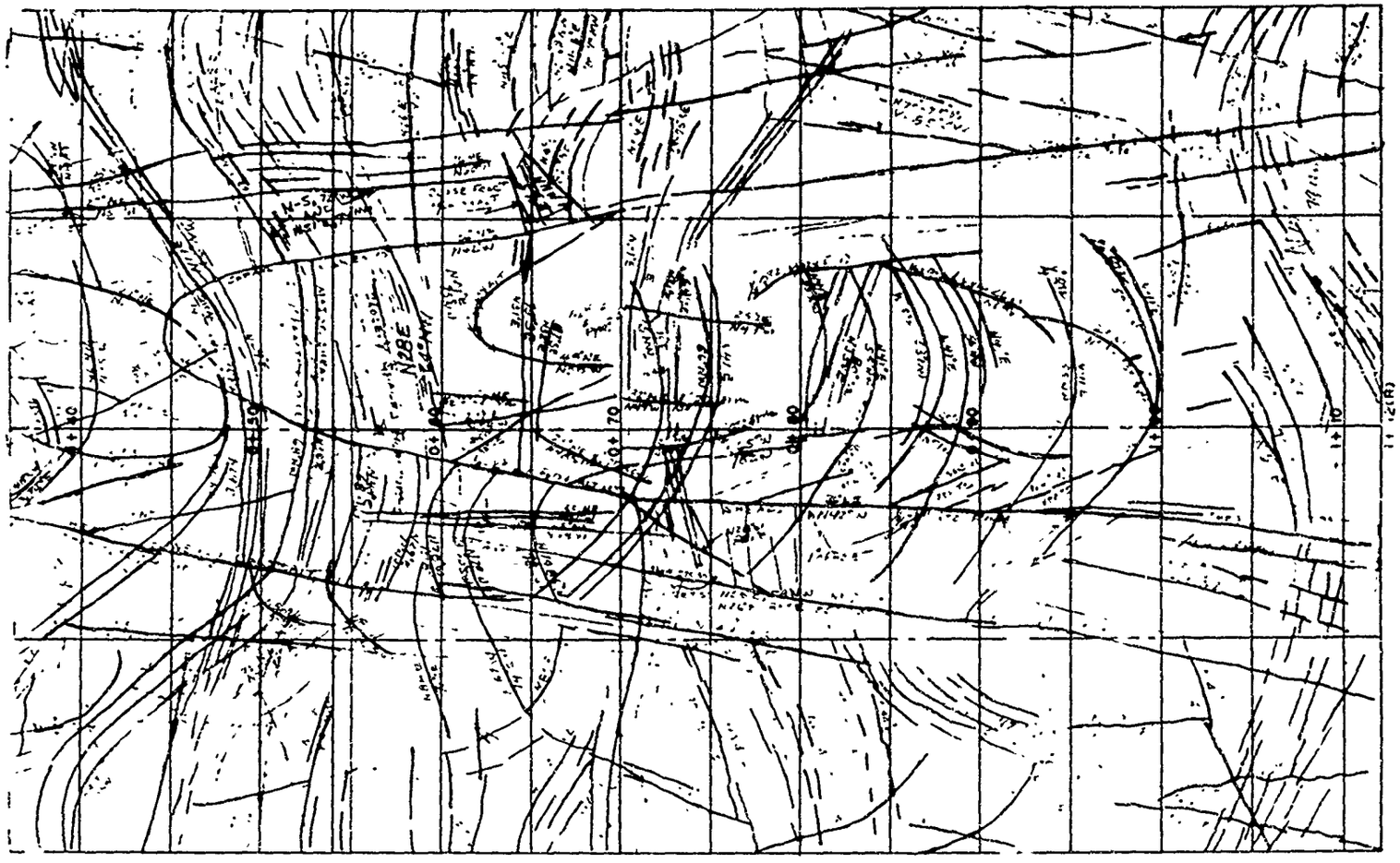

FIGURE 3.1 c GEOLOGICAL LOGS CR EAST WEST DRIFT
STATION 0+37 TO 1+12

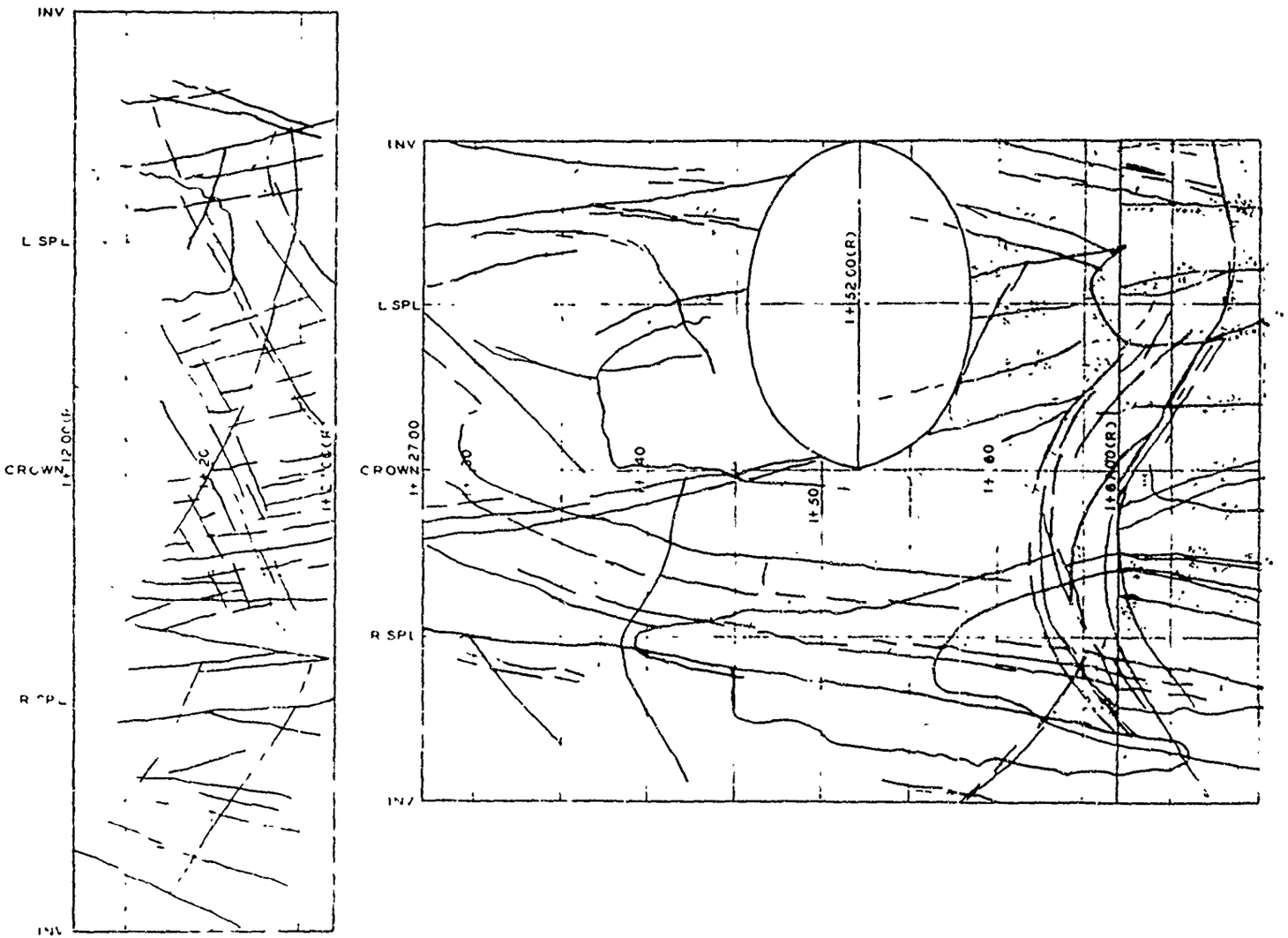

FIGURE 3.1 d GEOLOGICAL LOGS CR EAST WEST
STATION 1+12 TO 1+76

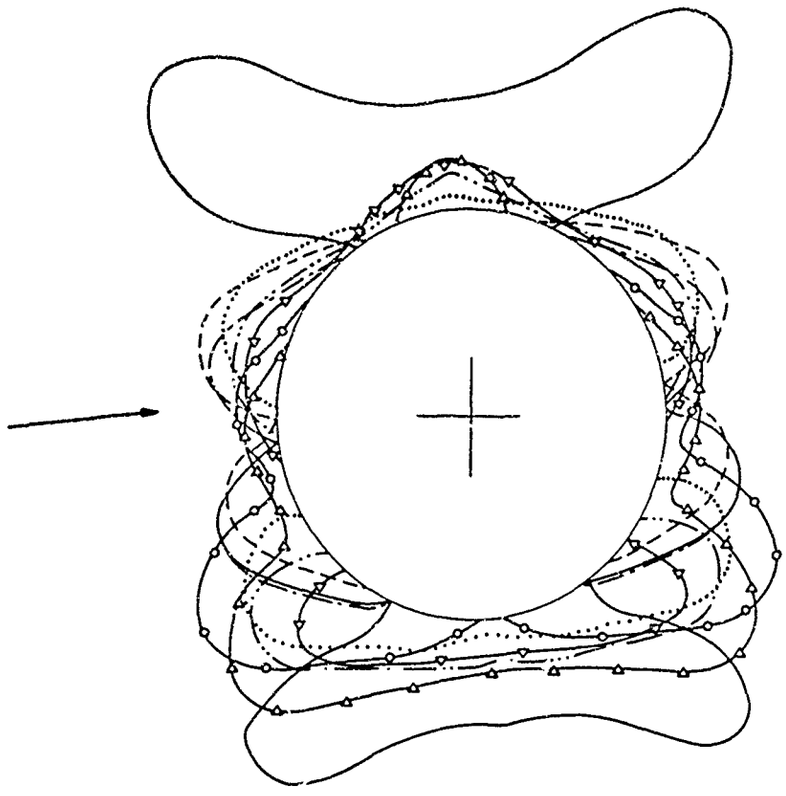

a

A Θ = 28°, β = 83°
B1 Θ = 86°, β = 81°
B2 Θ = -85°, β = 84°
C Θ = -10°, β = -40°
D1 Θ = 52°, β = 48°
D2 Θ = -67°, β = 60°
E1 Θ = 31°, β = 40°
E2 Θ = 23°, β = 40°

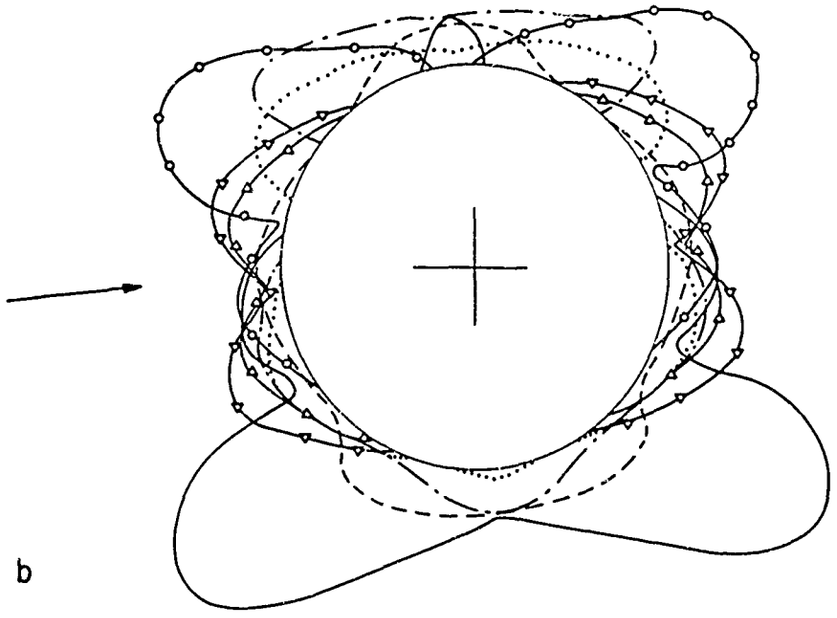

b

F Θ = 50°, β = 72°
G1 Θ = 30°, β = -40°
G2 Θ = 51°, β = -37°
G3 Θ = 18°, β = -33°
H Θ = -65°, β = 80°
I1 Θ = -77°, β = 52°
I2 Θ = 89°, β = 70°

FIGURE 3.2 JOINT INFLUENCE DIAGRAMS CR LATERAL
10,000 PSI BLAST c = 100 PSI

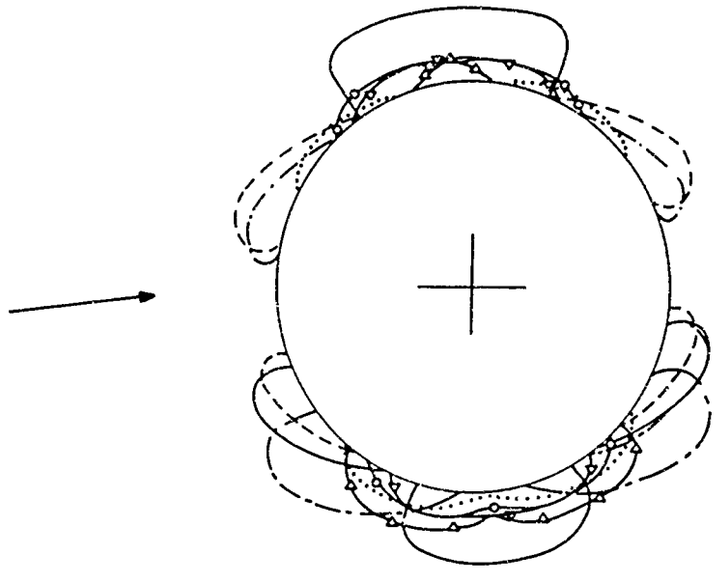

a

——— A Θ = 28°, β = 83°
—·—·— B1 Θ = 86°, β = 81°
– – – – – B2 Θ = -85°, β = 84°
····· C Θ = -10°, β = -40°
—△—△— D1 Θ = 52°, β = 48°
—▽—▽— E1 Θ = 31°, β = 40°
—○—○— E2 Θ = 23°, β = 40°

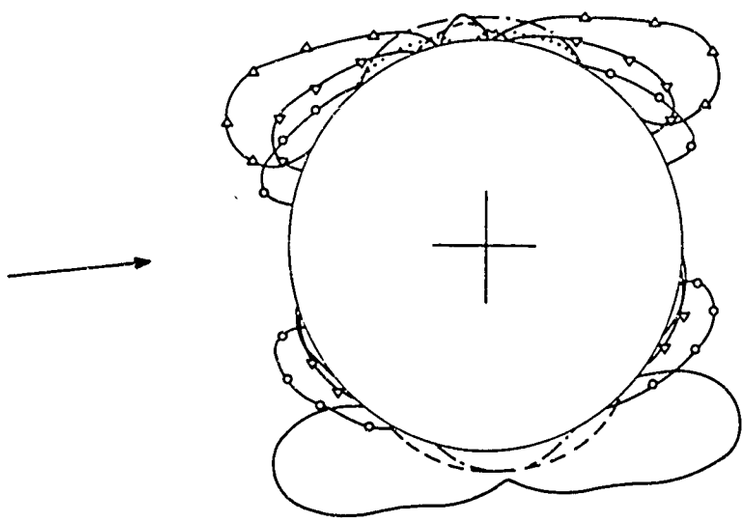

b

——— F Θ = 50°, β = 72°
—·—·— G1 Θ = 30°, β = -40°
– – – – – G2 Θ = 51°, β = -37°
····· G3 Θ = 18°, β = -33°
—△—△— H Θ = -65°, β = 80°
—▽—▽— I1 Θ = -77°, β = 52°
—○—○— I2 Θ = 89°, β = 70°

FIGURE 3.3 JOINT INFLUENCE DIAGRAMS C R LATERAL - 10,000 PSI BLAST c = 1000 PSI

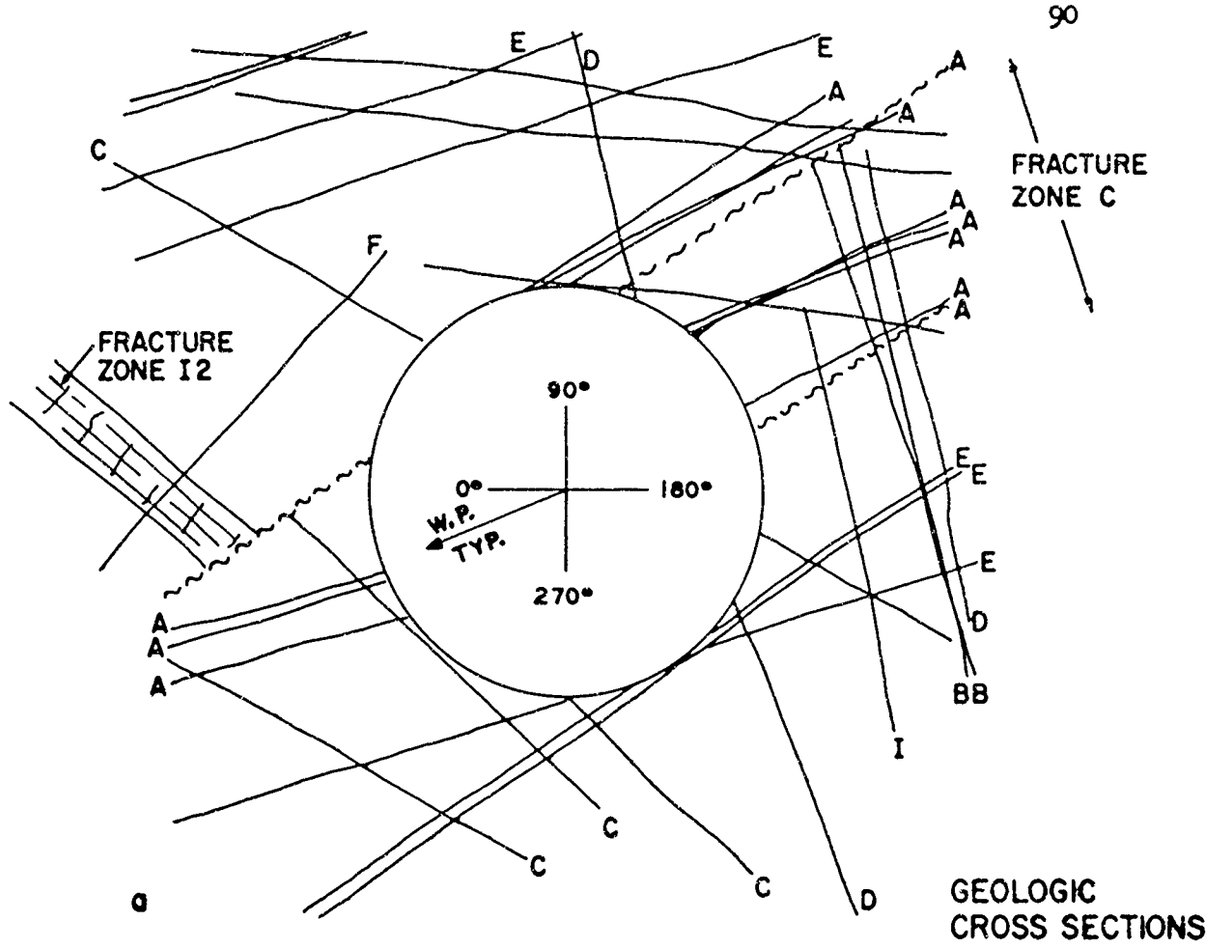

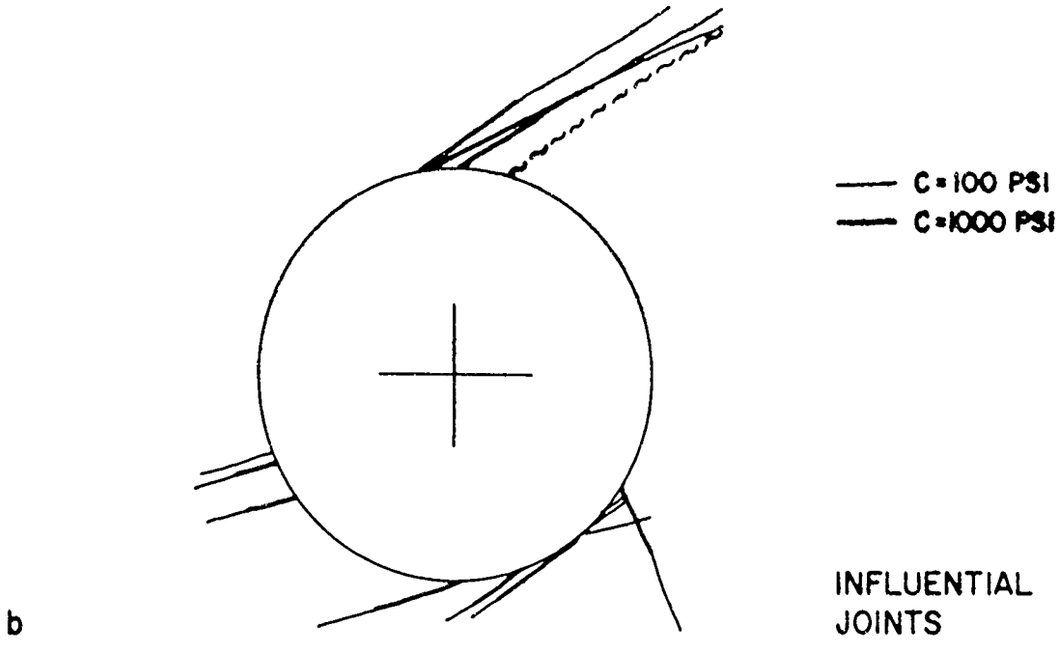

FIGURE 3.4 0+60, 16' DIAM., 16' ROCK BOLTS AT 2'

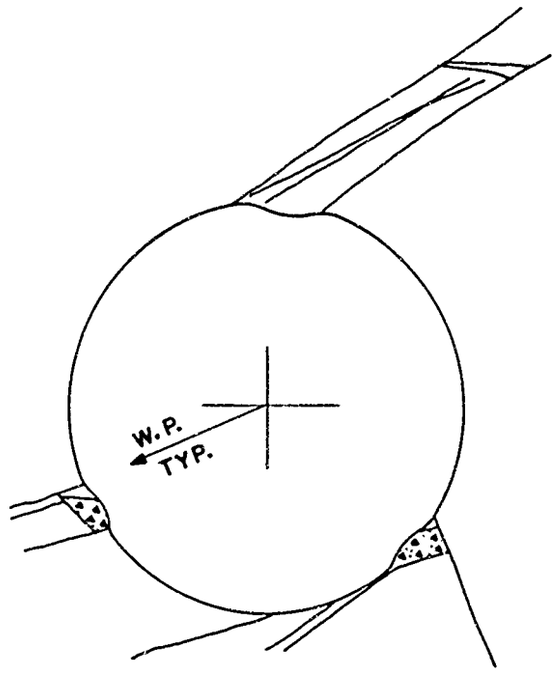

c = 100 PSI

c

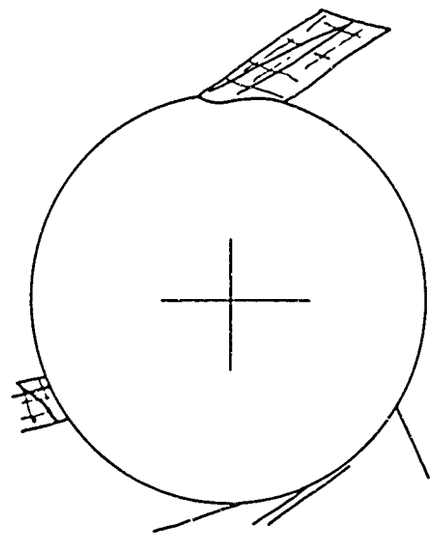

c = 1000 PSI

d

FIGURE 3.4 0 + 60, 16' DIAM., 16' ROCK BOLTS AT 2'
PREDICTED POST-SHOCK CROSS SECTIONS

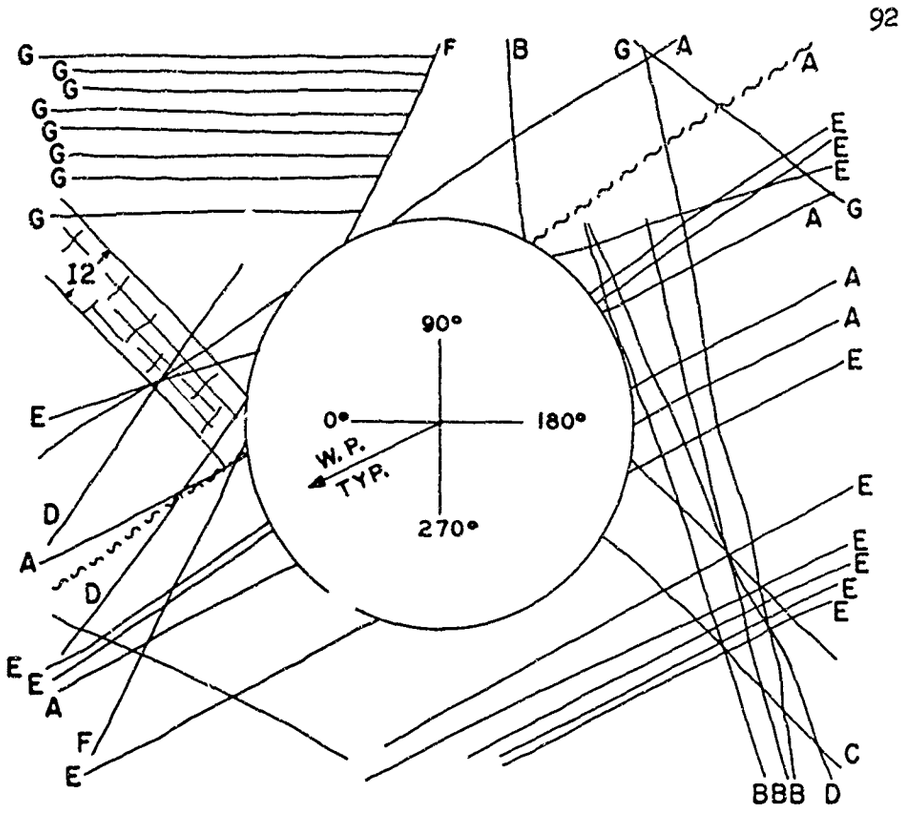

a

GEOLOGIC
CROSS SECTION

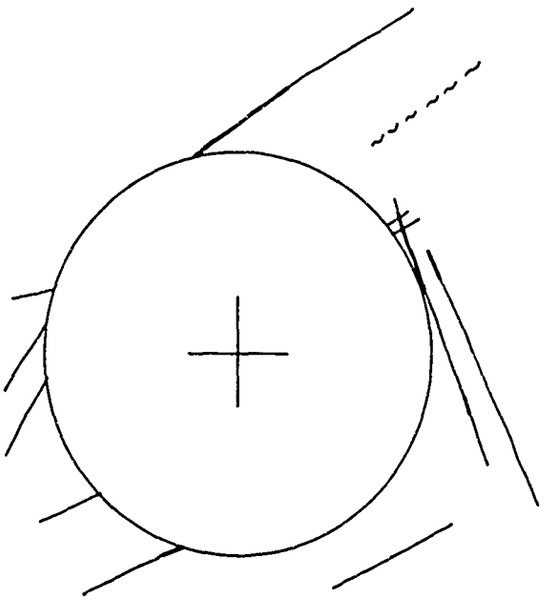

c = 100 PSI
c = 1000 PSI

b

INFLUENTIAL
JOINTS

FIGURE 3.5 0+70 , 16' DIAM. , 16' ROCK BOLTS AT 2'

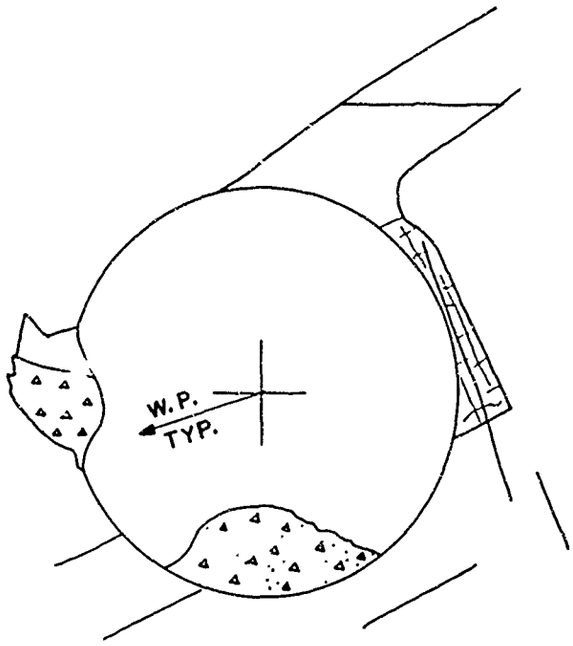

c = 100 PSI

c

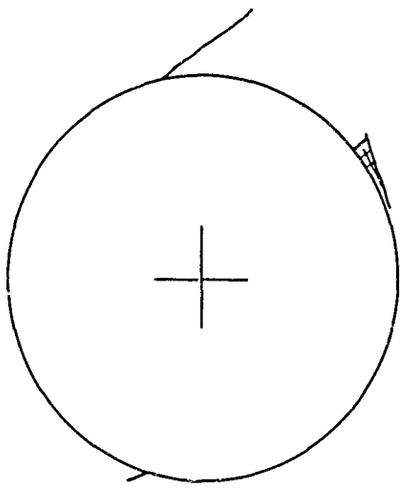

c = 1000 PSI

d

FIGURE 3.5 0+70 , 16' DIAM., 16' ROCK BOLTS AT 2'
PREDICTED POST-SHOCK CROSS SECTIONS

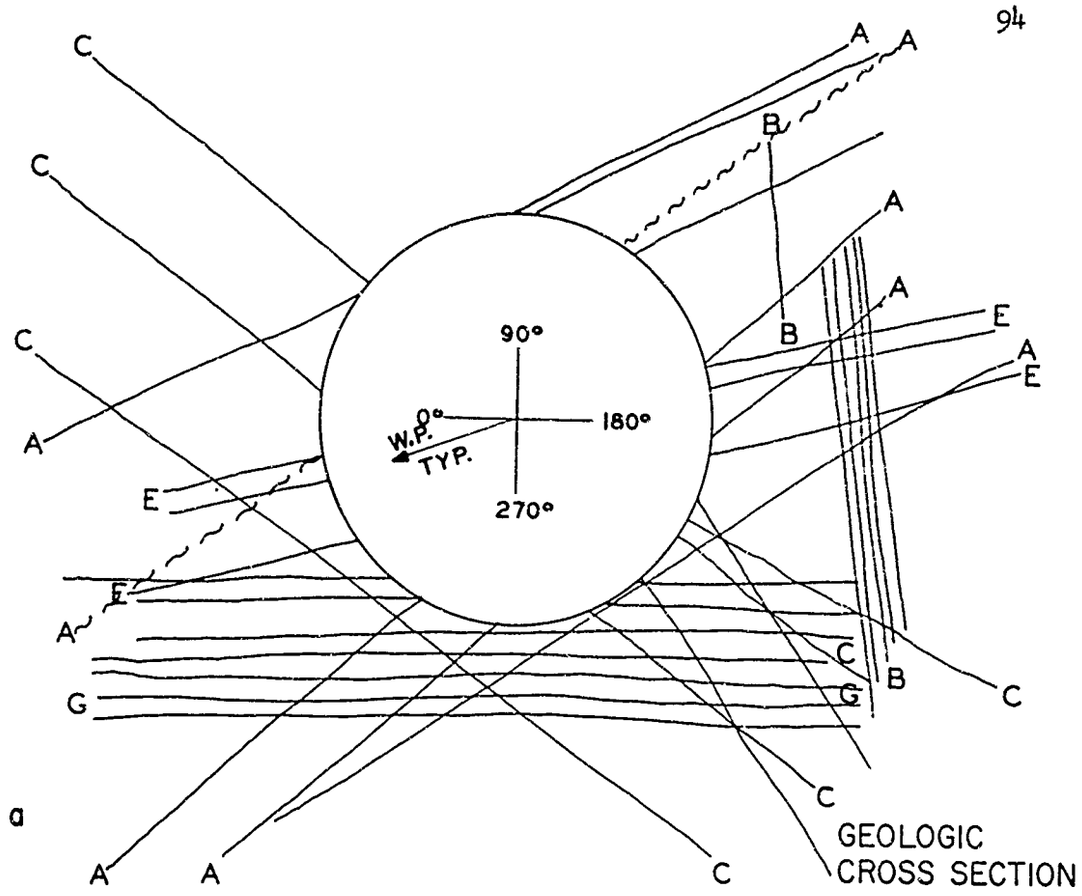

a GEOLOGIC CROSS SECTION

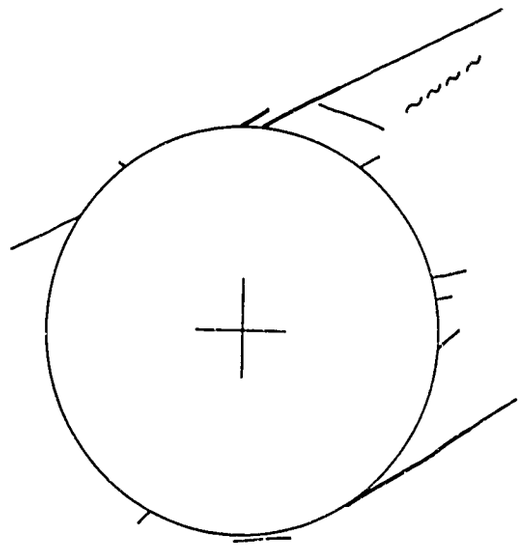

c = 100 PSI

c = 1000 PSI

b INFLUENTIAL JOINTS

FIGURE 3.6 0+80, 16' DIAM., 16' ROCK BOLTS AT 2'

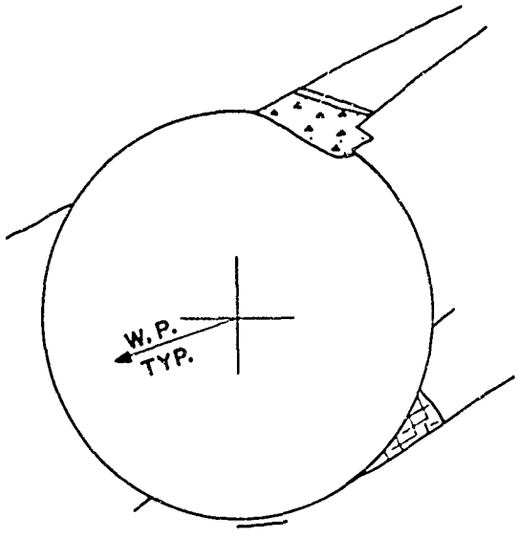

c = 100 PSI

c

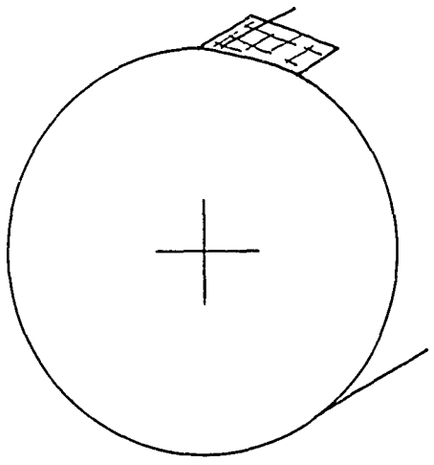

c = 1000 PSI

d

FIGURE 3.6 0 + 80 , 16' DIAM. , 16' ROCK BOLTS AT 2'
PREDICTED POST-SHOCK CROSS SECTION

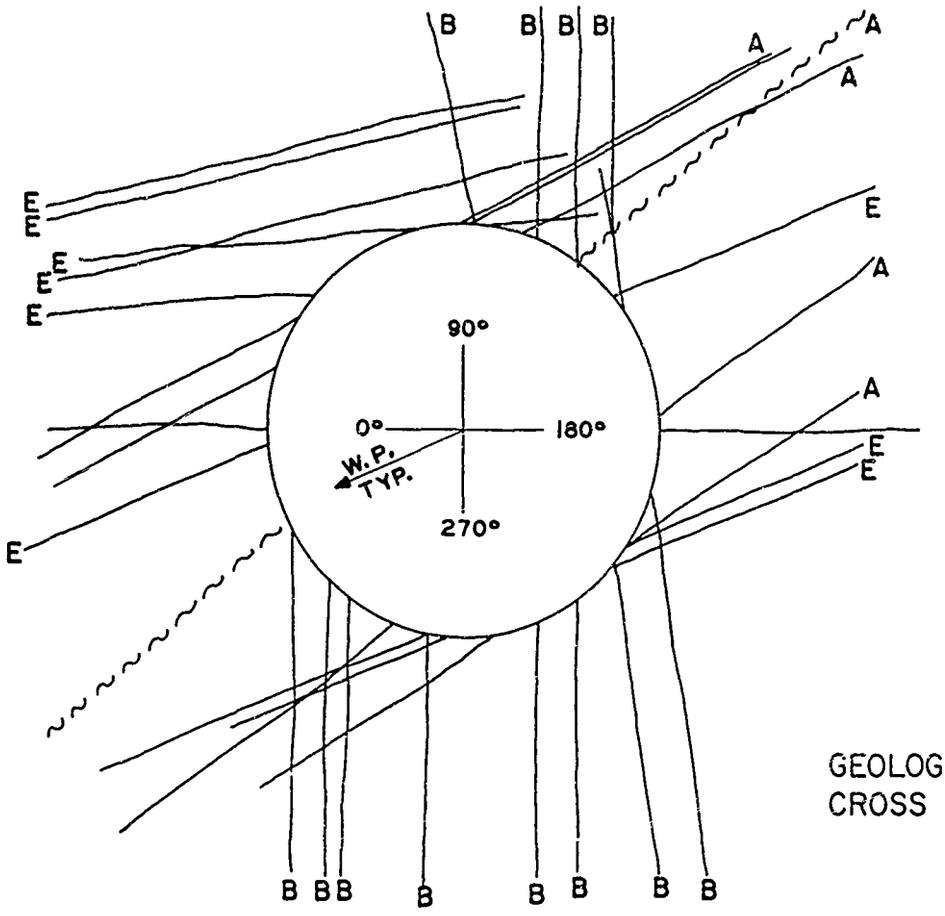

a

GEOLOGIC
CROSS SECTION

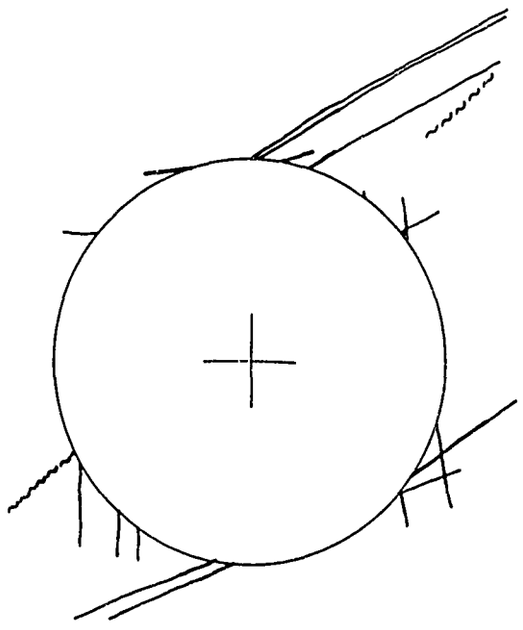

c = 100 PSI
c = 1000 PSI

b

INFLUENTIAL
JOINTS

FIGURE 3.7 0+90 , 16' DIAM., 16' ROCK BOLTS AT 2'

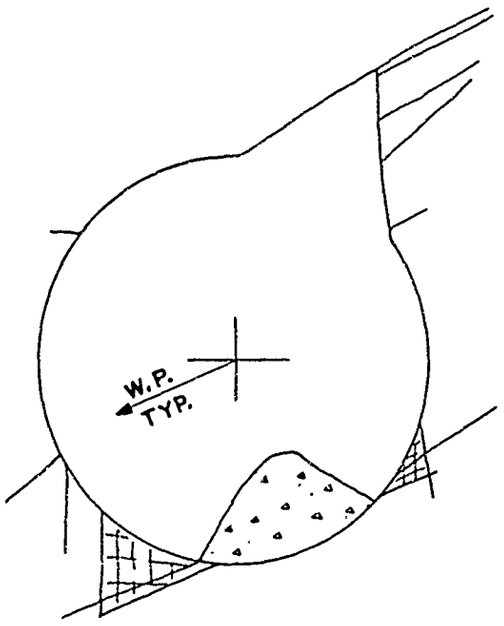

c = 100 PSI

c

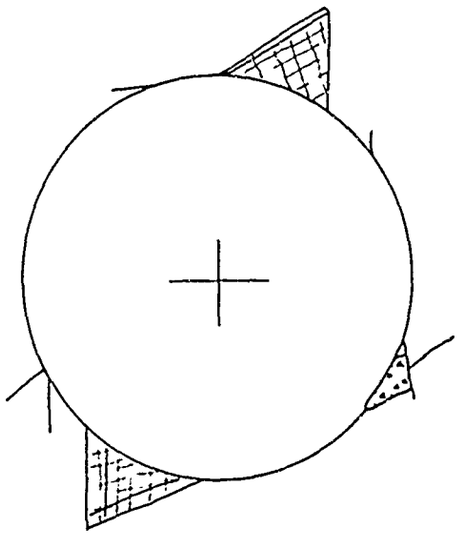

c = 1000 PSI

d

FIGURE 3.7 0+90, 16' DIAM., 16' ROCK BOLTS AT 2'
PREDICTED POST-SHOCK CROSS SECTIONS

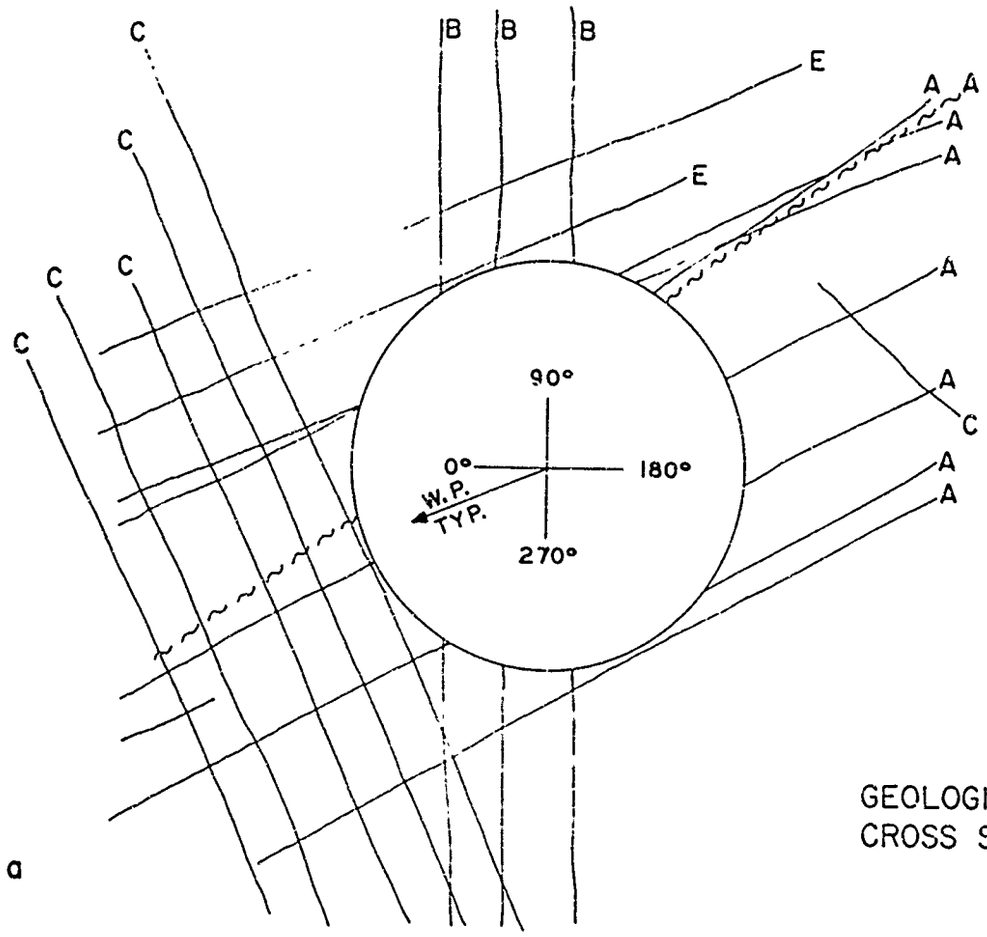

a

GEOLOGIC
CROSS SECTION

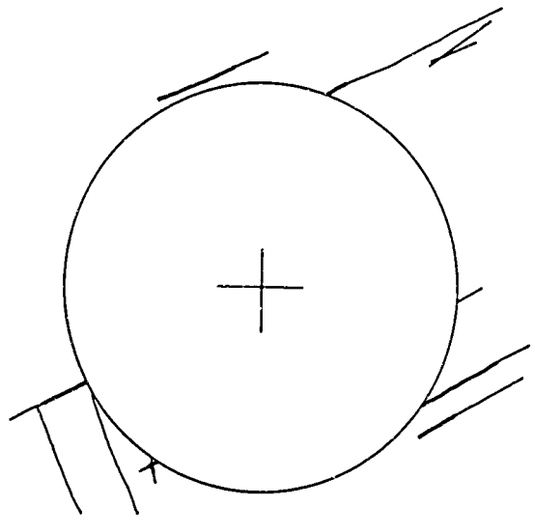

b

c = 100 PSI
c = 1000 PSI

INFLUENTIAL
JOINTS

FIGURE 3.8 1+00 , 16' DIAM., UNLINED

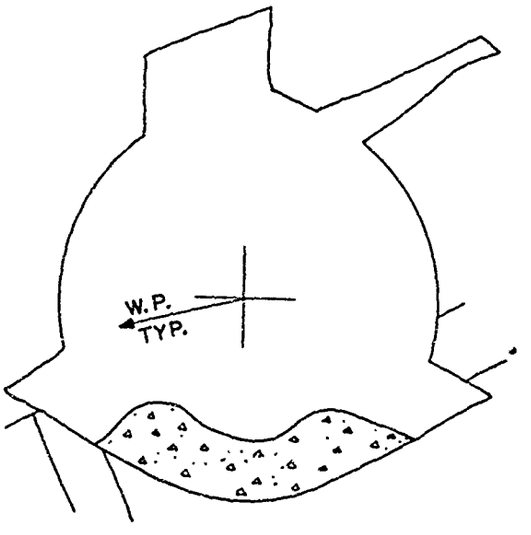

c = 100 PSI

c

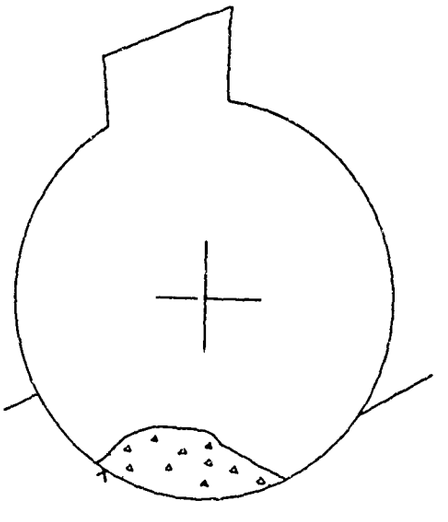

c = 1000 PSI

d

FIGURE 3.8 1+00 , 16' DIAM. , UNLINED
PREDICTED POST-SHOCK CROSS SECTIONS

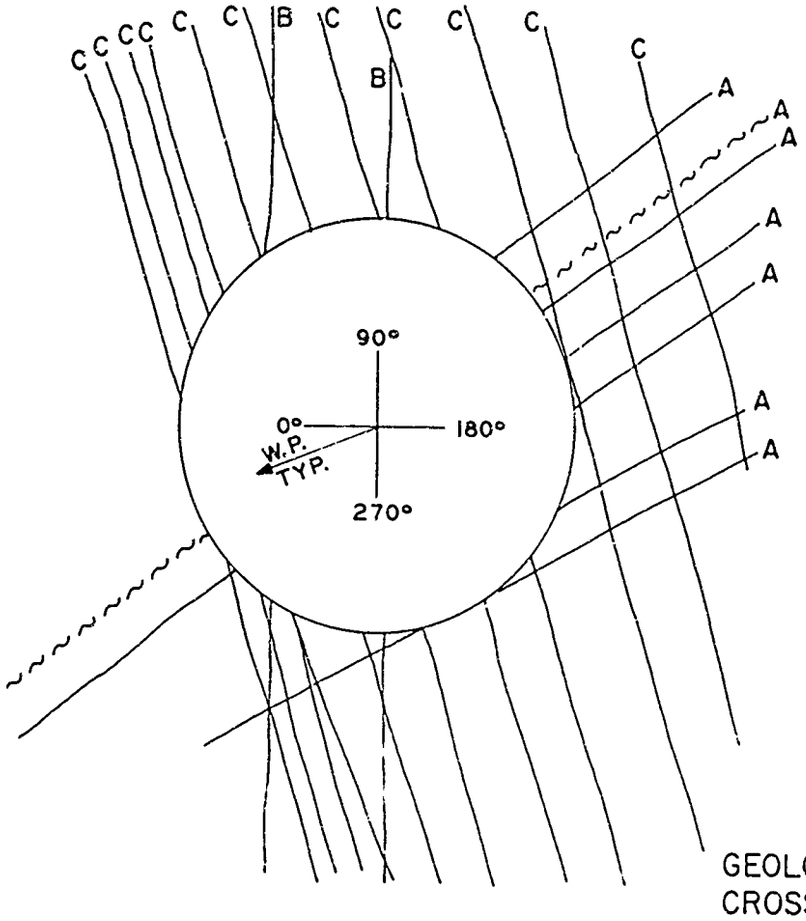

a

GEOLOGIC
CROSS SECTION

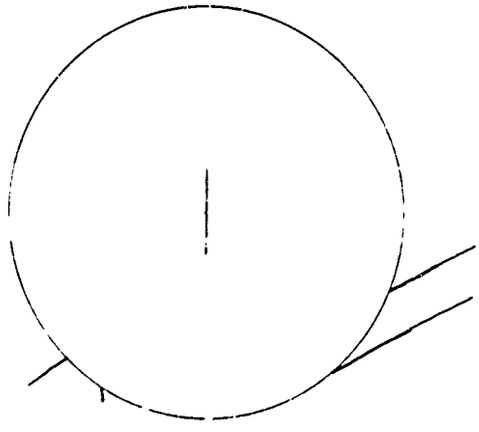

c = 100 PSI
c = 1000 PSI

b

INFLUENTIAL
JOINTS

FIGURE 5.9 1+10 , 16' DIAM. , UNLINED

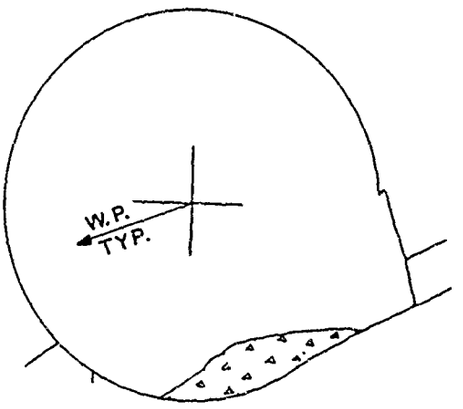

c = 100 PSI

c

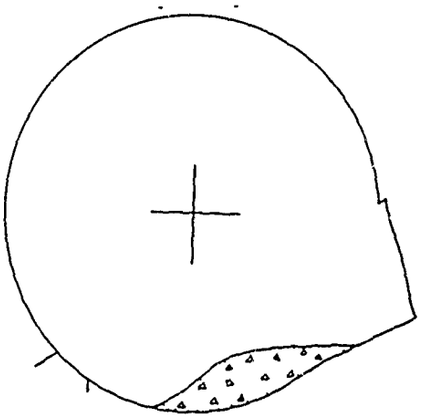

c = 1000 PSI

d

FIGURE 3.9 1+10 , 16' DIAM. , UNLINED
PREDICTED POST-SHOCK CROSS SECTION

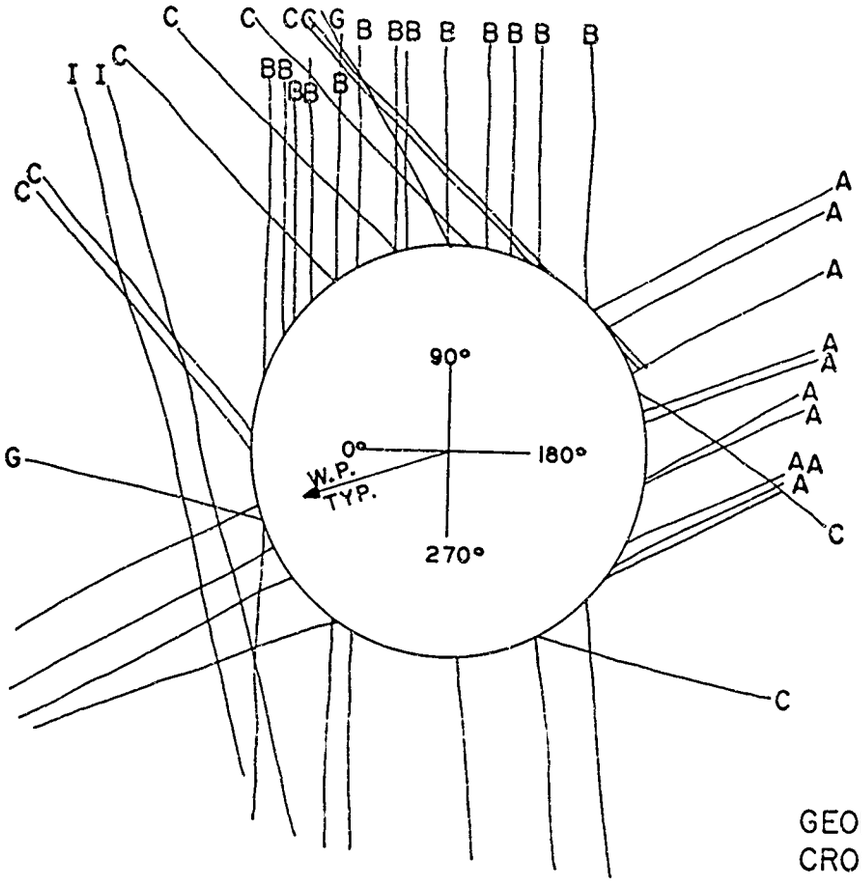

a

GEOLOGIC
CROSS SECTION

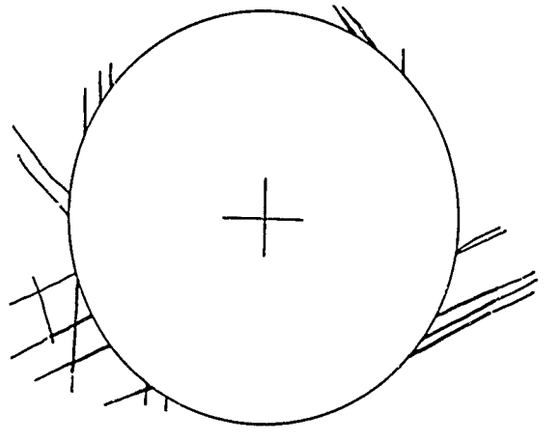

c = 100 PSI
c = 1000 PSI

b

INFLUENTIAL
JOINTS

FIGURE 3.10 1+20 , 18' DIAM. , UNLINED

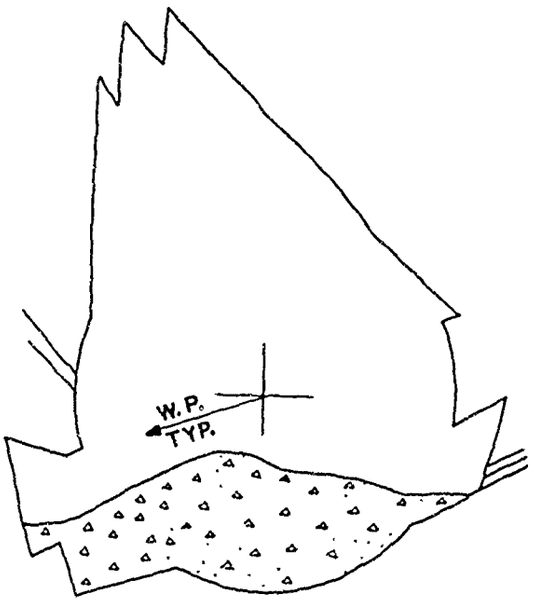

c = 100 PSI

c

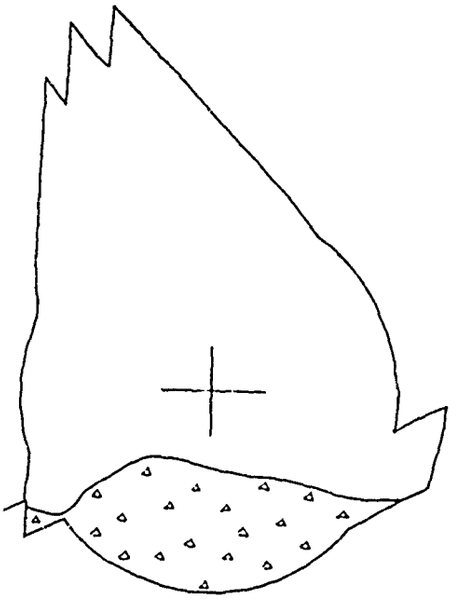

c = 1000 PSI

d

FIGURE 3.10 1+20 , 18' DIAM. , UNLINED
PREDICTED POST-SHOCK CROSS SECTIONS

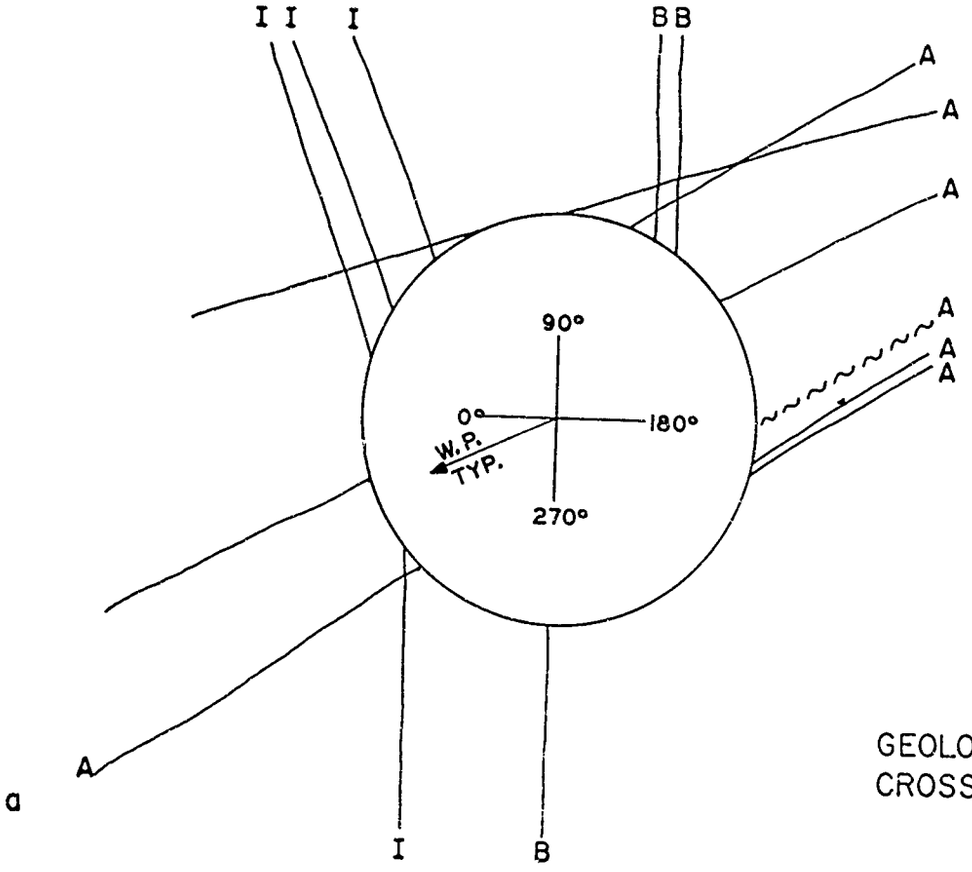

a

GEOLOGIC
CROSS SECTION

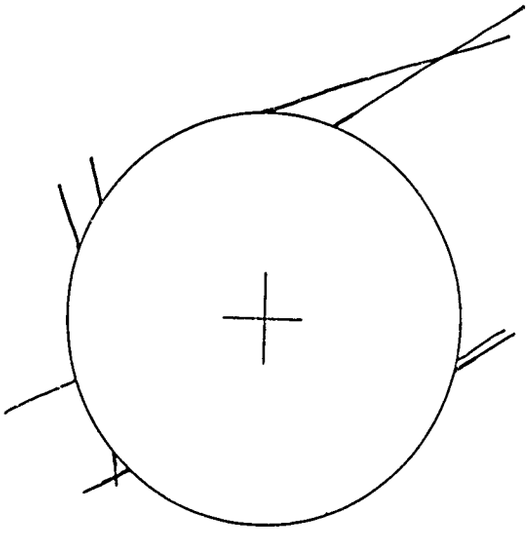

c = 100 PSI
c = 1000 PSI

b

INFLUENTIAL
JOINTS

FIGURE ... 1+30 , 13' DIAM. , 12' ROCK BOLTS AT 2'

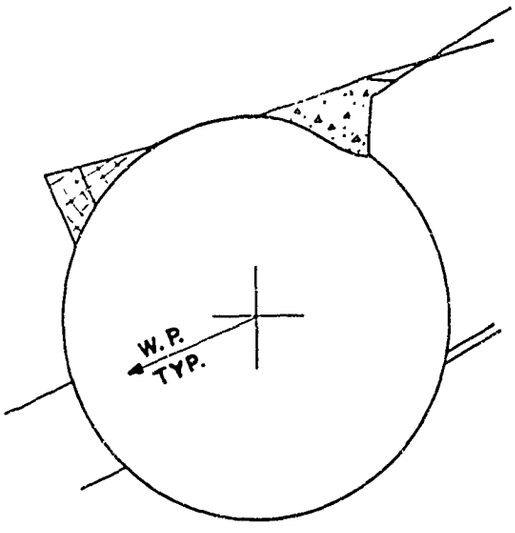

c = 100 PSI

c

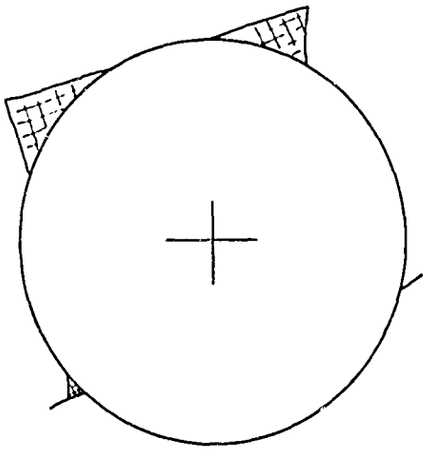

c = 1000 PSI

d

FIGURE 3.11 1+30 , 13' DIAM. , 12' ROCK BOLTS AT 2'
PREDICTED POST-SHOCK CROSS SECTION

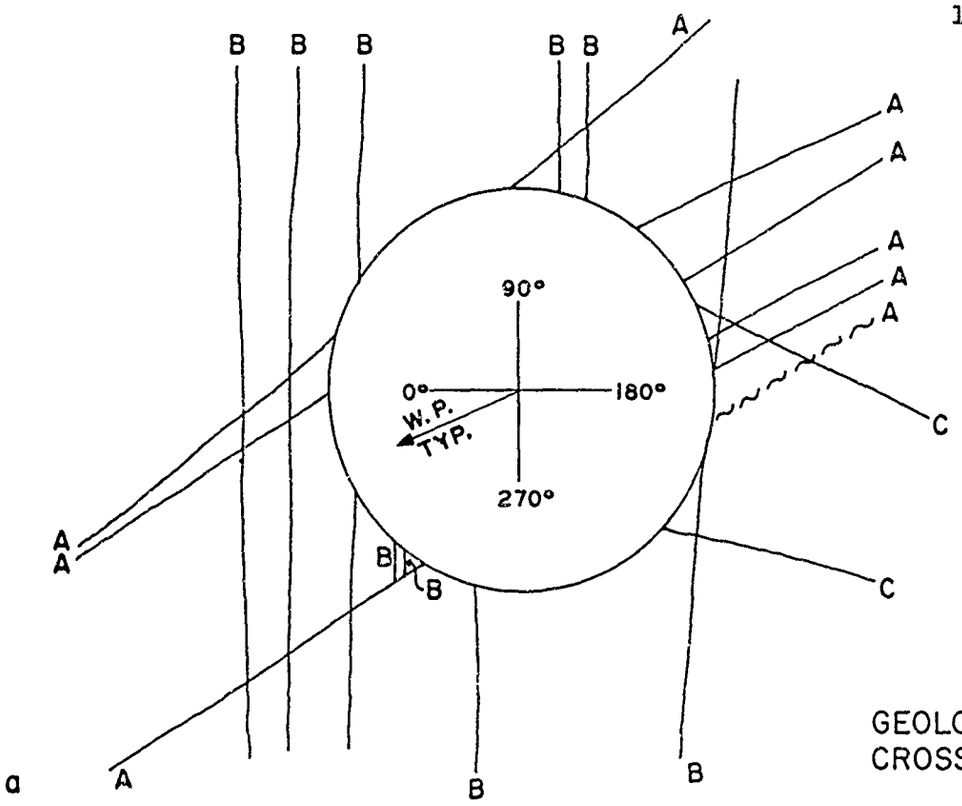

a

GEOLOGIC
CROSS SECTION

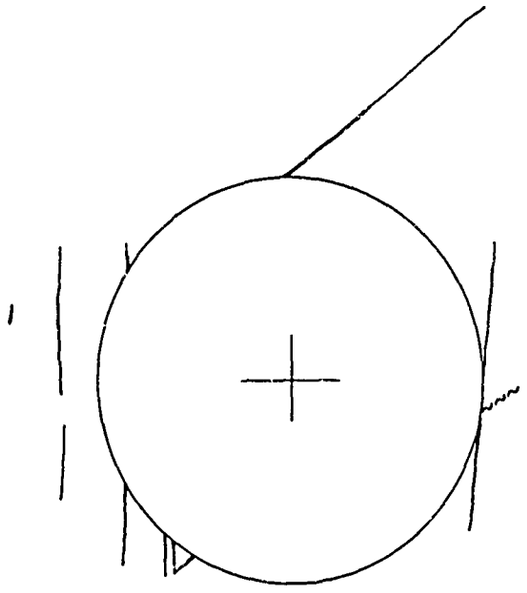

c = 100 PSI
c = 1000 PSI

b

INFLUENTIAL
JOINTS

FIGURE 3.12 1+40 , 13' DIAM. , 12' ROCK BOLTS AT 2'

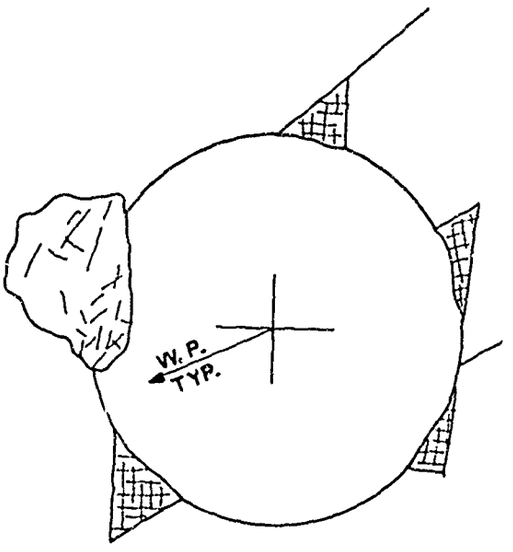

c = 100 PSI

c

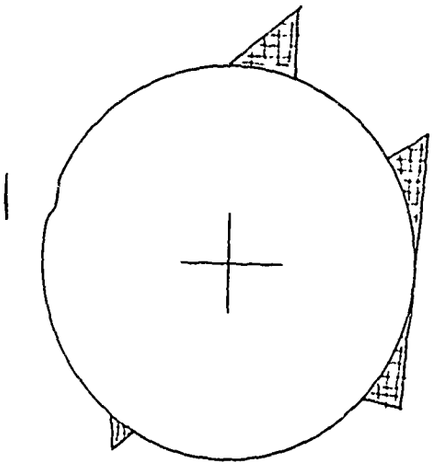

c = 1000 PSI

d

FIGURE 7.12 1+40 , 13' DIAM. , 12' ROCK BOLTS AT 2'
PREDICTED POST-SHOCK CROSS SECTIONS

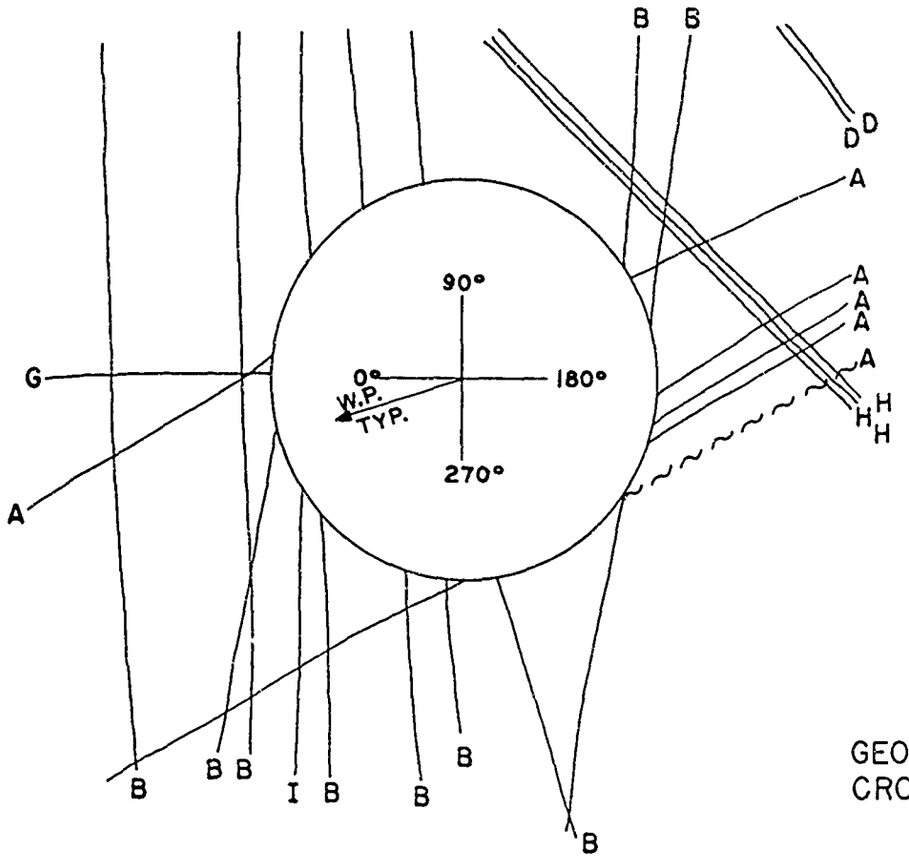

a

GEOLOGIC
CROSS SECTION

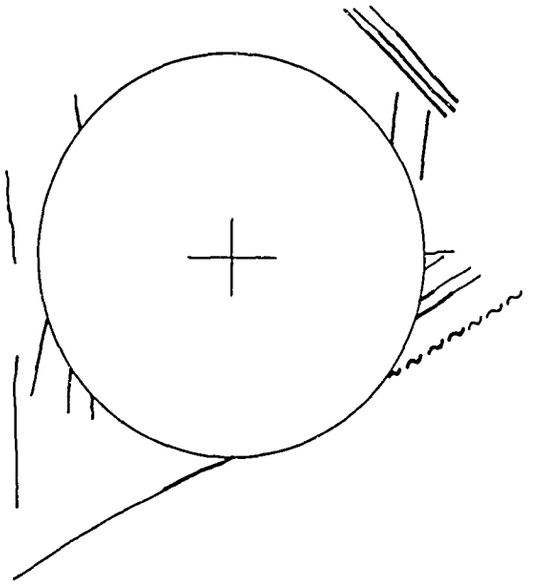

c = 100 PSI
c = 1000 PSI

b

INFLUENTIAL
JOINTS

FIGURE 3.13 1+60 , 13' DIAM. , 12' ROCK ANCHORS AT 2'

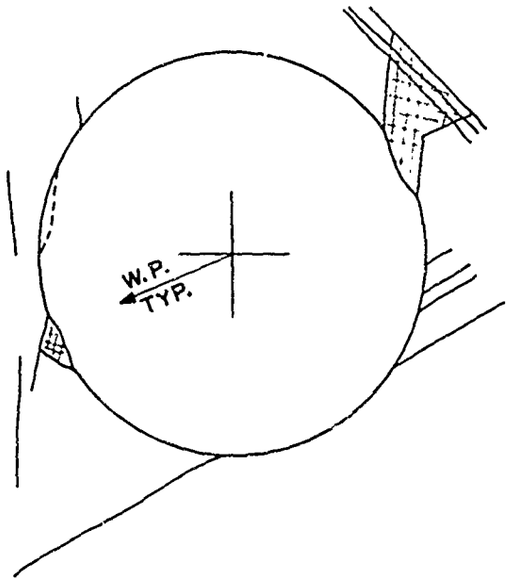

c = 100 PSI

c

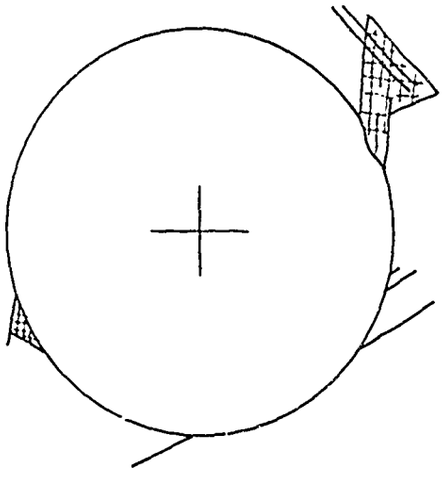

c = 1000 PSI

d

FIGURE 3.13 1+60 , 13' DIAM., 12' ROCK ANCHORS AT 2'
PREDICTED POST-SHOCK CROSS SECTIONS

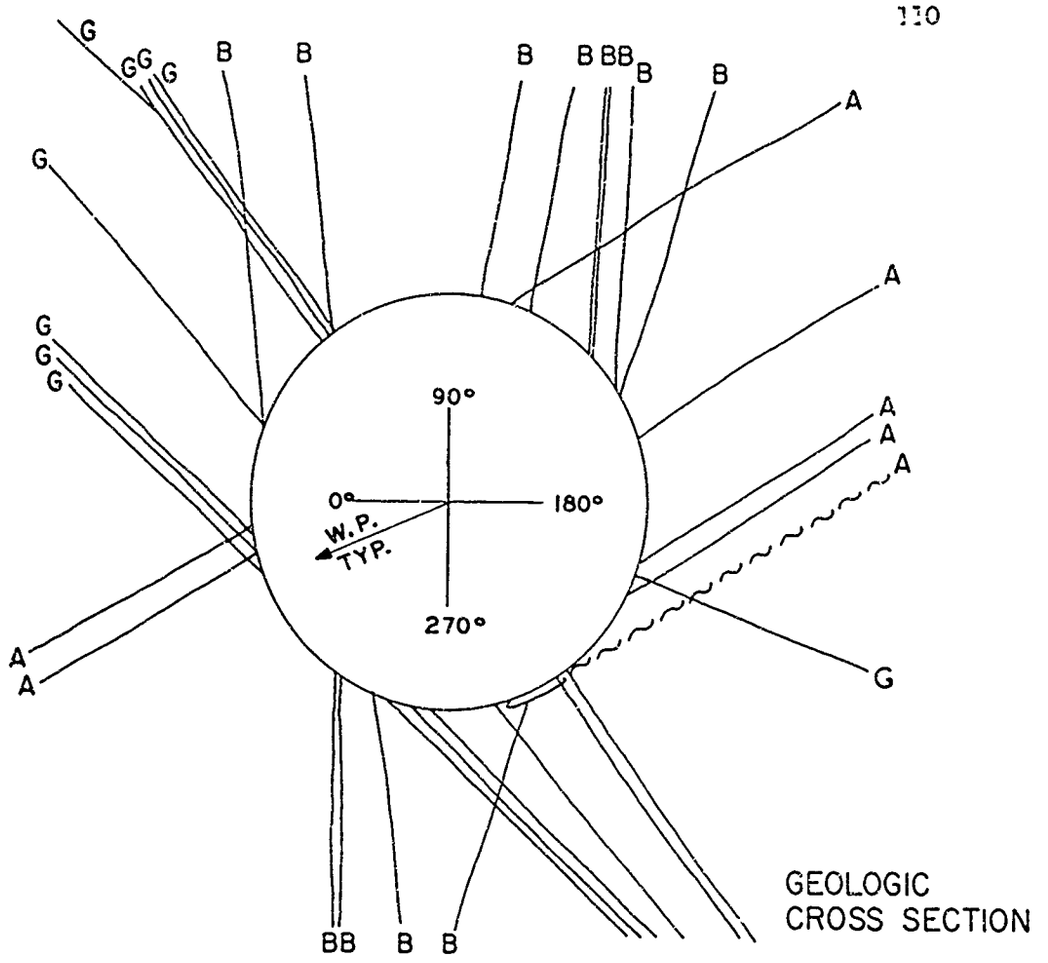

a

GEOLOGIC
CROSS SECTION

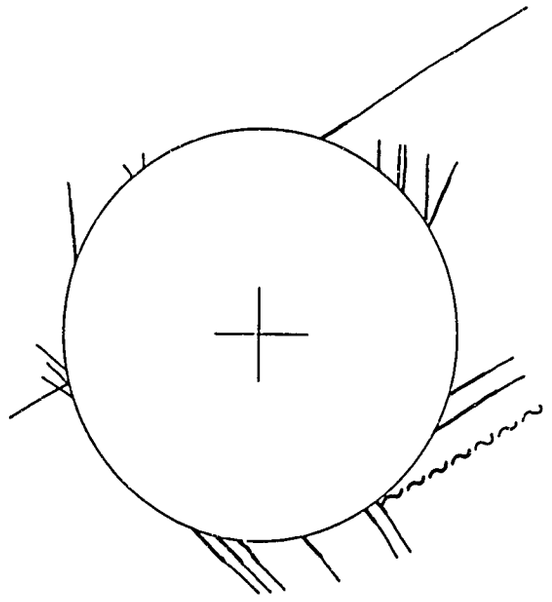

c = 100 PSI
c = 1000 PSI

b

INFLUENTIAL
JOINTS

FIGURE 3.14 1+70 , 9' DIAM. , UNLINED

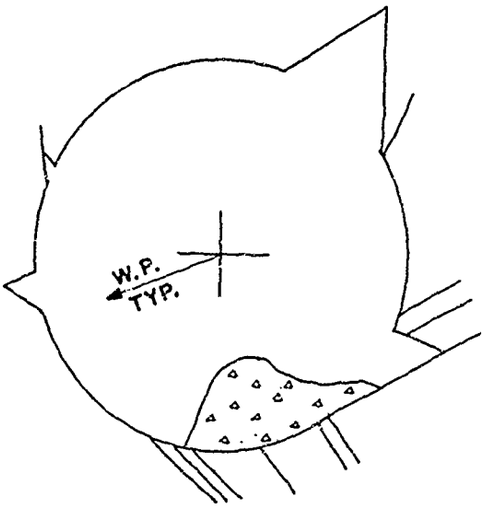

c = 100 PSI

c

d

c = 1000 PSI

FIGURE 3.14 I+70 , 9' DIAM , UNLINED
PREDICTED POST-SHOCK CRACK

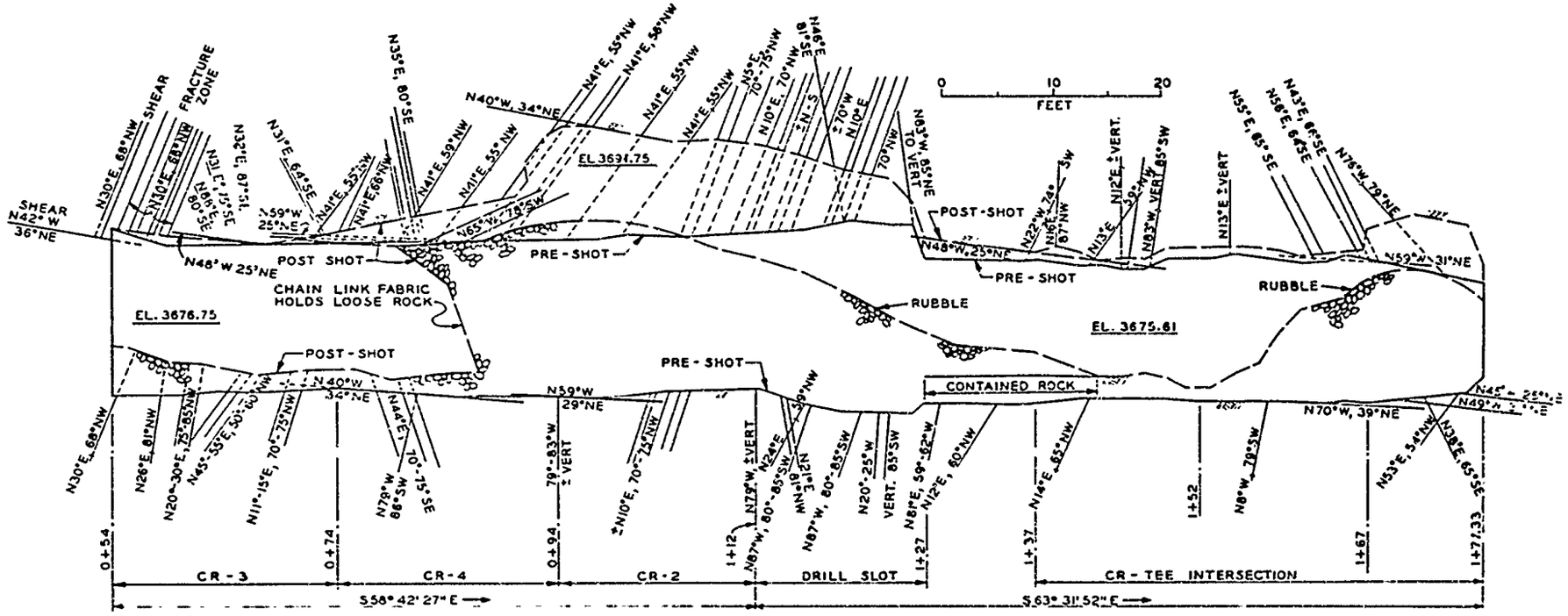

Fig. 3.15 Sectional elevation at centerline and geology - CR Drift

(Fig. 3.84 of POR 4015, Chapter 4)

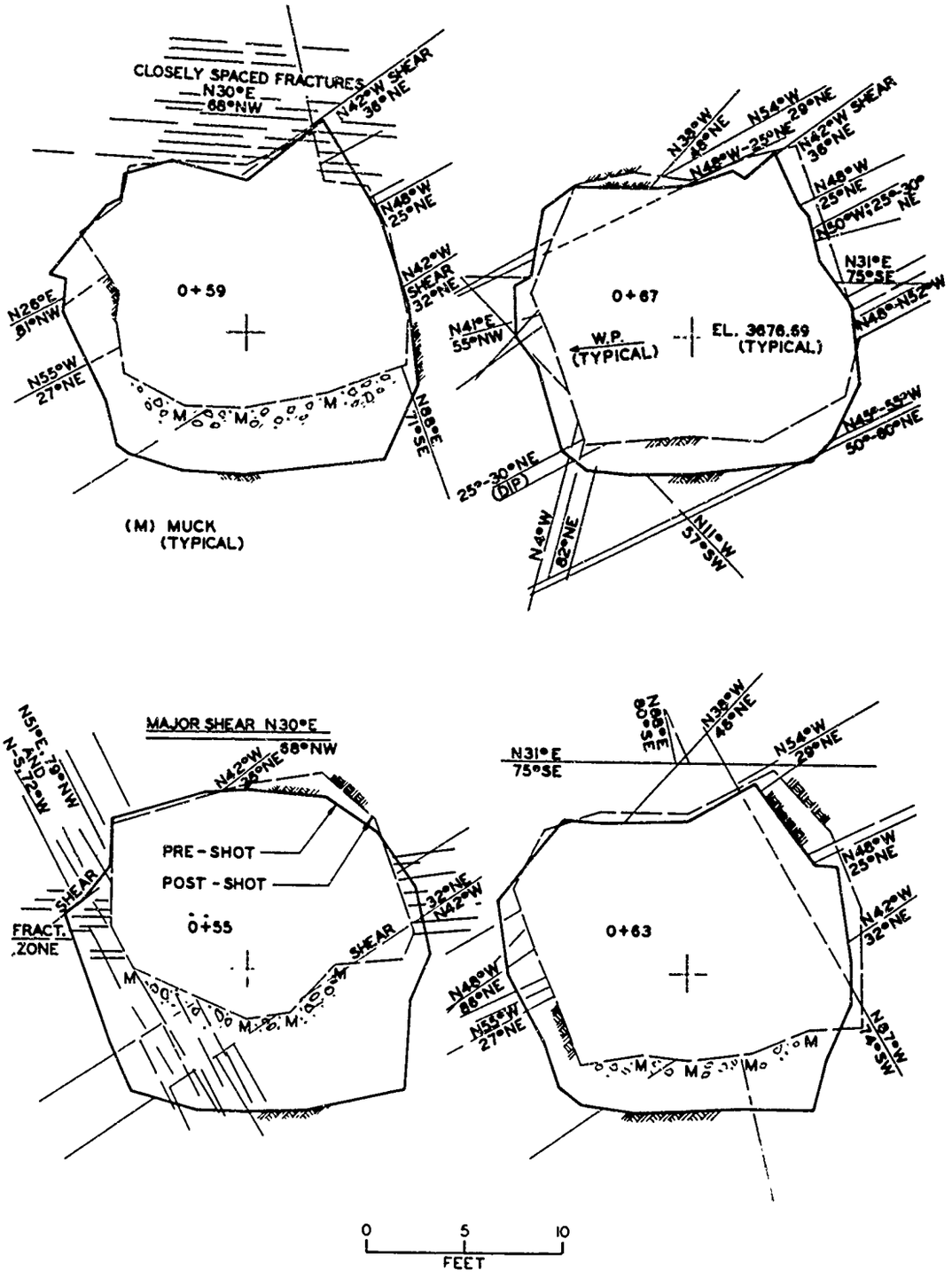

Figure 3.16 Cross sections and geology - CR Drift (1 of 10 sheets)

(Fig. 3.81 of POR 4015, Chapter 4

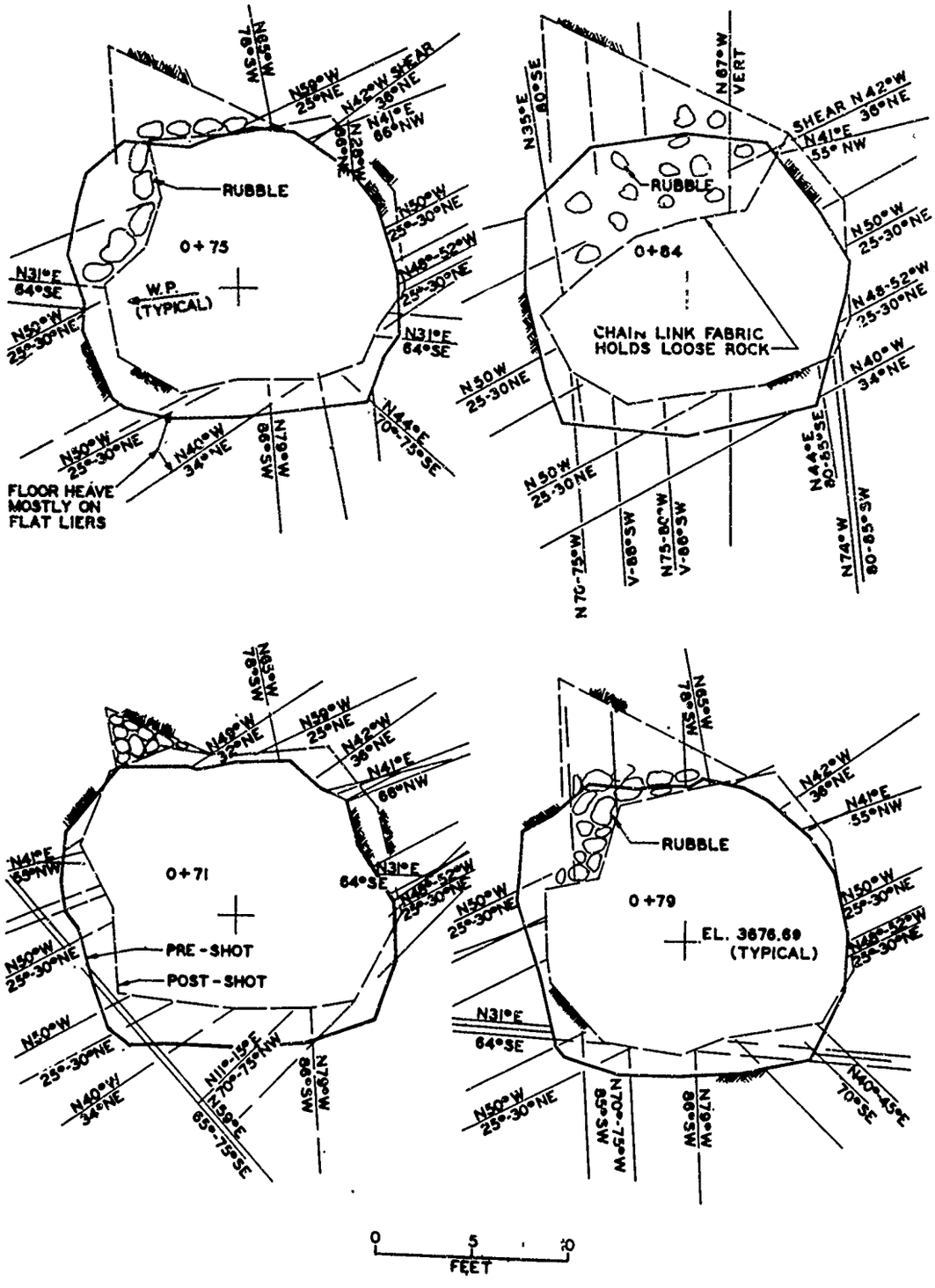

Figure 3.16 Continued (2 of 10 sheets)

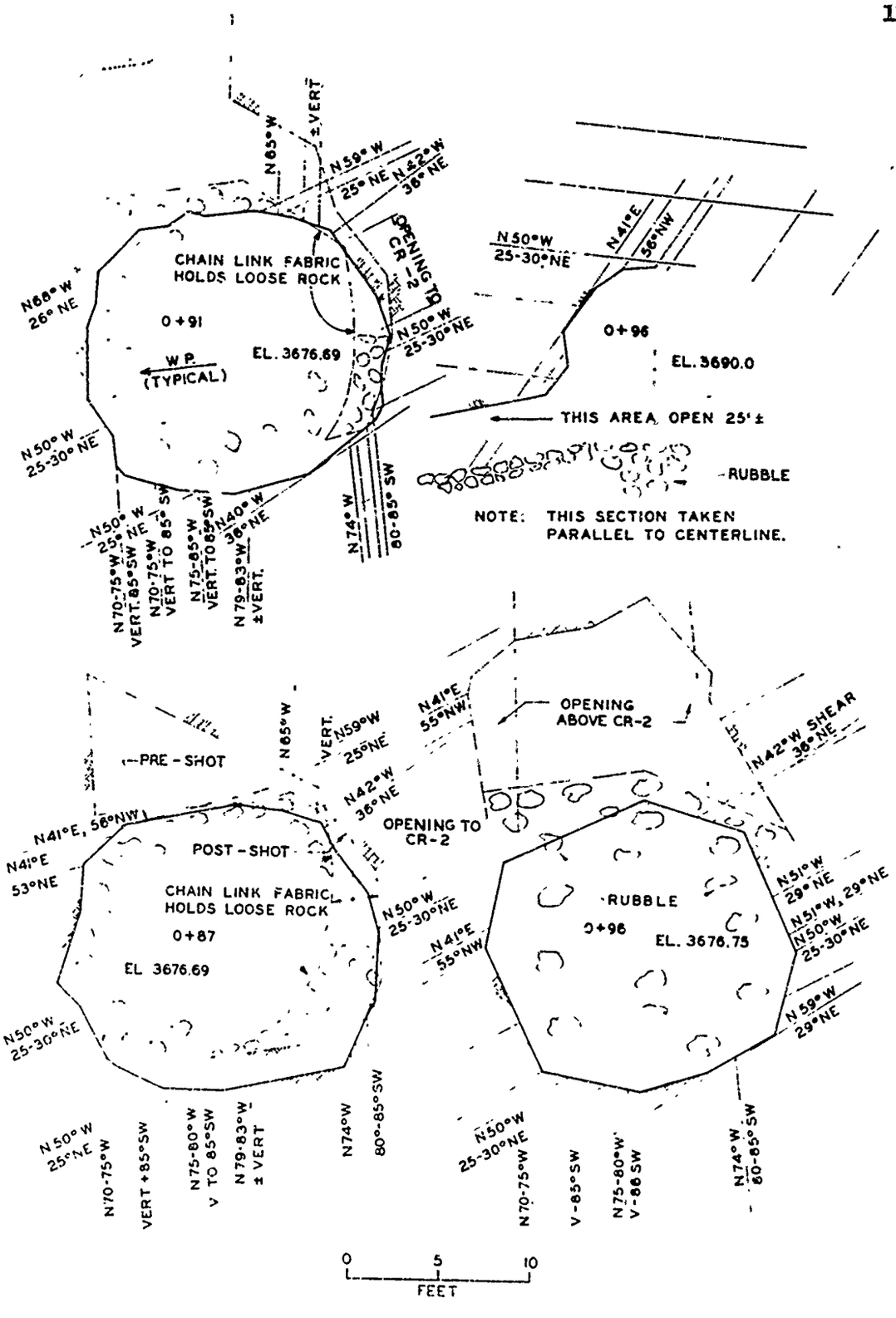

Figure 3.16 Continued (3 of 10 sheets)

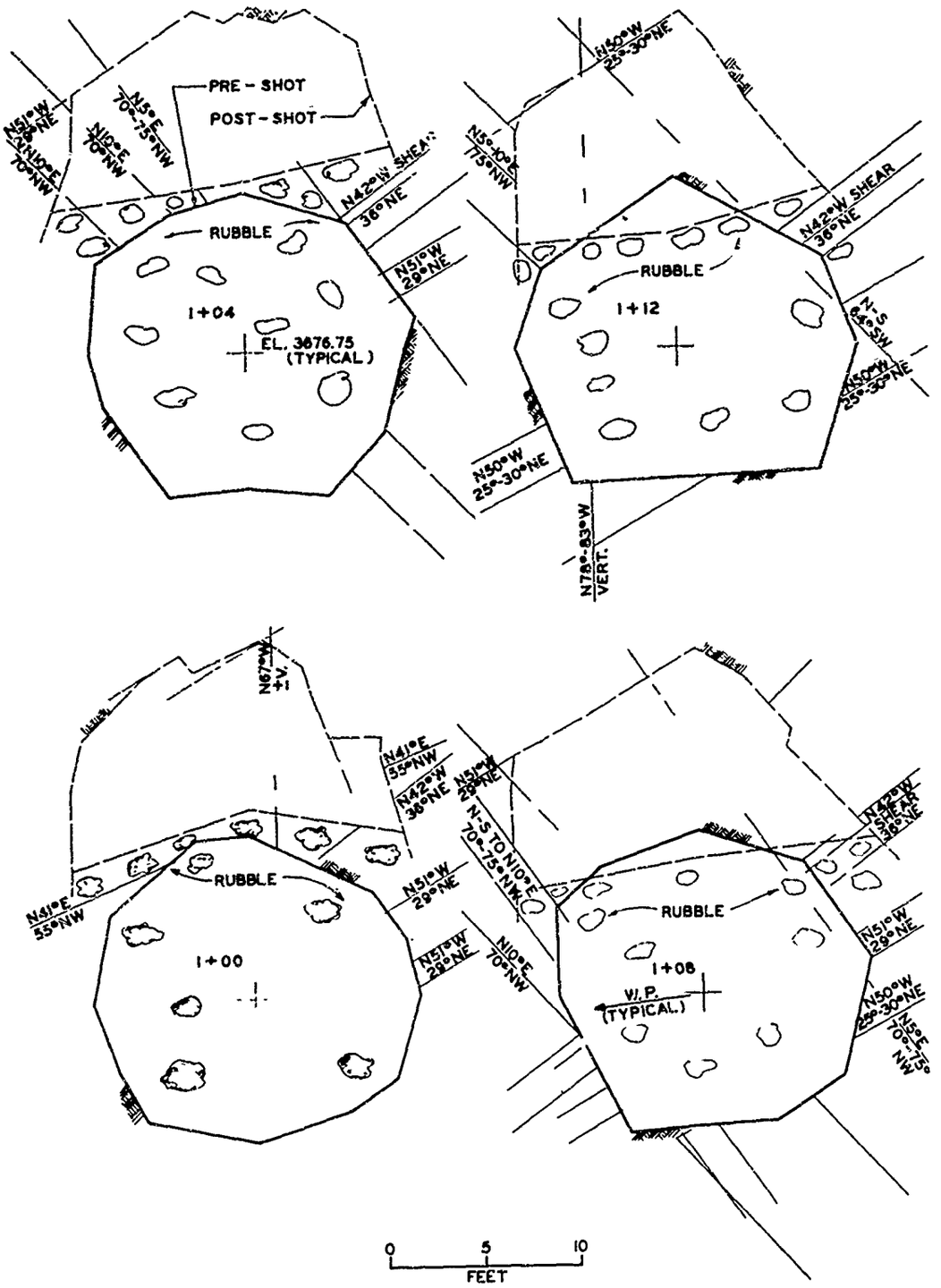

Figure 3.16 Continued (4 of 10 sheets)

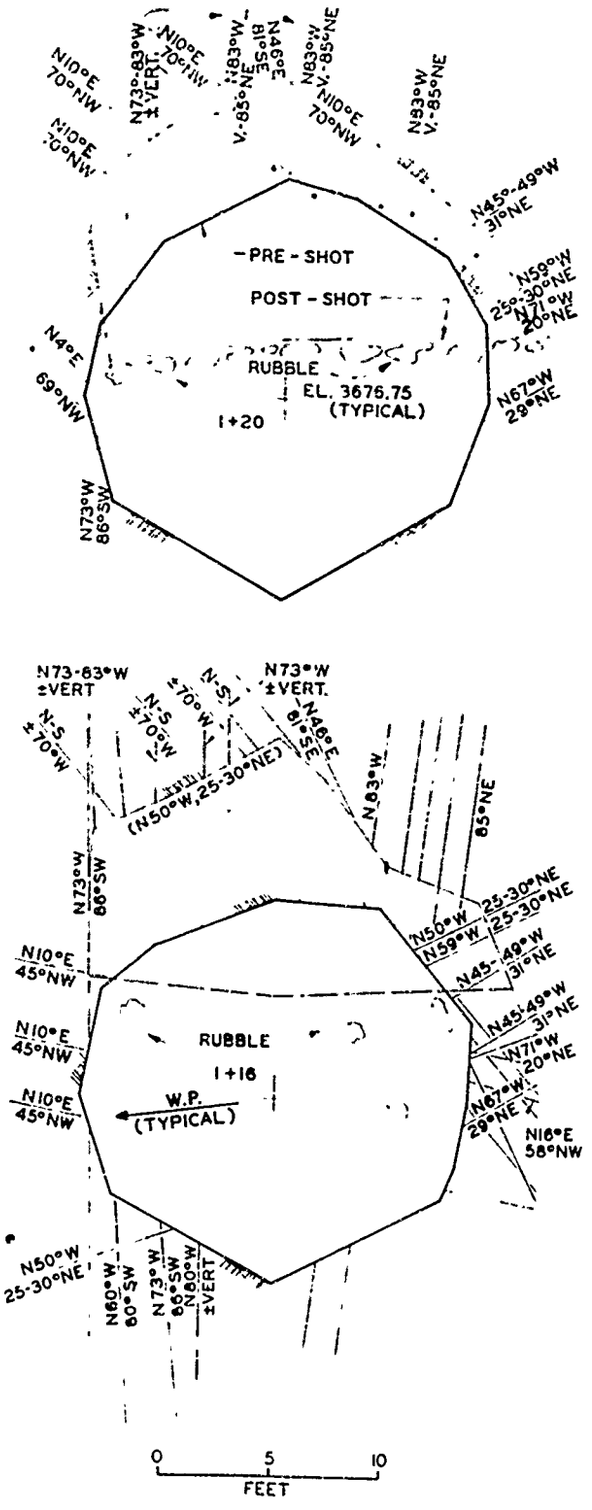

Figure 3.16 Continued (5 of 10 sheets)

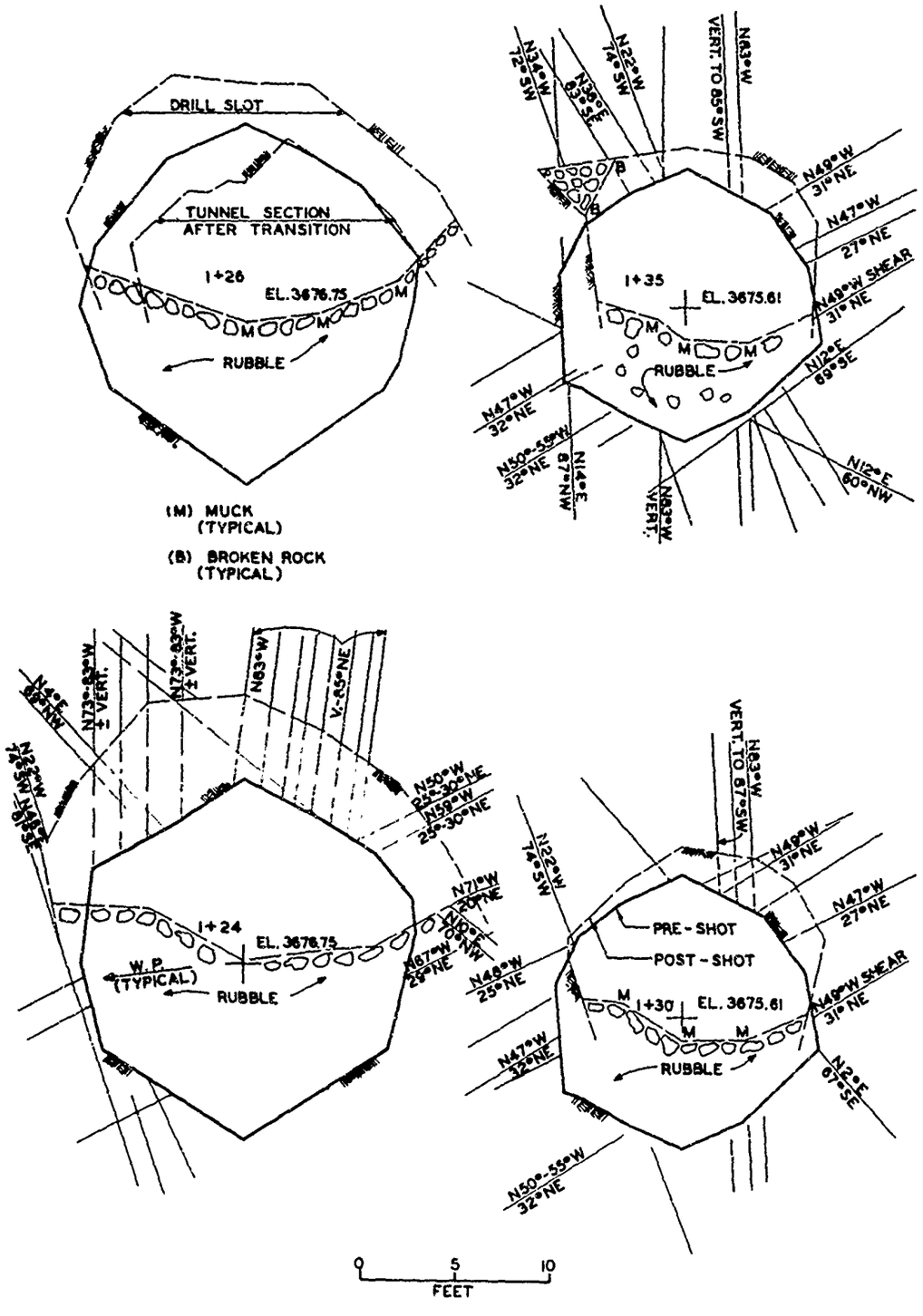

Figure 3.16 Continued (6 of 10 sheets)

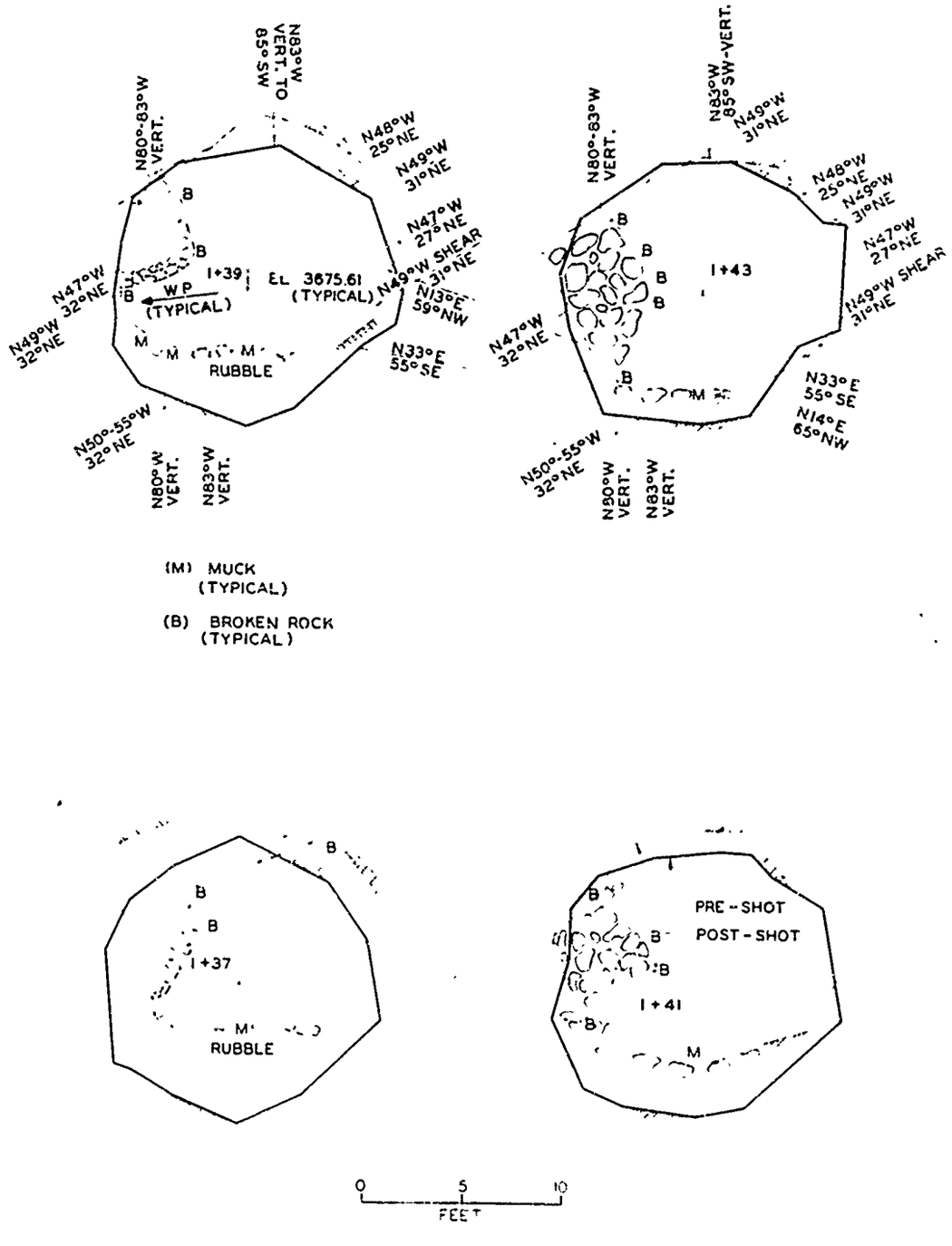

Figure 3.16 Continued (7 of 16 sheets)

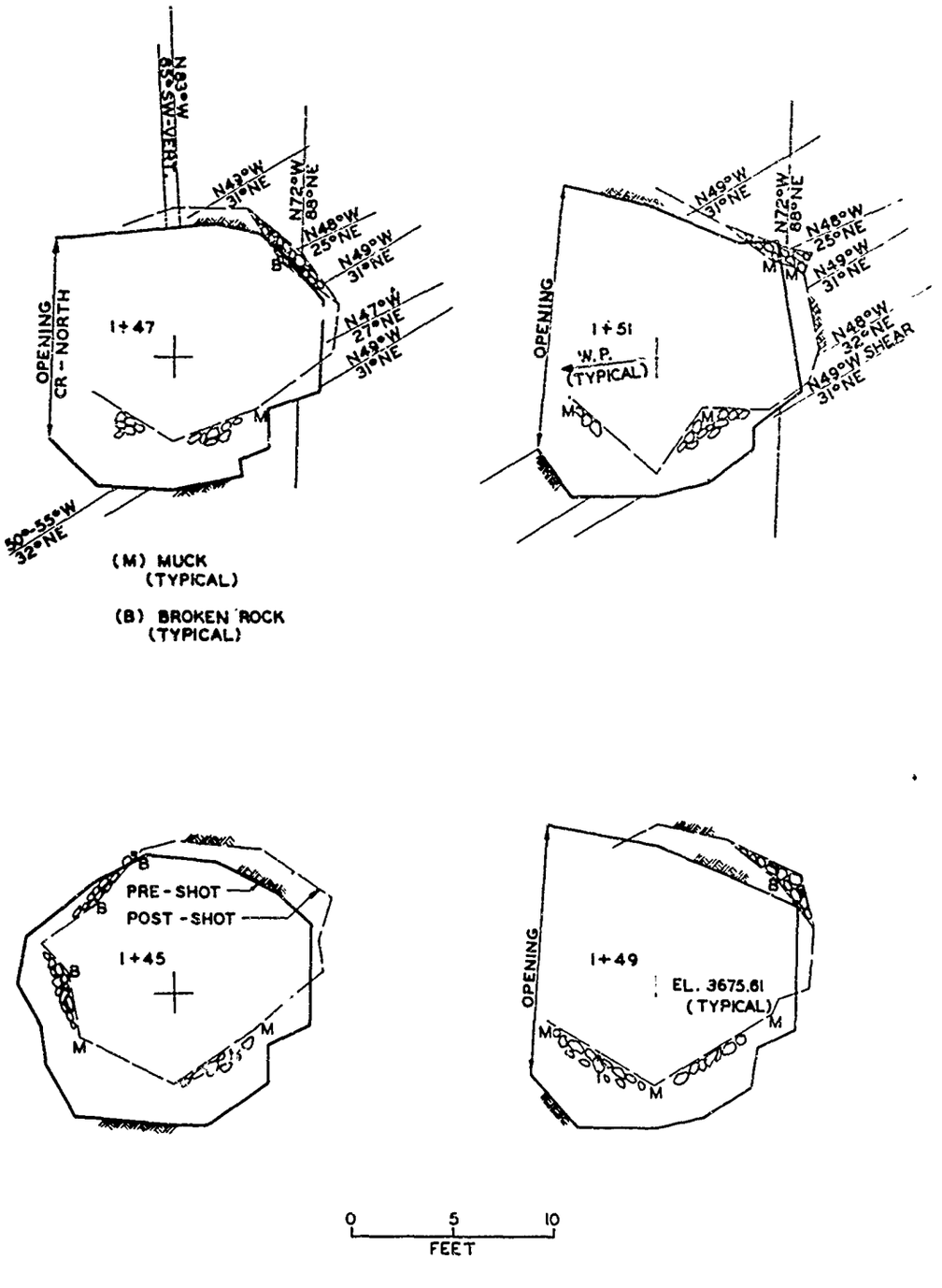

Figure 3.16 Continued (8 of 10 sheets)

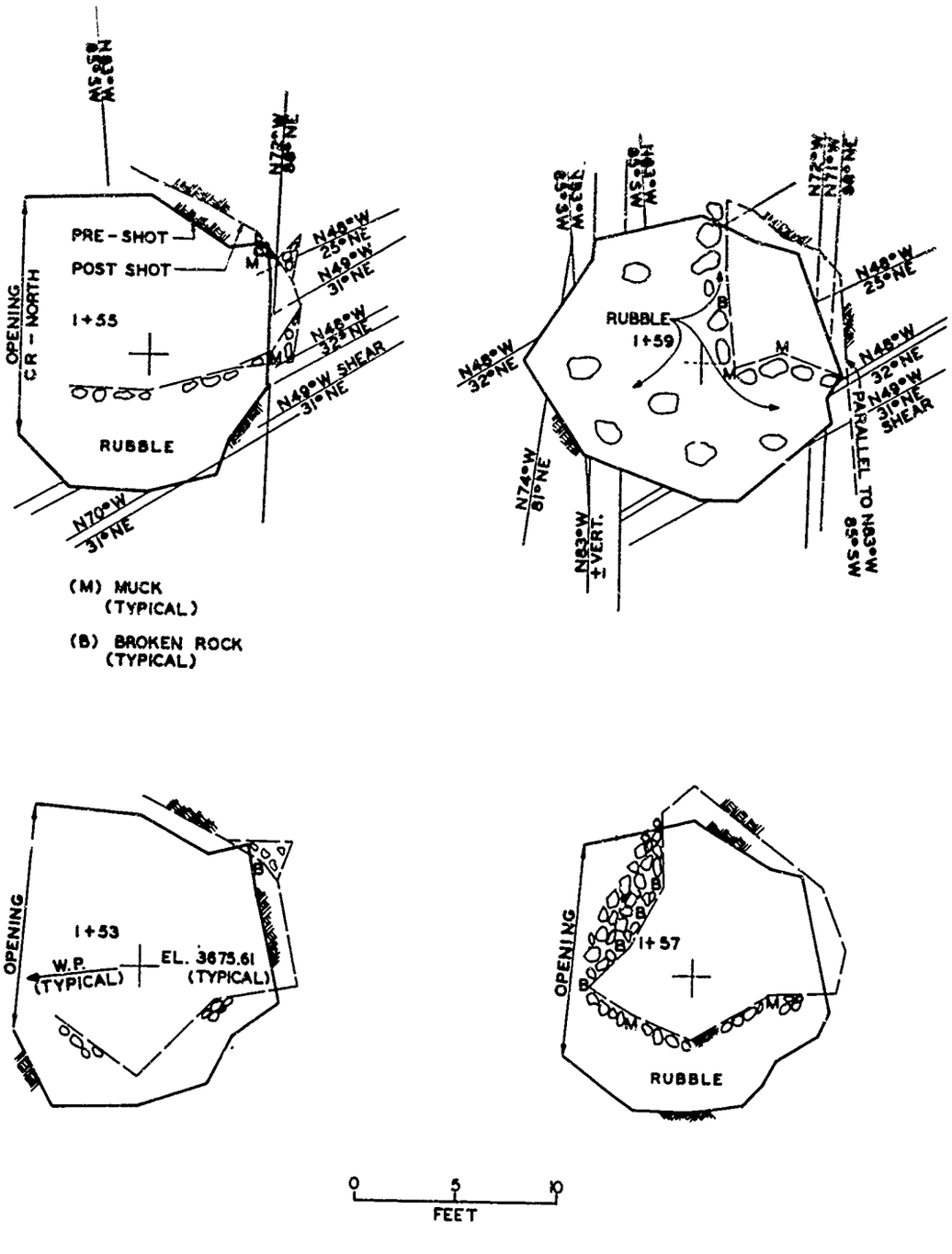

Figure 3.16 Continued (9 of 10 sheets)

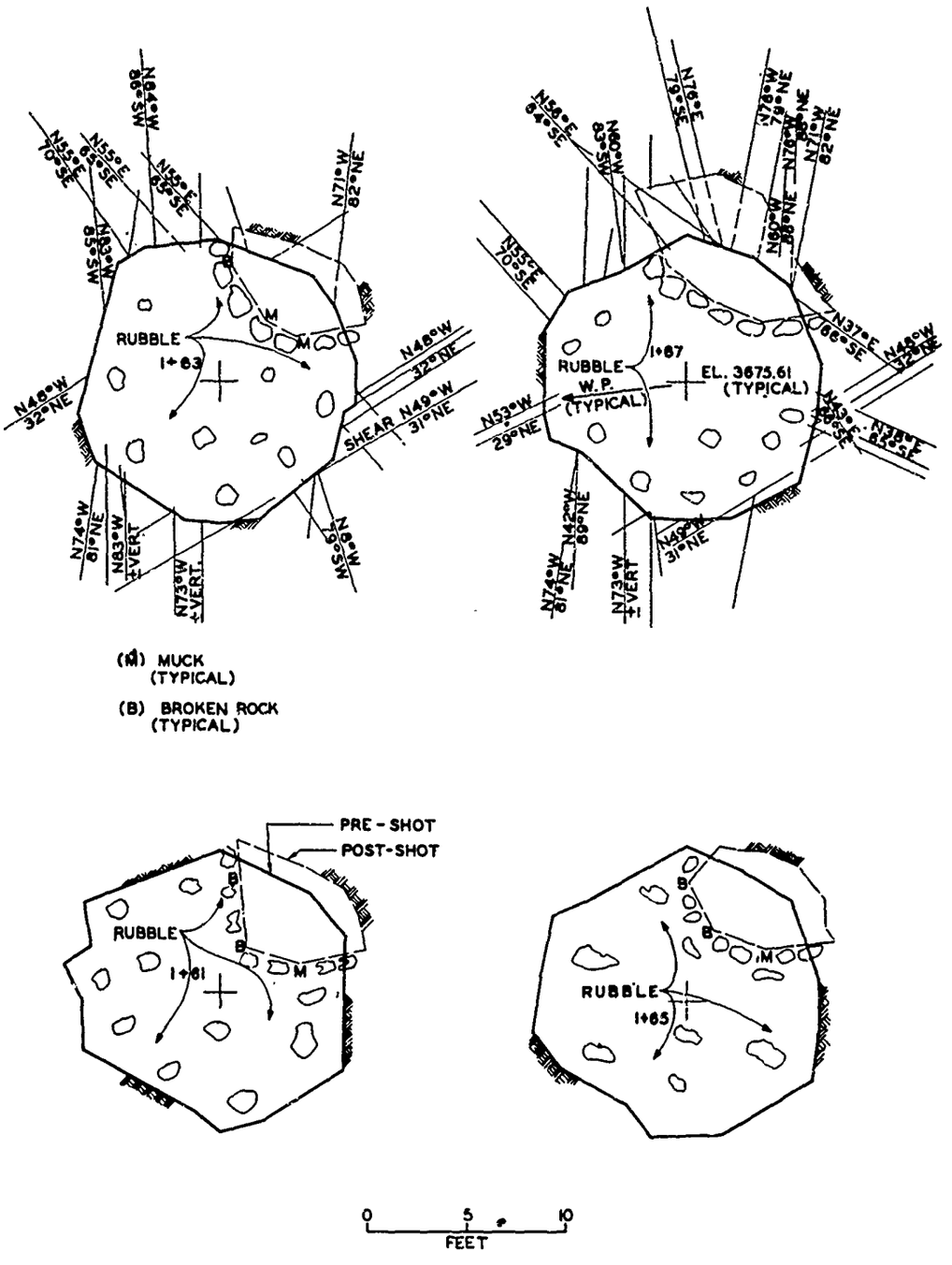

Figure 3.16 Continued (10 of 10 sheets).

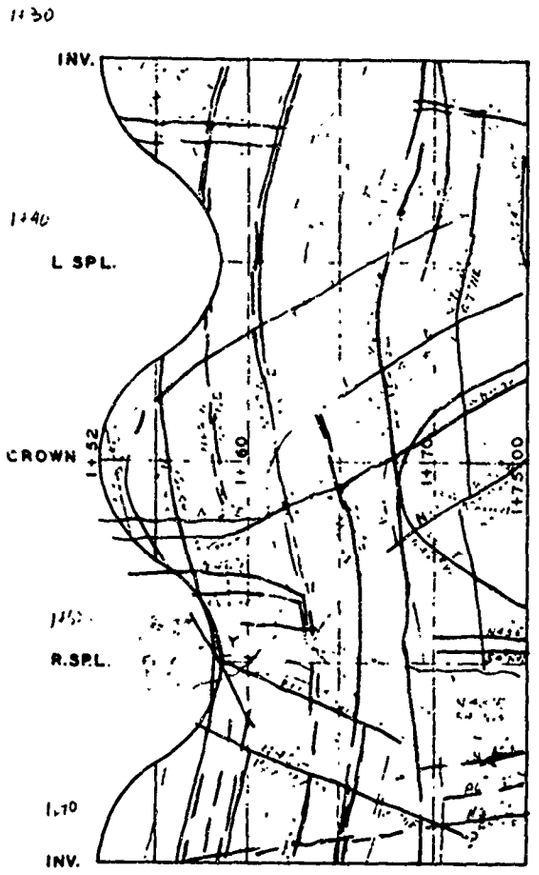

TEE INTERSECTION

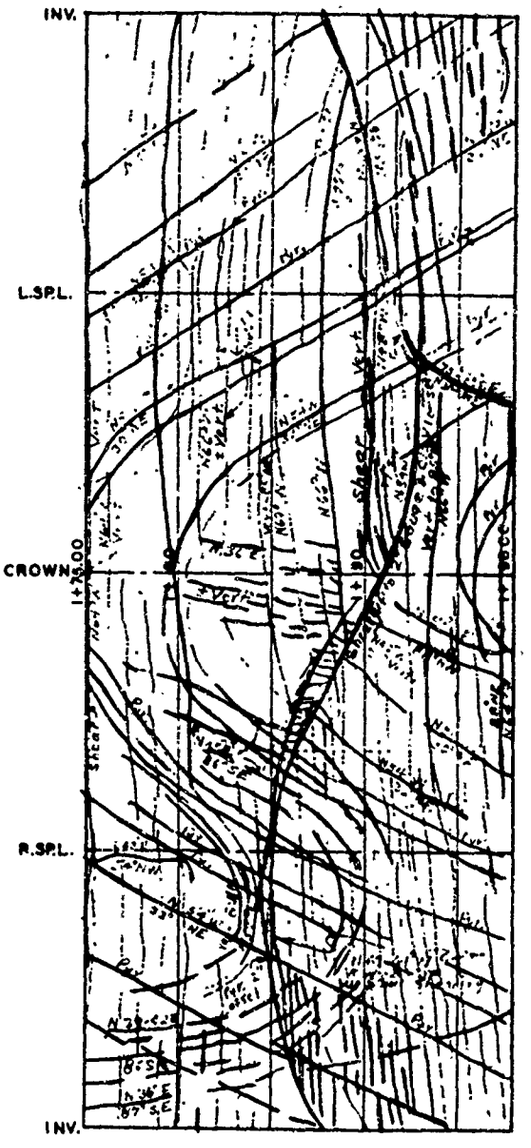

DRILL SLOT

FIGURE 3.17 a GEOLOGICAL LOGS CR NORTH DRIFT
STATION 1+52 TO 1+98

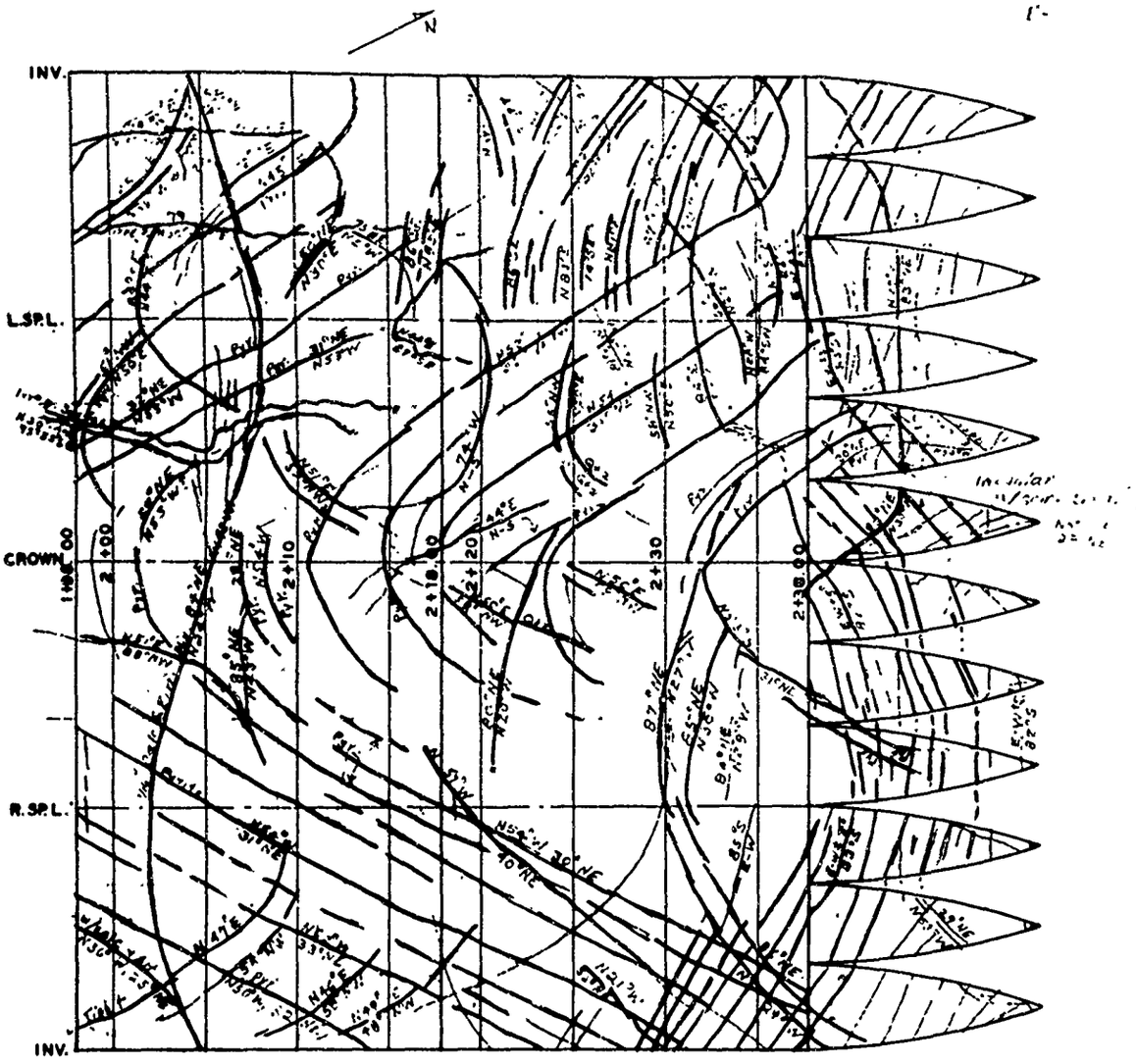

FIGURE 3.17 b GEOLOGICAL LOGS, CR NORTH DRIFT
STATION 1+98 TO END

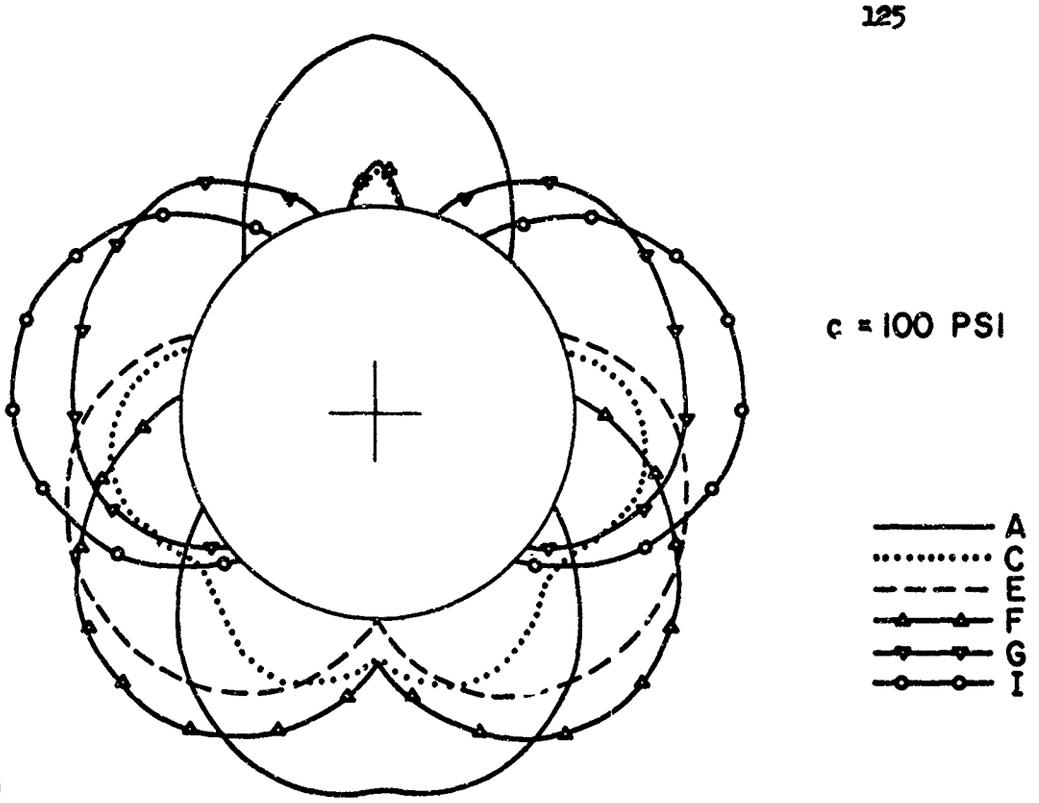

a

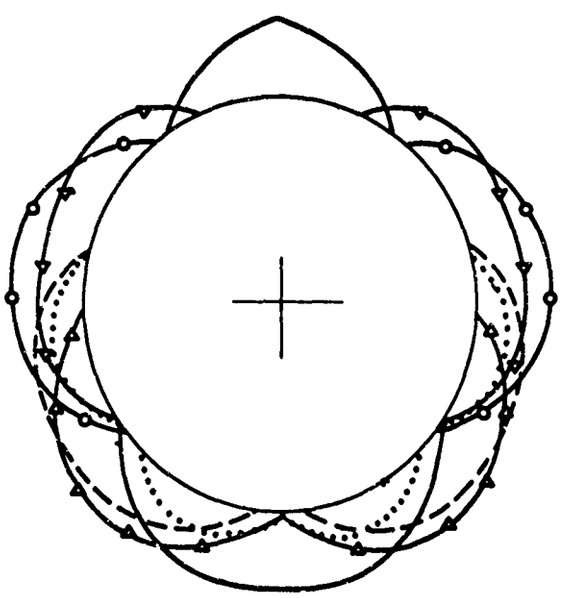

b

FIGURE 3.18 - JOINT INFLUENCE DIAGRAMS
CR DRIFT - 10,000 PSI BLAST

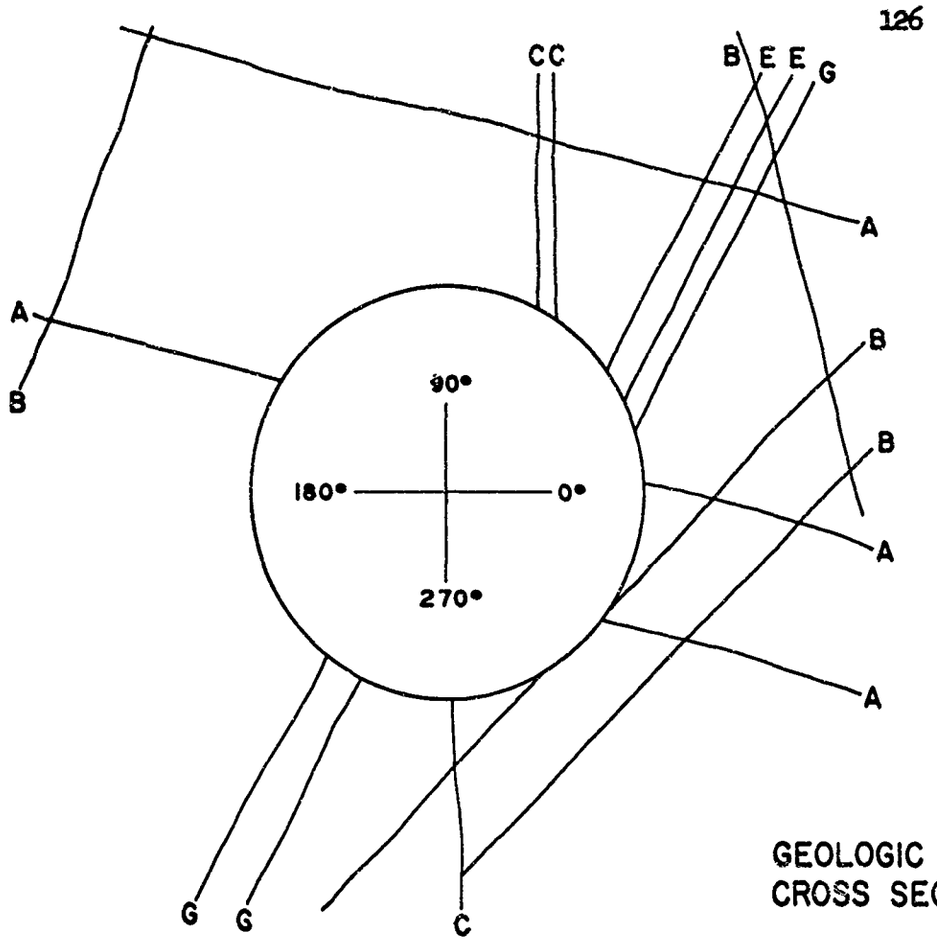

a

GEOLOGIC
CROSS SECTION

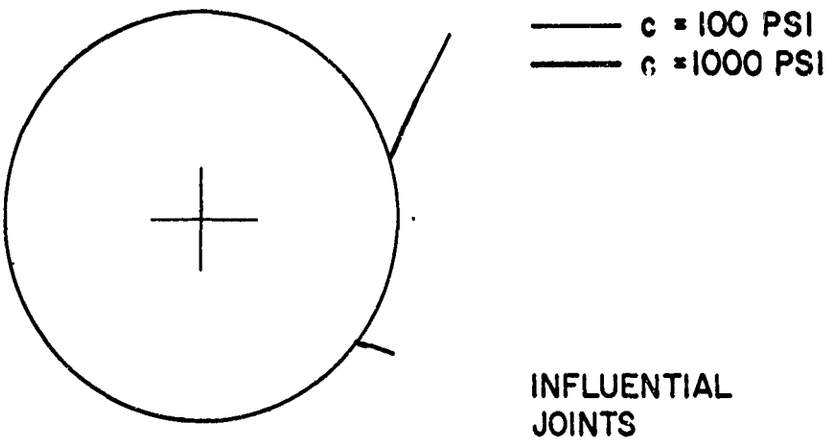

b

INFLUENTIAL
JOINTS

FIGURE 3.19 1+60, CR NORTH, 13' DIAM., 12' ROCK BOLTS AT 2'

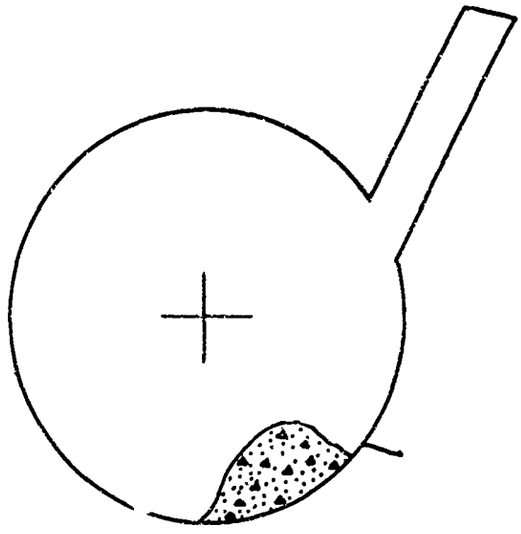

c = 100 PSI

c

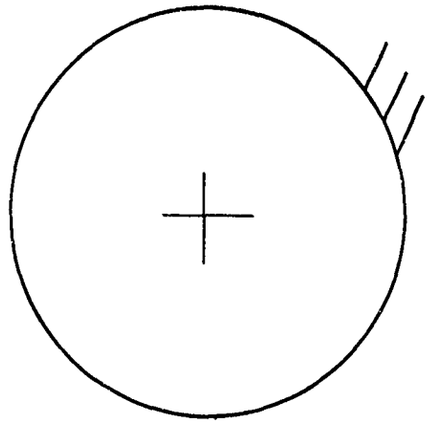

c = 1000 PSI

d

FIGURE 3.19 1+60 CR NORTH , 13' DIAM. , 12' ROCK BOLTS AT 2' PREDICTED POST - SHOCK CROSS SECTIONS

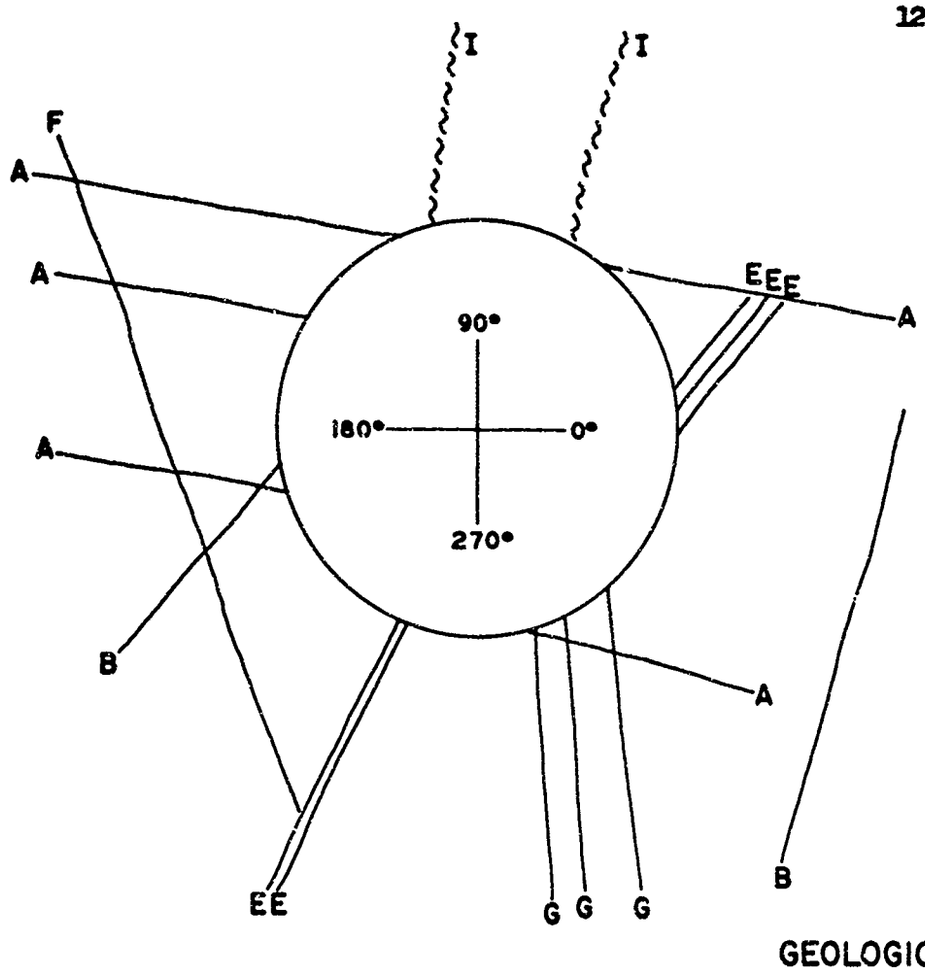

a

GEOLOGIC
CROSS SECTION

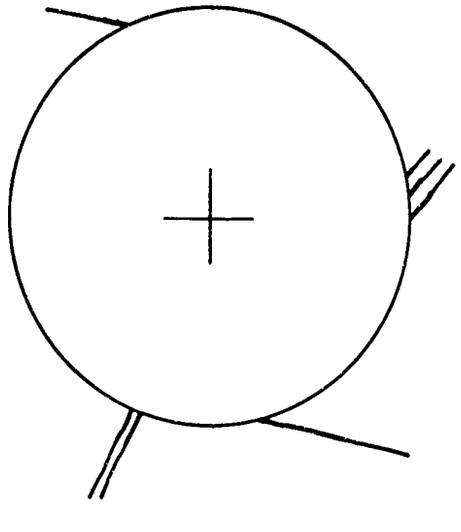

c = 100 PSI
c = 1000 PSI

b

INFLUENTIAL
JOINTS

FIGURE 3.20 I+70 CR NORTH, 13' DIAM., UNLINED

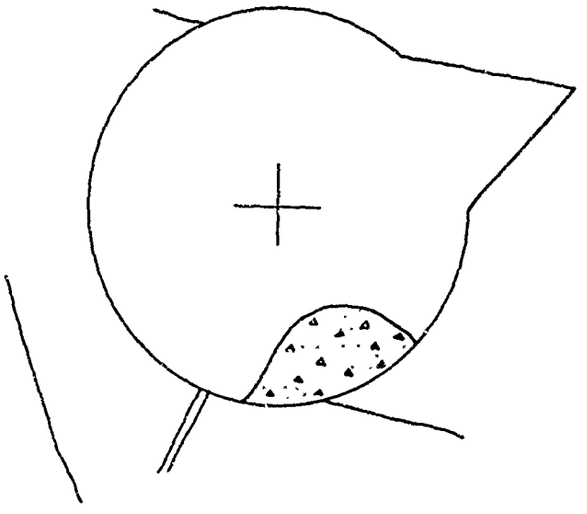

c = 100 PSI

c

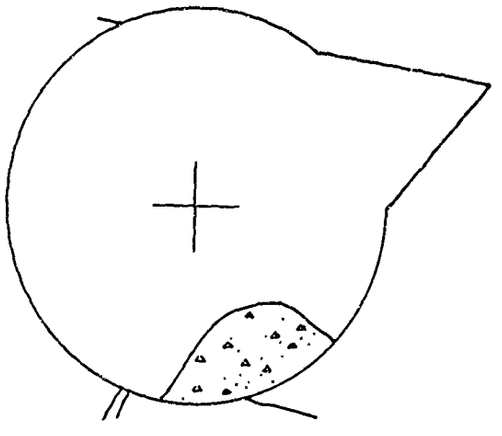

c = 1000 PSI

d

FIGURE 3.20 I+70 CR NORTH , 13' DIAM. , UNLINED
PREDICTED POST-SHOCK CROSS SECTIONS

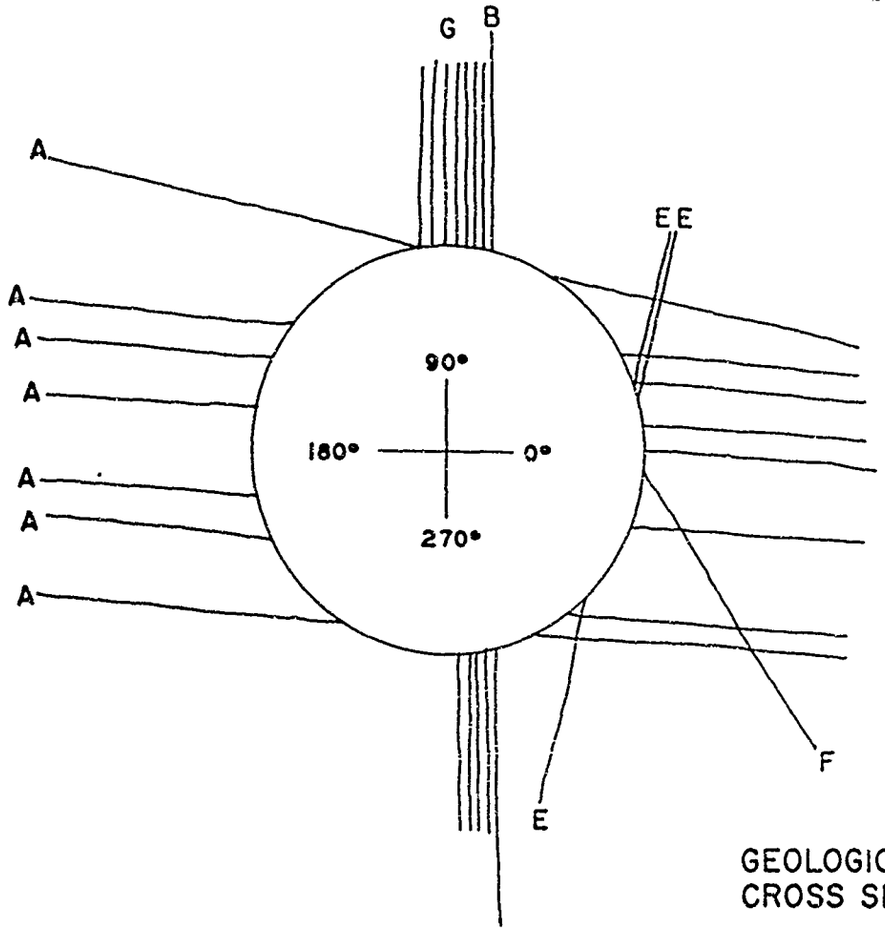

a

GEOLOGIC
CROSS SECTION

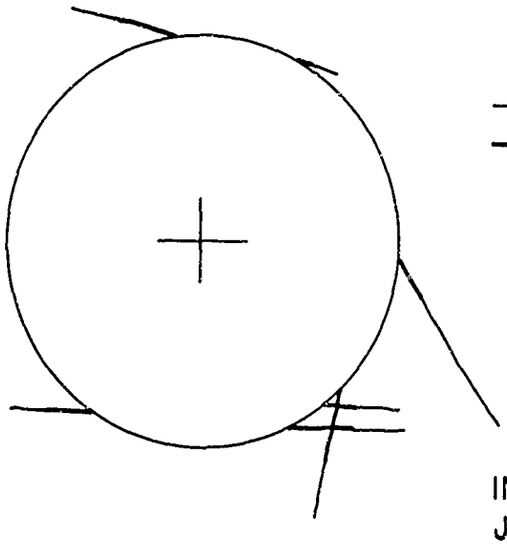

c = 100 PSI
c = 1000 PSI

b

INFLUENTIAL
JONTS

FIGURE 3.21 1+80 CR NORTH , 18' DIAM. , UNLINED

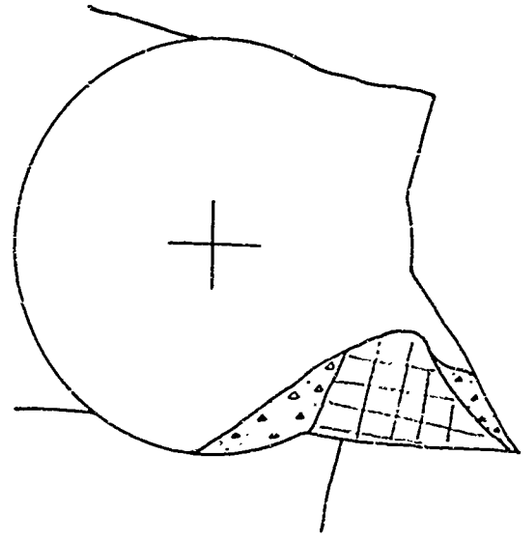

c = 100 PSI

c

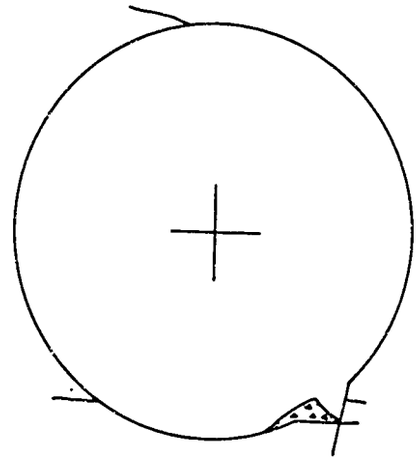

c = 1000 PSI

d

FIGURE 3.21 1+80 CR NORTH , 18' DIAM. , UNLINED
PREDICTED POST-SHOCK CROSS SECTIONS

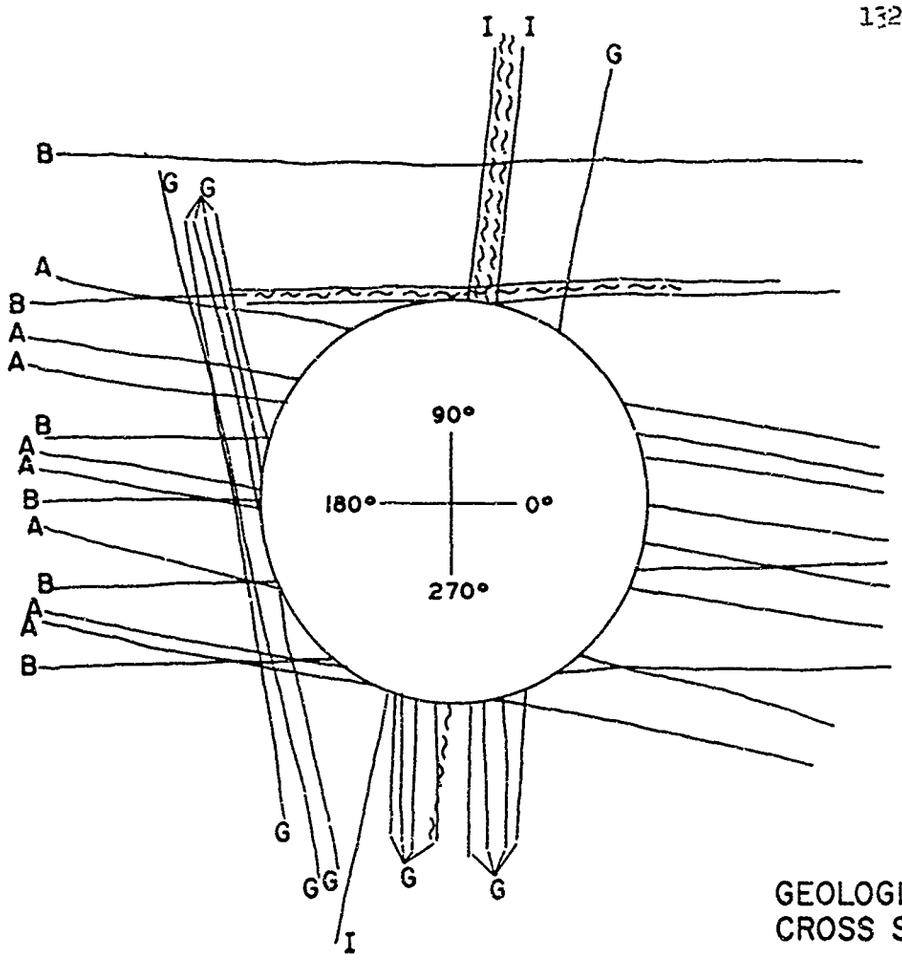

a

GEOLOGIC
CROSS SECTION

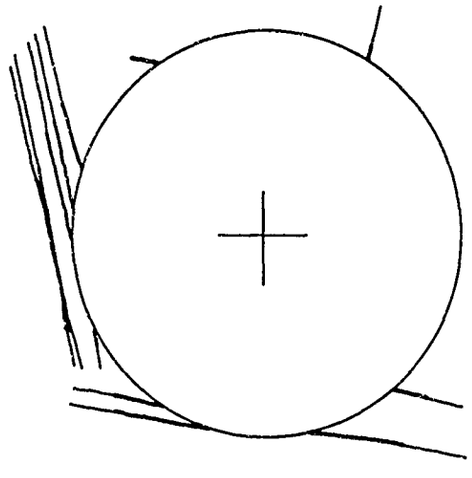

c = 100 PSI
c = 1000 PSI

b

INFLUENTIAL
JOINTS

FIGURE 3.22 1+90 CR NORTH , 18' DIAM. , UNLINED

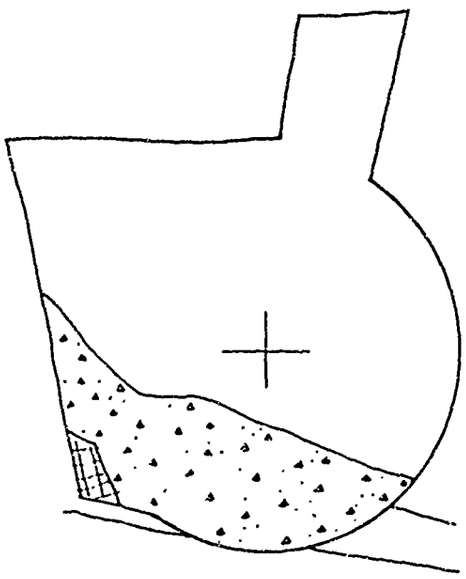

c = 100 PSI

c

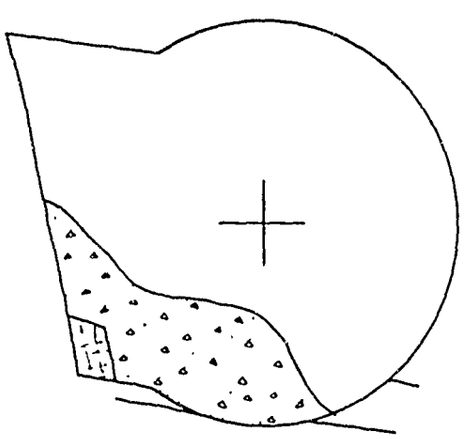

c = 1000 PSI

d

FIGURE 3.26 1+90 CR NORTH , 18' DIAM. , UNLINED
PREDICTED POST-SHOCK CROSS SECTIONS

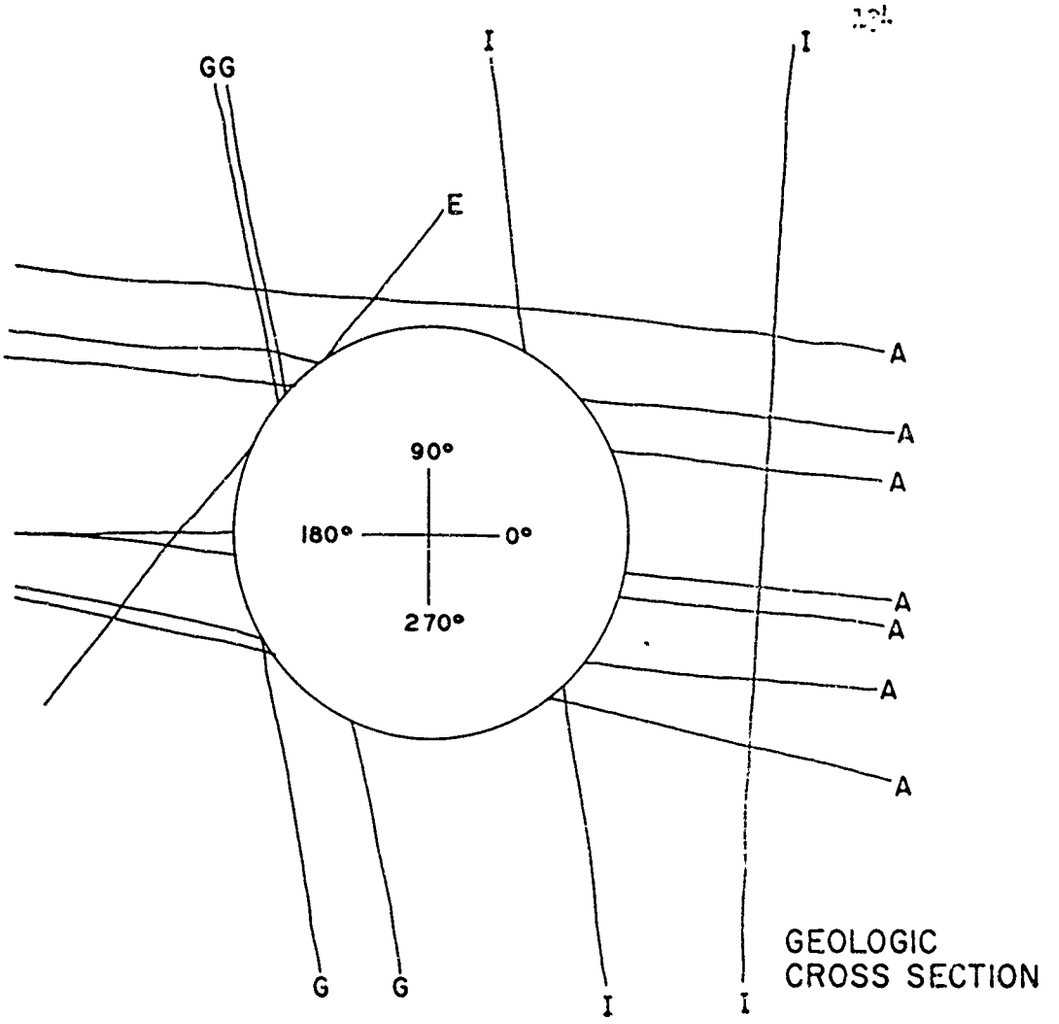

a

GEOLOGIC
CROSS SECTION

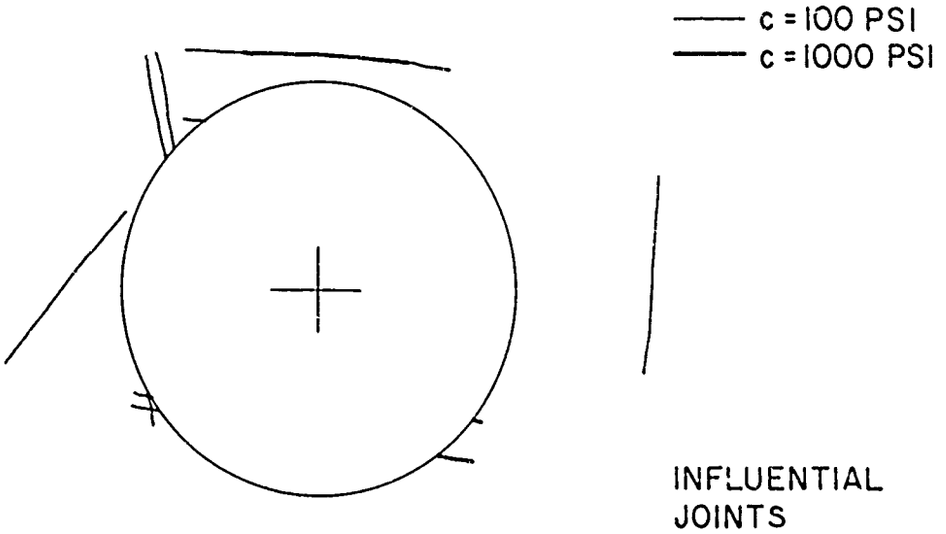

b

INFLUENTIAL
JOINTS

FIGURE 3.23 2+00 CR NORTH , 16' DIAM. , 16' ROCK BOLTS AT 2'

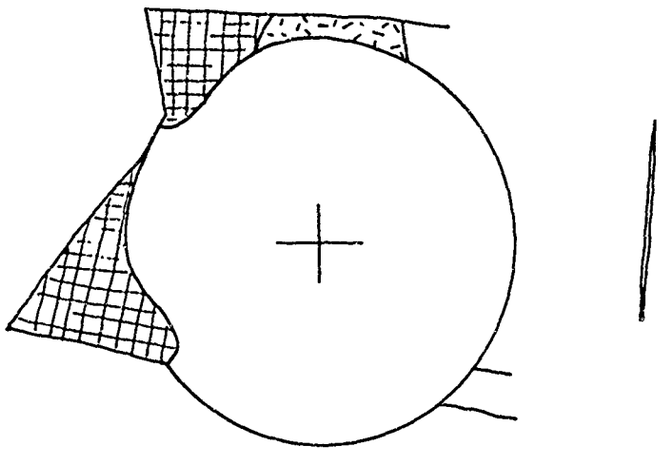

c = 100 PSI

c

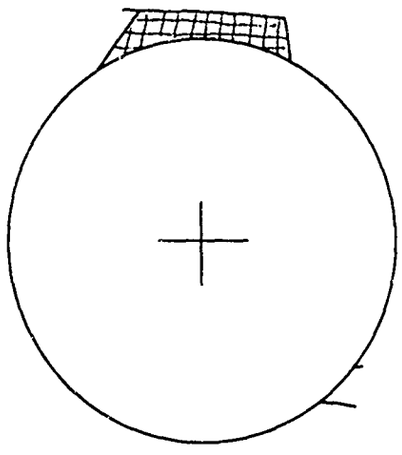

c = 1000 PSI

d

FIGURE 3.23 2+00 CR NORTH, 16' DIAM., 16' ROCK BOLTS AT 2' PREDICTED POST-SHOCK CROSS SECTIONS

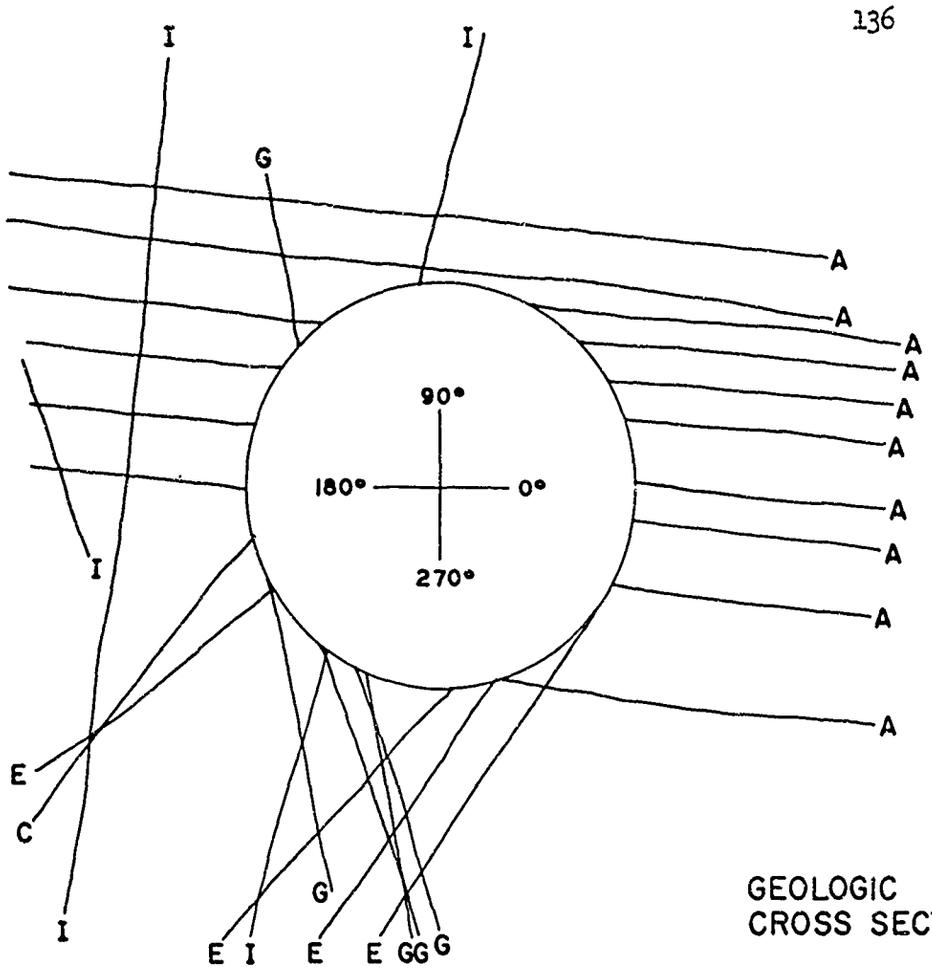

a

GEOLOGIC
CROSS SECTION

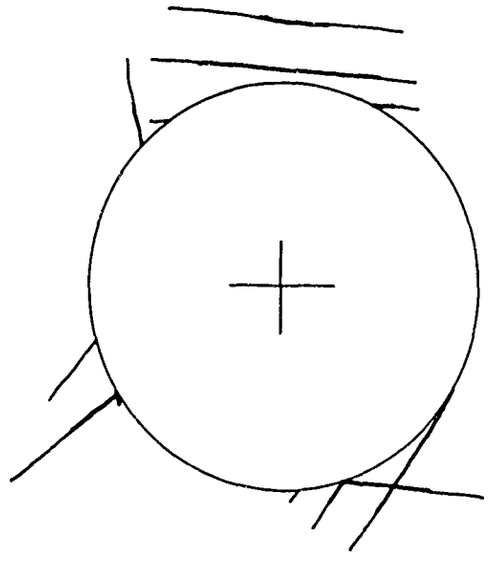

c = 100 PSI
c = 1000 PSI

INFLUENTIAL
JOINTS

b

FIGURE 3.2 2 + 10 CR NORTH , 16' DIAM. , 16' ROCK BOLTS AT 2'

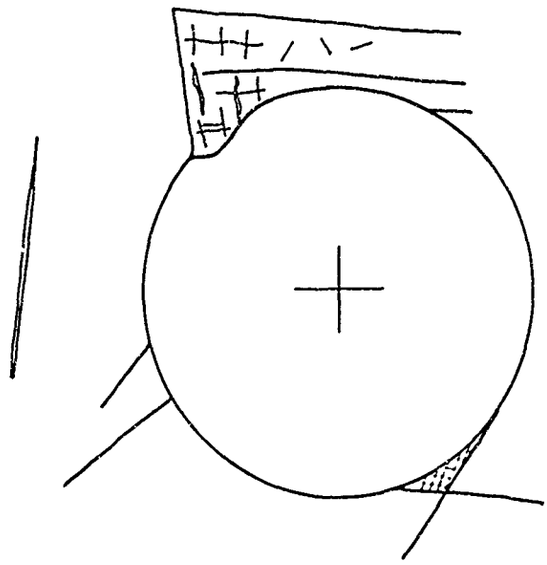

c = 100 PSI

c

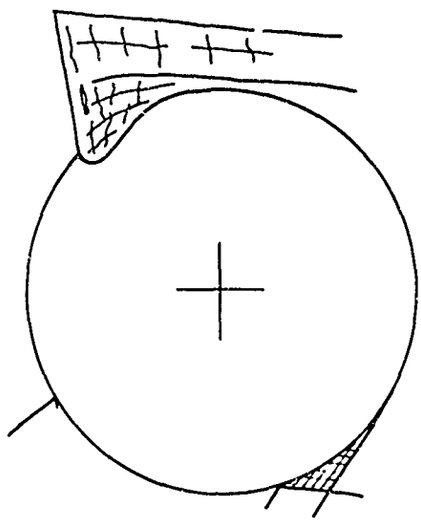

c = 1000 PSI

d

FIGURE 3:24 2+10 CR NORTH , 16' DIAM. , 16' ROCK BOLTS AT 2' PREDICTED POST-SHOCK CROSS SECTIONS

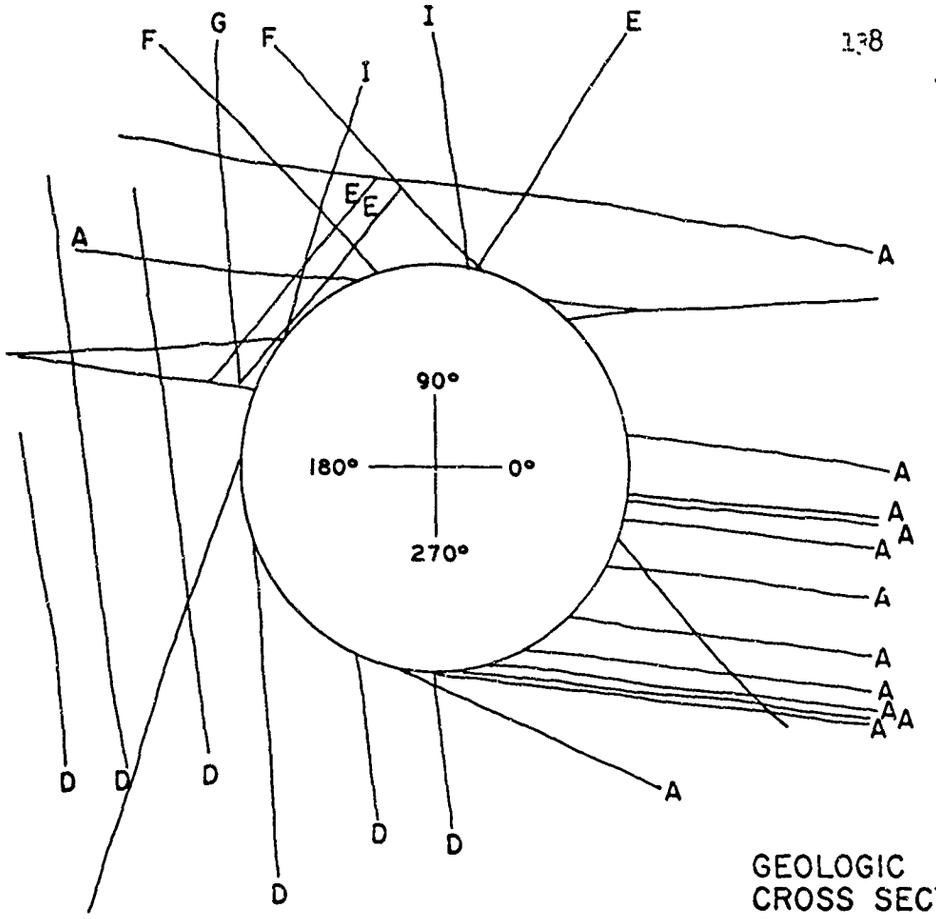

a

GEOLOGIC
CROSS SECTION

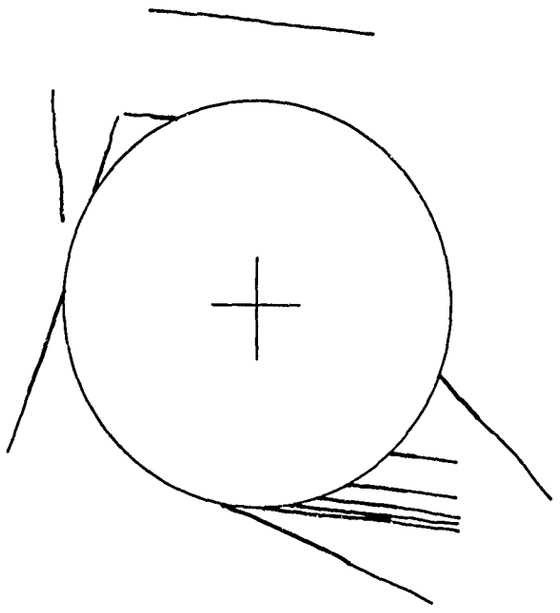

c = 100 PSI
c = 1000 PSI

b

INFLUENTIAL
JOINTS

FIGURE 3.25 2+20 CR NORTH , 16' DIAM. , 16' ROCK BOLTS AT 2'

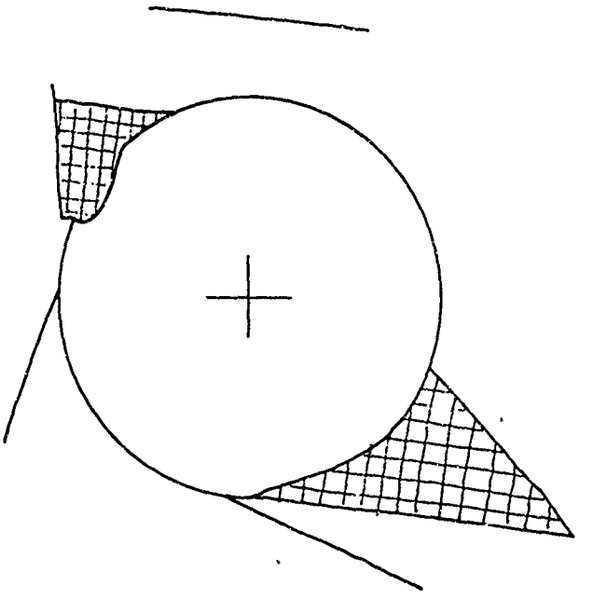

c = 100 PSI

c

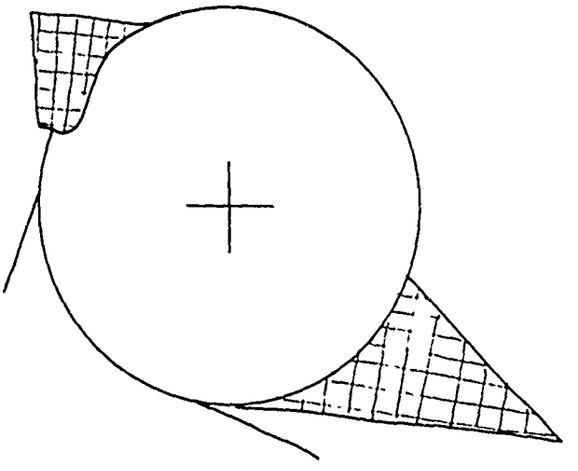

c = 1000 PSI

d

FIGURE 3.25 2+20 CR NORTH , 16' DIAM. , 16' ROCK BOLTS AT 2' PREDICTED POST-SHOCK CROSS SECTIONS

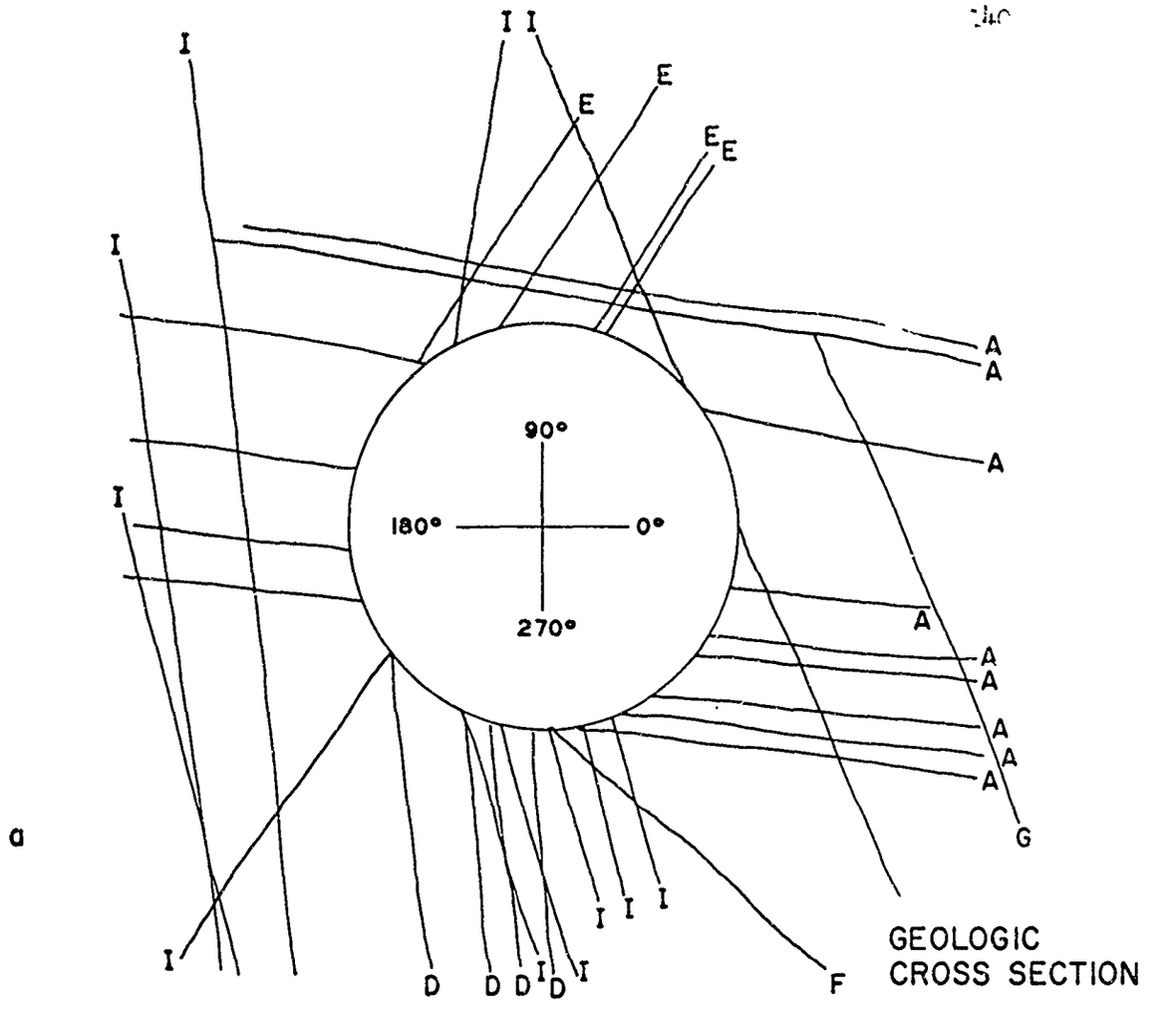

a

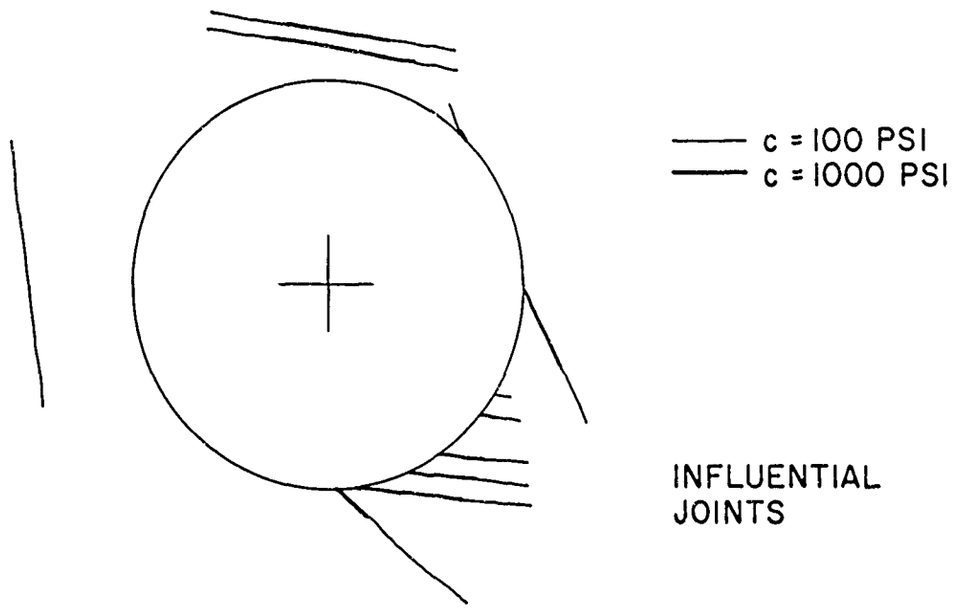

b

FIGURE 3.26 2+30 CR NORTH, 16' DIAM., 16' ROCK BOLTS AT 2'

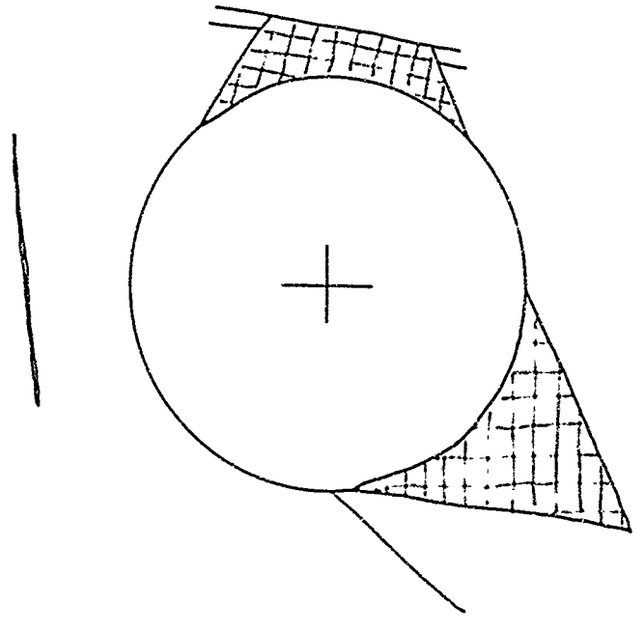

c = 100 PSI

c

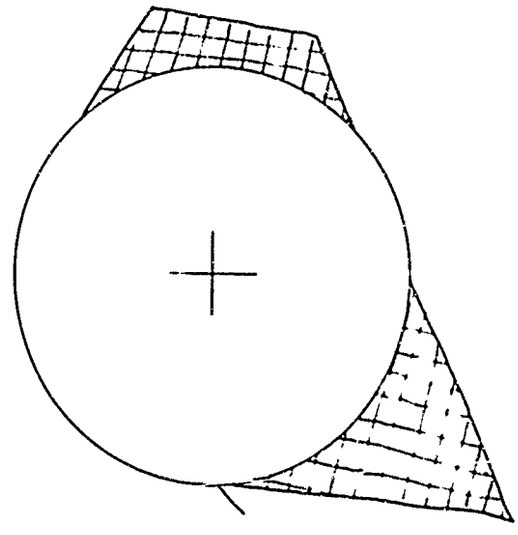

c = 1000 PSI

d

FIGURE 3.26 2+30 CR NORTH , 16' DIAM. , 16' ROCK BOLTS AT 2' PREDICTED POST-SHOCK CROSS SECTIONS

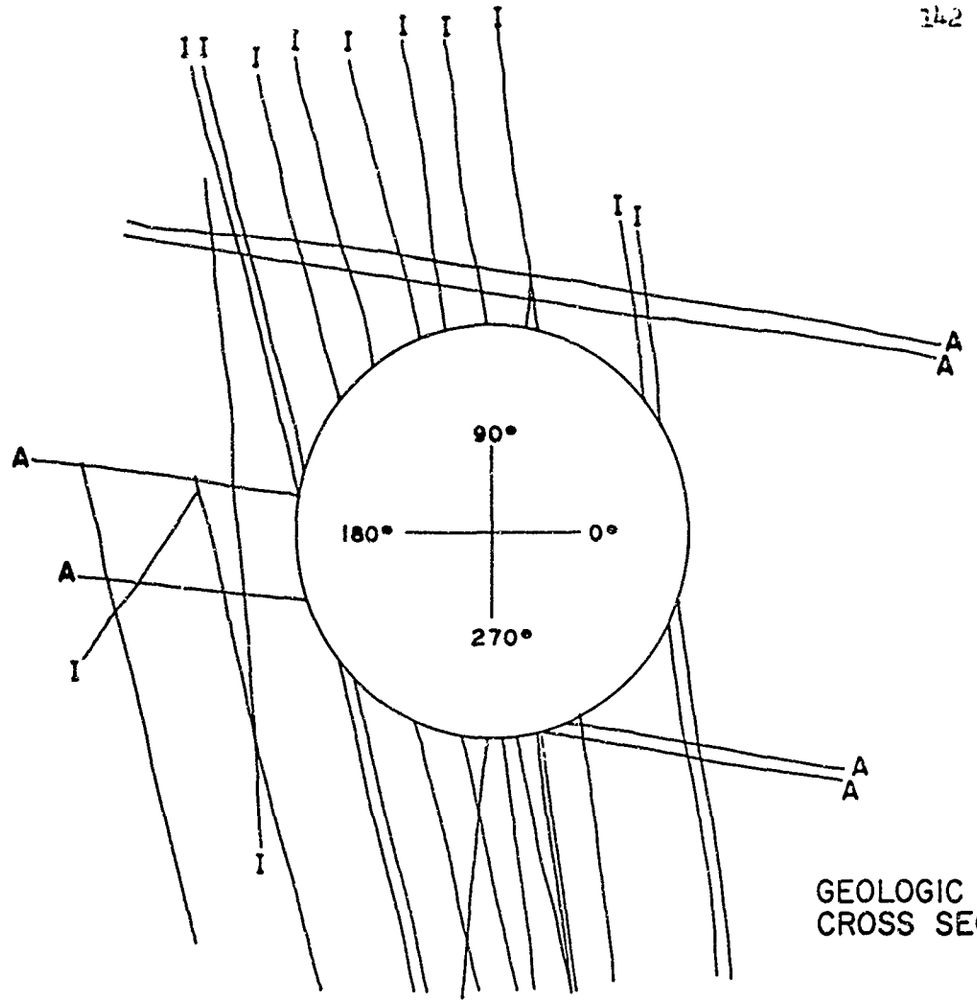

a

GEOLOGIC
CROSS SECTION

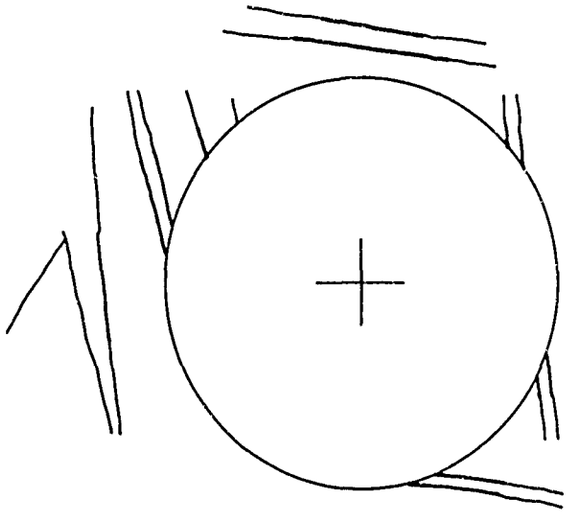

c = 100 PSI
c = 1000 PSI

b

INFLUENTIAL
JOINTS

FIGURE 3.27 2+38 CR NORTH , 16' DIAM. , 16' ROCK BOLTS AT 2'

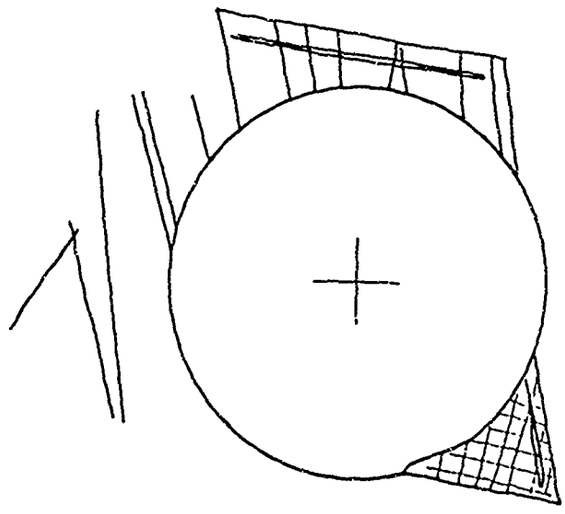

c = 100 PSI

c

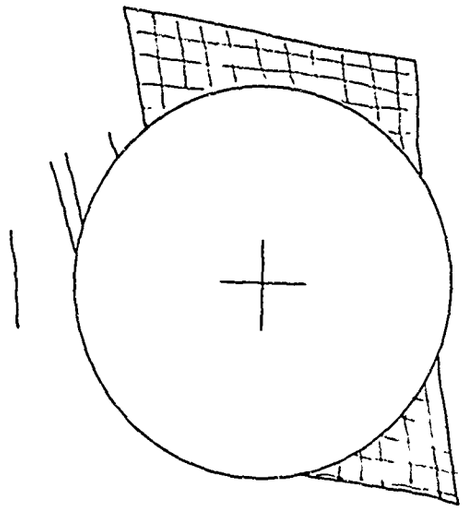

c = 1000 PSI

d

FIGURE 3.27 2+38 CR NORTH , 16' DIAM. , 16' ROCK BOLTS AT 2' PREDICTED POST-SHOCK CROSS SECTIONS

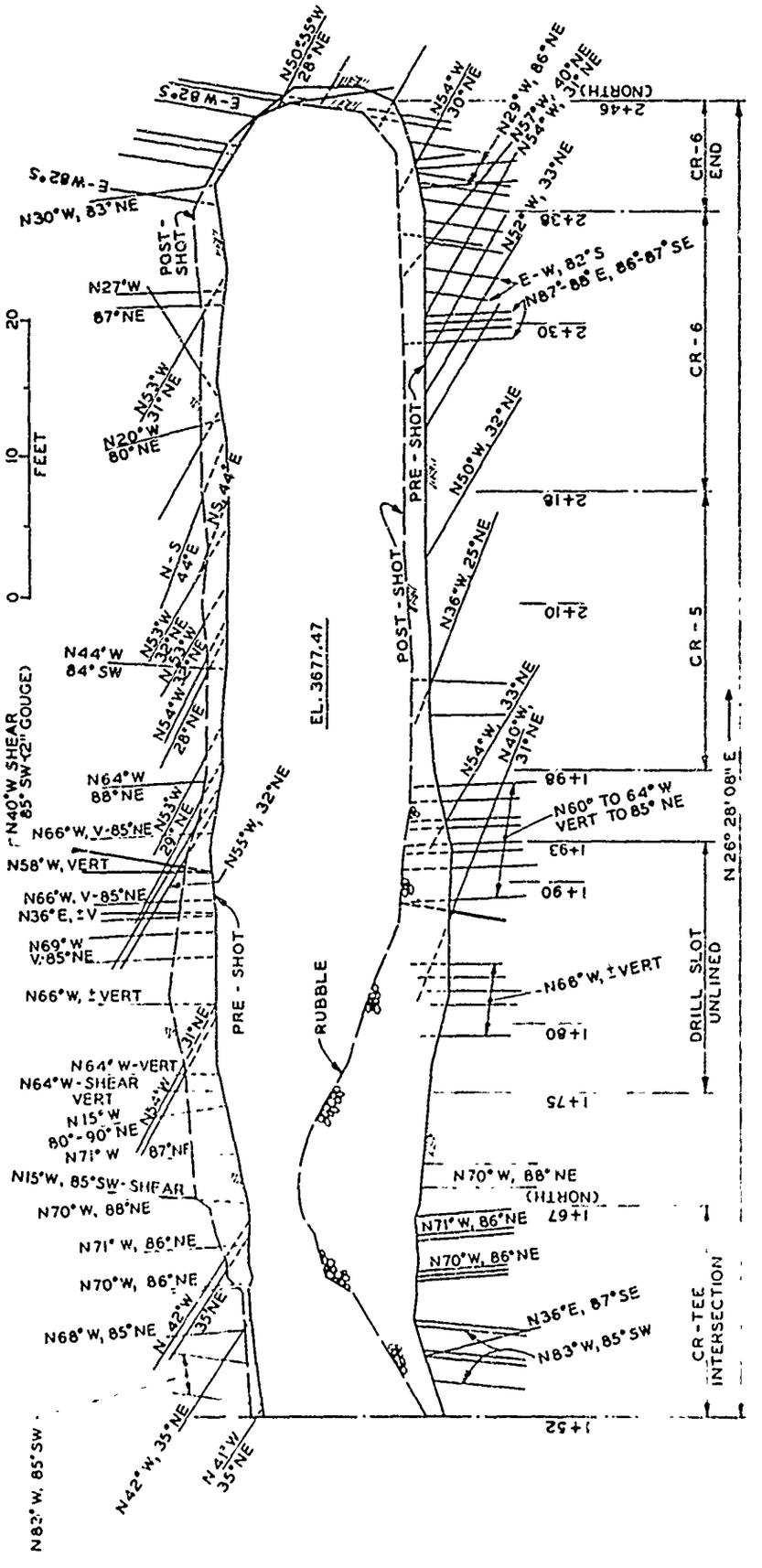

Fig. 3.28 Sectional elevation at centerline and geology - CR North Drift

(Fig. of POR 4015, Chapter 4)

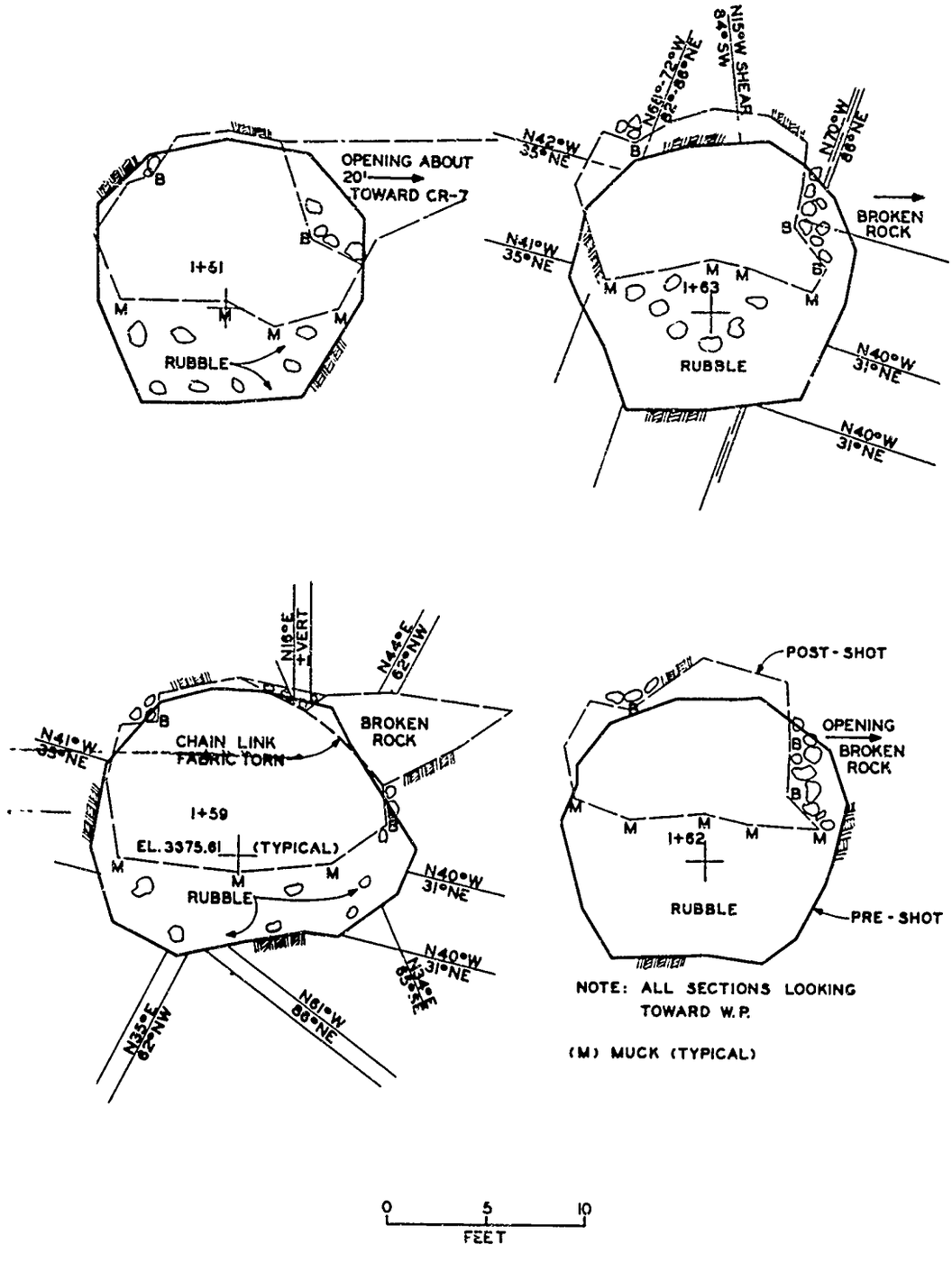

Figure 3.29 Cross sections and geology - CR North Drift (1 of 8 sheets)
(Fig. 3.82 of POR 4015, Chapter 4)

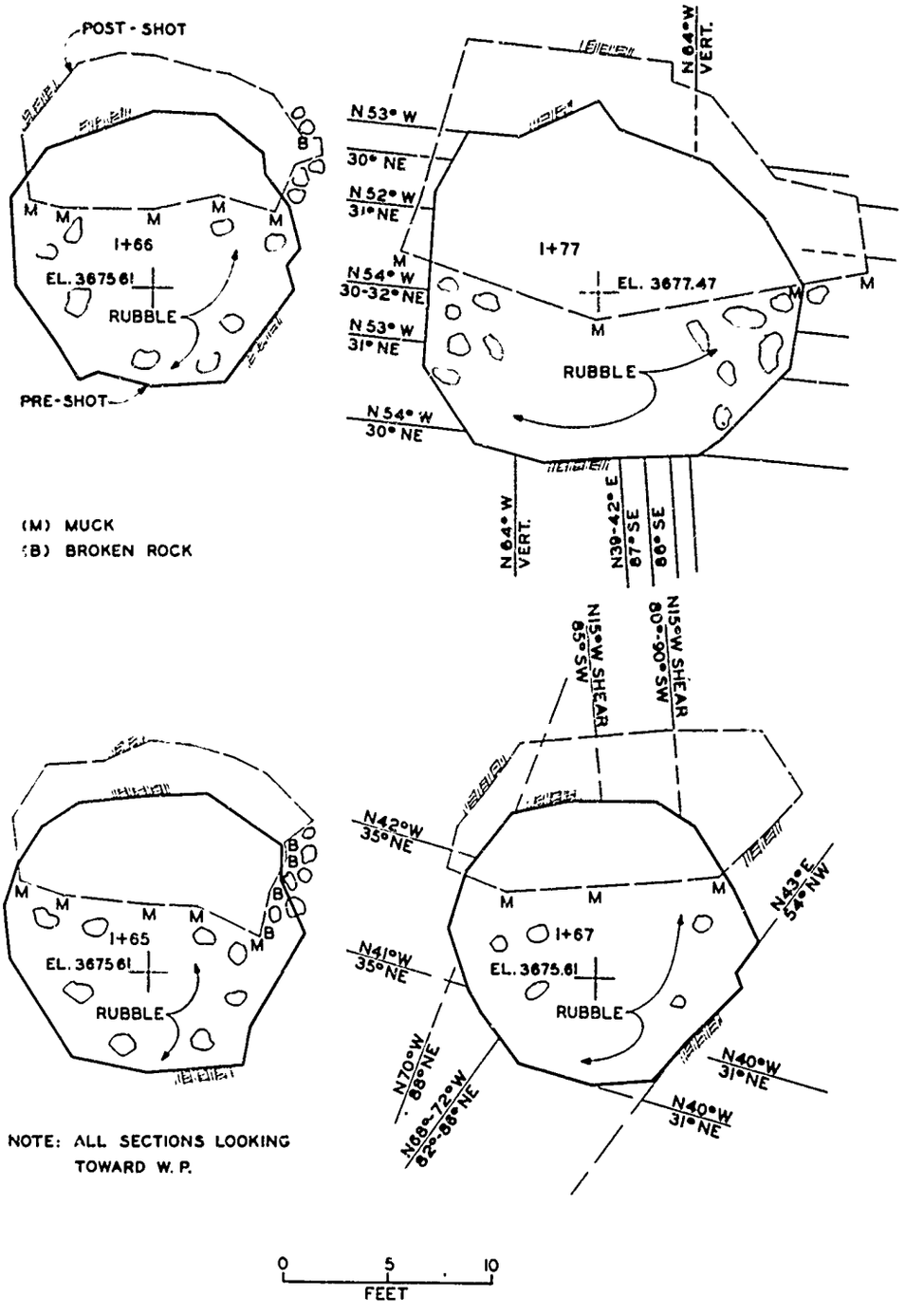

Figure 3.29 Continued (2 of 8 sheets)

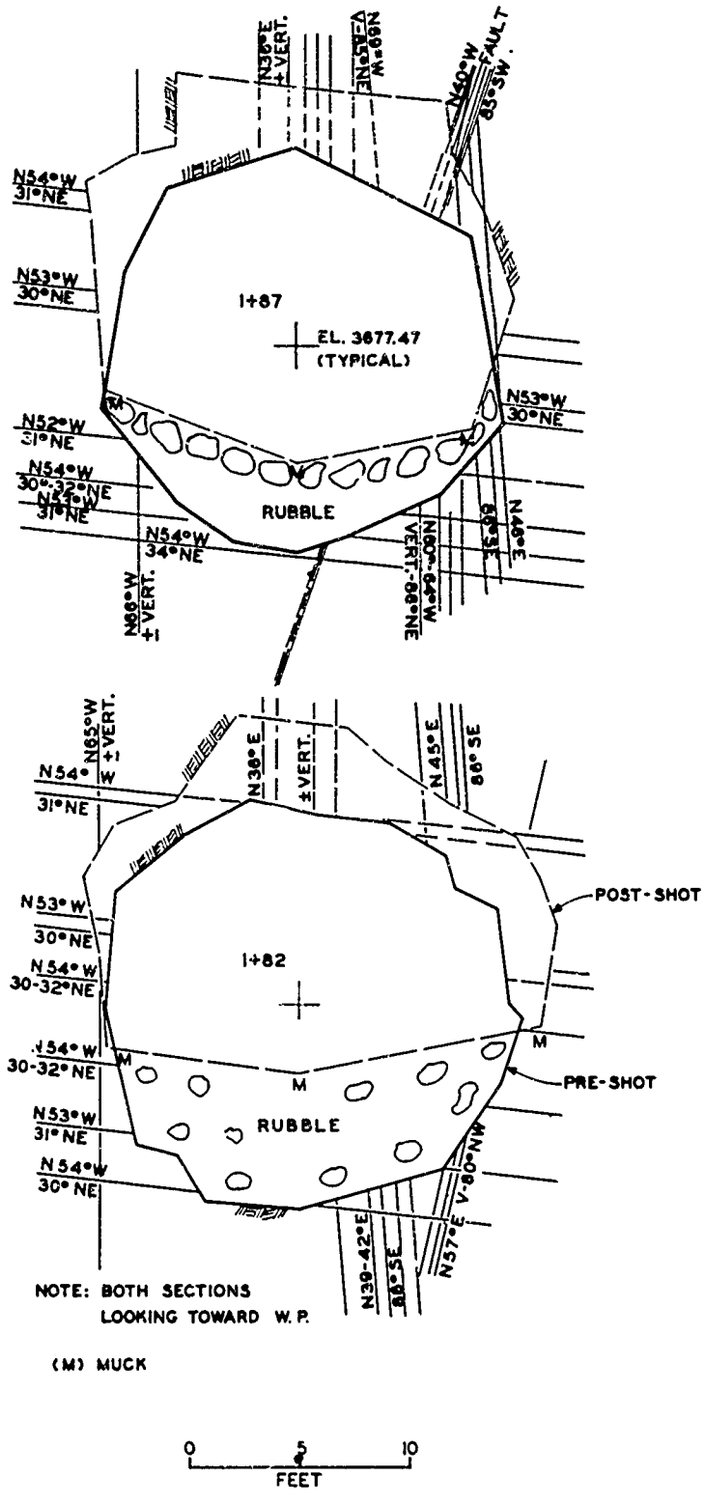

Figure 3.29 Continued (3 of 8 sheets)

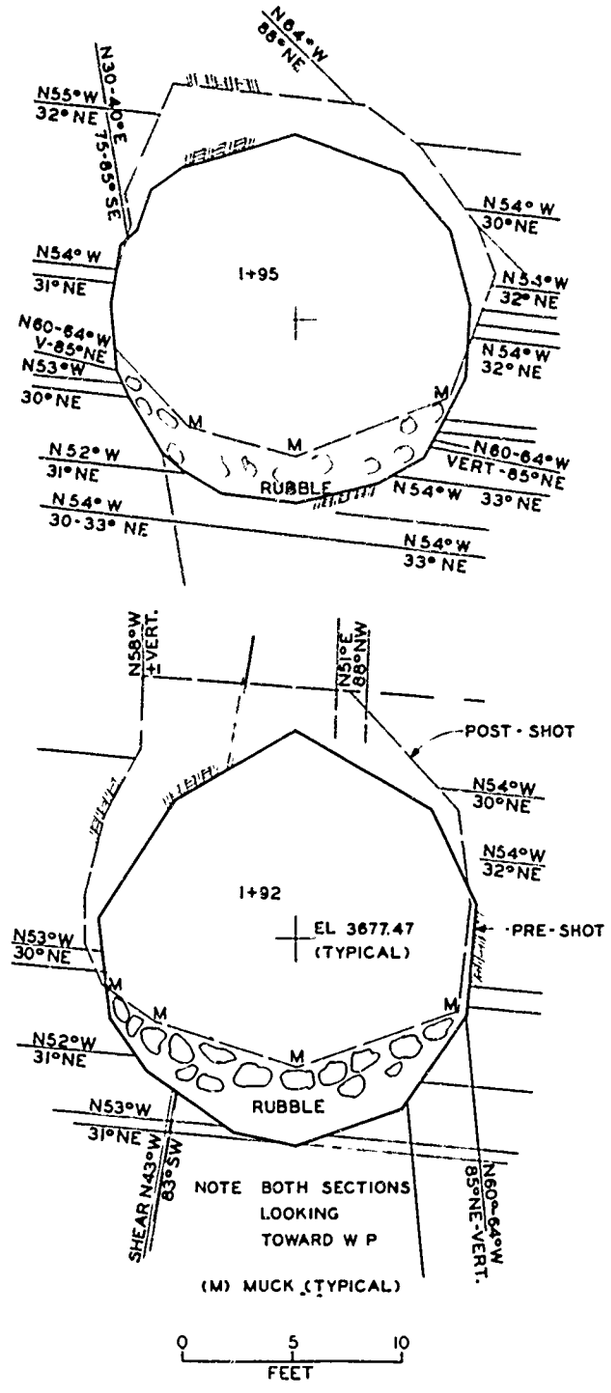

Figure 3.29 Continued (4 of 8 sheets)

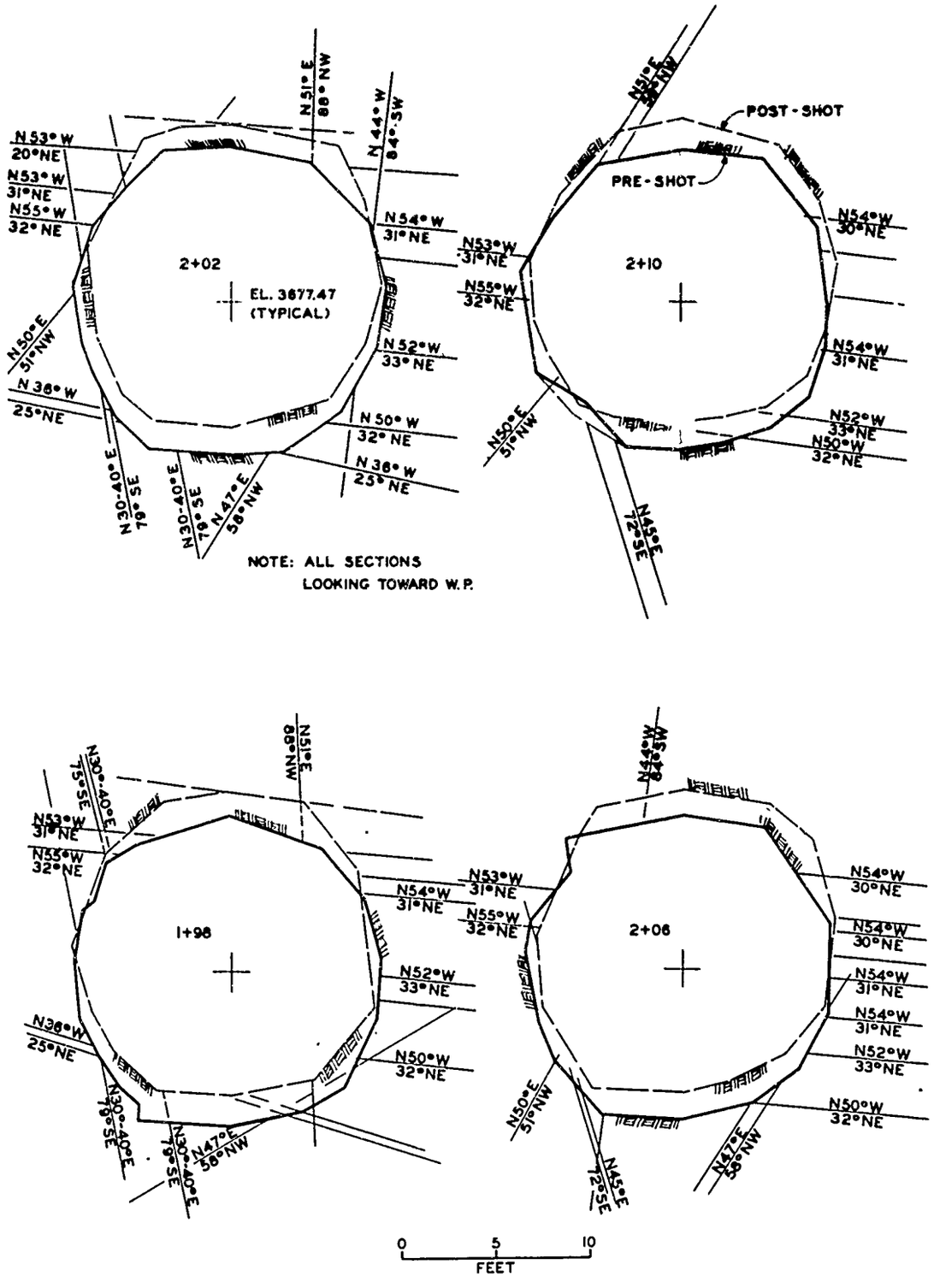

Figure 3.29 Continued (5 of 8 sheets)

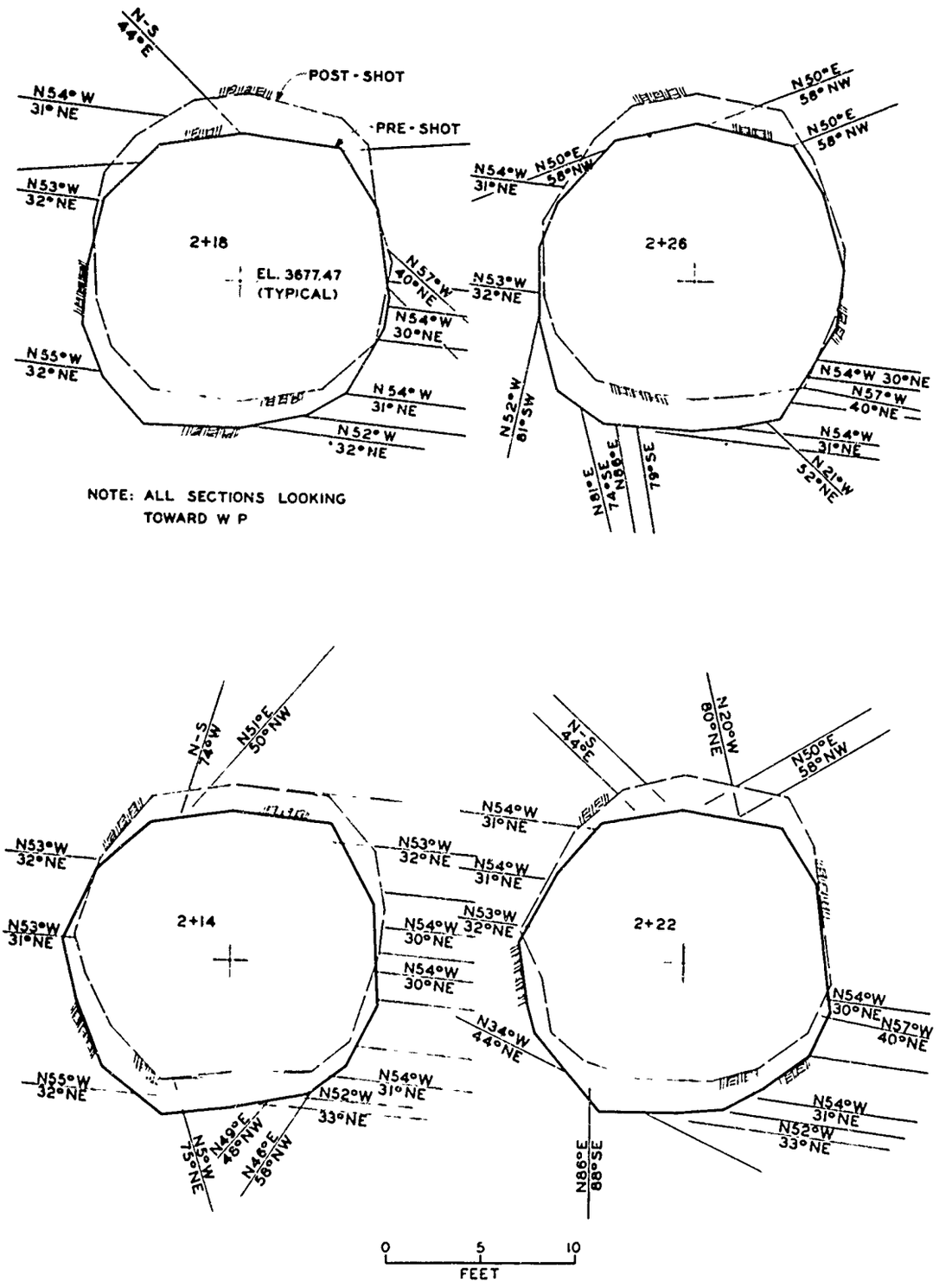

Figure 3.29 Continued (6 of 8 sheets)

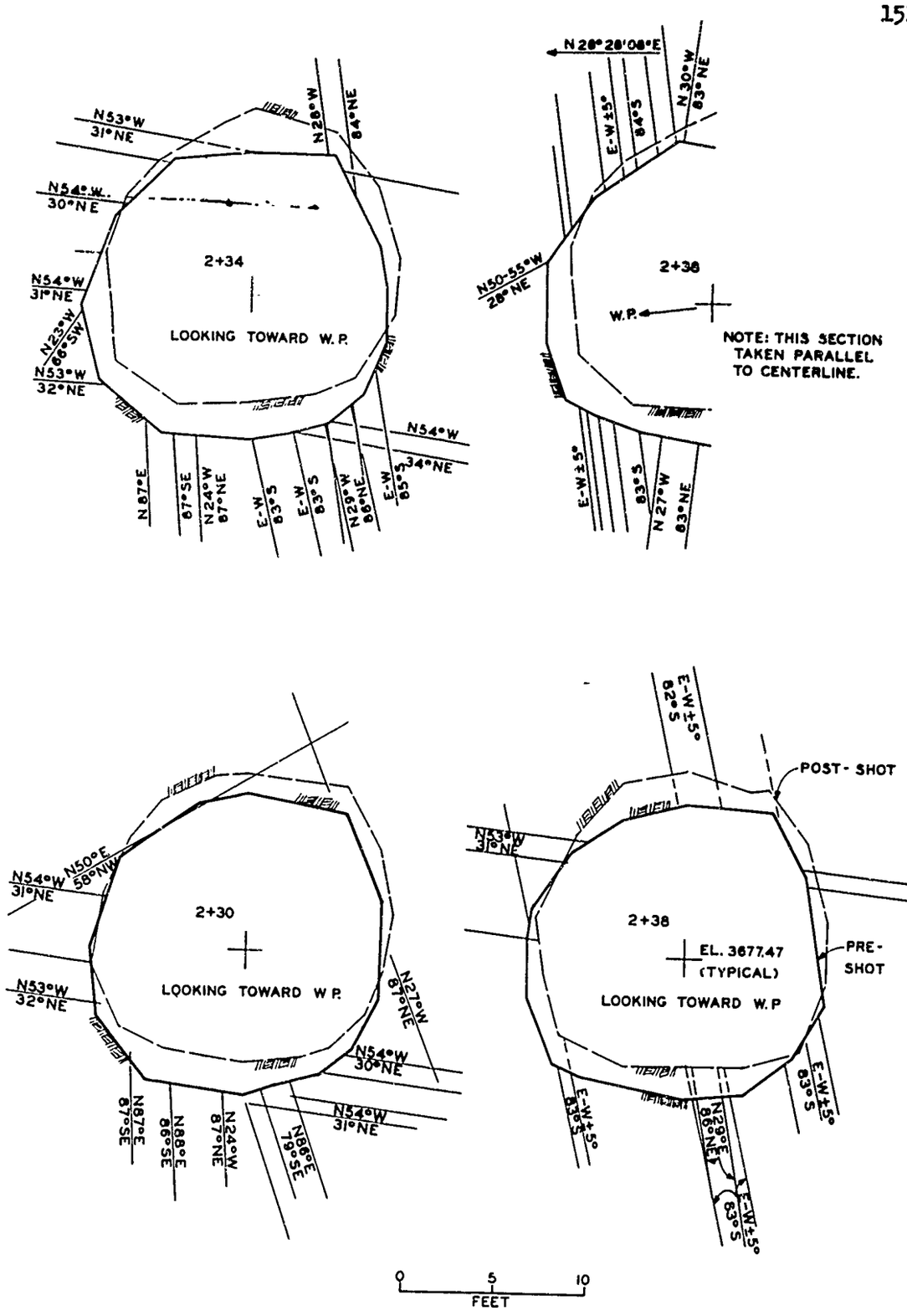

Figure 3.29 Continued (7 of 8 sheets)

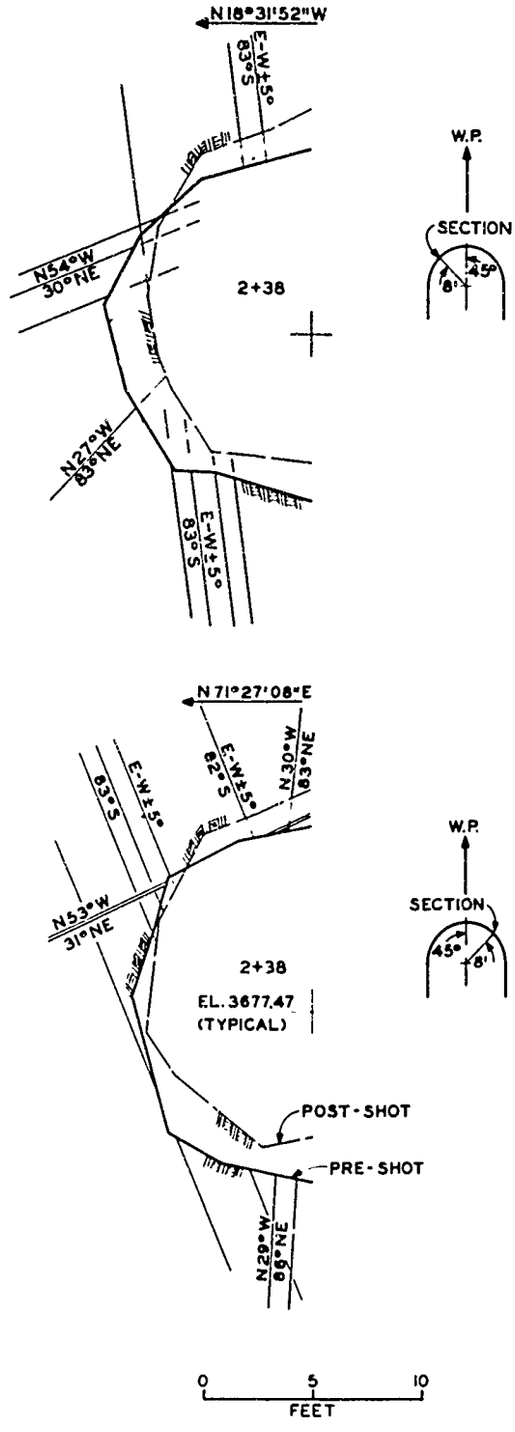

Figure 3.29 Continued (8 of 8 sheets)

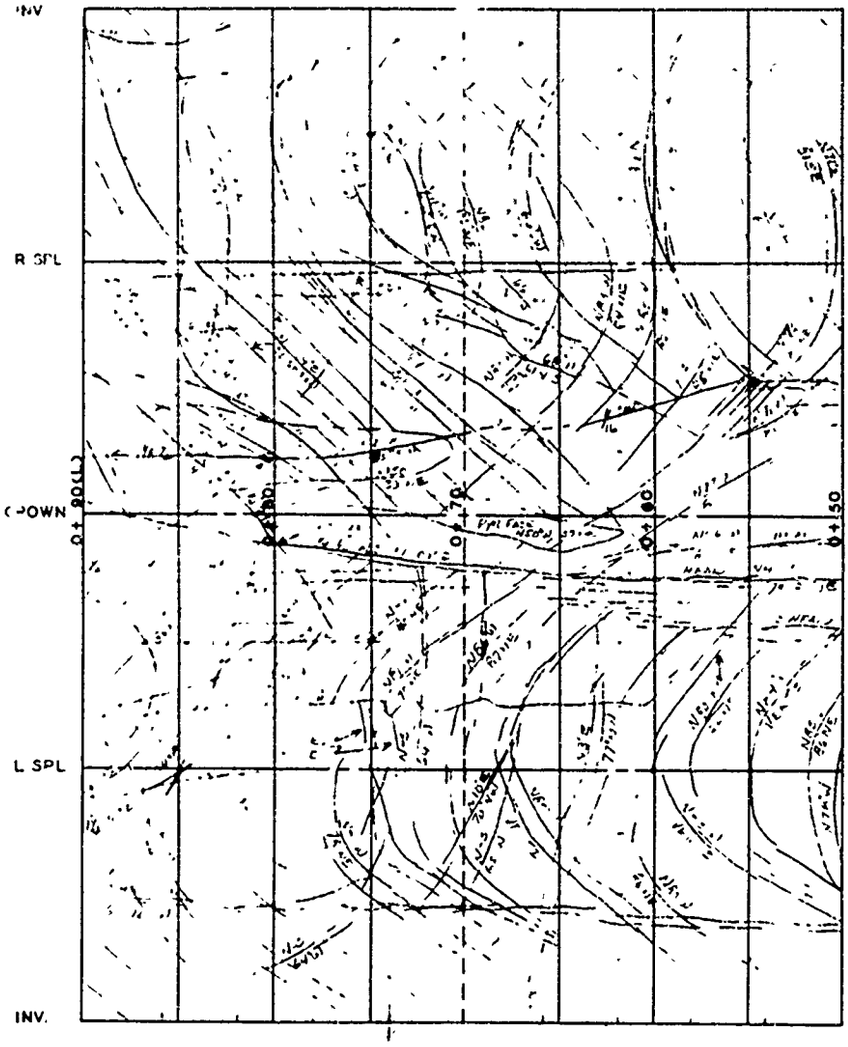

FIGURE 3.30 GEOLOGICAL LOGS DL 1,2
STATION 0+50 TO 0+90

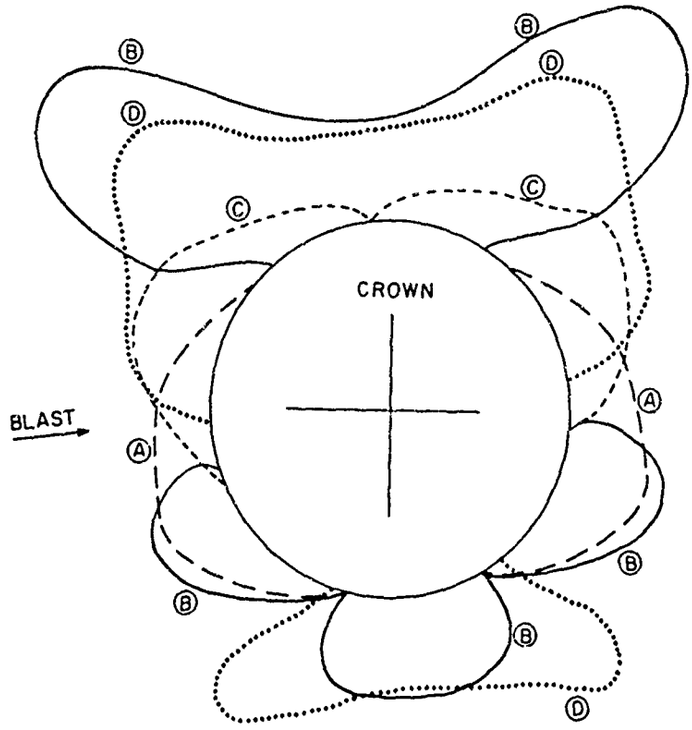

FIGURE 3.31 INFLUENCE DIAGRAMS FOR DL 1-2 DRIFT.
10,000 PSI BLAST PRESSURE.

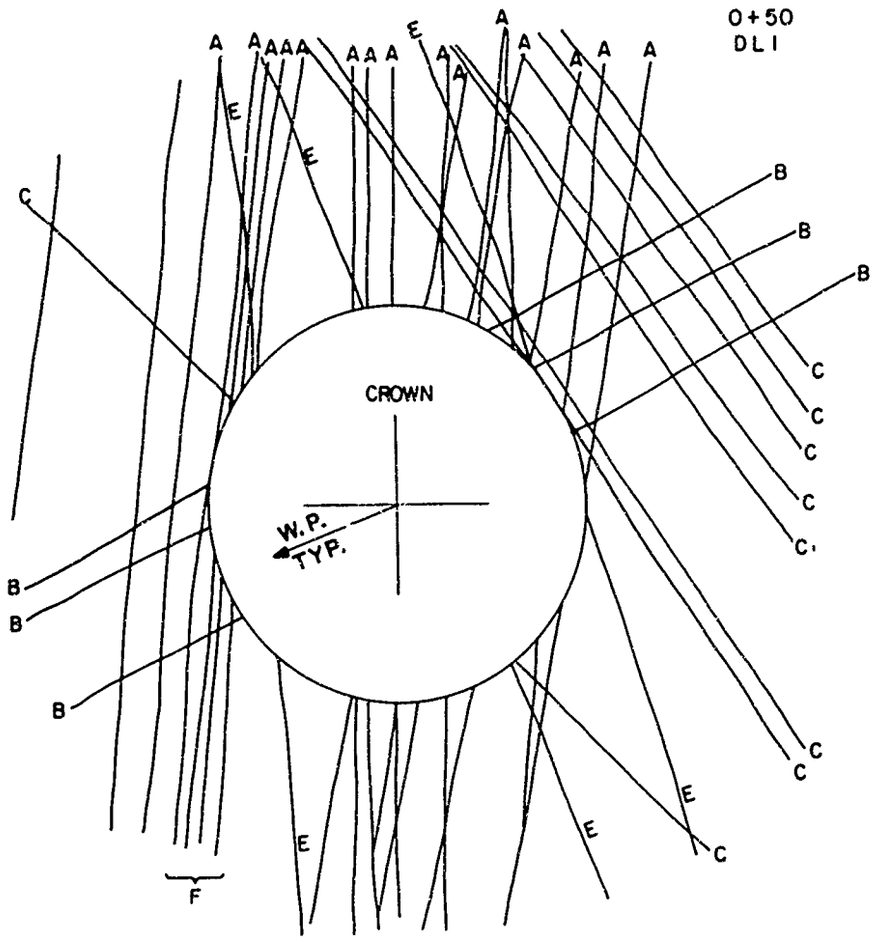

FIGURE 3.32a GEOLOGIC CROSS SECTION - STA 0+50

0+50

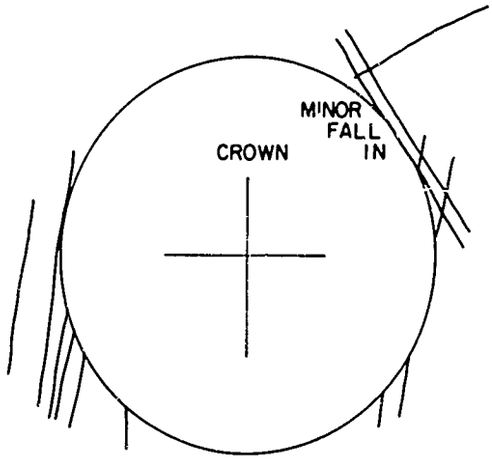

FIGURE 3.32b INFLUENTIAL JOINTS

0+50

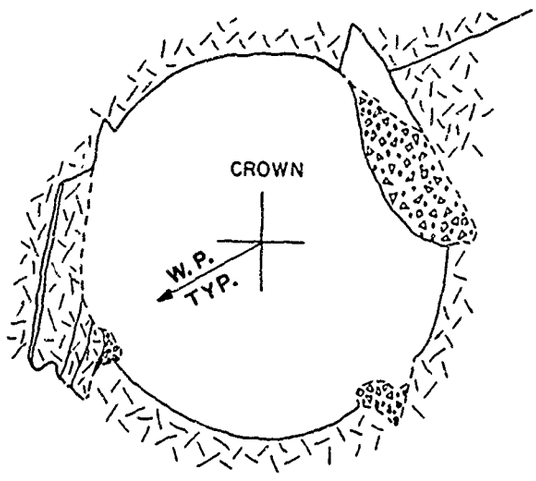

FIGURE 3.32c PREDICTED POST SHOCK SECTION

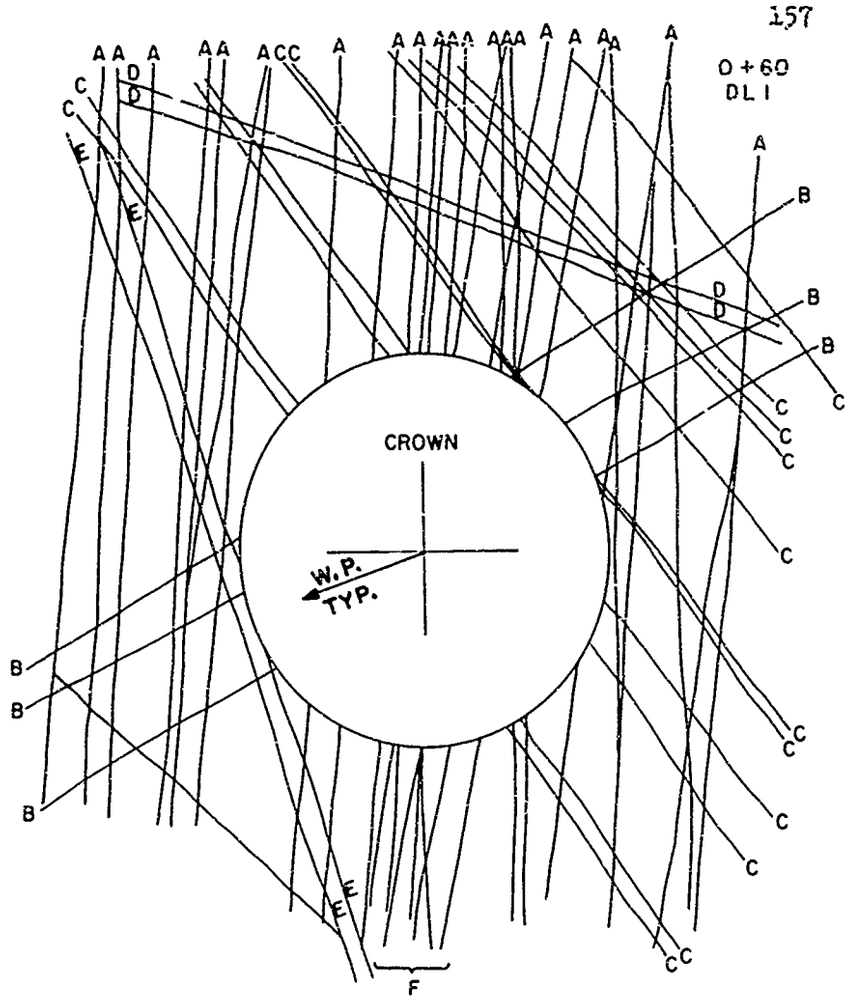

FIGURE 3.33a GEOLOGIC CROSS SECTION - STA 0+60

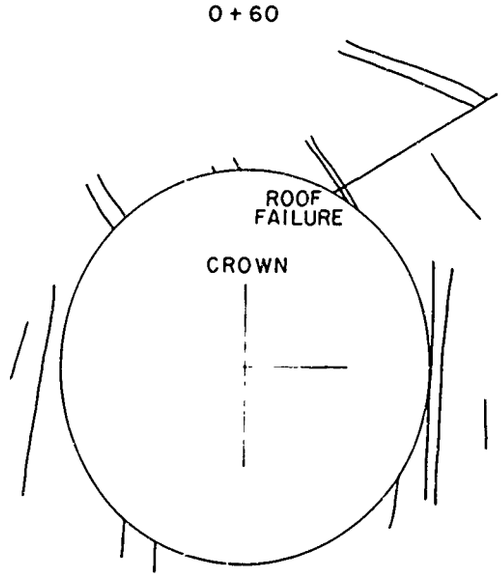

FIGURE 3.33b INFLUENTIAL JOINTS

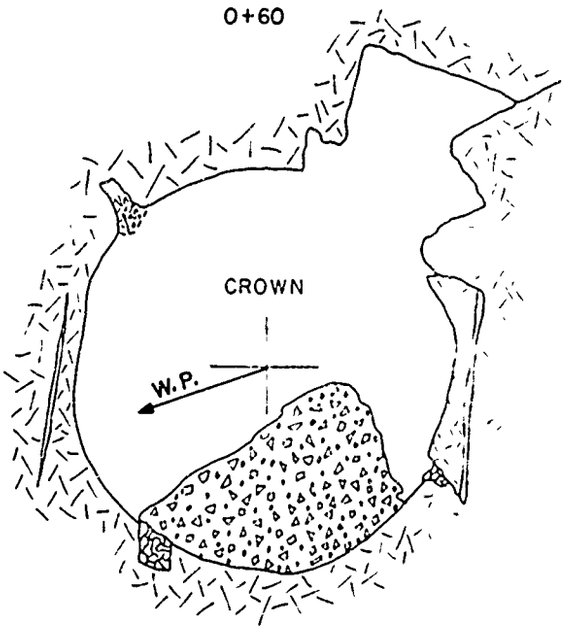

FIGURE 3.33c PREDICTED POST SHOCK SECTION

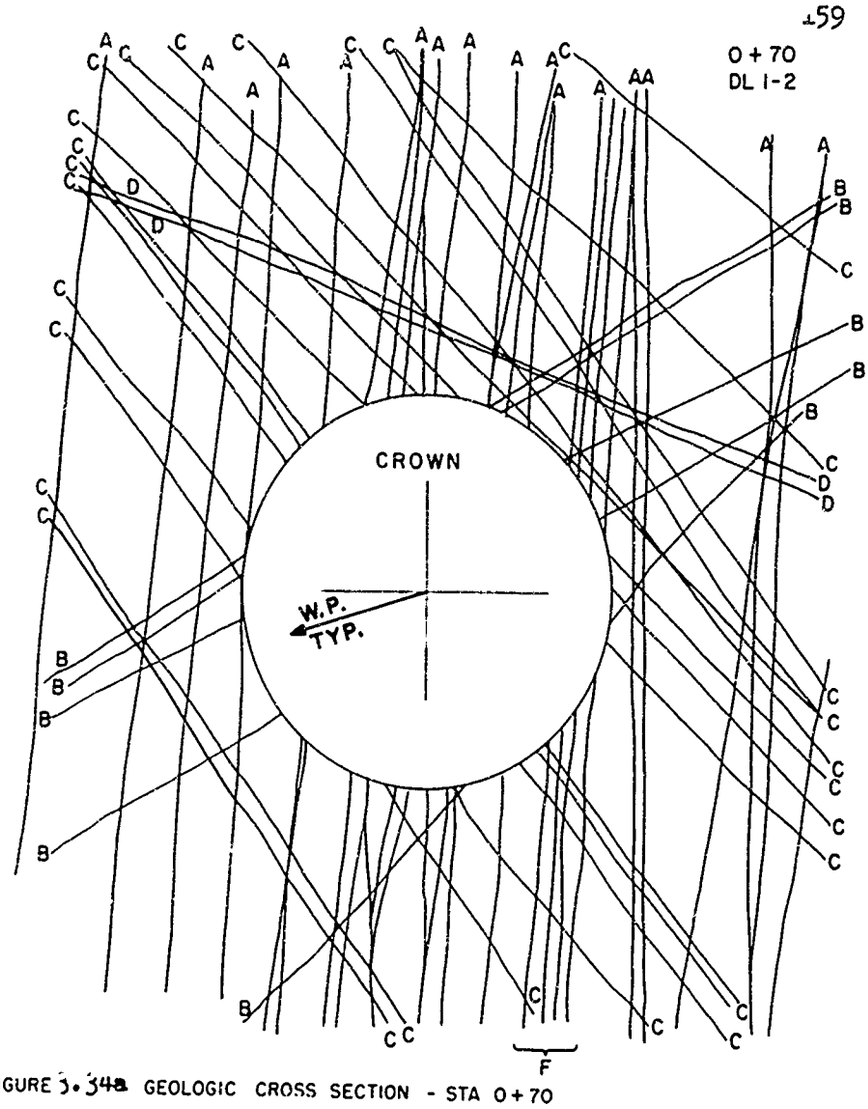

FIGURE 3.34a GEOLOGIC CROSS SECTION - STA 0+70

0 + 70

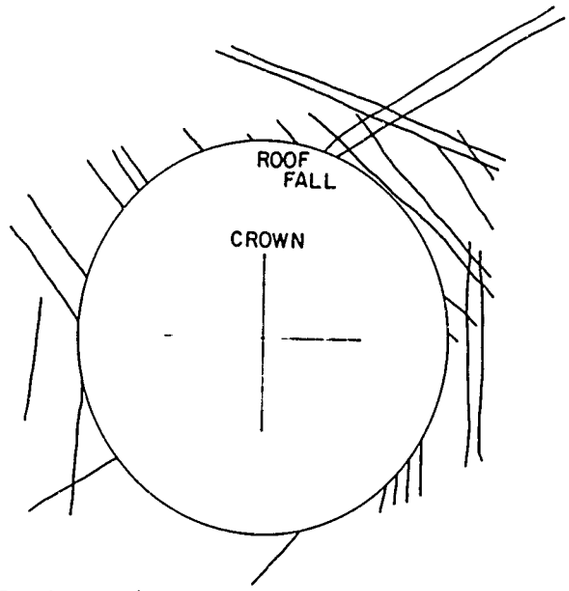

FIGURE 3.34b INFLUENTIAL JOINTS

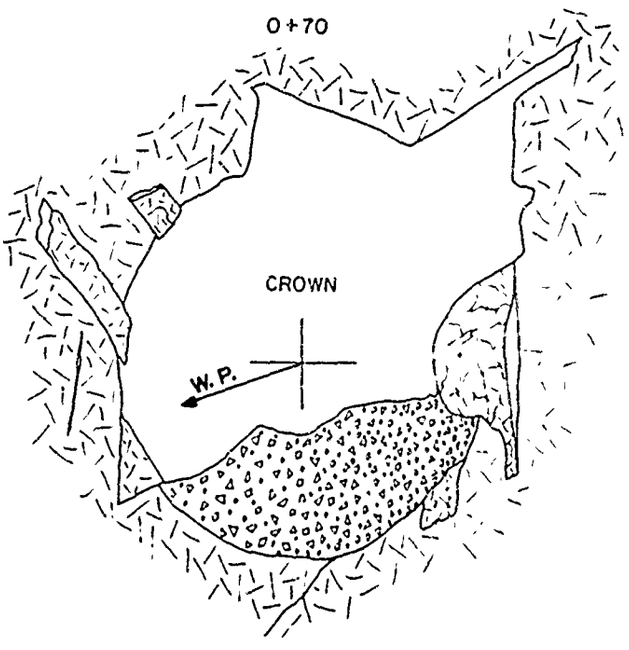

FIGURE 3.34cPREDICTED POST SHOCK SECTION

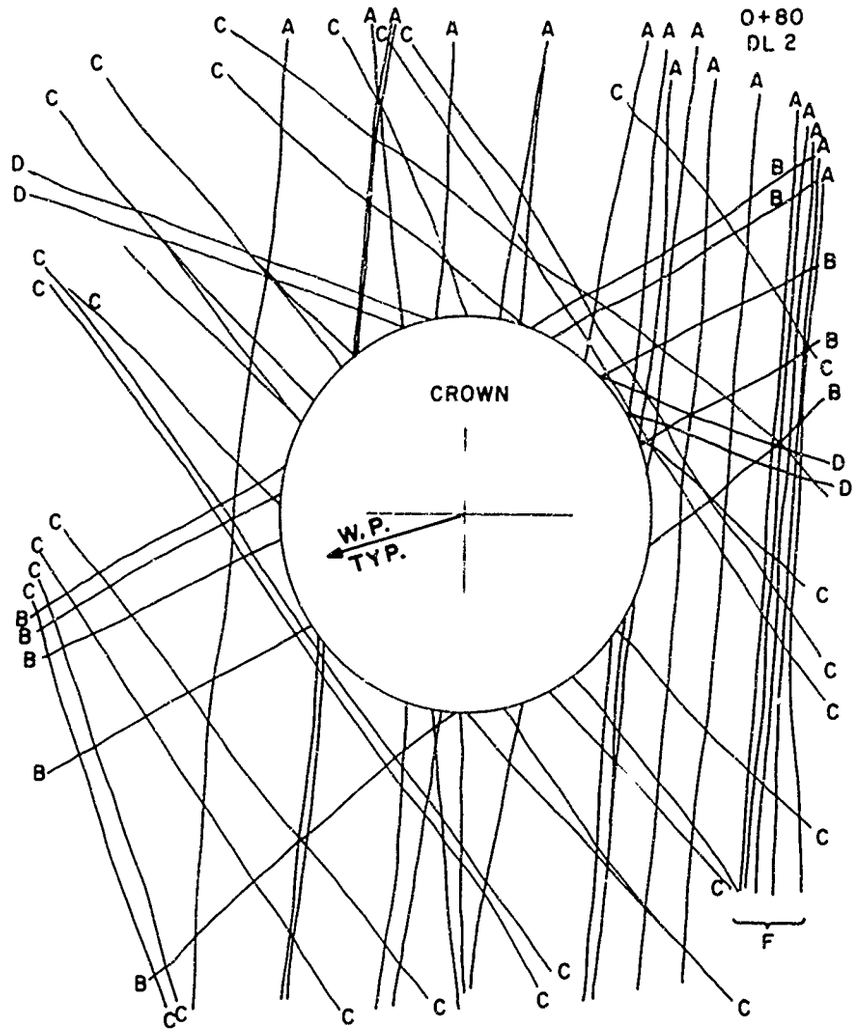

FIGURE 3.35a GEOLOGIC CROSS SECTION - STA 0+80

0+80

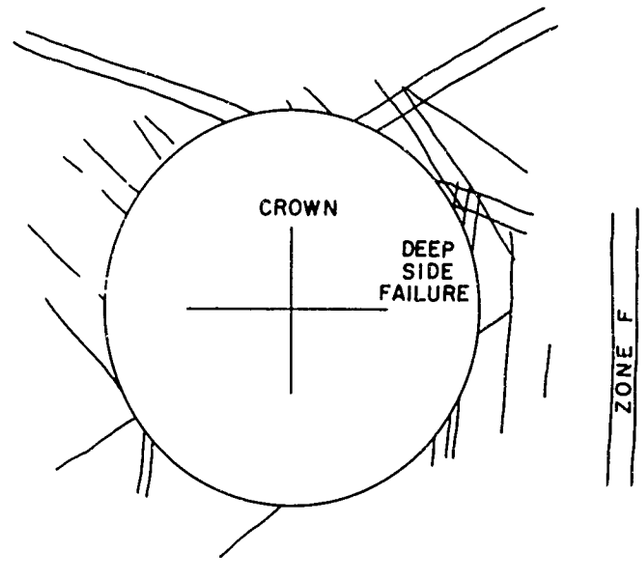

FIGURE 3.35b INFLUENTIAL JOINTS

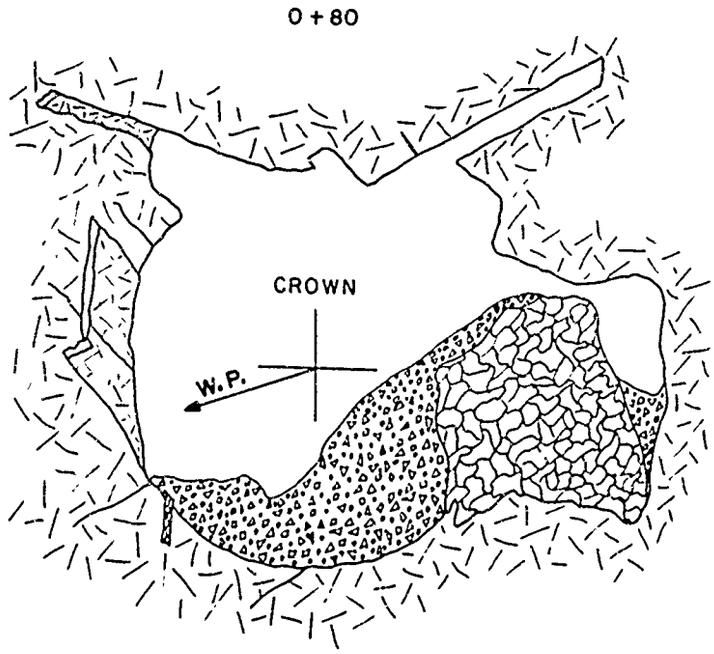

FIGURE 3.35c PREDICTED POST SHOCK SECTION

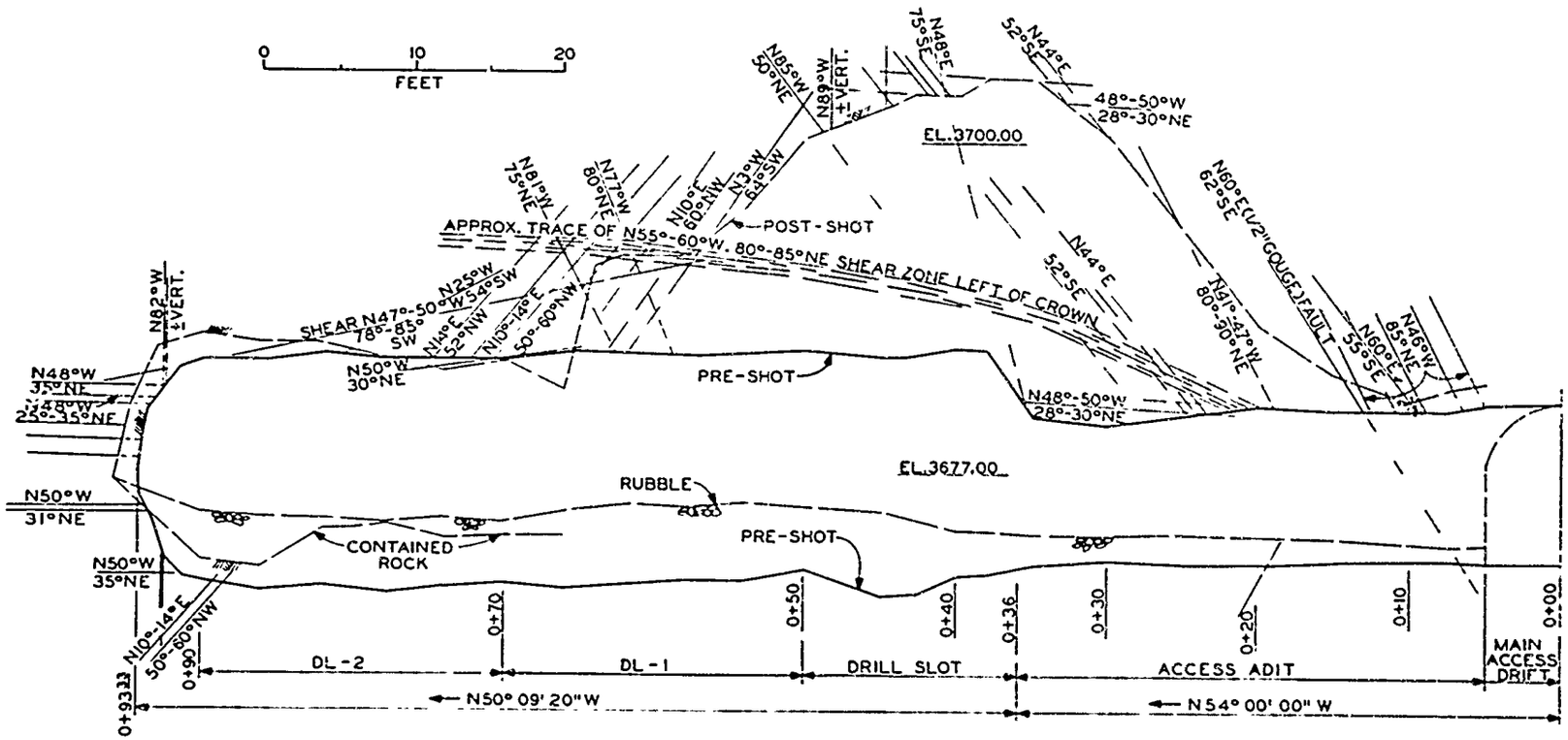

Fig. 3.36 Sectional elevation at centerline and geology - DL Drift

(Fig. 3.86 of POR 4015, Chapter 4)

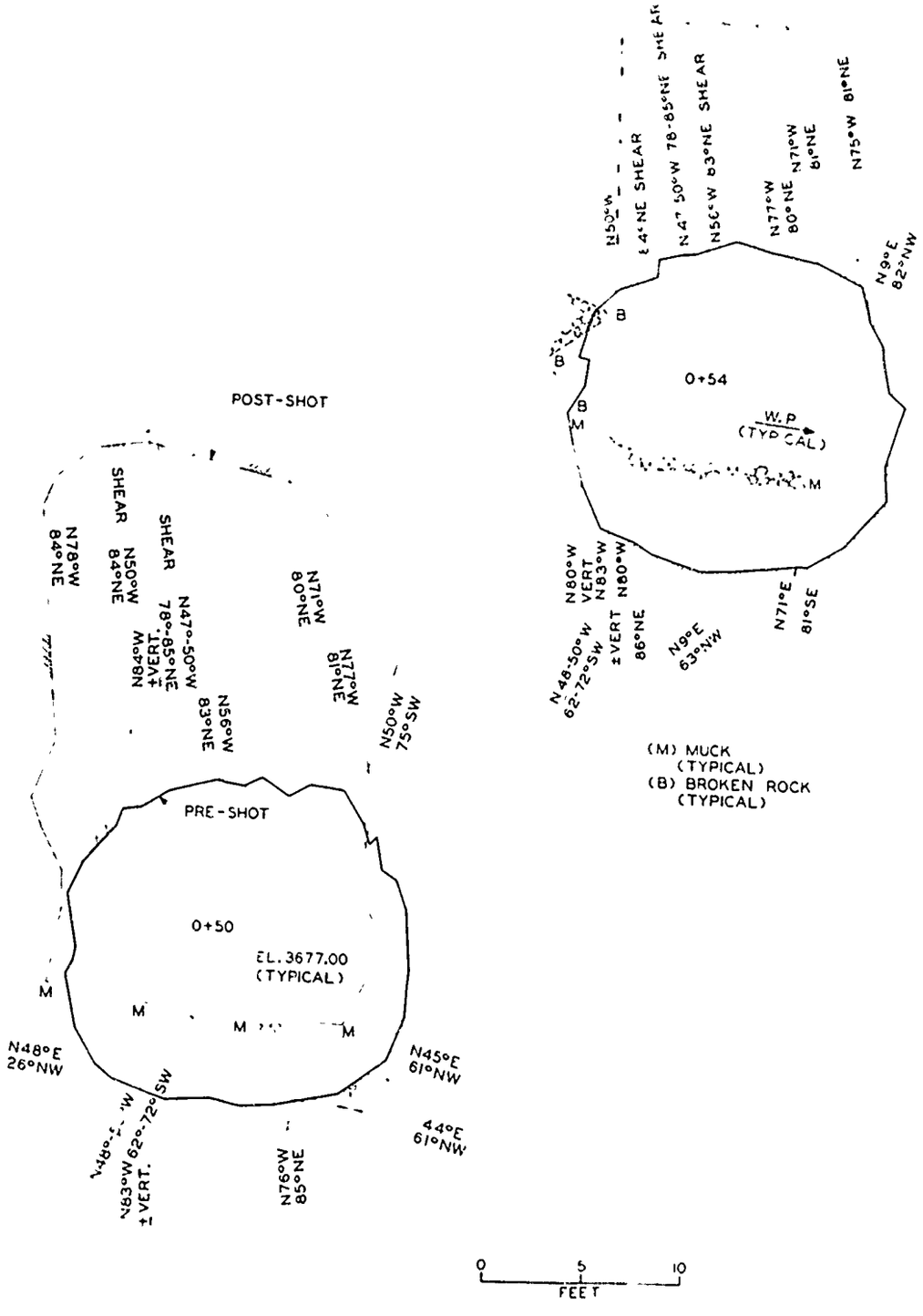

Fig. 3.37 Cross sections and geology - DL Drift (1 of 3 sheets)
(Fig. 3.83of POR 4015, Chapter 4)

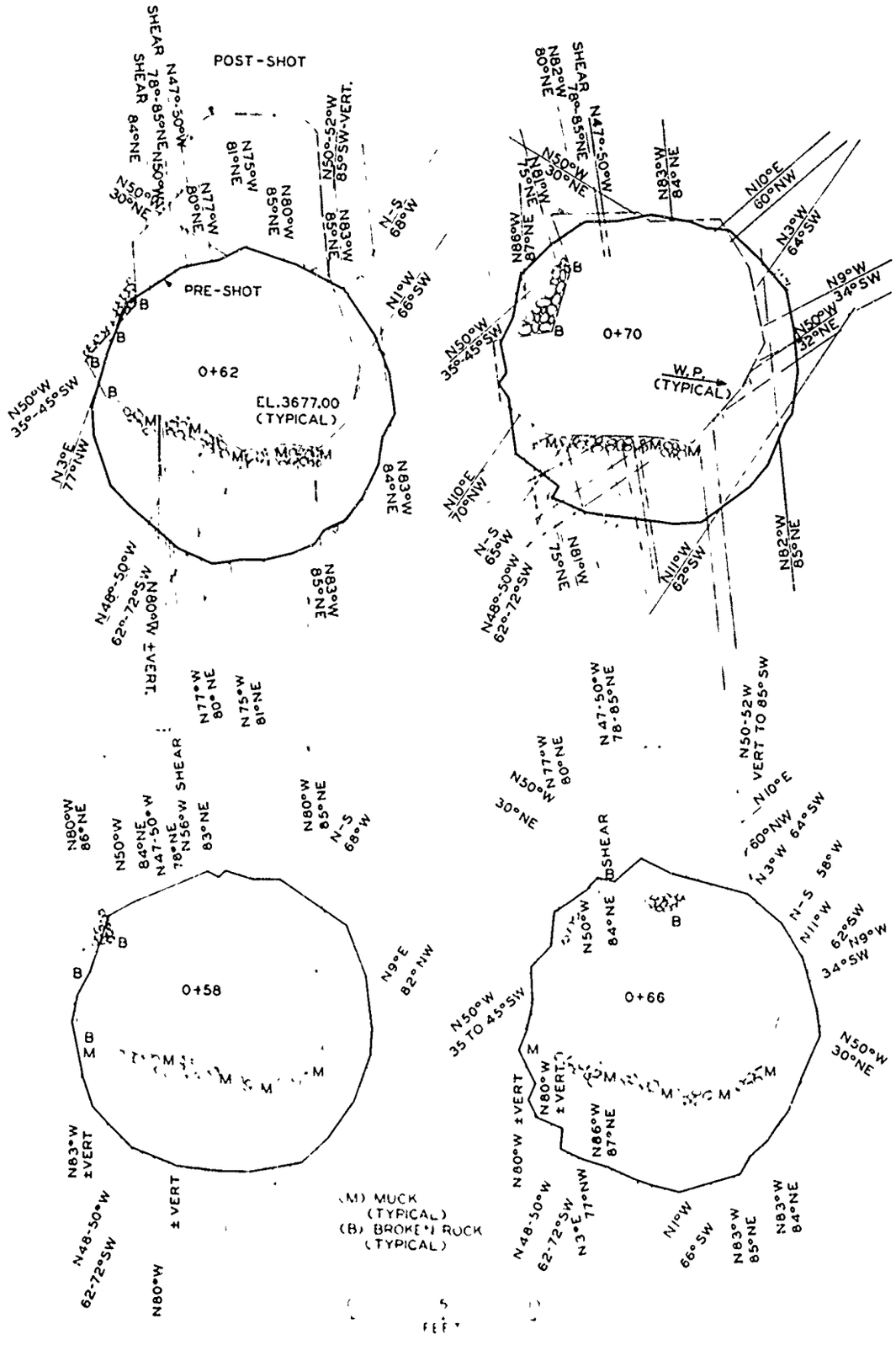

Fig. 3.37 Continued (2 of 3 sheets)

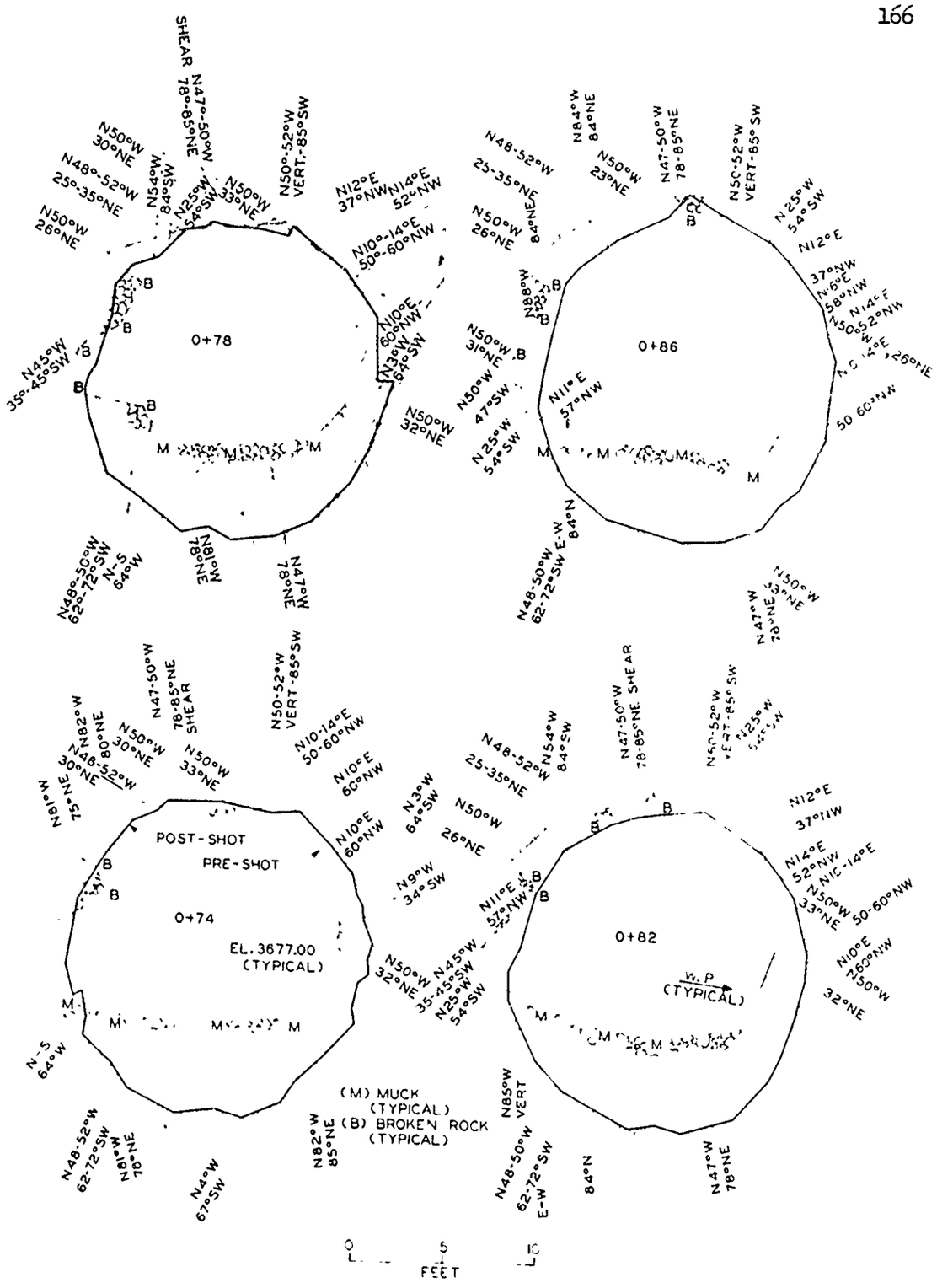

Figure 3.37 Continued (3 of 3 sheets)

4. CONCLUSIONS AND RECOMMENDATIONS

The problems for analysis posed by a jointed hard rock mass are not insurmountable. Provided that sufficient geological and engineering data about the rock can be garnered, it is possible to estimate the behavior of an excavation under given loading conditions.

The Piledriver test has demonstrated conclusively that the pattern of rock breakage and failures of rock bolted and unlined underground galleries at intermediate range depends primarily on geological conditions. Since these conditions exist before the blast, there is no a priori reason why they cannot be discerned with sufficient detail to define the geological conditions sufficiently well for analysis. The only real limitation is economic. (It is another question to define the loading conditions with certainty.)

With the development of bore hole television and photography devices, the expense of very detailed geological mapping should not be excessive for a gallery serving a valuable purpose. It is proposed that in a future project, an effort be made to make use of these devices so that geological cross sections can be prepared definitively showing the location of joints and fractures to a distance of at least one diameter around the tunnel.

Methods are becoming available for determining the strength and deformability properties of weakness planes in rock. Some of the available techniques of sampling and testing discontinuities in rock are reviewed in Section 2.4. In a future project, after the geological study has offered a classification of the weakness surfaces, grouping discontinuities together that are alike mechanically, it is proposed that a program of sampling and testing be conducted to determine the characteristic strength and stiffness of each group.

It is believed based upon the work of this project, that an analysis premised upon information of the quality proposed above would be trustworthy. Therefore, it should be possible to design reinforcement for an opening making optimum use of the reinforcing materials. In particular, rock bolt patterns can be unbalanced to strengthen the section in accordance with localized needs.

PERSONNEL AND ACKNOWLEDGEMENTS

R. E. Goodman served as principal investigator and prepared the report. He was assisted in these studies by several engineers. Mr. Fred Sage prepared the geological sections and assisted in the finite element studies of DL drift described in Section 2.5. Mr. Michael Cleary prepared geologic cross sections and participated in performing joint influence analysis for CR drift. Mr. Ashraf Mahtab assisted in analysis of joint test data.

The principal investigator is indebted to the individuals and companies who gave permission to study their methods and results of testing weakness planes in rock. Dr. Pierre Londe and Dr. J. Bernaix of Coyne and Bellier; Dr. Dusan Krsmanovic and his associates, Mr. Langof, Mr. Tufa, and Mr. Dolarovic, at the Faculty of Civil Engineering, Sarajevo; Dr. Knill and Dr. DeFreitas in the Geology Department at Imperial College, Dr. Evert Hoek, Dr. David Pentz, and Mr. John Verge of the Interdepartmental Rock Mechanics Project, Royal School of Mines, Imperial College, Mr. Jan Eurenius and Mr. Hans Fagerström of Vattenbyggnadsbyran, Stockholm; Professor Donald Deere and Mr. James Coulson of the Department of Civil Engineering, University of Illinois; Mr. Klaus John of Teknische Hochschule, Karlsruhe, Germany, Professor Bratislav Kujundzic, Professor Brcic, and Mr. Marcowitz of the Jaroslav Cerni Institute, Belgrade, Yugoslavia; Dr. Karel Drozd of IGHP, Prague, Czechoslovakia; and Dr. Manuel Rocna and Ing. Barosso of the National Civil Engineering Laboratory, Lisbon, Portugal. We appreciate the generosity of Electricité de France in permitting reproduction of figures from a Coyne and Bellier report about Vouglans Dam.

Other individuals who assisted in the preparation of the report are Mr. R. Heijdeman, Mr. Ellis Meyers, Miss Jeanie Chang and Mrs. Julia Estrella.

APPENDIX 1

FINITE ELEMENT ANALYSIS

COMPUTER PROGRAM

University of California, Berkeley
College of Engineering

COMPUTER PROGRAM FOR ANALYSIS OF JOINTED ROCK SYSTEMS*
WITH RESIDUAL STRESS AND ACCELERATION OPTIONS
- PLANE STRAIN - NONLINEAR ALONG TANGENTS - FINITE STRAIN -

PURPOSE

The purpose of this computer program is to determine displacements throughout a jointed rock body, stresses within rock blocks, and normal and tangential stresses on rock joints. The joints have no tensile strength and a finite shear strength. The blocks are orthotropic or isotropic, linear, elastic solids. A failure criterion is included, for the rock:

$$\tau_{oct} = N + D\,\sigma_{oct}{}^{B}$$

and for the joints:

$$s = c + \sigma \tan\phi$$

For tensile values of sigoctahedral, failure criterion in the rock is simply:

$$\sigma_{min} = \sigma_t \qquad (\sigma_t = \text{uniaxial tensile strength})$$

INPUT DATA

A. IDENTIFICATION CARD - (72H)

Columns 1 - 72 of this card contain information to be printed with results.

B. CONTROL CARD - (4I5, 2F10.2, 6I5)

Columns	1 - 5	Number of nodal points (900 maximum)
	6 - 10	Number of elements (670 maximum)
	11 - 15	Number of different materials (12 maximum)
	16 - 20	Number of boundary pressure cards (200 maximum)
	21 - 30	Acceleration in X direction
	31 - 40	Acceleration in Y direction
	41 - 45	Number of approximations (never less than 2 for jointed body)
	46 - 50	Code for running multiple problems (0 if second problem follows, 1 if no second problem follows)
	51 - 55	Residual stress code (reads residual stress if not equal to 0)

---

* Adapted from plane stress program by E. L. Wilson, July 1965, and joint stiffness and joint stress subroutines by R. L. Taylor and R. E. Goodman, July 1967.

2/68
7/68 Revision
9/68 Revision

56 - 60 Joint cut-off number: all materials with higher numbers are joints
61 - 65 Code to read punched deck output (effective strain deck) to restart problem at point of termination of last run (0 = no deck read; 1 = deck read)*
66 - 70 Number of joint elements (400 maximum)

C. MATERIAL PROPERTY CARDS

The following group of cards must be supplied for each different solid material and joint material. The last numbered solid material defines the solid's properties after tension or shear failure.

Solid Materials

First Card - (I5, F10.0)

Columns 1 - 5 Materials identification (any number from 1 to 12)
6 - 15 Mass density of materials

$$\frac{\gamma \text{ pounds/cu.ft.}}{g \text{ ft/sec}^2} = \text{pounds sec}^2/\text{ft}^2$$

Second Card - (7F10.0)

Columns 1 - 10 Tensile strength (input as positive quantity)
11 - 20 E compression
21 - 30 ν
31 - 40 E tension
41 - 50 N
51 - 60 D
61 - 70 B

$$\tau_{oct(\text{failure})} = N + D\ \sigma_{oct}^{B}$$

Joint Materials

First Card - (I5)

Columns 1 - 5 Number of joint materials

Second Card - (7F10.0)

Columns 1 - 10 Normal stiffness, psf/ft
11 - 20 Tangential stiffness, psf/ft
21 - 30 Joint cohesion, psf

*If number of joint materials was 0, the previous run will not have yielded punched output.

31 - 40	Joint friction angle, degrees
41 - 50	Tangential stiffness after slip occurs
51 - 60	Joint closure allowable (ft.); input as negative quantity

NOTE: If joint is non-stiff, the value of stiffness is probably 1/10 - 1/100 of the stiffness of the intervening block, e. g. $E_{block} = 1.0 \times 10^8$ psf, block thickness = 5.0 ft, then block stiffness is 2.0×10^7 psf/ft and a low joint stiffness K_t 10^6 psf/ft.

D. NODAL POINT CARDS - (I5, F5.0, 4F10.0)

One card for each nodal point with the follcwing information. Joint elements are obtained by double rows of nodal points at the same coordinates.

Columns	1 - 5	Nodal point number
	6 -10	Number which indicates if displacements or forces are to be specified
	11 -20	X - ordinate
	21 -30	Y - ordinate
	31 -40	XR
	41 -50	XZ

NOTE: If the number in column 10 is

0 XR is the specified X-load and XZ is the specified Y-load.
1 XR is the specified X-displacement and XZ is the specified Y-load.
2 XR is the specified X-load and XZ is the specified Y-displacement.
3 XR is the specified X-displacement and XZ is the specified Y-displacement.

All loads are considered to be total forces acting on an element of unit thickness. Nodal point cards must be in numerical sequence. If cards are omitted, the omitted nodal points are generated at equal intervals along a straight line between the defined nodal points. The necessary temperatures are determined by linear interpolation. The boundary code (column 10), XR, and XZ are set equal to zero.

E. ELEMENT CARDS - (6I5)

Solid Elements

One card for each element[1,2]

Columns	1 - 5	Element
	6 - 10	Nodal Point I
	11 - 15	Nodal Point J
	16 - 20	Nodal Point K
	21 - 25	Nodal Point L
	26 - 30	Material identification

[1]For a right-hand coordinate system, order nodal points counter-clockwise around.

[2]Maximum difference between nodal point I.D. must be less than 27.

Element cards must be in element number sequence. If element cards are omitted, the program automatically generates the omitted information by incrementing by one the preceding I, J, K, and L. The material identification code for the generated cards is set equal to the value of the last card. The last element card must always be supplied.

Triangular elements are also permissible; they are identified by repeating the last nodal point number (i.e. I, J, K, K). One-dimensional bar elements are identified by a nodal point numbering sequence of the form I, J, J, I.

Joint Elements

Nodal Point Naming convention for joint elements:

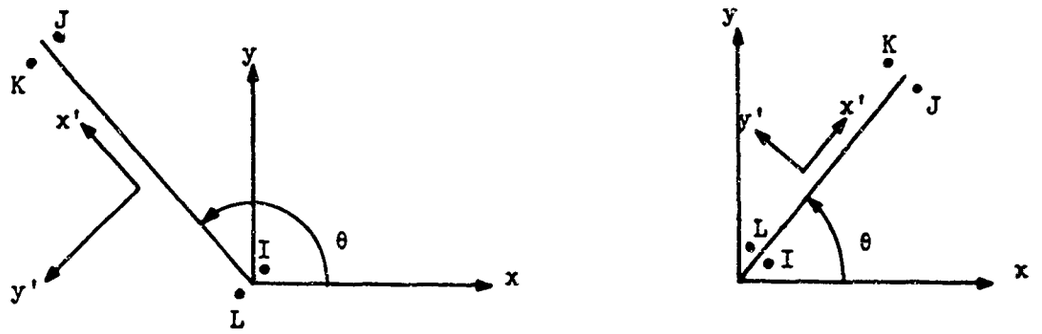

Nodal points must be numbered I, J, K, L proceeding from bottom left corner counterclockwise to upper left corner. Bottom and top are defined by x', y' system of coordinates created by rotation θ (180°) from x to x', where x' is along the length of the element.

F. PRESSURE CARDS - (2I5, 1F10.0)

One card for each boundary element which is subjected to a normal pressure.

Columns		
	1 - 5	Nodal Point I
	6 - 10	Nodal Point J
	11 - 20	Normal Pressure

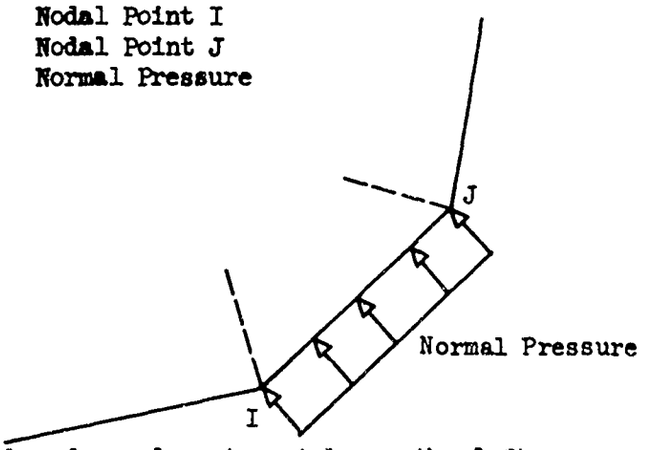

As shown above, the boundary element must be on the left as one progresses from I to J. Surface tensile force is input as a negative pressure. Joints cannot be placed on boundaries.

G. INCREMENTAL LOADING (15F5.2)

One card giving multiples of input pressure to be applied successively and cumulated.

Example:

For a problem with 3 pressure increments equal to 1000 psi, 4000 psi, and 2000 psi (total pressure: 7000 psi), with 1000 psi applied in F, the following card would be required:

Column 5	1
Column 10	4
Column 15	2

NOTE: The number of entries on this card must equal the number of approximations indicated on the control card.

H. SKEW BOUNDARIES

If the number in columns 5 - 10 of the nodal point card is other than 0, 1, 2, or 3, it is interpreted as the magnitude of an angle in degrees. This angle is shown below.

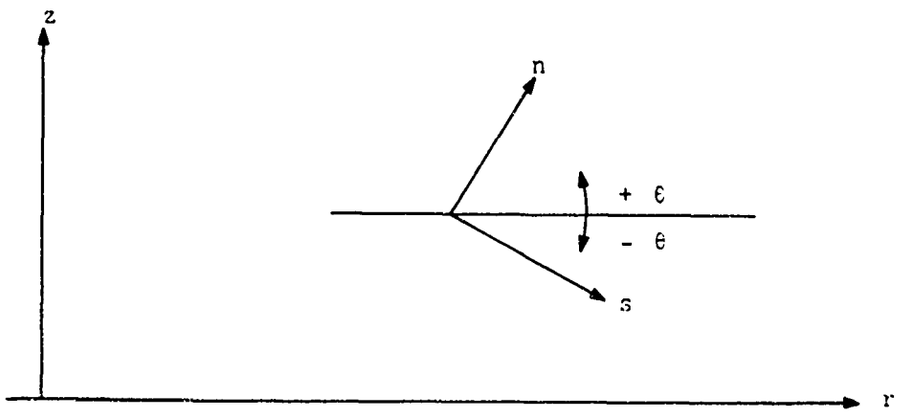

The terms in columns 31 - 50 of the nodal point card are then interpreted as follows:

XR is the specified load in the s-direction
XZ is the specified displacement in the n-direction

The angle θ must always be input as a negative angle and may range from -.001 to -180 degrees. Hence, + 1.0 degree is the same as -179.0 degrees. The displacements of these nodal points which are printed by the program are:

u_x = the displacement in the s-direction

u_y = the displacement in the n-direction

I. RESIDUAL STRESS CARDS

If residual stress code on the control card is not equal to 0, one card for each element must be supplied with the following information:

Columns	1 - 5	Element number
	6 - 7	Blank
	8 - 22	x-stress
	23 - 37	y-stress
	38 - 52	xy-stress

If cards are omitted, the stresses for the omitted elements are assumed equal to those supplied on the last card. If all elements have the same stresses, only the 1st and last element stresses may be supplied.

If element is a joint

Columns	1 - 5	Element number
	6 - 7	Blank
	8 - 22	Initial tangential stress
	23 - 37	Initial normal stress

J. EFFECTIVE STRAIN CARDS

These are punched by computer after last cycle of a run. If asked for by 1 in column 65 of the control card, the effective strain deck is read if placed behind the last data card in the data deck.

OUTPUT INFORMATION

The following information is developed and printed by the program:

1. Reprint of input data
2. Nodal point displacements*, for the preceding cycle and cumulative
3. Stresses at the center of each solid element*; principle stresses are cumulative
4. Stresses and relative displacements (of center top and bottom) of each joint element*, cumulative

---

*2., 3., and 4. are printed after each cycle.

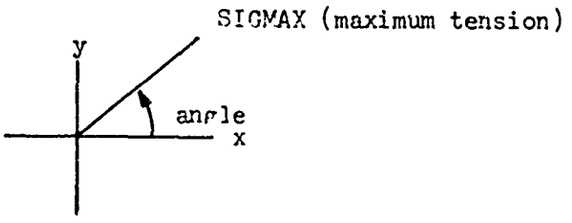

NOTE: New element corner positions are used to calculate new stiffnesses on each cycle (finite strain)

APPENDIX 1 (CONT.)

```
 FORTRAN PROGRAM FOR INCREMENTAL LOADING OF PLANE STRAIN STRUCTURES
PROPERTIES OF SOLID MATERIALS ARE MODIFIED IF STRESSES INDICATE FAILURE
    FAILURE LAW IS A POWER LAW IN TERMS OF OCTAHEDRAL STRESSES
UP TO 400 JOINT ELEMENTS CAN BE INTRODUCED        BANDWIDTH = 80

WRITTEN FOR USE ON CDC 6400, PROGRAM LENGTH 120000 OCTAL

ADAPTED FROM PLANE STRESS ROUTINE OF PROF E WILSON,


      PROGRAM MAIN (INPUT,OUTPUT, TAPE8, TAPE9, PUNCH)
C     PLANE STRAIN WITH JOINTS, CUMULATIVE LOADING, NON LINEAR ALONG TANGEN
C
      COMMON NUMNP,NUMEL,NUMMAT,NUMPC, ACELX,ACELY, N,VOL,TEMP,MTYPE,
     1 MED(12), E(8,12), RO(12),XXNN(12),R(900),Z(900),UR(900),UZ(900),
     2 CODE(900),IBC(200),JBC(200),PR(200),ANGLE(4),SIG(10),LBAD
      COMMON /ARG/ RRR(5),ZZZ(5),S(10,10),P(10),TT(4),LM(4),DD(3,3),
     1 HH(6,10),RR(4),ZZ(4),C(4,4),H(6,10),D(6,6),F(6,10),TP(6),XI(10)
     2,EE(7),IX(670,5),EPS(670),MTAG(670),RSTRS(4),RESID(670,3),
     3 NRES,PRFACT,NUMJT,SIGST(3,670)
      COMMON/BANARG/MBAND,NUMBLK,E(160),A(160,80)
      COMMON/JOINT/NSHELL,KCODE(400),FNST(400),FTST(400),EPSTST(400),
     2 EPSNST(400), PPP(8),MNN,NJ
      DIMENSION BST(1800), FACTOR(15)
C
C*****************************************************************
C     READ AND PRINT OF CONTROL INFORMATION AND MATERIAL PROPERTIES
C*****************************************************************
      LBAD=0
   50 READ 1000,HED,NUMNP,NUMEL,NUMMAT,NUMPC,ACELX,ACELY, NP, NEND,NRES,
     1 NSHELL,NSTAGE,NUMJT
      PRINT    2000, HED,NUMNP,NUMEL,NUMMAT,NUMPC,ACELX,ACELY,NUMJT,NP
C
      IF (NSHELL .EQ. 0)  NSHELL = 13
   56 DO 59 M=1,NUMMAT
      READ    1001, MTYPE,       RO(MTYPE)
      IF (MTYPE .GT. NSHELL)  GO TO 560
      PRINT 2011, MTYPE, RO(MTYPE)
      READ 1005, (E(J,MTYPE),J=1,7)
      PRINT 2010, (E(J,MTYPE),J=1,7)
      GO TO 59

  560 READ 1005, (E(J,MTYPE),J=1,6)
      PRINT 2017, MTYPE
      PRINT 2016,(E(J,MTYPE),J=1,6)
   59 CONTINUE
C
C*****************************************************************
C     READ AND PRINT OF NODAL POINT DATA
C*****************************************************************
      PRINT    2004
      L=0

   60 READ     1002, N,KCODE(N),R(N),Z(N),UR(N),UZ(N)
      NL=L+1
      ZX=N-L
      DR=(R(K)-R(L))/ZX
      DZ=(Z(N)-Z(L))/ZX
   70 L=L+1
      IF(N-L) 100,90,80
   80 CODE(L)=0.0
      R(L)=R(L-1)+DR
      Z(L)=Z(L-1)+DZ
      UR(L)=0.0
      UZ(L)=0.0
      GO TO 70
   90 PRINT    2002, (K,CODE(K),R(K),Z(K),UR(K),UZ(K),K=NL,N)
      IF(NUMNP-N) 100,110,60
  100 PRINT    2009, N
      LBAD = 1
      GO TO 60
  110 CONTINUE
C*****************************************************************
C     READ AND PRINT OF ELEMENT PROPERTIES
C*****************************************************************
      PRINT    2001
      N=0
  130 READ    1003, M,(IX(M,I),I=1,5)
  140 N=N+1
      IF (M-N) 170,170,150
  150 IX(N,1)=IX(N-1,1)+1
      IX(N,2)=IX(N-1,2)+1
      IX(N,3)=IX(N-1,3)+1
      IX(N,4)=IX(N-1,4)+1
      IX(N,5)=IX(N-1,5)
  170 PRINT    2003, N,(IX(N,I),I=1,5)
      IF (M-N) 180,180,140
  180 IF (NUMEL-N) 190,190,130
  190 CONTINUE
C*****************************************************************
C     READ AND PRINT OF PRESSURE BOUNDARY CONDITIONS
C*****************************************************************
      IF (NUMPC.EQ. 0) GO TO 310
  290 PRINT    2005
      DO 300 L=1,NUMPC
      READ 1004, IBC(L),JBC(L),PR(L)
  300 PRINT    2007, IBC(L),JBC(L),PR(L)
      PRINT 2029
      READ 2030, (FACTOR(I),I=1,NP)
      PRINT 2031, (FACTOR(I),I=1,NP)
  310 CONTINUE
C     ***********************************************
C     READ AND PRINT OF INITIAL DATA FOR THE PROBLEM
C     ***********************************************
      IF(NRES.EQ.0) GO TO 45
      PRINT 1006
      L=0
   47 READ 1007, N, (RESID(N,I),I=1,3)
      NL=L+1
   43 L=L+1
      IF(N-L) 40,41,42
   42 DO 46 I=1,3
   46 RESID(L,I)=RESID(L-1,I)
      GO TO 43
   41 PRINT 1007, (K, (RESID(K,I),I=1,3 ), K=NL,N )
      IF(NUMEL-N) 40,45,47
   40 PRINT 1008,N
      LBAD = 1
   45 CONTINUE
C*****************************************************************
C     READ OUTPUT OF PREVIOUS RUN TO RESTART PROBLEM
C*****************************************************************
      DO 312 N=1,NUMJT
  312 KCODE(N) =0
      KNP=2*NUMNP
      DO 313 K=1,KNP
  313 BST(K)=0.0
      IF(NSTAGE.EQ.0) GO TO 314
      PRINT 1017
      READ  1018, (N,MTAG(N),EPS(N),SIGST(1,N),SIGST(2,N),SIGST(3,N),
     1  N=1,NUMEL)
      PRINT 1018, (N,MTAG(N),EPS(N),SIGST(1,N),SIGST(2,N),SIGST(3,N),
     1  N=1,NUMEL)
      PRINT 1019
      READ 1020,(KCODE(N),EPSNST(N),EPSTST(N),FNST(N),FTST(N),N=1,NUMJT)
      PRINT1020,(KCODE(N),EPSNST(N),EPSTST(N),FNST(N),FTST(N),N=1,NUMJT)
      PRINT 1021
      READ 1022,(N,BST(2*N-1),BST(2*N),N=1,NUMNP)
      PRINT 1022,(N,BST(2*N-1),BST(2*N),N=1,NUMNP)
C*****************************************************************
C     DETERMINE BAND WIDTH
C*****************************************************************
  314 J=0
      DO 340 N=1,NUMEL
      DO 340 I=1,4
      DO 325 L=1,4
      KK=IABS(IX(N,I)-IX(N,L))
      IF(KK.LE.39)GO TO 315
      PRINT 2018, N
      LBAD=LBAD+1
  315 IF(KK-J) 325,325,320
  320 J=KK
  325 CONTINUE
  340 CONTINUE
      MBAND=2*J+2
      PRINT 2012,MBAND
      PRINT 2019,LBAD
      IF (LBAD.NE. 0)STOP
C*****************************************************************
C     SOLVE NON-LINEAR STRUCTURE BY SUCCESSIVE APPROXIMATIONS
C*****************************************************************
      IF(NRES.NE.0) GO TO 342
      DO 341 N=1,NUMEL
      DO 341 I=1,3
      RESID(N,I)=0.0
  341 CONTINUE
  342 CONTINUE
      IF(NSTAGE.NE.0) GO TO 380
      DO 350 N=1,NUMEL
      DO 307 I=1,3
  307 SIGST(I,N)=0.0
      MTAG(N)=1
  350 EPS(N)=0.0
      DO 360 N=1,NUMJT
      EPSNST(N)=0.
      EPSTST(N)=0.
      FNST(N)=0.
      FTST(N)=0.
  360 CONTINUE
  370 KNP=2*NUMNP
      DO 375 K=1,KNP
  375 BST(K)=0.0
C
  380 DO 500 NNN=1,NP
C     FORM STIFFNESS MATRIX
C
      DO 403 KN=1,NUMNP
      R(KN)=R(KN)+BST(2*N-1)
  403 Z(KN)=Z(KN)+BST(2*KN)
      PRFACT=FACTOR(NNN)
      CALL STIFF
C
C     SOLVE FOR DISPLACEMENTS
C
      CALL BANSOL
      DO 400 K=1,KNP
  400 BST(K)=B(K)+BST(K)
C
      PRINT 3000, NNN
      PRINT 2008
      PRINT  2006, (N,B(2*N-1),B(2*N),BST(2*N-1),BST(2*N),N=1,NUMNP)
C
C     COMPUTE STRESSES
C
      CALL STRESS
      CALL JTSTR
      NRES = 0
      NSTAGE =0
  500 CONTINUE
      IF(NUMJT.EQ.0) GO TO 501
      PUNCH 1018, (N,MTAG(N),EPS(N),SIGST(1,N),SIGST(2,N),SIGST(3,N),
     1  N=1,NUMEL)
      PUNCH1020,(KCODE(N),EPSNST(N),EPSTST(N),FNST(N),FTST(N),N=1,NUMJT)
      PUNCH 1022,(N,BST(2*N-1),BST(2*N),N=1,NUMNP)
  501 CONTINUE
C
C*****************************************************************
      IF ( NEND .EQ. 0 )  GO TO 50
```

```
C*********************************************************************
 1000 FORMAT(12A6/4I5,2F10.2,6I5)
 1001 FORMAT ( I5, F10.0)
 1002 FORMAT (I5, F5.0, 4F10.0)
 1003 FORMAT (6I5)
 1004 FORMAT (2I5,F10.0)
 1005 FORMAT (7F10.0)
 1006 FORMAT (29H1INITIAL STRESSES IN ROCK//8H ELEMENT 4X 9H X-STRESS 6X
     19H Y-STRESS 6X 10H XY-STRESS//)
 1007 FORMAT (I5,2X,3E15.4)
 1008 FORMAT (31H RESIDUAL STRESS INPUT ERROR N= I5)
 1017 FORMAT(*0 ELEMENT     MTAG        EPS        SIG 1      SIG 2      SIG3
     1    *)
 1018 FORMAT (2I10,4E12.3)
 1019 FORMAT (* KCODE     EPSNST     EPSTST     FNST       FTST*)
 1020 FORMAT (I5,4E10.2)
 1021 FORMAT( * N*    CUM X DISP              CUM Y DISP *)
 1022 FORMAT(I5,2E20.2)
 2000 FORMAT (1H1 12A6/
     1 30HO NUMBER OF NODAL POINTS------ I3 /
     2 30HO NUMBER OF ELEMENTS---------- I3 /
     3 30HO NUMBER OF DIFF. MATERIALS--- I3 /
     4 30HO NUMBER OF PRESSURE CARDS---- I5 /
     5 30HO X-ACCELERATION-------------- E12.4/
     6 30HO Y-ACCELERATION-------------- E12.4/
     7 30HO NUMBER OF JOINT ELEMENTS --- I3/
     8 30HO NUMBER OF APPROXIMATIONS---- I3)
 2001 FORMAT (49H1ELEMENT NO.     I     J     K     L    MATERIAL  )
 2002 FORMAT (I12, F12.2, 2F12.3, 2E24.7)
 2003 FORMAT (1I13,4I6,1I12)
 2004 FORMAT (108H1NODAL POINT        TYPE  X-ORDINATE  Y-ORDINATE  X LO
     1AD OR DISPLACEMENT  Y LOAD OR DISPLACEMENT            )
 2005 FORMAT (29HOPRESSURE BOUNDARY CONDITIONS/ 24H     I     J    PRESS
     1URE )
 2006 FORMAT (I12,4E20.7)
 2007 FORMAT (2I6,F12.3)
 2008 FORMAT(*0NODAL POINT  X DISPLACEMENT       Y DISPLACEMENT      CUM
     1 X DISPLACEMENT  CUM Y DISPLACEMENT*)
 2009 FORMAT (26HONODAL POINT CARD ERROR N= I5)
 2010 FORMAT (15HOITEMS. STRENGTH10X 5HE(C)  9X 6HNU     11X 4HE(T)
     1  10X 6H N       10X 4H D    10X  4H B    /7E15.5)
 2011 FORMAT (17HOMATERIAL NUMBER= I3, 15H. MASS DENSITY=  E12.4)
 2012 FORMAT (/6HMBAND= I5 /)
 2016 FORMAT (*0     KN              KT              C            PHI
     1       KT FINAL     MAX. CLOSURE  */ 6E15.4)
 2017 FORMAT (1HO10X,16H MATERIAL NUMBER(5)
 2018 FORMAT (24H ELEMENT CARD ERROR  N=  I4)
 2019 FORMAT (* LBAD =* I5)
 2029 FORMAT (*0 MULTIPLES OF INPUT PRESSURE SUCCESSIVELY APPLIED * /)
 2030 FORMAT(15F5.2)
 2031 FORMAT (15F7.2)
 3000 FORMAT (*1                                        INCREMENT NO.*I2)
C
      STOP
      END
```

```
      SUBROUTINE STIFF
C
      COMMON NUMNP,NUMEL,NUMMAT,NUMPC, ACELX,ACELY, N,VOL,TEMP,MTYPE,
     1 MED(12), E(12), RO(12),XNN(12),R(900),Z(900),UR(900),UZ(900),
     2 CODE(900),IBC(200),JBC(200),PR(200),ANGLE(4),SIG(10),LBAD
      COMMON /ARG/ RRR(5),ZZZ(5),S(10,10),P(10),TT(4),LM(4),DD(3,3),
     1 MM(6,10),RR(4),ZZ(4),C(4,4),H(6,10),D(6,6),F(6,10),TP(6),XI(10)
     2,EE(7),IX(670,5),E*S(670),MTAG(670),RSTRS(4),RESID(670,3),
     3 NRES,PRFACT,NUMJT,SIGST(3,670)
      COMMON/BANARG/MBAND,NUMBLK,B(160),A(160,80)
      COMMON/JOINT/NSHELL,KCODE(400),FNST(400),FTST(400),EPSTST(400),
     2 EPSNST(400), PPP(8),NNN,NJ
C
C*********************************************************************
C     INITIALIZATION
C*********************************************************************
      REWIND 9
      NB = 40
      ND=2*NB
      ND2=2*ND
      LBAD = 0
      NUMBLK=0
      NJ=0
C
      DO 50 N=1,ND2
      B(N)=0.0
      DO 50 M=1,ND
   50 A(N,M)=0.0
C*********************************************************************
C     FORM STIFFNESS MATRIX IN BLOCKS
C*********************************************************************
   60 NUMBLK=NUMBLK+1
      NN=NB*(NUMBLK+1)
      NM=NN-NB
      NL=NM-NB+1
      KSHIFT=2*NL-2
C
      DO 210 N=1,NUMEL
C
      IF (IX(N,5)) 210,210,65
   65 DO 80 I=1,4
      IF (IX(N,I)-NL) 80,70,70
   70 IF (IX(N,I)-NM) 90,90,80
   80 CONTINUE
      GO TO 210
C
   90 IF (IX(N,5) .LE. NSHELL)  GO TO 92
      CALL JTSTIF
      IF (VOL.GT. 0.0) GO TO 165
      PRINT 2003,N
      LBAD = 2
      GO TO 165
   92 CALL QUAD
      IX(N,5)=-IX(N,5)
C
      IF (VOL.LE. 0.) LBAD = 1
      IF (VOL .GT. 0.0) GO TO 144
      PRINT 2003, N
  144 IF (IX(N,5).EQ.IX(N,4)) GO TO 165
  145 DO 150 II=1,8
      CC=S(II,10)/S(10,10)
      P(II)=P(II)-CC*P(10)
      DO 150 JJ=1,9
  150 S(II,JJ)=S(II,JJ)-CC*S(10,JJ)
C
      DO 160 II=1,8
      CC=S(II,9)/S(9,9)
      P(II)=P(II)-CC*P(9)
      DO 160 JJ=1,8
  160 S(II,JJ)=S(II,JJ)-CC*S(9,JJ)
C
C          ADD ELEMENT STIFFNESS TO TOTAL STIFFNESS
C
  165 DO 166 I=1,4
  166 LM(I)=2*IX(N,I)-2
C
      DO 200 I=1,4
      DO 200 K=1,2
      II=LM(I)+K-KSHIFT
      KK=2*I-2+K
      B(II)=B(II)+P(KK)
      DO 200 J=1,4
      DO 200 L=1,2
      JJ=LM(J)+L-II+1-KSHIFT
      LL=2*J-2+L
      IF(JJ) 200,200,175
  175 IF(ND-JJ) 180,195,195
  180 PRINT    2004, N
      LBAD = 1
      GO TO 210
  195 A(II,JJ)=A(II,JJ)+S(KK,LL)
  200 CONTINUE
  210 CONTINUE
C
C     ADD CONCENTRATED FORCES WITHIN BLOCK
C
      DO 250 N=NL,NM
      K=2*N-KSHIFT
      B(K)=B(K)+UZ(N)
  250 B(K-1)=B(K-1)+UR(N)
C
C     BOUNDARY CONDITIONS
C
C       1. PRESSURE B.C.
C
      IF (NUMPC) 260,310,260
  260 DO 300 L=1,NUMPC
      I=IBC(L)
      J=JBC(L)
      PP=(PR(L)/2.)*PRFACT
```

```
      DZ=(Z(I)-Z(J))*PP
      DR=(R(J)-R(I))*PP
  264 II=2*I-KSHIFT
      JJ=2*J-KSHIFT
      IF (II) 280,280,265
  265 IF (II-ND) 270,270,280
  270 SINA=0.0
      COSA=1.0
      IF (CODE(I)) 271,272,272
  271 SINA=SIN(CODE(I))
      COSA=COS(CODE(I))
  272 B(II-1)=B(II-1)+(COSA*DZ+SINA*DR)
      B(II)=B(II)-(SINA*DZ-COSA*DR)
  280 IF (JJ) 300,300,285
  285 IF (JJ-ND) 290,290,300
  290 SINA=0.0
      COSA=1.0
      IF (CODE(J)) 291,292,292
  291 SINA=SIN(CODE(J))
      COSA=COS(CODE(J))
  292 B(JJ-1)=B(JJ-1)+(COSA*DZ+SINA*DR)
      B(JJ)=B(JJ)-(SINA*DZ-COSA*DR)
  300 CONTINUE
C
C       2. DISPLACEMENT B.C.
C
  310 DO 400 N=NL,NM
      IF (N-NUMNP) 315,315,400
  315 U=UR(N)
      N=2*N-1-KSHIFT
      IF (CODE(N)) 390,400,316
  316 IF (CODE(N)-1.) 317,370,317
  317 IF (CODE(N)-2.) 318,390,318
  318 IF (CODE(N)-3.) 390,380,390
  370 CALL MODIFY(A,B,ND2,MBAND,N,U)
      GO TO 400
  380 CALL MODIFY(A,B,ND2,MBAND,N,U)
  390 U=UZ(N)
      N=N+1
      CALL MODIFY(A,B,ND2,MBAND,N,U)
  400 CONTINUE
C
C     WRITE BLOCK OF EQUATIONS ON TAPE AND SHIFT UP LOWER BLOCK
C
      WRITE (9) (B(N),(A(N,M),M=1,MBAND),N=1,ND)
C
      DO 420 N=1,ND
      K=N+ND
      B(N)=B(K)
      B(K)=0.0
      DO 420 M=1,ND
      A(N,M)=A(K,M)
  420 A(K,M)=0.0
C
C     CHECK FOR LAST BLOCK
```

```
C
      IF (NM-NUMNP) 60,480,480
  480 CONTINUE
C*****************************************************************
      IF (LBAD .EQ. 0) GO TO 500
      PRINT 2005, LBAD
      STOP
  500 RETURN
C
 2003 FORMAT (26HONEGATIVE AREA ELEMENT NO. I4)
 2004 FORMAT (29HOBAND WIDTH EXCEEDS ALLOWABLE I4)
 2005 FORMAT ( * LBAD = *I5)
      END



      SUBROUTINE TRISTF(II,JJ,KK)
C
      COMMON NUMNP,NUMEL,NUMMAT,NUMPC, ACELX,ACELY, M,VOL,TEMP,MTYPE,
     1 HED(12), E(8,12), RO(12),XXNN(12),R(900),Z(900),UR(900),UZ(900),
     2 CODE(900),IBC(200),JBC(200),PR(200),ANGLE(4),SIG(10),LBAD
      COMMON /ARG/ RR(5),ZZZ(5),S(10,10),P(10),TT(4),LM(4),DD(3,3),
     1 HH(6,10),RR(4),ZZ(4),C(4,4),H(6,10),D(6,6),F(6,10),TP(6),X(10)
     2,EE(7),IX(670,5),EPS(670),MTAG(670),RSTRS(4),RESID(670,3),
     3 NRES,PRFACT,NUMJT,SIGST(3,670)
      COMMON/BANARG/MBAND,NUMBLK,B(160),A(160,80)
      COMMON/JOINT/NSHELL,KCODE(400),FNST(400),FTST(400),FPSTST(400),
     2 EPSNST(400), PPP(8),NNN,NJ
C
C       1. INITIALIZATION
C
      LM(1)=II
      LM(2)=JJ
      LM(3)=KK
C
      RR(1)=RR9(II)
      RR(2)=RRR(JJ)
      RR(3)=RRR(KK)
      RR(4)=RRR(II)
      ZZ(1)=ZZZ(II)
      ZZ(2)=ZZZ(JJ)
      ZZ(3)=ZZZ(KK)
      ZZ(4)=ZZZ(II)
C
   85 DO 100 I=1,6
      DO 90 J=1,10
      F(I,J)=0.0
   90 H(I,J)=0.0
      DO 100 J=1,6
  100 D(I,J)=0.0
C
C       3. FORM INTEGRAL(G)T*(C)*(G)
C
      COMM=RR(2)*(ZZ(3)-ZZ(1))+RR(1)*(ZZ(2)-ZZ(3))+RR(3)*(ZZ(1)-ZZ(2))



      XI(1)=COMM/2.0
      VOL=VOL+XI(1)
C
      D(2,2)=XI(1)*C(1,1)
      D(2,6)=XI(1)*C(1,2)
      D(3,3)=XI(1)*C(4,4)
      D(3,5)=XI(1)*C(4,4)
      D(5,5)=XI(1)*C(4,4)
      D(6,6)=XI(1)*C(2,2)
C
  108 DO 110 I=1,6
      DO 110 J=I,6
  110 D(J,I)=D(I,J)
C
C       4. FORM  COEFFICIENT-DISPLACEMENT TRANSFORMATION MATRIX
C
      DD(1,1)=(RR(2)*ZZ(3)-RR(3)*ZZ(2))/COMM
      DD(1,2)=(RR(3)*ZZ(1)-RR(1)*ZZ(3))/COMM
      DD(1,3)=(RR(1)*ZZ(2)-RR(2)*ZZ(1))/COMM
      DD(2,1)=(ZZ(2)-ZZ(3))/COMM
      DD(2,2)=(ZZ(3)-ZZ(1))/COMM
      DD(2,3)=(ZZ(1)-ZZ(2))/COMM
      DD(3,1)=(RR(3)-RR(2))/COMM
      DD(3,2)=(RR(1)-RR(3))/COMM
      DD(3,3)=(RR(2)-RR(1))/COMM
C
      DO 120 I=1,3
      J=2*LM(I)-1
      H(1,J)=DD(1,I)
      H(2,J)=DD(2,I)
      H(3,J)=DD(3,I)
      H(4,J+1) = DD(1,I)
      H(5,J+1)=DD(2,I)
  120 H(6,J+1)=DD(3,I)
C
C     ROTATE UNKNOWNS IF REQUIRED
C
      DO 129 J=1,2
      I=LM(J)
      IF (ANGLE(I)) 122,125,125
  122 SINA=SIN(ANGLE(I))
      COSA=COS(ANGLE(I))
      IJ=2*I
      DO 124 K=1,6
      TEM=H(K,IJ-1)
      H(K,IJ-1)=TEM*COSA+H(K,IJ)*S NA
  124 H(K,IJ)= -TEM*SINA+H(K,IJ)*COSA
  129 CONTINUE
C
C       5. FORM ELEMENT STIFFNESS MATRIX (H)T*(D)*(H)
C
      DO 130 J=1,10
      DO 130 K=1,6
      IF (H(K,J)) 128,130,128
  128 DO 129 I=1,6
```

```
  129 F(I,J)=F(I,J)+D(I,K)*H(K,J)
  130 CONTINUE
C
      DO 140 I=1,10
      DO 140 K=1,6
      IF (H(K,I)) 136,140,136
  136 DO 139 J=1,10
  139 S(I,J)=S(I,J)+H(K,I)*F(K,J)
  140 CONTINUE
C
C     FORM RESIDUAL STRESS CONTRIBUTIONS TO THE LOADS
C
  150 DO 160 I=1,10
  160 P(I)=P(I)+XI(1)*H(2,I)*(       -RSTRS(1) )
     1          +XI(1)*H(6,I)*(       -RSTRS(2) )
     2          +XI(1)*H(3,I)*(       -RSTRS(3) )
     3          +XI(1)*H(5,I)*(       -RSTRS(3) )
C
C     ACCELERATION LOADS
C
      COMM=RO(MTYPE)*XI(1)/3.0
      DO 170 I=1,3
      J=2*LM(I)-1
      P(J)=P(J)-ACELX*COMM
  170 P(J+1)=P(J+1)-ACELY*COMM
C
C     FORM STRAIN TRANSFORMATION MATRIX
C
  400 DO 410 I=1,6
      DO 410 J=1,10
  410 HH(I,J)=HH(I,J)+H(I,J)
C
  415 RETURN
C
      END



      SUBROUTINE QUAD
C
      COMMON NUMNP,NUMEL,NUMMAT,NUMPC, ACELX,ACELY, M,VOL,TEMP,MTYPE,
     1 HED(12), E(8,12), RO(12),XXNN(12),R(900),Z(900),UR(900),UZ(900),
     2 CODE(900),IBC(200),JBC(200),PR(200),ANGLE(4),SIG(10),LBAD
      COMMON /ARG/ RRR(5),ZZZ(5),S(10,10),P(10),TT(4),LM(4),DD(3,3),
     1 HH(6,10),RR(4),ZZ(4),C(4,4),H(6,10),D(6,6),F(6,10),TP(6),X(10)
     2,EE(7),IX(670,5),EPS(670),MTAG(670),RSTRS(4),RESID(670,3),
     3 NRES,PRFACT,NUMJT,SIGST(3,670)
      COMMON/BANARG/MBAND,NUMBLK,B(160),A(160,80)
      COMMON/JOINT/NSHELL,KCODE(400),FNST(400),FTST(400),FPSTST(400),
     2 EPSNST(400), PPP(8),NNN,NJ
C
      I=IX(N,1)
      J=IX(N,2)



      K=IX(N,3)
      L=IX(N,4)
      MTYPE=IX(N,5)
C
C     FORM STRESS STRAIN RELATIONSHIP FOR PLANE STRAIN
      DO 105 KK=1,7
  105 EE(KK)=E(KK+1,MTYPE)
C
C
      IF (MTAG(N)-2) 82,84,83
   82 EE(3)=EE(1)
      GO TO 84
   83 EE(1)=EE(3)
C
   84 EE(1)=EE(1)/(1.-EE(2)**2)
      EE(3)=EE(3)/(1.-EE(2)**2)
      EE(2)=EE(2)/(1.-EE(2))
C
      XX=EE(1)/EE(3)
      COMM=EE(1)/(XX-EE(2)**2)
      C(1,1)=COMM*XX
      C(1,2)=COMM*EE(2)
      C(1,3)=0.0
      C(2,1)=C(1,2)
      C(2,2)=COMM
      C(2,3)=0.0
      C(3,1)=0.0
      C(3,2)=0.0
      C(3,3)=.5*EE(1)/(XX+EE(2))
C
      SS=SIN(EPS(N))
      CC=COS(EPS(N))
      S2=SS*SS
      C2=CC*CC
      SC=SS*CC
C
      D(1,1)=S2
      D(1,2)=C2
      D(1,3)=0.0
      D(1,4)=-SC
      D(2,1)=C2
      D(2,2)=S2
      D(2,3)=0.0
      D(2,4)=SC
      D(3,1)=2.*SC
      D(3,2)=-D(3,1)
      D(3,3)=0.0
      D(3,4)=-C2+S2
C
      DO 88 II=1,3
      DO 88 JJ=1,4
      H(II,JJ)=0.0
      DO 88 KK=1,3
      H(II,JJ)=H(II,JJ) +C(II,KK)*D(KK,JJ)
   88 CONTINUE
```

```
C
      DO 89 II=1,4
      DO 89 JJ=1,6
      C(II,JJ)=0.0
      DO 89 KK=1,3
      C(II,JJ)=C(II,JJ)+D(KK,II)*H(KK,JJ)
   89 CONTINUE
C
C*****************************************************************
C     REPLACE RESIDUAL STRESSES FOR NTH ELEMENT BY RSTRS(IJ)
C*****************************************************************
C
      IF(NMES.EQ.0) GO TO 112
      DO 111 IJ=1,3
  111 RSTRS (IJ)=RESID(N,IJ)
      GO TO 114
  112 DO 113 IJ=1,3
  113 RSTRS(IJ)=0.
  114 RSTRS(4)=RSTRS(3)
C
C          FORM QUADRILATERAL STIFFNESS MATRIX
C
      RRR(5)=(R(I)+R(J)+R(K)+R(L))/4.0
      ZZZ(5)=(Z(I)+Z(J)+Z(K)+Z(L))/4.0
      DO 96 M=1,4
      MM=IX(N,M)
   93 RRR(M)=R(MM)
   94 ZZZ(M)=Z(MM)
C
      DO 100 II=1,10
      P(II)=0.0
      DO 95 JJ=1,6
   95 HH(JJ,II)=0.0
      DO 100 JJ=1,10
  100 S(II,JJ)=0.0
      DO 119 II=1,4
      JJ=IX(N,II)
  119 ANGLE(II)=CODE(JJ)/57.3
C
C     FORM BAR STIFFNESS
C
      IF (IX(N,2)-IX(N,3)) 250,240,250
  240 TT(1)=-EE(6)
      TT(2)=-EE(6)
      DR=R(J)-R(I)
      DZ=Z(J)-Z(I)
      XL=SQRT(DR**2+DZ**2)
      RRR(5)=(R(I)+R(J))/2.-2.*EE(4)*DZ/XL
      ZZZ(5)=(Z(I)+Z(J))/2.+2.*EE(4)*DR/XL
      CALL TRISTF(1,2,5)
      GO TO 130
  250 CONTINUE
C
      VOL = 0.0
      IF (K.NE. L) GO TO 125
```

```
      CALL QUAD
C
      DO 120 I=1,4
      II=2*I
      JJ=2*IX(N,I)
      P(II-1)=B(JJ-1)
  120 P(II)=B(JJ)
C
      DO 150 I=1,2
      RR(I)=P(I+8)
      DO 150 K=1,8
  150 RR(I)=RR(I)-S(I+8,K)*P(K)
C
      COMM=S(9,9)*S(10,10)-S(9,10)*S(10,9)
      IF (COMM) 155,160,155
  155 P(9)=(S(10,10)*RR(1)-S(9,10)*RR(2))/COMM
      P(10)=(-S(10,9)*RR(1)+S(9,9)*RR(2))/COMM
C
  160 DO 170 I=1,6
      TP(I)=0.0
      DO 170 K=1,10
  170 TP(I)=TP(I)+HH(I,K)*P(K)
C
C
      RR(1)=TP(2)
      RR(2)=TP(6)
      RR(3)=0.0
      RR(4)=TP(3)+TP(5)
C
  176 DO 180 I=1,4
      SIG(I)=RSTRS(I)
      RSTRS(I)=0.0
      DO 180 K=1,4
  180 SIG(I)=SIG(I)+C(I,K)*RR(K)
      SIG(3)=SIG(4)
      DO 190 I=1,3
      SIGST(I,M)=SIG(I)+SIGST(I,M)
  190 SIGST(3,M)=SIG(I)
C
C*****************************************************************
C     OUTPUT STRESSES
C*****************************************************************
C
C     CALCULATE PRINCIPAL STRESSES
C
      CC=(SIG(1)+SIG(2))/2.0
      BB=(SIG(1)-SIG(2))/2.0
      CR=SQRT(BB**2+SIG(3)**2)
      SIG(4)=CC+CR
      SIG(5)=CC-CR
      IF(BB.NE. 0.) GO TO 195
      EPS(N)=77777.
      GO TO 196
  195 EPS(N)=ATAN2(SIG(3),BB)/2.
  196 SIG(6)=57.296*EPS(N)
```

```
  120 CALL TRISTF(1,2,3)
      RRR(5)=(RRR(1)+RRR(2)+RRR(3))/3.0
      ZZZ(5)=(ZZZ(1)+ZZZ(2)+ZZZ(3))/3.0
      VOL=X(1)
      IF (VOL.GT. 0.) RETURN
      PRINT 1000,N
      RETURN
  125 CONTINUE
      CALL TRISTF(4,1,5)
      CALL TRISTF(1,2,5)
      CALL TRISTF(2,3,5)
      CALL TRISTF(3,4,5)
C
      IF(VOL.GT. 0.) GO TO 126
      PRINT 1000,N
  126 DO 140 II=1,6
      DO 140 JJ=1,10
      HH(II,JJ)=HH(II,JJ)/4.0
  140 CONTINUE
C
  130 RETURN
C
 1000 FORMAT ( * NEGATIVE AREA, ELEMENT NO.* I5)
      END
```

```
C
      MTAG(N)=1
      IF(SIG(4)) 261,261,260
  260 MTAG(N)=2
  261 IF(SIG(5)) 263,263,262
  262 MTAG(N)=3
  263 CONTINUE
C
C ****************************************************************
C      APPLY FAILURE CRITERION TAUOCT =LE= N + D*SIGOCT**B
C ****************************************************************
C
      SIGT = E(1,MTYPE)
      SIG(7)=EE(2)*(SIG(4)+SIG(5))
      SIGOCT =-(SIG(4)+SIG(5)+SIG(7))/3.0
      IF(SIGOCT.GE. 0.0) GO TO 290
      IF (SIG(4).LT. SIGT) GO TO 104
      IX(N,5)=NSHELL
      NFAIL =2
      GO TO 104
  290 TAUOCT = SQRT(((SIG(4)-SIG(5))**2)
     1 +((SIG(5)-SIG(7))**2)
     2 +((SIG(7)-SIG(4))**2))/3.0
      CONN = EE(4)
      COND = EE(5)
      CONB = EE(6)
      STREN = CONN + COND*(SIGOCT**CONB)
      IF(TAUOCT.LT.STREN) GO TO 104
      IX(N,5)=NSHELL
      NFAIL = 1
C
  104 IF (NPRINT) 110,105,110
  105 PRINT 2000
      NPRINT=50
  110 NPRINT=NPRINT-1
C
  305 PRINT 2001, N,RRR(5),ZZZ(5), (SIG(I),I=1,6),NFAIL
  300 CONTINUE
C
  320 RETURN
C
 2000 FORMAT (7H1EL.NO.   7X  1HX 7X 1HY 4X 8HX-STRESS 4X 8HY-STRESS 3X
     19HXY-STRESS 2X 10HMAX-STRESS 2X 10HMIN-STRESS 7H  ANGLE
     1 2X 17H FAILED IF 1 OR 2  )
 2001 FORMAT(I7,2F8.2,1P5E12.4,0PF7.2,I10)
      END
```

```
      SUBROUTINE MODIFY(A,B,NEQ,MBAND,N,U)
C
      DIMENSION A(160,80), B(160)
C
      DO 250 M=2,MBAND
```

```
      K=N-M+1
      IF(K) 235,235,230
  230 B(K)=B(K)-A(K,M)*U
      A(K,M)=0.0
  235 K=N+M-1
      IF(NEQ-K) 250,240,240
  240 B(K)=B(K)-A(N,M)*U
      A(N,M)=0.0
  250 CONTINUE
      A(N,1)=1.0
      B(M)=U
      RETURN
C
      END



      SUBROUTINE BANSOL
      COMMON/BANARG/MM,NUMBLK,B(160),A(160,80)
C
      NN= 80
      NL=NN+1
      NH=NN+NN
      REWIND 8
      REWIND 9
      NB=0
      GO TO 150
C**************************************************************************
C     REDUCE EQUATIONS BY BLOCKS
C**************************************************************************
C
C     1. SHIFT BLOCK OF EQUATIONS
C
  100 NB=NB+1
      DO 125 N=1,NN
      NM=NN+N
      B(N)=B(NM)
      B(NM)=0.0
      DO 125 M=1,MM
      A(N,M)=A(NM,M)
  125 A(NM,M)=0.0
C
C     2. READ NEXT BLOCK OF EQUATIONS INTO CORE
C
      IF (NUMBLK-NB) 150,200,150
  150 READ (9) (B(N),(A(N,M),M=1,MM),N=NL,NH)
      IF (NB) 200,100,200
C
C     3. REDUCE BLOCK OF EQUATIONS
C
  200 DO 300 N=1,NN
      IF (A(N,1)) 225,300,225
  225 B(N)=B(N)/A(N,1)


      DO 275 L=2,MM
      IF (A(N,L)) 230,275,230
  230 C=A(N,L)/A(N,1)
      I=N+L-1
      J=0
      DO 250 K=L,MM
      J=J+1
  250 A(I,J)=A(I,J)-C*A(N,K)
      B(I)=B(I)-A(N,L)*B(N)
      A(N,L)=C
  275 CONTINUE
  300 CONTINUE
C
C     4. WRITE BLOCK OF REDUCED EQUATIONS ON TAPE 2
C
      IF (NUMBLK-NB) 375,400,375
  375 WRITE (8) (B(N),(A(N,M),M=2,MM),N=1,NN)
      GO TO 100
C**************************************************************************
C     BACK-SUBSTITUTION
C**************************************************************************
  400 DO 450 M=1,NN
      N=NN+1-M
      DO 425 K=2,MM
      L=N+K-1
  425 B(N)=B(N)-A(N,K)*B(L)
      NM=N+NN
      B(NM)=B(N)
  450 A(NM,NB)=B(N)
      NB=NB-1
      IF (NB) 475,500,475
  475 BACKSPACE 8
      READ (8) (B(N),(A(N,M),M=2,MM),N=1,NN)
      BACKSPACE 8
      GO TO 400
C**************************************************************************
C     ORDER UNKNOWNS IN B ARRAY
C**************************************************************************
  500 K=0
      DO 600 NB=1,NUMBLK
      DO 600 N=1,NN
      NM=N+NN
      K=K+1
  600 B(K)=A(NM,NB)
C
      RETURN
C
      END



      SUBROUTINE JTSTIF
      COMMON NUMNP,NUMEL,NUMMAT,NUMPC, ACELR,ACELZ, [illegible]
     1 MED(12), E(8,12), RO(12),XANN( [illegible]
     2 CODE(900),IBC(200),JBC(200),PR(200),ANGLE(4),SIG(10),LBAD
      COMMON /ARG/ RRR(5),ZZZ(5),S(10,10),P(10),TT(4),LM(4),DD(3,3),
     1 HH(6,10),RR(4),ZZ(4),C(4,4),H(6,10),D(6,6),F(6,10),IP(6),XI(10)
     2,EE(7),IX(670,5),EPS(670),MTAG(670),RSTRS(4),RESID(670,3),
     3 NRES,PRFACT,NUMJT,SIGST(3,670)
      COMMON/JOINT/NSHELL,KCODE(400),FNST(400),FTST(400),EPSTST(400),
     2 EPSNST(400), PPP(8),NNN,NJ

      DIMENSION ESTIF(10,10)
      EQUIVALENCE (S(10,10),ESTIF(10,10))
      DIMENSION A(4,4),TR(2,2)
      DATA A/2.,1.,-1.,-2.,1.,2.,-2.,-1.,-1.,-2.,2.,1.,-2.,-1.,1.,2./
      REAL KS,KN,L
      NJ=NJ+1
C
C******************************************
C   REPLACE RESIDUAL STRESSES FOR NTH ELEMENT BY RESTRS(IJ)
C *********************************************************
C
      IF(NRES.EQ.0) GO TO 112
      DO 111 IJ=1,3
  111 RSTRS (IJ)=RESID(N,IJ)
      GO TO 114
  112 DO 113 IJ=1,3
  113 RSTRS(IJ)=0.
  114 RSTRS(4)=RSTRS(3)
C
  115 II=IX(N,1)
      JJ= IX(N,2)
      DR=R(JJ)-R(II)
      DZ=Z(JJ)-Z(II)
      L=SQRT(DR*DR+DZ*DZ)
      VOL = L
      IF(L.EQ.0.) GO TO 201
      MAT=IX(N,5)
      IX(N,5)=-IX(N,5)
C** MATERIAL PROPERTIES
      KN=E(1,MAT)
      IF(KCODE(NJ) GT.0) GO TO 40
      KS=E(2,MAT)
      GO TO 41
   40 KS=E(5,MAT)
   41 IF(FNST(NJ).LE.0.)GO TO 50
      KN=0.
      KS=0.
   50 IF(EPSNST(NJ).GT. E(6,MAT))GO TO 204
      KN=1000.*KN
  204 CONTINUE
      COMS=KS*L/6.
      COMN=KN*L/6.
C          INITIALIZE
      DO 100 II=1,8
      P(II)=0.0
      DO 100 JJ=1,8
  100 ESTIF(II,JJ)=0.0


      DO 160 I=1,4
      J=2*I-1
      PPP(J)=L*RSTRS(1)/2.
      J=2*I
  160 PPP(J)=L*RSTRS(2)/2.
      DO 161 I=1,4
  161 PPP(I)=-PPP(I)
      DO 200 II=1,4
      IS=2*II-1
      IN=2*II
      DO 200 JJ=1,4
      JS = 2*JJ-1
      JN = 2*JJ
      ESTIF (IS,JS) = COMS*A(II,JJ)
  200 ESTIF(IN,JN)=COMN*A(II,JJ)
C     ROTATE TO GLOBAL COORDINATES
      TR(1,1)=DR/L
      IF(TR(1,1).EQ.1.) RETURN
      TR(1,2)=DZ/L
      TR(2,1)=-DZ/L
      TR(2,2)=DR/L
      DO 400 NN=1,4
      DO 410 II=1,8
      JJ= 2*NN-1
      TEMP = ESTIF(II,JJ)
      DO 410 KK=1,2
      ESTIF(II,JJ)=TEMP*TR(1,KK)+ESTIF(II,2*NN)*TR(2,KK)
  410 JJ=JJ+1
      DO 420 II=1,8
      JJ=2*NN-1
      TEMP =ESTIF(JJ,II)
      DO 420 KK=1,2
      ESTIF(JJ,II)=TR(1,KK)*TEMP+TR(2,KK)*ESTIF(2*NN,II)
  420 JJ=JJ+1
  400 CONTINUE
      DO 401 I=1,4
      J=2*I-1
      II=2*I
      P(J)= PPP(J)*TR(2,2)+PPP(II)*TR( [illegible]
  401 P(II)=PPP(J)*TR(1,2)+PPP( [illegible]
      RETURN
  201 PRINT 2090, N
      RETURN
 2000 FORMAT(10E [illegible]
 2090 FORMAT(14H [illegible]
      END
```

```
     1 MM(6,10),RR(4),ZZ(4),C(4,6),H(6,10),D(6,6),F(6,10),IP(6),XI(10)
     2,EE(7),IX(670,5),EPS(670),MTAG(670),RSTRS(4),RESID(670,3),
     3 NREB,PRFACT,NUMJT,SIGST(3,670)
      COMMON/BANARS/MBAND,NUMBLK,B(160),A(160,80)
      COMMON/JOINT/NSHELL,KCODE(400),FNST(400),FTST(400),EPSTST(400),
     2 EPSNST(400), PPP(8),NNN,NJ

      DIMENSION V(6),U(6)
      REAL L,KN,KS
      N=0
      PRINT 1001
C  ********ESTABLISH DISPLACEMENTS ALONG AND NORMAL TO JOINT
      DO 500 N=1,NUMEL
      MAT=IX(N,5)
      IF(MAT.LE.NSHELL) GO TO 500
      M=N+1
      FTST(M)=FTST(M)+RESID(N,1)
      FNST(M)=FNST(M)+RESID(N,2)
      DO 10 I=1,3
   10 RESID(N,I)=0.
      I=IX(N,1)
      J= IX(N,2)
      DR=R(J)-R(I)
      DZ=Z(J)-Z(I)
      RJ=0.5*(R(J)+R(I))
      ZJ=0.5*(Z(J)+Z(I))
      L=SQRT(DR*DR+DZ*DZ)
      VOL = L
      DR=DR/L
      DZ=DZ/L
      DO 100 II=1,4
      K=IX(N,II)
      V(II)=-B(2*K-1)*DZ+B(2*K)*DR
  100 U(II)=B(2*K-1)*DR+B(2*K)*DZ
C **********  COMPUTE EFFECTIVE STRAIN
      KN=0.
      KS=0.0
      IF(EPSNST(M).GT.0.) GO TO 200
      KN=E(1,MAT)
      IF(EPSNST(M).GT.E(6,MAT))GO TO 203
      KN=1000.*KN
  203 IF(KCODE(M).GT.0) GO TO 201
      KS= E(2,MAT)
      GO TO 200
  201 KS = E(5,MAT)
  200 EPST=0.5*(U(4)-U(1)+U(3)-U(2))
      EPS(N)=0.5*(V(4)-V(1)+V(3)-V(2))
C   **********************************
C  COMPUTE NORMAL AND SHEAR FORCE PER UNIT LENGTH AND CALCULATE STRENGTH
C   **********************************
      FN=KN*EPS(N)+FNST(M)
  205 FT = KS*EPST +FTST(M)
      FTST(M)=FT
      FNST(M)=FN
      EPSNST(M)=EPS(N)+EPSNST(M)




      EPSTST(M)=EPST + EPSTST(M)
      CJ = E(3,MAT)
      PHIJ= E(4,MAT)
      PHIR=PHIJ*3.14159146/180.
      STREN = CJ+ABS(FN)*SIN(PHIR)/COS(PHIR)
      KCODE(M)=0
      IF (ABS(FT).LT.STREN) GO TO 210
      KCODE(M)=1
  210 PRINT 1000,N,RJ,ZJ,FN,FT,EPS(N),EPST,EPSNST(M),EPSTST(M),KCODE(M)
  500 CONTINUE
      RETURN
 1001 FORMAT('1 ELEM    X        Y        NORMAL STRESS  TANG STRESS    NOR
     1MAL DISP   TANG DISP     CUM NORM DISP   CUM TANG DISP 1 SHEARED')
 1000 FORMAT (I5,2F8.2,6E15.5,I10)
      END
```

APPENDIX 2

JOINT INFLUENCE ANALYSIS COMPUTER PROGRAM

FORTRAN PROGRAM TO GENERATE STRESSES BY KIRSCH SOLUTION FOR GIVEN FREE FIELD PRESSURES FORCING A CIRCULAR TUNNEL AND TO CALCULATE AND PLOT THE ZONES OF INFLUENCE AROUND THE TUNNEL OF JOINTS OF A GIVEN ORIENTATION AND A GIVEN COHESION AND FRICTION. PRODUCES A PLOT ON ON-LINE PRINTER

```
      PROGRAM KIRSCH (INPUT,OUTPUT)
C
      COMMON SIGX, SIGY, SIGZ, TAUXZ,FACTJ(10), C, DCL(10), DCL2(10),
     1       DCN(10), DCN2(10), DCM(10), MED(12), ITYPE(101,10),
     2       ROVERA(46,101), THETA(46), IPLOT(46,5,10), RPLOT(46,5,10),
     3       KMAX(46,10), ITH, IR, RADEND, NUMJTM, PHIR
      DIMENSION  CONTOR(5),BETA(10)
      REAL IPLOT
C
C     READ AND PRINT OF CONTROL INFORMATION
C     READ AND PRINT OF CONTROL INFORMATION
  199 READ 1000,(MED(I),I=1,12),NP
      IF (NP.GT.0) GO TO 999
      READ  1010, NUMJTM, RADINC, RADEND, THINC, P1, P2, GAM, S, C, PHI,
     1 SIGY1,BETA(1)
      PRINT   1001, (MED(I),I=1,12),NUMJTM,RADINC,RADEND,THINC,P1,P2,
     1 GAM,S,C,PHI
      PRINT 1008,SIGY1,BETA(1)
C
C     DETERMINE DIRECTION COSINES FOR BETA ORIENTATION
      DCM(1)=COS(BETA(1)*3.14159/180.0)
      DCN2(1)=(1.-DCM(1)**2)/(1.+S**2)
      DCN(1)=SQRT(DCN2(1))
      DCL(1)=-S*DCN(1)
      DCL2(1)=S**2*DCN2(1)
C
C     GENERATE SIGX AND SIG THETA FROM KIRSCH SOLUTION
      IR=IFIX((RADEND-1.)/RADINC)+1
      ITH=IFIX(90./THINC)+1
      P1PP2 = (P1 + P2) * 0.5
      P1MP2 = (P1 - P2) * 0.5
      PIR = 3.1415927 / 180.
      PHIR = PHI * PIR
      DO 1 J=1,ITH
      IF(J-1)  2,2,3
    2 THETA(J)=0.0
      GO TO 4
    3 THETA(J) = THETA(J-1) + THINC
    4 THETAR = PIR * THETA(J)
      THET2 = 2.0 * THETAR
      S2 = SIN(THETAR)**2
      C2 = COS(THETAR)**2
      SC= SIN(THETAR)*COS(THETAR)
      DO 11 I=1,IR
      IF(I-1)  5,5,6
    5 ROVERA(J,I)=1.0

      GO TO 7
    6 ROVERA(J,I)=ROVERA(J,I-1)+RADINC
    7 RAD2 = (1.0/ROVERA(J,I)) ** 2
      SIGRA = P1PP2 * (1.0 - RAD2)
      SIGRB = P1MP2 * (1.0 - RAD2*(4.0-3.0*RAD2)) * COS(THET2)
      SIGR = SIGRA + SIGRB
      SIGTHA = P1PP2 * (1.0 + RAD2)
      SIGTHB = P1MP2 * (1.0 + 3.0*RAD2*RAD2) * COS(THET2)
      SIGTH = SIGTHA - SIGTHB
      TAURTH = -P1MP2 * (1.0 + RAD2*(2.0-3.0*RAD2)) * SIN(THET2)
C     OBTAIN PRINCIPAL STRESSES
      R=SQRT(((SIGTH-SIGR)/2.)**2+TAURTH**2)
      SIGM=(SIGTH+SIGR)/2.0
      SIG1=SIGM+R
      SIG3=SIGM-R
      SIG2=0.0
C     OBTAIN XYZ STRESSES
      SIGX=SIGR*C2 - 2.*TAURTH*SC + SIGTH*S2
      SIGZ= SIGR*S2 + 2.*TAURTH*SC + SIGTH*C2
      TAUXZ=-(SIGTH-SIGR)*SC +TAURTH*(C2-S2)
      SIGY=SIG2 + SIGY1
C     DETERMINE FACTOR OF SAFETY FOR SLIDING ON JOINT
C
      DO 101  L=1,NUMJTM
      CALL JOINT(L)
C
C    ASSIGN A VALUE TO ITYPE. 1 IF IN ZONE OF SLIP, 2 IF OUTSIDE ZONE
C
      IF (FACTJ(L) - 1.0)  80, 80, 81
   80 ITYPE(I,L) = 1
      GO TO 101
   81 ITYPE(I,L) = 2
  101 CONTINUE
C     END OF IR LOOP
   11 CONTINUE
C
C     ESTABLISH COORDINATES FOR CONTOURS
C
      DO 51  L=1,NUMJTM
      K = 1
      DO 50  I=2,IR
      IF (ITYPE(I,L) - ITYPE(I-1,L))  21, 50, 23
   21 IPLOT(J,K,L) = 1H2
      GO TO 24
   23 IPLOT(J,K,L) = 1H1
   24 RPLOT(J,K,L) = ROVERA(J,I-1)
      K = K+1
   50 CONTINUE
   51 KMAX(J,L) = K-1
C
C     END OF J LOOP
    1 CONTINUE
      CALL PLOT
      GO TO 199
  999 RETURN
 1000 FORMAT (12A6, I2)
 1010 FORMAT (I10,3F10.4/ 8F10.4)
 1001 FORMAT(1H1,12A6/23HONUMBER OF ORIENTATIONS  9X,I5/
     1 19HO1NCREMENT OF RADII  6X,F10.4/ 17HOOUTERMOST RADIUS  8X,F10.4/
     219HOINCREMENT OF THETA   6X,F10.4/20HO::ORIZONTAL PRESSURE  6X,F10.
     32/18HOVERTICAL PRESSURE   7X,F10.2/16HOPOISSON'S RATIO  9X,F10.4/
     418HOSLOPE OF XZ TRACE  7X,F10.4/
     5              9HOCOHESION   25X,F10.4/ 18HOANGLE OF FRICTION
     6  15X,F10.4)
 1002 FORMAT(1H1,3X,2H L 8X, 2H M 8X,  2H N  )
 1003 FORMAT(1HO,3F10.4)
 1008 FORMAT(1HO/ 10H SIGY1 =          F10.4/11HOBETA(1) = 5X,F10.1)
 1020 FORMAT(6E10.4)
      END
      SUBROUTINE JOINT(L)
C
      COMMON SIGX, SIGY, SIGZ, TAUXZ,FACTJ(10), C, DCL(10), DCL2(10),
     1       DCM(10), DCN2(10), DCN(10), MED(12), ITYPE(101,10),
     2       ROVERA(46,101), THETA(46), IPLOT(46,5,10), RPLOT(46,5,10),
     3       KMAX(46,10), ITH, IR, RADEND, NUMJTM, PHIR
C
C     OBTAIN SHEAR AND NORMAL STRESSES ON JOINT
C
      SIGN=DCL2(L)*SIGX+DCM(L)**2*SIGY+ DCN2(L)*SIGZ+2.*DCM(L)*DCL(L)*
     1TAUXZ
      TRACT2=(DCL(L)*SIGX+DCM(L)*TAUXZ)**2+(DCM(L)*SIGY1)**2+(DCL(L)*
     1TAUXZ+DCM(L)*SIGZ)**2
      TAU = SQRT(ABS(TRACT2-SIGN**2))
C
C     FIND FACTOR OF SAFETY IN JOINT
C
      SHSTR=C+SIGN*TAN(PHIR)
      IF(TAU) 21,21,22
   21 FACTJ(L)=1.E+10
      GO TO 23
   22 FACTJ(L)=SHSTR/TAU
   23 RETURN
      END
      SUBROUTINE PLOT
C
      COMMON SIGX, SIGY, SIGZ, TAUXZ,FACTJ(10), C, DCL(10), DCL2(10),
     1       DCM(10), DCN2(10), DCN(10), MED(12), ITYPE(101,10),
     2       ROVERA(46,101), THETA(46), IPLOT(46,5,10), RPLOT(46,5,10),
     3       KMAX(46,10), ITH, IR, RADEND, NUMJTM, PHIR
      DIMENSION A(101)
      REAL IPLOT
C
      IH = ITH + 1
      TIMES = IR / (RADEND - 1.0)
C
C     INITIALIZE PRINTING LINE FOR BORDER
      DO 900 L=1,NUMJTM
   90 DO 91  I=2,100
   91 A(I) = 1H-
      DO 92  I=1,101,5

   92 A(I) = 1H+
      KOUNT = 5
C
C     PRINT TITLE AND UPPER BORDER
      ASSIGN 102 TO NEXT
  100 PRINT 101, MED, DCL(L), DCM(L), DCN(L)
  101 FORMAT (1H1///23X,12A6//36X,3HL =F10.4,7H    M =F10.4,7H    N =F10
     1.4///)
      GO TO NEXT
  102 PRINT 103
  103 FORMAT (8X,1H1,29X,1H1,29X,1H2,29X,1H2,29X,1H3)
C
  300 DO 320  JX=1,ITH
      J = IH - JX
      IF (KMAX(J,L))  303, 303, 301
  301 KK = KMAX(J,L)
      DO 302  K=1,KK
      I =(RPLOT(J,K,L) - 1.0) * TIMES + 0.5
  302 A(I) = IPLOT(J,K,L)
  303 IF (KOUNT - 5)  304, 306, 320
  306 PRINT 305, A
  305 FORMAT (8X,101A1)
      KOUNT = KOUNT + 1
      GO TO 308
  306 PRINT 307, THETA(J), A, THETA(J)
  307 FORMAT (5X,F2.0,1X,101A1,F3.0)
      KOUNT = 1
  308 IF (J - 2)  320, 310, 315
  310 DO 311  I=2,100
  311 A(I) = 1H-
      DO 312  I=1,101,5
  312 A(I) = 1H+
      GO TO 320
  315 DO 316  I=2,100
  316 A(I) = 2H /
  320 CONTINUE
      PRINT 103
C
C     PRINT VALUES OF PLOTTED POINTS
      ASSIGN 400 TO NEXT
      GO TO 100
  400 PRINT 401
  401 FORMAT (29X,5HTHETA14X,5(3HR/A15X))
      DO 410  J=1,ITH
      IF (KMAX(J,L))  410, 410, 402
  402 KK = KMAX(J,L)
      PRINT 403, THETA(J), (RPLOT(J,K,L), K=1,KK)
  403 FORMAT (10X,6F18.2)
  410 CONTINUE
C
  900 CONTINUE
      RETURN
      END
```

UNCLASSIFIED
Security Classification

200

DOCUMENT CONTROL DATA - R & D

(Security classification of title, body of abstract and indexing annotation must be entered when the overall report is classified)

1. ORIGINATING ACTIVITY *(Corporate author)*

Omaha District, Corps of Engineers
Omaha, Nebraska 68102

2a. REPORT SECURITY CLASSIFICATION
UNCLASSIFIED

2b. GROUP

3. REPORT TITLE

EFFECT OF JOINTS ON THE STRENGTH OF TUNNELS

4. DESCRIPTIVE NOTES *(Type of report and inclusive dates)*
Interim

5. AUTHOR(S) *(First name, middle initial, last name)*

Richard E. Goodman

6. REPORT DATE	7a. TOTAL NO. OF PAGES	7b. NO. OF REFS
September 1968	200	10

8a. CONTRACT OR GRANT NO.	9a. ORIGINATOR'S REPORT NUMBER(S)
Contract No. DACA45-67-C-0015 Mod. P001	
b. PROJECT NO.	Technical Report No. 5
c. Work Unit No. OW-1-03-013	9b. OTHER REPORT NO(S) *(Any other numbers that may be assigned this report)*
d.	

10. DISTRIBUTION STATEMENT

This document has been approved for public release and sale; its distribution is unlimited.

11. SUPPLEMENTARY NOTES	12. SPONSORING MILITARY ACTIVITY
Reference: Technical Reports No. 2 and 3 Sept., 1966 and 1967, same originating agency.	Department of the Army Office of the Chief of Engineers Washington, D. C. 20315

13. ABSTRACT

Rock and joint properties were reviewed as a basis for developing the analyses. The review discussed: failure criteria for the rock; and joint properties. Improved methods of sampling and testing joints were explored in detail. Pile Driver test sections were used as a basis for analysis.

Two approaches of analysis of the rock to predict performance of rock bolted and unlined test sections were used. The first method called finite element was used on one section only. This method's complexity prevented its application to other sections. Discontinuities, heterogeneities, and local failures can be taken into account by finite elements, but the representation is only two dimensional. Joint influence analysis, the second method, was applied to many sections. In comparison to the finite element method, joint influence analysis is relatively simple to use. Joints and rock bolts are assumed not to modify the stress distribution in the joint influence analysis; however, the method represents a three dimensional approach.

Comparisons were made to post-shot cross sections of the Pile Driver openings to evaluate the methods of analysis. The finite element method is more powerful; the joint influence analysis is easier to use.

DD FORM 1 NOV 65 1473 REPLACES DD FORM 1473, 1 JAN 64, WHICH IS OBSOLETE FOR ARMY USE.

UNCLASSIFIED
Security Classification

14. KEY WORDS	LINK A		LINK B		LINK C	
	ROLE	WT	ROLE	WT	ROLE	WT
Finite Element						
Jointed Rock						
Joint Influence						
Joint Properties						
Joint Testing						
Joint Sampling						
Rock						
Rock Mechanics						
Rock Stress						
Rock Failure						